

*ARMY RESEARCH LABORATORY*



## **Direct-Sequence Communication Systems**

**by Don Torrieri**

**ARL-TR-3175**

**March 2004**

## **NOTICES**

### **Disclaimers**

The findings in this report are not to be construed as an official Department of the Army position unless so designated by other authorized documents.

Citation of manufacturer's or trade names does not constitute an official endorsement or approval of the use thereof.

Destroy this report when it is no longer needed. Do not return it to the originator.

# **Army Research Laboratory**

Adelphi, MD 20783-1197

---

---

**ARL-TR-3175**

**March 2004**

---

## **Direct-Sequence Communication Systems**

**Don Torrieri**

**Computational and Information Sciences Directorate, ARL**

**REPORT DOCUMENTATION PAGE**

*Form Approved*  
*OMB No. 0704-0188*

Public reporting burden for this collection of information is estimated to average 1 hour per response, including the time for reviewing instructions, searching existing data sources, gathering and maintaining the data needed, and completing and reviewing the collection information. Send comments regarding this burden estimate or any other aspect of this collection of information, including suggestions for reducing the burden, to Department of Defense, Washington Headquarters Services, Directorate for Information Operations and Reports (0704-0188), 1215 Jefferson Davis Highway, Suite 1204, Arlington, VA 22202-4302. Respondents should be aware that notwithstanding any other provision of law, no person shall be subject to any penalty for failing to comply with a collection of information if it does not display a currently valid OMB control number.

**PLEASE DO NOT RETURN YOUR FORM TO THE ABOVE ADDRESS.**

<b>1. REPORT DATE (DD-MM-YYYY)</b> March 2004		<b>2. REPORT TYPE</b> Final		<b>3. DATES COVERED (From - To)</b>	
<b>4. TITLE AND SUBTITLE</b> Direct-Sequence Communication Systems				<b>5a. CONTRACT NUMBER</b>	
				<b>5b. GRANT NUMBER</b>	
				<b>5c. PROGRAM ELEMENT NUMBER</b>	
<b>6. AUTHOR(S)</b> Don Torrieri				<b>5d. PROJECT NUMBER</b>	
				<b>5e. TASK NUMBER</b>	
				<b>5f. WORK UNIT NUMBER</b>	
<b>7. PERFORMING ORGANIZATION NAME(S) AND ADDRESS(ES)</b> U.S. Army Research Laboratory ATTN: AMSRL-CI-C 2800 Powder Mill Road Adelphi, MD 20783-1197				<b>8. PERFORMING ORGANIZATION REPORT NUMBER</b>  ARL-TR-3175	
<b>9. SPONSORING/MONITORING AGENCY NAME(S) AND ADDRESS(ES)</b> U.S. Army Research Laboratory 2800 Powder Mill Road Adelphi, MD 20783-1197				<b>10. SPONSOR/MONITOR'S ACRONYM(S)</b>	
				<b>11. SPONSOR/MONITOR'S REPORT NUMBER(S)</b>	
<b>12. DISTRIBUTION/AVAILABILITY STATEMENT</b> Approved for public release; distribution unlimited.					
<b>13. SUPPLEMENTARY NOTES</b>					
<b>14. ABSTRACT</b> This report presents a comprehensive review of the state of the art of direct-sequence communication systems. Although it is largely self-contained mathematically, the report presumes a thorough understanding of modern digital communications. To limit the report to approximately 200 pages, only the most vital aspects of the theory are emphasized, but the cited references provide many details and minor topics.					
<b>15. SUBJECT TERMS</b> Direct sequence, spread spectrum, code-division multiple access					
<b>16. SECURITY CLASSIFICATION OF:</b>			<b>17. LIMITATION OF ABSTRACT</b> UL	<b>18. NUMBER OF PAGES</b> 205	<b>19a. NAME OF RESPONSIBLE PERSON</b> Don Torrieri
<b>a. REPORT</b> Unclassified	<b>b. ABSTRACT</b> Unclassified	<b>c. THIS PAGE</b> Unclassified			<b>19b. TELEPHONE NUMBER (Include area code)</b> (301) 394-2484

# Contents

<b>Preface</b>	<b>xii</b>
<b>1. Definitions and Concepts</b>	<b>1</b>
<b>2. Spreading Sequences and Waveforms</b>	<b>4</b>
2.1 Random Binary Sequence . . . . .	4
2.2 Shift-Register Sequences . . . . .	6
2.3 Periodic Autocorrelations . . . . .	11
2.4 Polynomials over the Binary Field . . . . .	15
2.5 Long Nonlinear Sequences . . . . .	19
<b>3. Systems with Coherent PSK and Random Spreading Sequences</b>	<b>23</b>
3.1 Tone Interference at Carrier Frequency . . . . .	26
3.2 General Tone Interference . . . . .	27
3.3 Gaussian Interference . . . . .	31
<b>4. Quaternary Systems with Random Spreading Sequences</b>	<b>32</b>
<b>5. Pulsed Interference</b>	<b>38</b>
<b>6. Despreading with Matched Filters</b>	<b>47</b>
6.1 Matched Filters . . . . .	48
6.2 Noncoherent Systems . . . . .	52
6.3 Multipath-Resistant Coherent System . . . . .	56
<b>7. Code Synchronization</b>	<b>60</b>

7.1	Acquisition with Matched Filter . . . . .	63
7.2	Serial-Search Acquisition . . . . .	64
7.3	Acquisition Correlator . . . . .	80
7.4	Code Tracking . . . . .	88
<b>8.</b>	<b>Rejection of Narrowband Interference</b>	<b>93</b>
8.1	Time-Domain Adaptive Filtering . . . . .	94
8.2	Transform-Domain Processing . . . . .	97
8.3	Nonlinear Filtering . . . . .	99
<b>9.</b>	<b>Detection of Direct-Sequence Signals</b>	<b>105</b>
9.1	Ideal Detection . . . . .	106
9.2	Wideband Radiometer . . . . .	109
<b>10.</b>	<b>Direct-Sequence Code-Division Multiple Access</b>	<b>116</b>
10.1	Orthogonal Sequences . . . . .	117
10.2	Sequences with Small Cross-Correlations . . . . .	119
10.3	Symbol Error Probability for Direct-Sequence Systems . . . . .	124
10.4	Complex-Valued Quaternary Sequences . . . . .	125
10.5	Direct-Sequence Systems with PSK and Random Sequences . . . . .	129
10.6	Quadrature Direct-Sequence Systems with Random Sequences . . . . .	137
10.7	Wideband Direct-Sequence CDMA . . . . .	140
10.8	Cellular Networks and Power Control . . . . .	149
<b>11.</b>	<b>Multiuser Detectors</b>	<b>152</b>
11.1	Optimum Detectors . . . . .	153

11.2	Decorrelating detector . . . . .	156
11.3	MMSE Detector . . . . .	160
11.4	Interference Cancellers . . . . .	162
11.5	Successive Interference Canceller . . . . .	162
11.6	Parallel Interference Canceller . . . . .	163
<b>Appendices</b>		<b>165</b>
<b>A. Inequalities</b>		<b>165</b>
A.1	Jensen's Inequality . . . . .	165
A.2	Chebyshev's Inequality . . . . .	166
<b>B. Probability Distributions</b>		<b>169</b>
B.1	Chi-Square Distribution . . . . .	169
B.2	Central Chi-Square Distribution . . . . .	171
B.3	Rice Distribution . . . . .	171
B.4	Rayleigh Distribution . . . . .	173
B.5	Sum of Independent, Exponentially Distributed Random Variables . . . . .	174
<b>C. Signal Representations</b>		<b>177</b>
C.1	Bandpass Signals . . . . .	177
C.2	Stationary Stochastic Processes . . . . .	179
C.3	Sampling Theorems . . . . .	185
<b>D. Adaptive Filters</b>		<b>189</b>
<b>References</b>		<b>192</b>

---

**List of Figures**

1	Examples of (a) data modulation and (b) spreading waveform . . . . .	2
2	Functional block diagram of direct-sequence systemn with PSK or DPSK: (a) transmitter and (b) receiver . . . . .	3
3	Spectra of desired signal and interference: (a) wideband-filter output and (b) demodulator input . . . . .	3
4	Sample function of a random binary sequence . . . . .	4
5	General feedback shift register with $m$ stages . . . . .	6
6	(a) Three-stage linear feedback shift register and (b) contents after successive shifts . . . . .	7
7	Linear feedback shift register: (a) standard representation and (b) high-speed form . . . . .	9
8	(a) Nonmaximal linear feedback shift register and (b) state diagrams . . . .	12
9	Autocorrelations of maximal sequence and random binary sequence . . . . .	14
10	Power spectral density of maximal sequence . . . . .	14
11	Linear generator of binary sequence with period $N$ . . . . .	21
12	(a) Nonlinear generator and (b) its linear equivalent . . . . .	22
13	Nonlinear generator that uses a multiplexer . . . . .	23
14	Basic elements of correlator for direct-sequence signal with coherent PSK . .	24
15	Symbol error probability of binary direct-sequence system with tone interference at carrier frequency and $G = 17$ dB . . . . .	30
16	Symbol error probability for direct-sequence system with PSK, rectangular and sinusoidal chip waveforms, $G = 17$ dB, $\mathcal{E}_s/N_0 = 14$ dB, and $GS/I = 10$ dB in the presence of tone interference . . . . .	30

17	Receiver for direct-sequence signal with dual quaternary modulation; CMF = chip-matched filter; SSG = spreading sequence generator. Delay = 0 for QPSK; delay = $T_c/2$ for OQPSK and MSK . . . . .	33
18	Symbol error probability for quaternary and binary direct-sequence systems with $G = 17$ dB, $\mathcal{E}_s/N_0 = 14$ dB, and $GS/I = 10$ dB in the presence of tone interference . . . . .	35
19	Receiver for direct-sequence signal with balanced quaternary modulation (delay = 0 for QPSK and delay = $T_c/2$ for OQPSK and MSK); CMF = chip-matched filter; SSG = spreading sequence generator . . . . .	36
20	Symbol error probability for direct-sequence systems with balanced QPSK and dual quaternary modulations, rectangular and sinusoidal chip waveforms, $G = 17$ dB, $\mathcal{E}_s/N_0 = 14$ dB, and $GS/I = 10$ dB in the presence of tone interference . . . . .	38
21	Worst-case performance against pulsed interference for convolutional codes of constraint length $K$ , rate $r$ , $\mathcal{E}_b/N_0 = 20$ dB, and hard decisions . . . . .	41
22	Worst-case performance against pulsed interference for convolutional codes of constraint length $K$ , rate $r$ , $\mathcal{E}_b/N_0 = 20$ dB and maximum-likelihood (ML) and AGC metrics . . . . .	43
23	Performance against pulsed interference for convolutional code with white-noise metric, and $K = 7$ , $r = 1/2$ , and $\mathcal{E}_b/N_0 = 20$ dB . . . . .	45
24	Performance against pulsed interference for convolutional code with erasures, $K = 7$ , $r = 1/2$ , and $\mathcal{E}_b/N_0 = 20$ dB . . . . .	46
25	Worst-case performance against pulsed interference for convolutional codes with ideal erasure decoding, constraint length $K$ , rate $r$ , and $\mathcal{E}_b/N_0 = 20$ dB . . . . .	47
26	Matched filter that uses a SAW transversal filter . . . . .	50
27	SAW elastic convolver . . . . .	51
28	Chip configurations within convolver at time instants $t = 4T_c, 5T_c$ , and $6T_c$ when $t_0 = 0$ , $L/v = T_c$ , and $T = 4T_c$ . . . . .	53
29	Direct-sequence system with binary code-shift keying: (a) transmitter and (b) receiver . . . . .	53
30	Receiver for direct-sequence system with differential phase-shift keying . . . . .	56

31	Recirculation loop . . . . .	57
32	Coherent decision-directed demodulator . . . . .	59
33	Conceptual waveforms of demodulator: (a) matched-filter output, (b) recirculation loop input or output, and (c) baseband integrator input . . . . .	60
34	Digital matched filter . . . . .	64
35	Configuration of a serial-search acquisition system enabled by a matched filter	65
36	Serial-search acquisition system . . . . .	66
37	Flow graph of multiple-dwell system with consecutive-count strategy . . . . .	67
38	Flow graph of multiple-dwell system with up-down strategy . . . . .	67
39	Trajectories of search positions: (a) uniform search and (b) broken-center $Z$ search . . . . .	67
40	Trajectories of expanding-window search positions: (a) broken-center and (b) continuous-center search . . . . .	75
41	Trajectories of alternating search positions: (a) uniform search and (b) nonuniform search . . . . .	75
42	Circular state diagram for serial-search acquisition . . . . .	77
43	Subsidiary state diagram for determination of $H_0(z)$ for consecutive-count double-dwell system . . . . .	78
44	Subsidiary state diagram for calculation of $H_D(z)$ and $H_M(z)$ for consecutive-count double-dwell system with two-state collective state . . . . .	79
45	Noncoherent correlator for acquisition system. CMF = chip matched filter. SSG = spreading sequence generator . . . . .	81
46	NMAT versus $\mathcal{E}_c/N_0$ for single-dwell system in presence of fast Rayleigh fading or no fading. Values of $P_f$ and $M$ are optimized . . . . .	86
47	NMAT versus $\mathcal{E}_c/N_0$ for double-dwell systems in presence of fast Rayleigh fading. Step size is $\Delta = 1/2$ . Values of $P_{F1}$ , $P_{F2}$ , $M_1$ , and $M_2$ are optimized (brackets) appears on the contents list . . . . .	87
48	Delay-locked loop . . . . .	89

49	Discriminator characteristic of delay-locked loop for $\delta = 1/2$ . . . . .	91
50	Tau-dither loop . . . . .	92
51	Direct-sequence receiver with processor for rejecting narrowband interference	94
52	(a) Processor using adaptive filter and (b) two-sided adaptive transversal filter	95
53	Processor with decision-directed adaptive filter . . . . .	96
54	Transform-domain processor . . . . .	97
55	Adaptive ACM filter . . . . .	104
56	Radiometers: (a) passband, (b) baseband with integration, and (c) baseband with sampling at rate $1/W$ and summation . . . . .	110
57	Probability of detection versus $\mathcal{E}/N_0$ for wideband radiometer with $P_F = 10^{-3}$ and various values of $TW$ . Solid curves are the $\hat{N}_0 = N_0$ ; dashed curve is for $\hat{N}_0 = 1.001N_0$ . . . . .	114
58	Energy-to-noise-density ratio versus $TW$ for wideband radiometer with $P_D = 0.99$ and various values of $P_F$ and $h$ . . . . .	116
59	Gold sequence generator . . . . .	122
60	(a) Feedback shift register for a quaternary sequence and (b) contents after successive shifts . . . . .	127
61	Product of quaternary data and spreading sequences . . . . .	128
62	Receiver for direct-sequence system with complex quaternary spreading sequences. CMF is chip-matched filter . . . . .	129
63	Symbol error probability of direct-sequence system with PSK in presence of single multiple-access interference signal and $\mathcal{E}_s/N_0 = 15$ dB . . . . .	135
64	Symbol error probability of direct-sequence system with PSK in presence of $K - 1$ equal-power multiple-access interference signals and $\mathcal{E}_s/N_0 = 15$ dB . . . . .	135
65	Symbol error probability of direct-sequence system with PSK in presence of 3 equal-power multiple-access interference signals and $\mathcal{E}_s/N_0 = 15$ dB . . . . .	137
66	Symbol error probability of quadriphase direct-sequence system in presence of 3 equal-power multiple-access interference signals and $\mathcal{E}_s/N_0 = 15$ dB . . . . .	139

67	Multicarrier direct-sequence CDMA system: (a) transmitter and (b) receiver	142
68	Symbol error probability for multicarrier systems with $L$ carriers . . . . .	145
69	Symbol error probability for single-carrier systems and $L \leq 4$ multipath components with different multipath intensity vectors . . . . .	147
70	Information-bit error probability for multicarrier system with $L = 32$ and for single-carrier systems with $\Gamma_1 = (.505, .495, 0)$ and $\Gamma_2 = (.995, .990, 0)$ . Error-correcting code is BCH(63, 36) . . . . .	149
71	Geometry of cellular network with base station at center of each hexagon. Two concentric tiers of cells surrounding a central cell are shown . . . . .	150
72	Architecture of decorrelating detector and MMSE detector. Filter bank comprises parallel correlators . . . . .	156
73	Successive interference canceller with $K$ detector-generators to produce signal estimates for subtraction . . . . .	161
74	Structure of detector-generator for signal $i$ . . . . .	162
75	Second canceller of multistage canceller using successive interference cancellers	163
76	Parallel interference canceller for two signals . . . . .	163
77	Multistage parallel interference canceller for two signals. $D$ =delay . . . . .	163

---

## List of Tables

1	Primitive Polynomials . . . . .	20
---	---------------------------------	----

---

## Preface

---

This report presents a comprehensive review of the state of the art of direct-sequence communication systems. Although it is largely self-contained mathematically, the report presumes a thorough understanding of modern digital communications. To limit the report to approximately 200 pages, only the most vital aspects of the theory are emphasized, but the cited references provide many details and minor topics. Sections 1 and 2 cover the basic definitions and concepts and the fundamental properties of spreading sequences. Sections 3 and 4 derive the symbol error probabilities of coherent systems in the presence of tone or Gaussian interference. Methods of suppressing pulsed interference are analyzed in Section 5. In Section 6, the role of matched filters in direct-sequence systems is examined. Code synchronization, which is the most significant issue in the design of direct-sequence systems, is analyzed in Section 7. Several supplementary methods of rejecting narrowband interference are presented in Section 8. The detection of the existence of a direct-sequence signal by both an ideal receiver and the more practical wideband radiometer are analyzed in Section 9. Section 10 explains and develops the theory of direct-sequence code-division multiple access, which is the dominant technology of third and fourth generation cellular mobile communications. Multiuser detectors, which have current and potential applications in cellular receivers, are discussed in Section 11. The four appendices provide extensive derivations of mathematical results that are used in the main text.

---

## 1. Definitions and Concepts

---

A *spread-spectrum signal* is a signal that has an extra modulation that expands the signal bandwidth beyond what is required by the underlying data modulation. Spread-spectrum communication systems [1], [2], [3] are useful for suppressing interference, making interception difficult, accommodating fading and multipath channels, and providing a multiple-access capability. The most practical and dominant methods of spread-spectrum communications are direct-sequence modulation and frequency hopping of digital communications.

A *direct-sequence signal* is a spread-spectrum signal generated by the direct mixing of the data with a spreading waveform before the final carrier modulation. Ideally, a direct-sequence signal with binary phase-shift keying (PSK) or differential PSK (DPSK) data modulation can be represented by

$$s(t) = Ad(t)p(t) \cos(2\pi f_c t + \theta) \quad (1-1)$$

where  $A$  is the signal amplitude,  $d(t)$  is the data modulation,  $p(t)$  is the spreading waveform,  $f_c$  is the carrier frequency, and  $\theta$  is the phase at  $t = 0$ . The data modulation is a sequence of nonoverlapping rectangular pulses of duration  $T_s$ , each of which has an amplitude  $d_i = +1$  if the associated data symbol is a 1 and  $d_i = -1$  if it is a 0. Equation (1-1) implies that  $s(t) = Ap(t)\cos[2\pi f_c t + \theta + \pi d(t)]$ , which explicitly exhibits the phase-shift keying by the data modulation. The *spreading waveform* has the form

$$p(t) = \sum_{i=-\infty}^{\infty} p_i \psi(t - iT_c) \quad (1-2)$$

where each  $p_i$  equals  $+1$  or  $-1$  and represents one *chip* of the *spreading sequence*. The *chip waveform*  $\psi(t)$  is ideally confined to the interval  $[0, T_c]$  to prevent interchip interference in the receiver. A rectangular chip waveform has  $\psi(t) = w(t, T_c)$ , where

$$w(t, T) = \begin{cases} 1, & 0 \leq t < T \\ 0, & \text{otherwise} \end{cases} \quad (1-3)$$

Figure 1 depicts an example of  $d(t)$  and  $p(t)$  for a rectangular chip waveform.

*Message privacy* is provided by a direct-sequence system if a transmitted message cannot be recovered without knowledge of the spreading sequence. To ensure message privacy, which is assumed henceforth, the data-symbol transitions must coincide with the chip transitions. Since the transitions coincide, the *processing gain*  $G = T_s/T_c$  is an integer equal to the number of chips in a symbol interval. If  $W$  is the bandwidth of  $p(t)$  and  $B$  is the bandwidth of  $d(t)$ , the spreading due to  $p(t)$  ensures that  $s(t)$  has a bandwidth  $W \gg B$ .

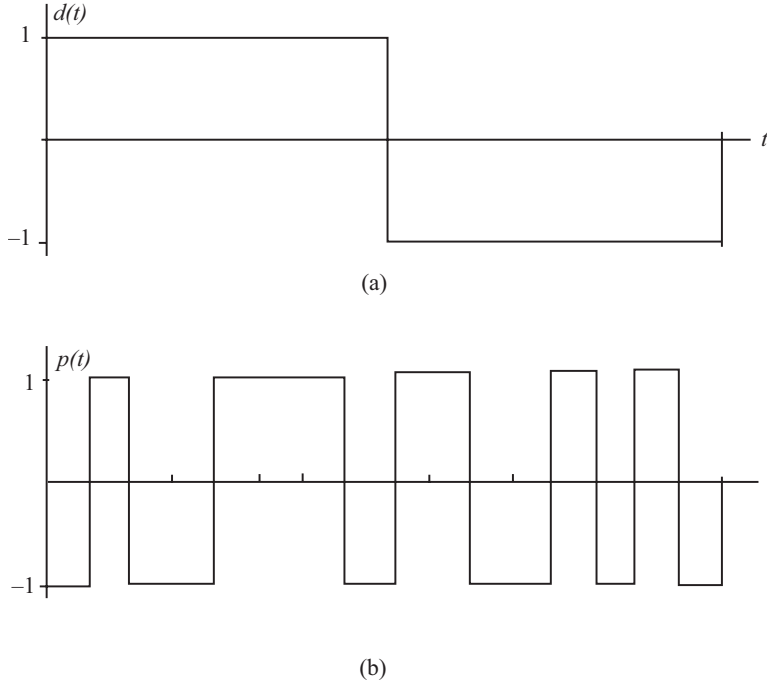


Figure 1. Examples of (a) data modulation and (b) spreading waveform.

Figure 2 is a functional or conceptual block diagram of the basic operation of a direct-sequence system with PSK. To provide message privacy, data symbols and chips, which are represented by digital sequences of 0's and 1's, are synchronized by the same clock and then modulo-2 added in the transmitter. The adder output is converted according to  $0 \rightarrow -1$  and  $1 \rightarrow +1$  before the chip and carrier modulations. Assuming that chip and symbol synchronization has been established, the received signal passes through the wideband filter and is multiplied by a synchronized local replica of  $p(t)$ . If  $\psi(t)$  is rectangular, then  $p(t) = \pm 1$  and  $p^2(t) = 1$ . Therefore, if the filtered signal is given by (1-1), the multiplication yields the *despread signal*

$$s_1(t) = p(t)s(t) = Ad(t) \cos(2\pi f_c t + \theta) \quad (1-4)$$

at the input of the PSK demodulator. Since the despread signal is a PSK signal, a standard coherent demodulator extracts the data symbols.

Figure 3(a) is a qualitative depiction of the relative spectra of the desired signal and narrowband interference at the output of the wideband filter. Multiplication by the spreading waveform produces the spectra of Figure 3(b) at the demodulator input. The signal bandwidth is reduced to  $B$ , while the interference energy is spread over a bandwidth exceeding  $W$ . Since the filtering action of the demodulator then removes most of the interference spectrum that does not overlap the signal spectrum, most of the original interference energy is eliminated. An approximate measure of the interference rejection capability is given by the ratio  $W/B$ . Whatever the precise definition of a bandwidth,  $W$

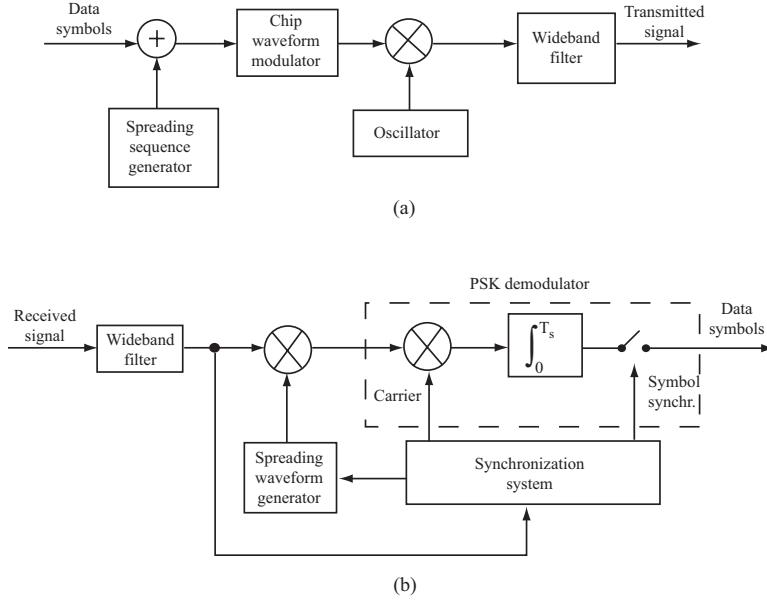


Figure 2. Functional block diagram of direct-sequence system with PSK or DPSK: (a) transmitter and (b) receiver.

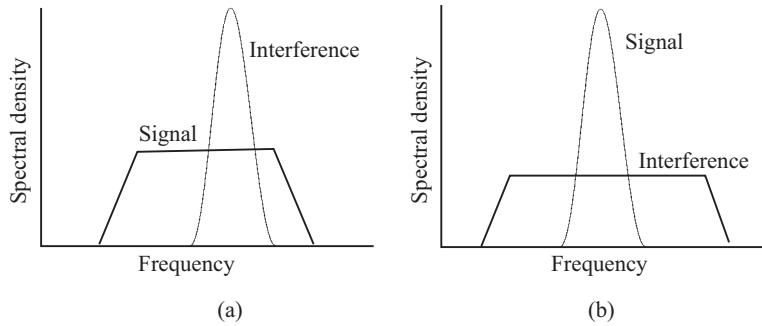


Figure 3. Spectra of desired signal and interference: (a) wideband-filter output and (b) demodulator input.

and  $B$  are proportional to  $1/T_c$  and  $1/T_s$ , respectively, with the same proportionality constant. Therefore,

$$G = \frac{T_s}{T_c} = \frac{W}{B} \tag{1-5}$$

which links the processing gain with the interference rejection illustrated in the figure. Since its spectrum is unchanged by the despreading, white Gaussian noise is not suppressed by a direct-sequence system.

In practical systems, the wideband filter in the transmitter is used to limit the out-of-band radiation. This filter and the propagation channel disperse the chip waveform so that it is no longer confined to  $[0, T_c]$ . To avoid interchip interference in the receiver, the filter might be designed to generate a pulse that satisfies the Nyquist criterion for no intersymbol

interference. A convenient representation of a direct-sequence signal when the chip waveform may extend beyond  $[0, T_c]$  is

$$s(t) = A \sum_{i=-\infty}^{\infty} d_{\lfloor i/G \rfloor} p_i \psi(t - iT_c) \cos(2\pi f_c t + \theta) \quad (1-6)$$

where  $\lfloor x \rfloor$  denotes the integer part of  $x$ . When the chip waveform is assumed to be confined to  $[0, T_c]$ , then (1-6) can be expressed by (1-1) and (1-2).

## 2. Spreading Sequences and Waveforms

### 2.1 Random Binary Sequence

A *random binary sequence*  $x(t)$  is a stochastic process that consists of independent, identically distributed symbols, each of duration  $T$ . Each symbol takes the value  $+1$  with probability  $1/2$  or the value  $-1$  with probability  $1/2$ . Therefore,  $E[x(t)] = 0$  for all  $t$ , where  $E[\ ]$  denotes the expected value, and

$$P[x(t) = i] = 1/2, \quad i = +1, -1 \quad (2-1)$$

where  $P[A]$  denotes the probability of event  $A$ . The process is wide-sense stationary if the location of the first symbol transition or start of a new symbol after  $t = 0$  is a random variable uniformly distributed over the half-open interval  $(0, T]$ . A sample function of a *wide-sense-stationary random binary sequence*  $x(t)$  is illustrated in Figure 4.

The *autocorrelation* of a stochastic process  $x(t)$  is defined as

$$R_x(t, \tau) = E[x(t)x(t + \tau)] \quad (2-2)$$

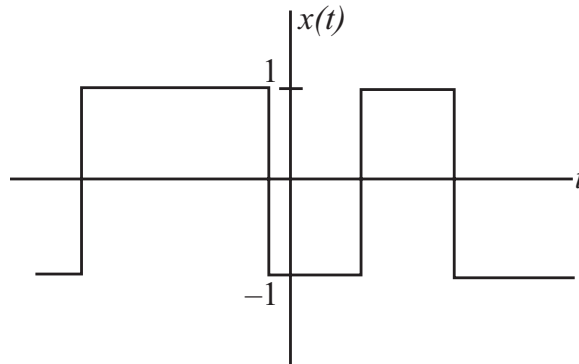


Figure 4. Sample function of a random binary sequence.

If  $x(t)$  is a wide-sense stationary process, then  $R_x(t, \tau)$  is a function of  $\tau$  alone, and the autocorrelation is denoted by  $R_x(\tau)$ . From the theorem of total probability, the definition of a conditional probability, and (2-1), it follows that the autocorrelation of a random binary sequence is

$$\begin{aligned} R_x(t, \tau) &= \frac{1}{2}P[x(t + \tau) = 1|x(t) = 1] - \frac{1}{2}P[x(t + \tau) = -1|x(t) = 1] \\ &\quad + \frac{1}{2}P[x(t + \tau) = -1|x(t) = -1] - \frac{1}{2}P[x(t + \tau) = 1|x(t) = -1] \end{aligned} \quad (2-3)$$

where  $P[A|B]$  denotes the conditional probability of event  $A$  given the occurrence of event  $B$ . From the theorem of total probability, it follows that

$$\begin{aligned} P[x(t + \tau) = i|x(t) = i] + P[x(t + \tau) = -i|x(t) = i] &= 1, \\ i &= +1, -1 \end{aligned} \quad (2-4)$$

Since both of the following probabilities are equal to the probability that  $x(t)$  and  $x(t + \tau)$  differ,

$$P[x(t + \tau) = 1|x(t) = -1] = P[x(t + \tau) = -1|x(t) = 1] \quad (2-5)$$

Substitution of (2-4) and (2-5) into (2-3) yields

$$R_x(t, \tau) = 1 - 2P[x(t + \tau) = 1|x(t) = -1] \quad (2-6)$$

If  $|\tau| \geq T$ , then  $x(t)$  and  $x(t + \tau)$  are independent random variables because  $t$  and  $t + \tau$  are in different symbol intervals. Therefore,

$$P[x(t + \tau) = 1|x(t) = -1] = P[x(t + \tau) = 1] = 1/2$$

and (2-6) implies that  $R_x(t, \tau) = 0$  for  $|\tau| \geq T$ . Further simplification is possible for a stationary random binary sequence. If  $|\tau| < T$ , then  $x(t)$  and  $x(t + \tau)$  are independent only if a symbol transition occurs in the half-open interval  $I_0 = (t, t + \tau]$ . Consider any half-open interval  $I_1$  of length  $T$  that includes  $I_0$ . Exactly one transition occurs in  $I_1$ . Since the first transition for  $t > 0$  is assumed to be uniformly distributed over  $(0, T]$ , the probability that a transition in  $I_1$  occurs in  $I_0$  is  $|\tau|/T$ . If a transition occurs in  $I_0$ , then  $x(t)$  and  $x(t + \tau)$  are independent and differ with probability  $1/2$ ; otherwise,  $x(t) = x(t + \tau)$ . Consequently,  $P[x(t + \tau) = 1|x(t) = -1] = |\tau|/2T$  if  $|\tau| < T$ . Substitution of the preceding results into (2-6) gives the *autocorrelation of the stationary random binary sequence*:

$$R_x(t, \tau) = R_x(\tau) = \Lambda\left(\frac{\tau}{T}\right) \quad (2-7)$$

where the *triangular function* is defined by

$$\Lambda(t) = \begin{cases} 1 - |t|, & |t| \leq 1 \\ 0, & |t| > 1 \end{cases} \quad (2-8)$$

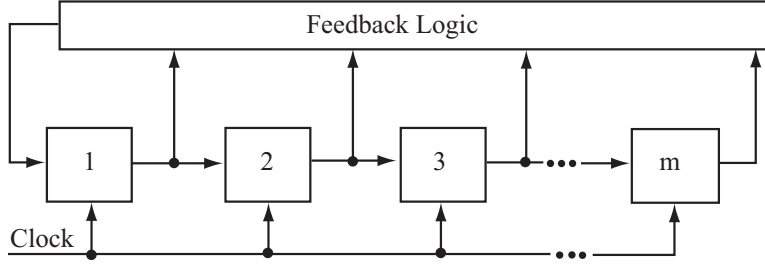


Figure 5. General feedback shift register with  $m$  stages.

## 2.2 Shift-Register Sequences

Ideally, one would prefer a random binary sequence as the spreading sequence. However, practical synchronization requirements in the receiver force one to use periodic binary sequences. A *shift-register sequence* is a periodic binary sequence generated by combining the outputs of feedback shift registers. A *feedback shift register*, which is diagrammed in Figure 5, consists of consecutive two-state memory or storage stages and feedback logic. Binary sequences drawn from the alphabet  $\{0,1\}$  are shifted through the shift register in response to clock pulses. The *content* of each stage is identical to its output. The contents of the stages are logically combined to produce the input to the first stage. The initial contents of the stages and the feedback logic determine the successive contents of the stages. A feedback shift register and its output are called *linear* when the feedback logic consists entirely of modulo-2 adders (exclusive-OR gates). Figure 6(a) illustrates a linear feedback shift register with three stages and an output sequence extracted from the final stage. The input to the first stage is the modulo-2 sum of the contents of the second and third stages. After each clock pulse, the contents of the first two stages are shifted to the right, and the input to the first stage becomes its content. If the initial contents of the shift-register stages are 0 0 1, the subsequent contents after successive shifts are listed in Figure 6(b). Since the shift register returns to its initial state after 7 shifts, the periodic output sequence extracted from the final stage has a period of 7 bits.

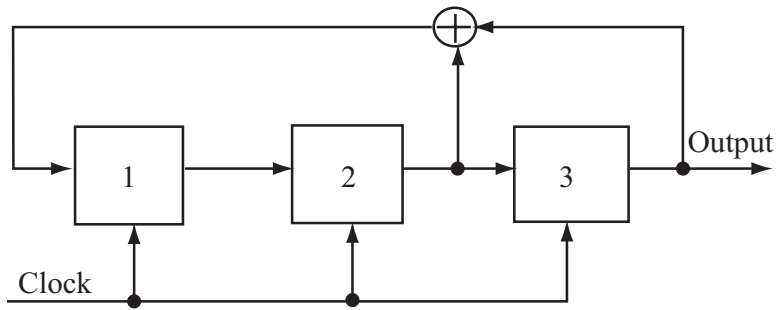
Let  $s_j(i)$  denote the content of stage  $j$  after clock pulse  $i$ . The *state* of the shift register after clock pulse  $i$  is the vector

$$\mathbf{S}(i) = [s_1(i) \ s_2(i) \ \dots \ s_m(i)], \quad i \geq 0 \quad (2-9)$$

where  $\mathbf{S}(0)$  is the initial state. The *zero state* is the state for which all the contents are 0's. From the definition of a shift register, it follows that

$$s_j(i) = s_{j-k}(i-k), \quad i \geq k \geq 0, \quad k \leq j \leq m \quad (2-10)$$

where  $s_0(i)$  denotes the input to stage 1 after clock pulse  $i$ . If  $a_i$  denotes the state of bit  $i$  of the output sequence, then  $a_i = s_m(i)$ . The state of a feedback shift register uniquely



(a)

Shift	Contents		
	Stage 1	Stage 2	Stage 3
Initial	0	0	1
1	1	0	0
2	0	1	0
3	1	0	1
4	1	1	0
5	1	1	1
6	0	1	1
7	0	0	1

(b)

Figure 6. (a) Three-stage linear feedback shift register and (b) contents after successive shifts.

determines the subsequent sequence of states and the output sequence. The period  $N$  of a periodic sequence  $\{a_i\}$  is defined as the smallest positive integer for which  $a_{i+N} = a_i, i \geq 0$ . Since the number of distinct states of an  $m$ -stage shift register is  $2^m$ , the sequence of states and the output sequence have period  $N \leq 2^m$ .

The *Galois field* of two elements, which is denoted by  $GF(2)$ , consists of the symbols 0 and 1 and the operations of modulo-2 addition and modulo-2 multiplication. These binary operations are defined by

$$\begin{aligned} 0 \oplus 0 &= 0, & 0 \oplus 1 &= 1, & 1 \oplus 0 &= 1, & 1 \oplus 1 &= 0 \\ 0 \cdot 0 &= 0, & 0 \cdot 1 &= 0, & 1 \cdot 0 &= 0, & 1 \cdot 1 &= 1 \end{aligned} \quad (2-11)$$

where  $\oplus$  denotes modulo-2 addition. From these equations, it is easy to verify that the field is closed under both modulo-2 addition and modulo-2 multiplication and that both operations are *associative* and *commutative*. Since  $-1$  is defined as that element which when added to 1 yields 0, we have  $-1 = 1$ , and subtraction is the same as addition. From (2-11), it follows that the additive identity element is 0, the multiplicative identity is 1, and the multiplicative inverse of 1 is  $1^{-1} = 1$ . The substitutions of all possible symbol combinations verify the *distributive laws*:

$$a(b \oplus c) = ab \oplus ac, \quad (b \oplus c)a = ba \oplus ca \quad (2-12)$$

where  $a, b$ , and  $c$  can each equal 0 or 1. The equality of subtraction and addition implies that if  $a \oplus b = c$ , then  $a = b \oplus c$ .

The input to stage 1 of a linear feedback shift register is

$$s_0(i) = \sum_{k=1}^m c_k s_k(i), \quad i \geq 0 \quad (2-13)$$

where the operations are modulo-2 and the feedback coefficient  $c_k$  equals either 0 or 1, depending on whether the output of stage  $k$  feeds a modulo-2 adder. An  $m$ -stage shift register is defined to have  $c_m = 1$ ; otherwise, the final state would not contribute to the generation of the output sequence, but would only provide a one-shift delay. For example, Figure 6 gives  $c_1 = 0, c_2 = c_3 = 1$ , and  $s_0(i) = s_2(i) \oplus s_3(i)$ . A general representation of a linear feedback shift register is shown in Figure 7(a). If  $c_k = 1$ , the corresponding switch is closed; if  $c_k = 0$ , it is open.

Since the output bit  $a_i = s_m(i)$ , (2-10) and (2-13) imply that for  $i \geq m$ ,

$$a_i = s_0(i - m) = \sum_{l=1}^m c_l s_l(i - m) = \sum_{l=1}^m c_l s_m(i - l)$$

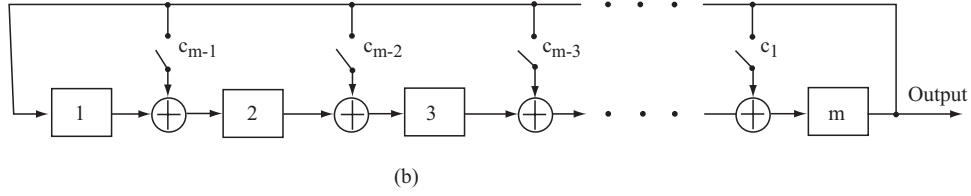
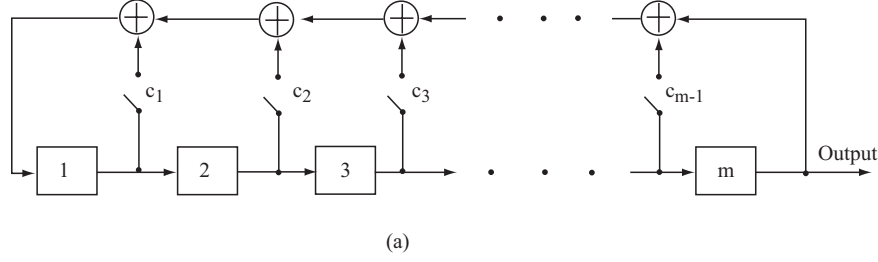


Figure 7. Linear feedback shift register: (a) standard representation and (b) high-speed form.

which indicates that each output bit satisfies the *linear recurrence relation*:

$$a_i = \sum_{k=1}^m c_k a_{i-k}, \quad i \geq m \quad (2-14)$$

The first  $m$  output bits are determined solely by the initial state:

$$a_i = s_{m-i}(0), \quad 0 \leq i \leq m-1 \quad (2-15)$$

Figure 7(a) is not necessarily the best way to implement the feedback shift register that produces the sequence satisfying (2-14). Figure 7(b) illustrates an implementation that allows higher-speed operation. From this diagram, it follows that

$$s_j(i) = s_{j-1}(i-1) \oplus c_{m-j+1} s_m(i-1), \quad i \geq 1, \quad 2 \leq j \leq m \quad (2-16)$$

$$s_1(i) = s_m(i-1) \quad i \geq 1 \quad (2-17)$$

Repeated application of (2-16) implies that

$$\begin{aligned} s_m(i) &= s_{m-1}(i-1) \oplus c_1 s_m(i-1), \quad i \geq 1 \\ s_{m-1}(i-1) &= s_{m-2}(i-2) \oplus c_2 s_m(i-2), \quad i \geq 2 \\ &\vdots \\ s_2(i-m+2) &= s_1(i-m+1) \oplus c_{m-1} s_m(i-m+1), \quad i \geq m-1 \end{aligned} \quad (2-18)$$

Addition of these  $m$  equations yields

$$s_m(i) = s_1(i-m+1) \oplus \sum_{k=1}^{m-1} c_k s_m(i-k), \quad i \geq m-1 \quad (2-19)$$

Substituting (2-17) and then  $a_i = s_m(i)$  into (2-19), we obtain

$$a_i = a_{i-m} \oplus \sum_{k=1}^{m-1} c_k a_{i-k}, \quad i \geq m \quad (2-20)$$

Since  $c_m = 1$ , (2-20) is the same as (2-14). Thus, the two implementations can produce the same output sequence indefinitely if the first  $m$  output bits coincide. However, they require different initial states and have different sequences of states. Successive substitutions into the first equation of sequence (2-18) yields

$$s_m(i) = s_{m-i}(0) \oplus \sum_{k=1}^i c_k s_m(i-k), \quad 1 \leq i \leq m-1 \quad (2-21)$$

Substituting  $a_i = s_m(i)$ ,  $a_{i-k} = s_m(i-k)$ , and  $j = m-i$  into (2-21) and then using binary arithmetic, we obtain

$$s_j(0) = a_{m-j} \oplus \sum_{k=1}^{m-j} c_k a_{m-j-k}, \quad 1 \leq j \leq m \quad (2-22)$$

If  $a_0, a_1, \dots, a_{m-1}$  are specified, then (2-22) gives the corresponding initial state of the high-speed shift register.

The sum of binary sequence  $\mathbf{a} = (a_0, a_1, \dots)$  and binary sequence  $\mathbf{b} = (b_0, b_1, \dots)$  is defined to be the binary sequence  $\mathbf{a} \oplus \mathbf{b}$ , each bit of which is the modulo-2 sum of the corresponding bits of  $\mathbf{a}$  and  $\mathbf{b}$ . Thus, if  $\mathbf{d} = \mathbf{a} \oplus \mathbf{b}$  we can write

$$d_i = a_i \oplus b_i, \quad i \geq 0 \quad (2-23)$$

Suppose that  $\mathbf{a}$  and  $\mathbf{b}$  are generated by the same linear feedback shift register, but may differ because the initial states may be different. For the sequence  $\mathbf{d} = \mathbf{a} \oplus \mathbf{b}$ , (2-23) and the associative and distributive laws of binary fields imply that

$$\begin{aligned} d_i &= \sum_{k=1}^m c_k a_{i-k} \oplus \sum_{k=1}^m c_k b_{i-k} = \sum_{k=1}^m (c_k a_{i-k} \oplus c_k b_{i-k}) \\ &= \sum_{k=1}^m c_k (a_{i-k} \oplus b_{i-k}) = \sum_{k=1}^m c_k d_{i-k} \end{aligned} \quad (2-24)$$

Since the linear recurrence relation is identical,  $\mathbf{d}$  can be generated by the same linear feedback logic as  $\mathbf{a}$  and  $\mathbf{b}$ . Thus, if  $\mathbf{a}$  and  $\mathbf{b}$  are two output sequences of a linear feedback shift register, then  $\mathbf{a} \oplus \mathbf{b}$  is also. If  $\mathbf{a} = \mathbf{b}$ , then  $\mathbf{a} \oplus \mathbf{b}$  is the sequence of all 0's, which can be generated by any linear feedback shift register.

If a linear feedback shift register reached the zero state at some time, it would always remain in the zero state, and the output sequence would subsequently be all 0's. Since a

linear  $m$ -stage feedback shift register has exactly  $2^m - 1$  nonzero states, the period of its output sequence cannot exceed  $2^m - 1$ . A sequence of period  $2^m - 1$  generated by a linear feedback shift register is called a *maximal* or *maximal-length sequence*. If a linear feedback shift register generates a maximal sequence, then all of its nonzero output sequences are maximal, regardless of the initial states.

Out of  $2^m$  possible states, the content of the last stage, which is the same as the output bit, is a 0 in  $2^{m-1}$  states. Among the nonzero states, the output bit is a 0 in  $2^{m-1} - 1$  states. Therefore, in one period of a maximal sequence, the number of 0's is exactly  $2^{m-1} - 1$ , while the number of 1's is exactly  $2^{m-1}$ .

Given the binary sequence  $\mathbf{a}$ , let  $\mathbf{a}(j) = (a_j, a_{j+1}, \dots)$  denote a shifted binary sequence. If  $\mathbf{a}$  is a maximal sequence and  $j \neq 0$ , modulo  $2^m - 1$ , then  $\mathbf{a} \oplus \mathbf{a}(j)$  is not the sequence of all 0's. Because it is generated by the same shift register as  $\mathbf{a}$ ,  $\mathbf{a} \oplus \mathbf{a}(j)$  must be a maximal sequence and, hence, some cyclic shift of  $\mathbf{a}$ . We conclude that the modulo-2 sum of a maximal sequence and a cyclic shift of itself by  $j$  digits, where  $j \neq 0$ , modulo  $2^m - 1$ , produces another cyclic shift of the original sequence. This property is succinctly written as

$$\mathbf{a} \oplus \mathbf{a}(j) = \mathbf{a}(k), \quad j \neq 0 \text{ (modulo } 2^m - 1) \quad (2-25)$$

In contrast, a non-maximal linear sequence  $\mathbf{a} \oplus \mathbf{a}(j)$  is not necessarily a cyclic shift of  $\mathbf{a}$  and may not even have the same period. As an example, consider the linear feedback shift register depicted in Figure 8. The possible state transitions depend on the initial state. Thus, if the initial state is 0 1 0, then the first state diagram indicates that there are four possible states and, hence, the output sequence has a period of four. The output sequence is  $\mathbf{a} = (0, 1, 0, 1, 0, 1, \dots)$ , which implies that  $\mathbf{a}(1) = (1, 0, 1, 0, 1, 0, \dots)$  and  $\mathbf{a} \oplus \mathbf{a}(1) = (1, 1, 1, 1, 1, 1, \dots)$ ; this result indicates that (2-25) is not satisfied for any  $k$ .

### 2.3 Periodic Autocorrelations

A binary sequence  $\mathbf{a}$  with components  $a_i \in GF(2)$ , can be mapped into a binary antipodal sequence  $\mathbf{p}$  with components  $p_i \in \{-1, +1\}$  by means of the transformation

$$p_i = (-1)^{a_i+1}, \quad i \geq 0 \quad (2-26)$$

or, alternatively,  $p_i = (-1)^{a_i}$ . The *periodic autocorrelation* of a periodic binary sequence  $\mathbf{a}$  with period  $N$  is defined as

$$\theta_p(j) = \frac{1}{N} \sum_{i=0}^{N-1} p_i p_{i+j} \quad (2-27)$$

Substitution of (2-26) into (2-27) yields

$$\theta_p(j) = \frac{1}{N} \sum_{i=0}^{N-1} (-1)^{a_i+a_{i+j}} = \frac{1}{N} \sum_{i=0}^{N-1} (-1)^{a_i \oplus a_{i+j}} = \frac{A_j - D_j}{N} \quad (2-28)$$

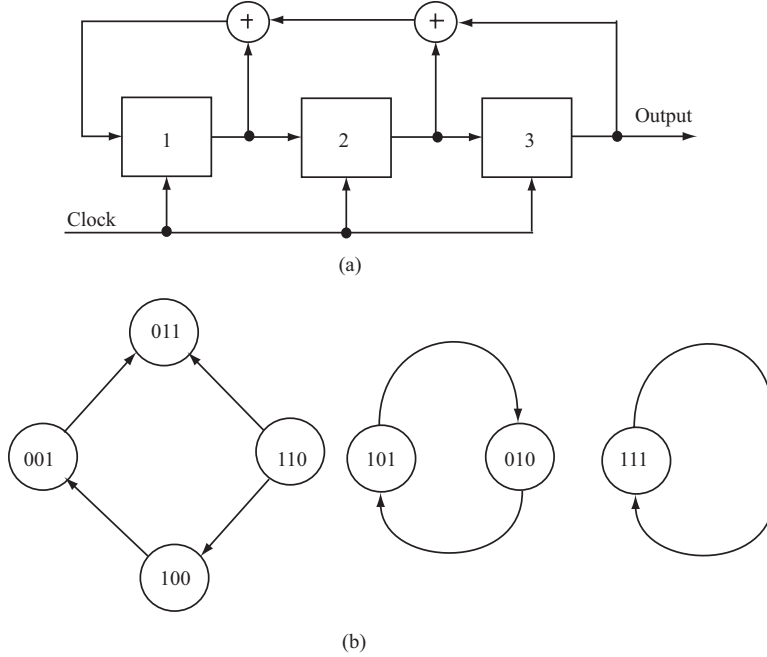


Figure 8. (a) Nonmaximal linear feedback shift register and (b) state diagrams.

where  $A_j$  denotes the number of agreements in the corresponding bits of  $\mathbf{a}$  and  $\mathbf{a}(j)$ , and  $D_j$  denotes the number of disagreements. Equivalently,  $A_j$  is the number of 0's in one period of  $\mathbf{a} \oplus \mathbf{a}(j)$ , and  $D_j = N - A_j$  is the number of 1's.

Consider a maximal sequence. From (2-25), it follows that  $A_j$  equals the number of 0's in a maximal sequence if  $j \neq 0$ , modulo  $N$ . Thus,  $A_j = (N - 1)/2$  and, similarly,  $D_j = (N + 1)/2$  if  $j \neq 0$ , modulo  $N$ . Therefore,

$$\theta_p(j) = \begin{cases} 1, & j = 0(\text{mod } N) \\ -\frac{1}{N}, & j \neq 0(\text{mod } N) \end{cases} \quad (2-29)$$

The *periodic autocorrelation* of a periodic function  $x(t)$  with period  $T$  is defined as

$$R_x(\tau) = \frac{1}{T} \int_c^{c+T} x(t)x(t + \tau)dt \quad (2-30)$$

where  $\tau$  is the relative delay variable and  $c$  is an arbitrary constant. It follows that  $R_x(\tau)$  has period  $T$ . We derive the periodic autocorrelation of  $p(t)$  assuming an ideal periodic spreading waveform of infinite extent and a rectangular chip waveform. If the spreading sequence has period  $N$ , then  $p(t)$  has period  $T = NT_c$ . Equations (1-2) and (2-30) with  $c = 0$  yield the autocorrelation of  $p(t)$ :

$$R_p(\tau) = \frac{1}{NT_c} \sum_{i=0}^{N-1} p_i \sum_{l=0}^{N-1} p_l \int_0^{NT_c} \psi(t - iT_c)\psi(t - lT_c + \tau) dt \quad (2-31)$$

If  $\tau = jT_c$ , where  $j$  is an integer, then  $\psi(t) = w(t, T_c)$ , (1-3), and (2-31) yield

$$R_p(jT_c) = \frac{1}{N} \sum_{i=0}^{N-1} p_i p_{i+j} = \theta_p(j) \quad (2-32)$$

Any delay can be expressed in the form  $\tau = jT_c + \epsilon$ , where  $j$  is an integer and  $0 \leq \epsilon < T_c$ . Therefore, (2-31) and  $\psi(t) = w(t, T_c)$  give

$$\begin{aligned} R_p(jT_c + \epsilon) &= \frac{1}{NT_c} \sum_{i=0}^{N-1} p_i p_{i+j} \int_0^{NT_c} w(t - iT_c, T_c) w(t - iT_c + \epsilon, T_c) dt \\ &\quad + \frac{1}{NT_c} \sum_{i=0}^{N-1} p_i p_{i+j+1} \int_0^{NT_c} w(t - iT_c, T_c) w(t - iT_c + \epsilon - T_c, T_c) dt \end{aligned} \quad (2-33)$$

Using (2-32) and (1-3) in (2-33), we obtain

$$R_p(jT_c + \epsilon) = \left(1 - \frac{\epsilon}{T_c}\right) \theta_p(j) + \frac{\epsilon}{T_c} \theta_p(j+1) \quad (2-34)$$

For a maximal sequence, the substitution of (2-29) into (2-34) yields  $R_p(\tau)$  over one period:

$$R_p(\tau) = \frac{N+1}{N} \Lambda\left(\frac{\tau}{T_c}\right) - \frac{1}{N}, \quad |\tau| \leq NT_c/2 \quad (2-35)$$

where  $\Lambda()$  is the triangular function defined by (2-8). Since it has period  $NT_c$ , the autocorrelation can be compactly expressed as

$$R_p(\tau) = -\frac{1}{N} + \frac{N+1}{N} \sum_{i=-\infty}^{\infty} \Lambda\left(\frac{\tau - iNT_c}{T_c}\right) \quad (2-36)$$

Over one period, this autocorrelation resembles that of a random binary sequence, which is given by (2-7) with  $T = T_c$ . Both autocorrelations are shown in Figure 9.

A straightforward calculation or the use of tables gives the Fourier transform of the triangular function:

$$\begin{aligned} \mathcal{F} \left\{ \Lambda\left(\frac{t}{T}\right) \right\} &= \int_{-\infty}^{\infty} \Lambda\left(\frac{t}{T}\right) \exp(-j2\pi ft) dt \\ &= T \text{sinc}^2 fT \end{aligned} \quad (2-37)$$

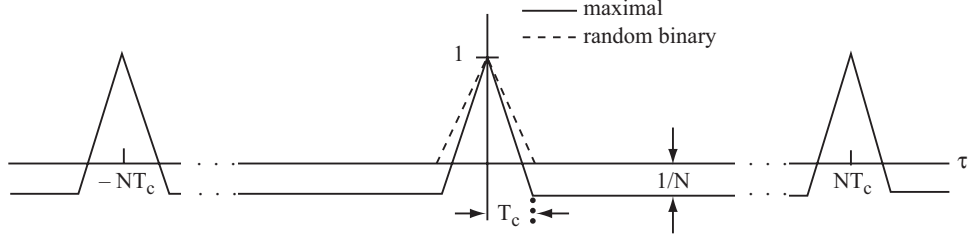


Figure 9. Autocorrelations of maximal sequence and random binary sequence.

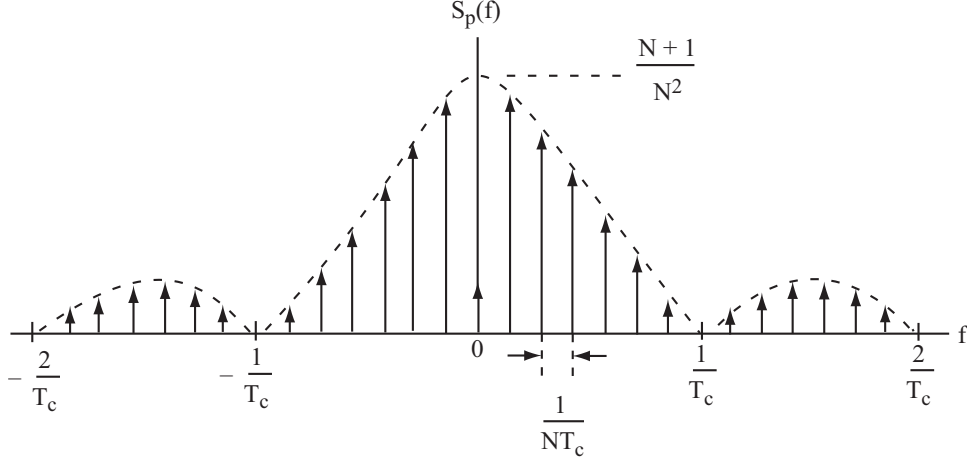


Figure 10. Power spectral density of maximal sequence.

where  $j = \sqrt{-1}$  and  $\text{sinc } x = (\sin \pi x)/\pi x$ . Since the infinite series in (2-36) is a periodic function of  $\tau$ , it can be expressed as a complex exponential Fourier series. From (2-37) and the fact that the Fourier transform of a complex exponential is a delta function, we obtain

$$\mathcal{F} \left\{ \sum_{i=-\infty}^{\infty} \Lambda \left( \frac{t - iNT_c}{T_c} \right) \right\} = \frac{1}{N} \sum_{i=-\infty}^{\infty} \text{sinc}^2 \left( \frac{i}{N} \right) \delta \left( f - \frac{i}{NT_c} \right) \quad (2-38)$$

where  $\delta(\cdot)$  is the Dirac delta function. Applying this identity to (2-36), we determine  $S_p(f)$ , the *power spectral density* of  $p(t)$ , which is defined as the Fourier transform of  $R_p(\tau)$ :

$$S_p(f) = \frac{N+1}{N^2} \sum_{\substack{i=-\infty \\ i \neq 0}}^{\infty} \text{sinc}^2 \left( \frac{i}{N} \right) \delta \left( f - \frac{i}{NT_c} \right) + \frac{1}{N^2} \delta(f) \quad (2-39)$$

This function, which consists of an infinite series of delta functions, is sketched in Figure 10.

A *pseudonoise* or *pseudorandom sequence* is a periodic binary sequence with a nearly even balance of 0's and 1's and an autocorrelation that roughly resembles, over one period, the autocorrelation of a random binary sequence. Pseudonoise sequences provide practical spreading sequences because their autocorrelations facilitate code synchronization in the receiver (Section 7). Other sequences have peaks that hinder synchronization.

To derive the power spectral density of a direct-sequence signal with a periodic spreading sequence, it is necessary to define the *average autocorrelation* of  $x(t)$ :

$$\bar{R}_x(\tau) = \lim_{T \rightarrow \infty} \frac{1}{2T} \int_{-T}^T R_x(t, \tau) dt \quad (2-40)$$

The limit exists and may be nonzero if  $x(t)$  has finite power and infinite duration. If  $x(t)$  is stationary,  $\bar{R}_x(\tau) = R_x(\tau)$ . The *average power spectral density*  $\bar{S}_x(f)$  is defined as the Fourier transform of the average autocorrelation.

For the direct-sequence signal of (1-1),  $d(t)$  is modeled as a random binary sequence with autocorrelation given by (2-7), and  $\theta$  is modeled as a random variable uniformly distributed over  $[0, 2\pi)$  and statistically independent of  $d(t)$ . Neglecting the constraint that the bit transitions must coincide with chip transitions, we obtain the autocorrelation of the direct-sequence signal  $s(t)$ :

$$R_s(t, \tau) = \frac{A^2}{2} p(t)p(t + \tau) \Lambda\left(\frac{\tau}{T_s}\right) \cos 2\pi f_c \tau \quad (2-41)$$

where  $p(t)$  is the periodic spreading waveform. Substituting this equation into (2-40) and using (2-30), we obtain

$$\bar{R}_s(\tau) = \frac{A^2}{2} R_p(\tau) \Lambda\left(\frac{\tau}{T_s}\right) \cos 2\pi f_c \tau \quad (2-42)$$

where  $R_p(\tau)$  is the periodic autocorrelation of  $p(t)$ . For a maximal spreading sequence, the convolution theorem, (2-42), (2-37), and (2-39) provide the average power spectral density of  $s(t)$ :

$$\bar{S}_s(f) = \frac{A^2}{4} [S_{s1}(f - f_c) + S_{s1}(f + f_c)] \quad (2-43)$$

where the lowpass equivalent density is

$$S_{s1}(f) = \frac{T_s}{N^2} \text{sinc}^2 f T_s + \frac{N+1}{N^2} T_s \sum_{\substack{i=-\infty \\ i \neq 0}}^{\infty} \text{sinc}^2\left(\frac{i}{N}\right) \text{sinc}^2\left(f T_s - \frac{i T_s}{N T_c}\right) \quad (2-44)$$

For a random binary sequence,  $S_s(f) = \bar{S}_s(f)$  is given by (2-43) with  $S_{s1}(f) = T_c \text{sinc}^2 f T_c$ .

## 2.4 Polynomials over the Binary Field

Polynomials allow a compact description of the dependence of the output sequence of a linear feedback shift register on its feedback coefficients and initial state. A *polynomial* over the binary field  $GF(2)$  has the form

$$f(x) = f_0 + f_1 x + f_2 x^2 + \cdots + f_n x^n \quad (2-45)$$

where the coefficients  $f_0, f_1, \dots, f_n$  are elements of  $GF(2)$  and the symbol  $x$  is an indeterminate introduced for convenience in calculations. The *degree* of a polynomial is the largest power of  $x$  with a nonzero coefficient. The *sum* of two polynomials,  $f(x)$  and  $g(x)$ , over  $GF(2)$  is another polynomial over  $GF(2)$  defined as

$$f(x) + g(x) = \sum_{i=0}^{\max(n_1, n_2)} (f_i \oplus g_i) x^i \quad (2-46)$$

where the addition of the coefficients is modulo 2,  $n_1$  is the degree of  $f(x)$ ,  $n_2$  is the degree of  $g(x)$ , and  $\max(n_1, n_2)$  denotes the larger of  $n_1$  and  $n_2$ . For example,

$$(1 + x^2 + x^3) + (1 + x^2 + x^4) = x^3 + x^4 \quad (2-47)$$

The *product* of two polynomials over  $GF(2)$  is another polynomial over  $GF(2)$  defined as

$$f(x)g(x) = \sum_{i=0}^{n_1+n_2} \left( \sum_{j=0}^i f_j g_{i-j} \right) x^i \quad (2-48)$$

where the inner addition is modulo 2. For example,

$$(1 + x^2 + x^3)(1 + x^2 + x^4) = 1 + x^3 + x^5 + x^6 + x^7 \quad (2-49)$$

It is easily verified that associative, commutative, and distributive laws apply to polynomial addition and multiplication.

The *characteristic polynomial* associated with a linear feedback shift register of  $m$  stages is defined as

$$f(x) = 1 + \sum_{i=1}^m c_i x^i \quad (2-50)$$

where  $c_m = 1$  assuming that stage  $m$  contributes to the generation of the output sequence. The *generating function* associated with the output sequence is defined as

$$G(x) = \sum_{i=0}^{\infty} a_i x^i \quad (2-51)$$

Substitution of (2-14) into this equation yields

$$\begin{aligned} G(x) &= \sum_{i=0}^{m-1} a_i x^i + \sum_{i=m}^{\infty} \sum_{k=1}^m c_k a_{i-k} x^i \\ &= \sum_{i=0}^{m-1} a_i x^i + \sum_{k=1}^m c_k x^k \sum_{i=m}^{\infty} a_{i-k} x^{i-k} \\ &= \sum_{i=0}^{m-1} a_i x^i + \sum_{k=1}^m c_k x^k \left[ G(x) + \sum_{i=0}^{m-k-1} a_i x^i \right] \end{aligned} \quad (2-52)$$

Combining this equation with (2-50), and defining  $c_0 = 1$ , we obtain

$$\begin{aligned}
G(x)f(x) &= \sum_{i=0}^{m-1} a_i x^i + \sum_{k=1}^m c_k x^k \left( \sum_{i=0}^{m-k-1} a_i x^i \right) \\
&= \sum_{k=0}^{m-1} c_k x^k \left( \sum_{i=0}^{m-k-1} a_i x^i \right) = \sum_{k=0}^{m-1} \sum_{i=0}^{m-k-1} c_k a_i x^{k+i} \\
&= \sum_{k=0}^{m-1} \sum_{j=k}^{m-1} c_k a_{j-k} x^j = \sum_{j=0}^{m-1} \sum_{k=0}^j c_k a_{j-k} x^j
\end{aligned} \tag{2-53}$$

Therefore,

$$G(x) = \frac{\sum_{i=0}^{m-1} x^i \left( \sum_{k=0}^i c_k a_{i-k} \right)}{f(x)}, \quad c_0 = 1 \tag{2-54}$$

Thus, the generating function of the output sequence generated by a linear feedback shift register with characteristic polynomial  $f(x)$  may be expressed in the form  $G(x) = \phi(x)/f(x)$ , where the degree of  $\phi(x)$  is less than the degree of  $f(x)$ . The output sequence is said to be *generated* by  $f(x)$ . Equation (2-54) explicitly shows that the output sequence is completely determined by the feedback coefficients  $c_k, k = 1, 2, \dots, m$ , and the initial state  $a_i = s_{m-i}(0), i = 0, 1, \dots, m - 1$ .

In Figure 6, the feedback coefficients are  $c_1 = 0, c_2 = 1$ , and  $c_3 = 1$ , and the initial state gives  $a_0 = 1, a_1 = 0$ , and  $a_2 = 0$ . Therefore,

$$G(x) = \frac{1 + x^2}{1 + x^2 + x^3} \tag{2-55}$$

Performing the long polynomial division according to the rules of binary arithmetic yields  $1 + x^3 + x^5 + x^6 + x^7 + x^{10} + \dots$ , which implies the output sequence listed in the figure.

The polynomial  $p(x)$  is said to *divide* the polynomial  $b(x)$  if there is a polynomial  $h(x)$  such that  $b(x) = h(x)p(x)$ . A polynomial  $p(x)$  over  $GF(2)$  of degree  $m$  is called *irreducible* if  $p(x)$  is not divisible by any polynomial over  $GF(2)$  of degree less than  $m$  but greater than zero. If  $p(x)$  is irreducible over  $GF(2)$ , then  $p(0) \neq 0$ , for otherwise  $x$  would divide  $p(x)$ . If  $p(x)$  has an even number of terms, then  $p(1) = 0$  and the fundamental theorem of algebra implies that  $x + 1$  divides  $p(x)$ . Therefore, an irreducible polynomial over  $GF(2)$  must have an odd number of terms, but this condition is not sufficient for irreducibility. For example,  $1 + x + x^2$  is irreducible, but  $1 + x + x^5 = (1 + x^2 + x^3)(1 + x + x^2)$  is not.

If a shift-register sequence  $\{a_i\}$  is periodic with period  $n$ , then its generating function  $G(x) = \phi(x)/f(x)$  may be expressed as

$$\begin{aligned}
G(x) &= g(x) + x^n g(x) + x^{2n} g(x) + \cdots \\
&= g(x) \sum_{i=0}^{\infty} x^{in} \\
&= \frac{g(x)}{1 + x^n}
\end{aligned} \tag{2-56}$$

where  $g(x)$  is a polynomial of degree  $n - 1$ . Therefore,

$$g(x) = \frac{\phi(x)(1 + x^n)}{f(x)}$$

Suppose that  $f(x)$  and  $\phi(x)$  have no common factors, which is true if  $f(x)$  is irreducible since  $\phi(x)$  is of lower degree than  $f(x)$ . Then  $f(x)$  must divide  $1 + x^n$ . Conversely, if the characteristic polynomial  $f(x)$  divides  $1 + x^n$ , then  $f(x)h(x) = 1 + x^n$  for some polynomial  $h(x)$ , and

$$G(x) = \frac{\phi(x)}{f(x)} = \frac{\phi(x)h(x)}{1 + x^n}$$

which has the form of (2-56). Thus,  $f(x)$  generates a sequence of period  $n$  for all  $\phi(x)$  and, hence, all initial states.

A polynomial over  $GF(2)$  of degree  $m$  is called *primitive* if the smallest positive integer  $n$  for which the polynomial divides  $1 + x^n$  is  $n = 2^m - 1$ . Thus, a primitive characteristic polynomial of degree  $m$  can generate a sequence of period  $2^m - 1$ , which is the period of a maximal sequence generated by a characteristic polynomial of degree  $m$ . Suppose that a primitive characteristic polynomial of positive degree  $m$  could be factored so that  $f(x) = f_1(x)f_2(x)$ , where  $f_1(x)$  is of positive degree  $m_1$  and  $f_2(x)$  is of positive degree  $m - m_1$ . A partial-fraction expansion yields

$$\frac{1}{f(x)} = \frac{a(x)}{f_1(x)} + \frac{b(x)}{f_2(x)}$$

Since  $f_1(x)$  and  $f_2(x)$  can serve as characteristic polynomials, the period of the first term in the expansion cannot exceed  $2^{m_1} - 1$  while the period of the second term cannot exceed  $2^{m-m_1} - 1$ . Therefore, the period of  $1/f(x)$  cannot exceed  $(2^{m_1} - 1)(2^{m-m_1} - 1) \leq 2^m - 3$ , which contradicts the assumption that  $f(x)$  is primitive. Thus, a *primitive characteristic polynomial must be irreducible*.

**Theorem.** *A characteristic polynomial of degree  $m$  generates a maximal sequence of period  $2^m - 1$  if and only if it is a primitive polynomial.*

**Proof.** To prove sufficiency, we observe that if  $f(x)$  is a primitive characteristic polynomial, it divides  $1 + x^n$  for  $n = 2^m - 1$  so a maximal sequence of period  $2^m - 1$  is

generated. If a sequence of smaller period could be generated, then the irreducible  $f(x)$  would have to divide  $1 + x^{n_1}$  for  $n_1 < n$ , which contradicts the assumption of a primitive polynomial. To prove necessity, we observe that if the characteristic polynomial  $f(x)$  generates a maximal sequence with period  $n = 2^m - 1$ , then  $f(x)$  cannot divide  $1 + x^{n_1}$ ,  $n_1 < n$ , because a sequence with a smaller period would result, and such a sequence cannot be generated by a maximal sequence generator. Since  $f(x)$  does divide  $1 + x^n$ , it must be a primitive polynomial.  $\square$

Primitive polynomials are difficult to find, but many have been tabulated (e.g., [4]). Those for which  $m \leq 7$  and one of those of minimal coefficient weight for  $8 \leq m \leq 25$  are listed in Table 1 as octal numbers in increasing order (e.g.,  $51 \leftrightarrow 1\ 0\ 1\ 1\ 0\ 0 \leftrightarrow 1 + x^2 + x^3$ ). For any positive integer  $m$ , the number of different primitive polynomials of degree  $m$  over  $GF(2)$  is

$$\lambda(m) = \frac{\phi_e(2^m - 1)}{m} \quad (2-57)$$

where the *Euler function*  $\phi_e(n)$  is the number of positive integers that are less than and relatively prime to the positive integer  $n$ . If  $n$  is a prime number,  $\phi_e(n) = n - 1$ . In general,

$$\phi_e(n) = n \prod_{i=1}^k \frac{\nu_i - 1}{\nu_i} \leq n - 1 \quad (2-58)$$

where  $\nu_1, \nu_2, \dots, \nu_k$  are the prime integers that divide  $n$ . Thus,  $\lambda(6) = \phi_e(63)/6 = 6$  and  $\lambda(13) = \phi_e(8191)/13 = 630$ .

## 2.5 Long Nonlinear Sequences

A *long sequence* or *long code* is a spreading sequence with a period that is much longer than the data-symbol duration and may even exceed the message duration. A *short sequence* or *short code* is a spreading sequence with a period that is equal to or less than the data-symbol duration. Since short sequences are susceptible to interception and long linear sequences are inherently susceptible to mathematical cryptanalysis [1], long nonlinear pseudonoise sequences and programmable code generators are needed for communications with a high level of security. However, if a modest level of security is acceptable, short or moderate-length pseudonoise sequences are preferable for rapid acquisition, burst communications, and multiuser detection.

The algebraic structure of linear feedback shift registers makes them susceptible to cryptanalysis. Let

$$\mathbf{c} = [c_1\ c_2\ \dots\ c_m]^T \quad (2-59)$$

denote the column vector of the  $m$  feedback coefficients of an  $m$ -stage linear feedback shift register, where  $T$  denotes the transpose. The column vector of  $m$  successive sequence bits

Table 1. Primitive Polynomials.

Degree	Primitive	Degree	Primitive	Degree	Primitive
2	7	7	103	8	534
3	51		122	9	1201
	31		163	10	1102
4	13		112	11	5004
	32		172	12	32101
5	15		543	13	33002
	54		523	14	30214
	57		532	15	300001
	37		573	16	310012
	76		302	17	110004
	75		323	18	1020001
6	141		313	19	7400002
	551		352	20	1100004
	301		742	21	50000001
	361		763	22	30000002
	331		712	23	14000004
	741		753	24	702000001
			772	25	110000002

produced by the shift register starting at bit  $i$  is

$$\mathbf{a}_i = [a_i \ a_{i+1} \ \dots \ a_{i+m-1}]^T, \quad (2-60)$$

Let  $\mathbf{A}(i)$  denote the  $m \times m$  matrix with columns consisting of the  $\mathbf{a}_j$  vectors for  $i \leq j \leq i + m - 1$ :

$$\mathbf{A}(i) = \begin{bmatrix} a_{i+m-1} & a_{i+m-2} & \cdots & a_i \\ a_{i+m} & a_{i+m-1} & \cdots & a_{i+1} \\ \vdots & \vdots & & \vdots \\ a_{i+2m-2} & a_{i+2m-3} & \cdots & a_{i+m-1} \end{bmatrix} \quad (2-61)$$

The linear recurrence relation (2-14) indicates that the output sequence and feedback coefficients are related by

$$\mathbf{a}_{i+m} = \mathbf{A}(i)\mathbf{c}, \quad i \geq 0 \quad (2-62)$$

If  $2m$  consecutive sequence bits are known, then  $\mathbf{A}(i)$  and  $\mathbf{a}_{i+n}$  are completely known for some  $i$ . If  $\mathbf{A}(i)$  is invertible, then the feedback coefficients are derived from

$$\mathbf{c} = \mathbf{A}^{-1}(i)\mathbf{a}_{i+m}, \quad i \geq 0 \quad (2-63)$$

The output sequence of a shift register is completely determined by the feedback coefficients and any state vector. Since any  $m$  successive sequence bits determine a state

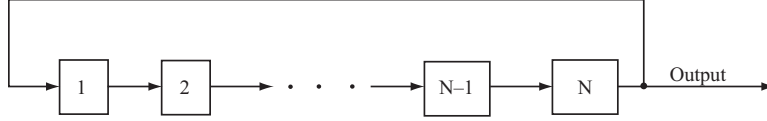


Figure 11. Linear generator of binary sequence with period  $N$ .

vector,  $2m$  successive bits provide enough information to reproduce the output sequence unless  $\mathbf{A}(i)$  is not invertible. In that case, a few more bits are needed.

If a binary sequence has period  $N$ , it can always be generated by a  $N$ -stage linear feedback shift register by connecting the output of the last stage to the input of the first stage and inserting  $N$  consecutive bits of the sequence into the output sequence, as illustrated in Figure 11. The polynomial associated with one period of the binary sequence is

$$g(x) = \sum_{i=0}^{N-1} a_i x^i \quad (2-64)$$

Let  $\gcd(g(x), 1 + x^N)$  denote the greatest common polynomial divisor of the polynomials  $g(x)$  and  $1 + x^N$ . Then (2-56) implies that the generating function of the sequence may be expressed as

$$G(x) = \frac{g(x)/\gcd(g(x), 1 + x^N)}{(1 + x^N)/\gcd(g(x), 1 + x^N)} \quad (2-65)$$

If  $\gcd(g(x), 1 + x^N) \neq 1$ , the degree of the denominator of  $G(x)$  is less than  $N$ . Therefore, the sequence represented by  $G(x)$  can be generated by a linear feedback shift register with fewer stages than  $N$  and with the characteristic function given by the denominator. The appropriate initial state can be determined from the coefficients of the numerator.

The *linear equivalent* of the generator of a sequence is the linear shift register with the fewest stages that produces the sequence. The number of stages in the linear equivalent is called the *linear complexity* of the sequence. If the linear complexity is equal to  $m$ , then (2-63) determines the linear equivalent after the observation of  $2m$  consecutive sequence bits. Security improves as the period of a sequence increases, but there are practical limits to the number of shift-register stages. To produce sequences with a long enough period for high security, the feedback logic in Figure 5 often must be nonlinear. Alternatively, one or more shift-register outputs or several outputs of shift-register stages may be applied to a nonlinear device to produce the sequence [5]. Nonlinear generators with relatively few shift-register stages can produce sequences of enormous linear complexity. As an example, Figure 12(a) depicts a nonlinear generator in which two stages of a linear feedback shift register have their outputs applied to an AND gate to produce the output sequence. The initial contents of the shift-register stages are indicated by the enclosed binary numbers. Since the linear generator produces a maximal sequence of length 7, the output sequence



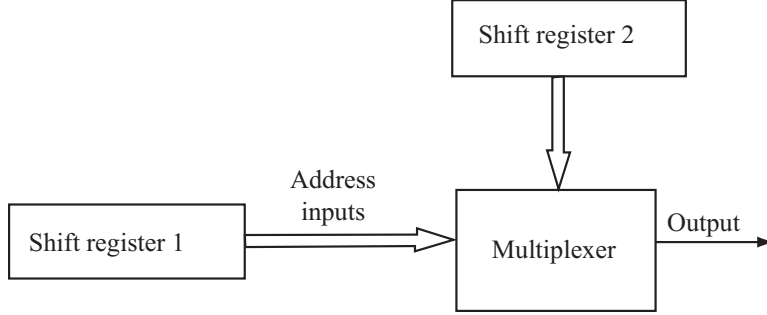


Figure 13. Nonlinear generator that uses a multiplexer.

---

### 3. Systems with Coherent PSK and Random Spreading Sequences

---

A received direct-sequence signal with PSK data modulation and ideal carrier synchronization can be represented by (1-1) or (1-6) with  $\theta = 0$  to reflect the absence of phase uncertainty. Assuming that the chip waveform is well approximated by a waveform  $\psi(t)$  of duration  $T_c$ , the received signal is

$$s(t) = \sqrt{2S}d(t)p(t) \cos 2\pi f_c t \quad (3-1)$$

where  $S$  is the average power,  $d(t)$  is the data modulation,  $p(t)$  is the spreading waveform, and  $f_c$  is the carrier frequency. The data modulation is a sequence of nonoverlapping rectangular pulses, each of which has an amplitude equal to  $+1$  or  $-1$ . Each pulse of  $d(t)$  represents a data symbol and has a duration of  $T_s$ . The spreading waveform has the form

$$p(t) = \sum_{i=-\infty}^{\infty} p_i \psi(t - iT_c) \quad (3-2)$$

where  $p_i$  is equal to  $+1$  or  $-1$  and represents one chip of a spreading sequence  $\{p_i\}$ . It is convenient, and entails no loss of generality, to normalize the energy content of the chip waveform according to

$$\frac{1}{T_c} \int_0^{T_c} \psi^2(t) dt = 1 \quad (3-3)$$

Because the transitions of a data symbol and the chips coincide on both sides of a symbol, the *processing gain*, defined as

$$G = \frac{T_s}{T_c} \quad (3-4)$$

is an integer equal to the number of chips in a symbol interval.

A practical direct-sequence system differs from the functional diagram of Figure 2. The transmitter needs practical devices, such as a power amplifier and a filter, to limit out-of-band radiation. In the receiver, the radio-frequency front end includes devices for wideband filtering and automatic gain control. These devices are assumed to have a negligible effect on the operation of the demodulator, at least for the purposes of this analysis. Thus, the front-end circuitry is omitted from Figure 14, which shows the optimum demodulator in the form of a correlator for the detection of a single symbol in the presence of white Gaussian noise. This correlator is more practical and flexible for digital processing than the alternative one shown in Figure 2. It is a suboptimal but reasonable approach against non-Gaussian interference. An equivalent matched-filter demodulator is implemented with a transversal filter or tapped delay line and a stored spreading sequence. However, the matched-filter implementation is not practical for a long sequence that extends over many data symbols. If the chip-rate synchronization in Figure 14 is accurate, then the demodulated sequence and the receiver-generated spreading sequence are multiplied together, and  $G$  successive products are added in an accumulator to produce the decision variable. The effective sampling rate of the decision variable is the symbol rate.

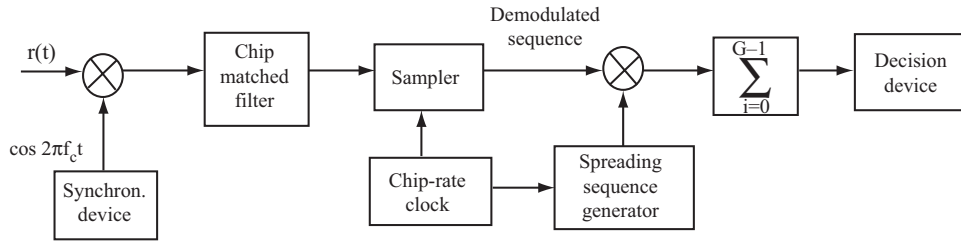


Figure 14. Basic elements of correlator for direct-sequence signal with coherent PSK.

The sequence generator, multiplier, and summer function as a discrete-time filter matched to the spreading sequence.

In the subsequent analysis, perfect phase, sequence, and symbol synchronization are assumed. The received signal is

$$r(t) = s(t) + i(t) + n(t) \quad (3-5)$$

where  $i(t)$  is the interference, and  $n(t)$  denotes the zero-mean white Gaussian noise. The chip matched filter has impulse response  $\psi(-t)$ . Its output is sampled at the chip rate to provide  $G$  samples per data symbol. If  $d(t) = d_0$  over  $[0, T_s]$ , then (3-1) to (3-5) indicate that the demodulated sequence corresponding to this data symbol is

$$Z_i = \int_{iT_c}^{(i+1)T_c} r(t)\psi(t - iT_c) \cos 2\pi f_c t dt = S_i + J_i + N_i, \quad 0 \leq i \leq G - 1 \quad (3-6)$$

where

$$S_i = \int_{iT_c}^{(i+1)T_c} s(t)\psi(t - iT_c) \cos 2\pi f_c t dt = p_i d_0 \sqrt{\frac{S}{2}} T_c \quad (3-7)$$

$$J_i = \int_{iT_c}^{(i+1)T_c} i(t)\psi(t - iT_c) \cos 2\pi f_c t dt \quad (3-8)$$

$$N_i = \int_{iT_c}^{(i+1)T_c} n(t)\psi(t - iT_c) \cos 2\pi f_c t dt \quad (3-9)$$

and it is assumed that  $f_c \gg 1/T_c$  so that the integral over a double-frequency term in (3-7) is negligible. The input to the decision device is

$$V = \sum_{i=0}^{G-1} p_i Z_i = d_0 \sqrt{\frac{S}{2}} T_s + V_1 + V_2 \quad (3-10)$$

where

$$V_1 = \sum_{\nu=0}^{G-1} p_\nu J_\nu \quad (3-11)$$

$$V_2 = \sum_{\nu=0}^{G-1} p_\nu N_\nu \quad (3-12)$$

Suppose that  $d_0 = +1$  represents the logic symbol 1 and  $d_0 = -1$  represents the logic symbol 0. The decision device produces the symbol 1 if  $V > 0$  and the symbol 0 if  $V < 0$ . An error occurs if  $V < 0$  when  $d_0 = +1$  or if  $V > 0$  when  $d_0 = -1$ . The probability that  $V = 0$  is zero.

The white Gaussian noise has autocorrelation

$$R_n(\tau) = \frac{N_0}{2} \delta(t - \tau) \quad (3-13)$$

where  $N_0/2$  is the two-sided noise power spectral density. Since  $E[n(t)] = 0$ , (3-12) implies that  $E[V_2] = 0$ . A straightforward calculation using (3-9), (3-12), (3-13), the limited duration of  $\psi(t)$ , and  $f_c \gg 1/T_c$  yields

$$\text{var}(V_2) = \frac{1}{4} N_0 T_s \quad (3-14)$$

It is natural and analytically desirable to model a long spreading sequence as a random binary sequence. The random-binary-sequence model does not seem to obscure important exploitable characteristics of long sequences and is a reasonable approximation even for short sequences in networks with asynchronous communications. A random binary sequence consists of statistically independent symbols, each of which takes the value +1 with probability  $\frac{1}{2}$  or the value -1 with probability  $\frac{1}{2}$ . Thus,  $E[p_i] = E[p(t)] = 0$ . It then follows from (3-10) to (3-12) that  $E[V_1] = E[V_2] = 0$ , and the mean value of the decision variable is

$$E[V] = d_0 \sqrt{\frac{S}{2}} T_s \quad (3-15)$$

for the direct-sequence system with coherent PSK. Since  $p_i$  and  $p_j$  are independent for  $i \neq j$ ;

$$E[p_i p_j] = 0, \quad i \neq j \quad (3-16)$$

Therefore, the independence of  $p_i$  and  $J_j$  for all  $i$  and  $j$  implies that  $E[p_i J_i p_j J_j] = 0, i \neq j$ , and hence

$$\text{var}(V_1) = \sum_{i=0}^{G-1} E[J_i^2] \quad (3-17)$$

### 3.1 Tone Interference at Carrier Frequency

When tone interference has the same carrier frequency as the desired signal, a nearly exact, closed-form equation for the symbol error probability can be derived. The tone interference has the form

$$i(t) = \sqrt{2I} \cos(2\pi f_c t + \phi) \quad (3-18)$$

where  $I$  is the average power and  $\phi$  is the phase relative to the desired signal. Assuming that  $f_c \gg 1/T_c$ , (3-8), (3-11), (3-18) and a change of variables give

$$V_1 = \sqrt{\frac{I}{2}} \cos \phi \sum_{i=0}^{G-1} p_i \int_0^{T_c} \psi(t) dt \quad (3-19)$$

A rectangular chip waveform has  $\psi(t) = w(t, T_c)$ , which is given by (1-3). For sinusoidal pulses in the spreading waveform,  $\psi(t) = \psi_s(t, T_c)$ , where

$$\psi_s(t, T) = \begin{cases} \sqrt{2} \sin\left(\frac{\pi}{T}t\right), & 0 \leq t \leq T \\ 0, & \text{otherwise} \end{cases} \quad (3-20)$$

Let  $k_1$  denote the number of chips in  $[0, T_s]$  for which  $p_i = +1$ ; the number for which  $p_i = -1$  is  $G - k_1$ . Equations (3-19), (1-3), and (3-20) yield

$$V_1 = \sqrt{\frac{I\kappa}{2}} T_c (2k_1 - G) \cos \phi \quad (3-21)$$

where

$$\kappa = \begin{cases} 1, & \text{rectangular pulses} \\ \frac{8}{\pi^2}, & \text{sinusoidal pulses} \end{cases} \quad (3-22)$$

These equations indicate that the use of sinusoidal pulses instead of rectangular pulses effectively reduces the interference power by a factor  $8/\pi^2$  if  $V_1 \neq 0$ . Thus, the advantage of sinusoidal pulses is 0.91 dB against tone interference at the carrier frequency. Equation (3-21) indicates that tone interference at the carrier frequency would be completely rejected if  $k_1 = G/2$  in every symbol interval.

In the random-binary-sequence model,  $p_i$  is equally likely to be +1 or -1. Therefore, the conditional symbol error probability given the value of  $\phi$  is

$$P_s(\phi) = \sum_{k_1=0}^G \binom{G}{k_1} \left(\frac{1}{2}\right)^G \left[ \frac{1}{2} P_s(\phi, k_1, +1) + \frac{1}{2} P_s(\phi, k_1, -1) \right] \quad (3-23)$$

where  $P_s(\phi, k_1, d_0)$  is the conditional symbol error probability given the values of  $\phi$ ,  $k_1$  and  $d_0$ . Under these conditions,  $V_1$  is a constant, and  $V$  has a Gaussian distribution. Equations (3-10) and (3-21) imply that the conditional expected value of  $V$  is

$$E[V|\phi, k_1, d_0] = d_0 \sqrt{\frac{S}{2}} T_s + \sqrt{\frac{I\kappa}{2}} T_c (2k_1 - G) \cos \phi \quad (3-24)$$

The conditional variance of  $V$  is equal to the variance of  $V_2$ , which is given by (3-14). Using the Gaussian density to evaluate  $P_s(\phi, k_1, +1)$  and  $P_s(\phi, k_1, -1)$  separately and then consolidating the results yields

$$P_s(\phi, k_1, d_0) = Q \left[ \sqrt{\frac{2\mathcal{E}_s}{N_0}} + d_0 \sqrt{\frac{2IT_c\kappa}{GN_0}} (2k_1 - G) \cos \phi \right] \quad (3-25)$$

where  $\mathcal{E}_s = ST_s$  is the energy per symbol,

$$Q(x) = \frac{1}{\sqrt{2\pi}} \int_x^\infty \exp\left(-\frac{y^2}{2}\right) dy = \frac{1}{2} \operatorname{erfc}\left(\frac{x}{\sqrt{2}}\right) \quad (3-26)$$

and  $\operatorname{erfc}(\cdot)$  is the complementary error function. Assuming that  $\phi$  is uniformly distributed over  $[0, 2\pi)$  and exploiting the periodicity of  $\cos \phi$ , we obtain the symbol error probability

$$P_s = \frac{1}{\pi} \int_0^\pi P_s(\phi) d\phi \quad (3-27)$$

where  $P_s(\phi)$  is given by (3-23) and (3-25).

### 3.2 General Tone Interference

To simplify the preceding equations for  $P_s$  and to examine the effects of tone interference with a carrier frequency different from the desired frequency, a Gaussian approximation is used. Consider interference due to a single tone of the form

$$i(t) = \sqrt{2I} \cos(2\pi f_1 t + \theta_1) \quad (3-28)$$

where  $I$ ,  $f_1$ , and  $\theta_1$  are the average power, frequency, and phase angle of the interference signal at the receiver. The frequency  $f_1$  is assumed to be close enough to the desired

frequency  $f_c$  that the tone is undisturbed by the initial wideband filtering that precedes the correlator. If  $f_1 + f_c \gg f_d = f_1 - f_c$  so that a term involving  $f_1 + f_c$  is negligible, (3-28) and (3-8) and a change of variable yield

$$J_i = \sqrt{\frac{I}{2}} \int_0^{T_c} \psi(t) \cos(2\pi f_d t + \theta_1 + i2\pi f_d T_c) dt \quad (3-29)$$

For a rectangular chip waveform, evaluation of the integral and trigonometry yield

$$J_i = \sqrt{\frac{I}{2}} T_c \operatorname{sinc}(f_d T_c) \cos(i2\pi f_d T_c + \theta_2) \quad (3-30)$$

where

$$\theta_2 = \theta_1 + \pi f_d T_c \quad (3-31)$$

Substituting (3-30) into (3-17) and expanding the squared cosine, we obtain

$$\operatorname{var}(V_1) = \frac{1}{4} I T_c^2 \operatorname{sinc}^2(f_d T_c) \left[ G + \sum_{i=0}^{G-1} \cos(i4\pi f_d T_c + 2\theta_2) \right] \quad (3-32)$$

To evaluate the inner summation, we use the identity

$$\sum_{\nu=0}^{n-1} \cos(a + \nu b) = \cos\left(a + \frac{n-1}{2} b\right) \frac{\sin(nb/2)}{\sin(b/2)} \quad (3-33)$$

which is proved by using mathematical induction and trigonometric identities. Evaluation and simplification yield

$$\operatorname{var}(V_1) = \frac{1}{4} I T_s T_c \operatorname{sinc}^2(f_d T_c) \left[ 1 + \frac{\operatorname{sinc}(2f_d T_s)}{\operatorname{sinc}(2f_d T_c)} \cos 2\phi \right] \quad (3-34)$$

where

$$\phi = \theta_2 + \pi f_d (T_s - T_c) = \theta_1 + \pi f_d T_s \quad (3-35)$$

Given the value of  $\phi$ , the  $J_i$  in (3-30) are uniformly bounded constants, and hence the terms of  $V_1$  in (3-11) are independent and uniformly bounded. Since  $\operatorname{var}(V_1) \rightarrow \infty$  as  $G \rightarrow \infty$ , the central limit theorem [6] implies that when  $G$  is large, the conditional distribution of  $V_1$  is approximately Gaussian. Thus,  $V$  is nearly Gaussian with mean given by (3-15) and  $\operatorname{var}(V) = \operatorname{var}(V_1) + \operatorname{var}(V_2)$ . Because of the symmetry of the model, the conditional symbol error probability may be calculated by assuming  $d_0 = 1$  and evaluating the probability that  $V < 0$ . A straightforward derivation using (3-34) indicates that the conditional symbol error probability is well approximated by

$$P_s(\phi) = Q \left[ \sqrt{\frac{2\mathcal{E}_s}{N_{0e}(\phi)}} \right] \quad (3-36)$$

where

$$N_{0e}(\phi) = N_0 + IT_c \text{sinc}^2(f_d T_c) \left[ 1 + \frac{\text{sinc}(2f_d T_s)}{\text{sinc}(2f_d T_c)} \cos 2\phi \right] \quad (3-37)$$

and  $N_{0e}(\phi)/2$  can be interpreted as the *equivalent two-sided power spectral density* of the interference plus noise, given the value of  $\phi$ . For sinusoidal pulses, a similar derivation yields (3-36) with

$$N_{0e}(\phi) = N_0 + IT_c \left( \frac{8}{\pi^2} \right) \left( \frac{\cos \pi f_d T_c}{1 - 4f_d^2 T_c^2} \right)^2 \left[ 1 + \frac{\text{sinc}(2f_d T_s)}{\text{sinc}(2f_d T_c)} \cos 2\phi \right] \quad (3-38)$$

To explicitly exhibit the reduction of the interference power by the factor  $G$ , we may substitute  $T_c = T_s/G$  in (3-37) or (3-38). A comparison of these two equations confirms that sinusoidal pulses provide a  $\pi^2/8 = 0.91$  dB advantage when  $f_d = 0$ , but this advantage decreases as  $|f_d|$  increases and ultimately disappears. The preceding analysis can easily be extended to multiple tones, but the resulting equations are complicated.

If  $\theta_1$  in (3-35) is modeled as a random variable that is uniformly distributed over  $[0, 2\pi)$ , then the modulo- $2\pi$  character of  $\cos 2\phi$  in (3-37) implies that its distribution is the same as it would be if  $\phi$  were uniformly distributed over  $[0, 2\pi)$ . Therefore, we can henceforth assign a uniform distribution for  $\phi$ . The symbol error probability, which is obtained by averaging  $P_s(\phi)$  over the range of  $\phi$ , is

$$P_s = \frac{2}{\pi} \int_0^{\pi/2} Q \left[ \sqrt{\frac{2\mathcal{E}_s}{N_{0e}(\phi)}} \right] d\phi \quad (3-39)$$

where the fact that  $\cos 2\phi$  takes all its possible values over  $[0, \pi/2]$  has been used to shorten the integration interval.

Figure 15 depicts the symbol error probability as a function of the despread signal-to-interference ratio,  $GS/I$ , for one tone-interference signal, rectangular pulses,  $f_d = 0$ ,  $G = 50 = 17$  dB, and  $\mathcal{E}_s/N_0 = 14$  dB and 20 dB. One pair of curves are computed using the approximate model of (3-37) and (3-39), while the other pair are derived from the nearly exact model of (3-23), (3-25), and (3-27) with  $\kappa = 1$ . For the nearly exact model,  $P_s$  depends not only on  $GS/I$ , but also on  $G$ . A comparison of the two curves indicates that the error introduced by the Gaussian approximation is on the order of or less than 0.1 dB when  $P_s \geq 10^{-6}$ . This example and others provide evidence that the Gaussian approximation introduces insignificant error if  $G \geq 50$  and practical values for the other parameters are assumed.

Figure 16 uses the approximate model to plot  $P_s$  versus the normalized frequency offset  $f_d T_c$  for rectangular and sinusoidal chip waveforms,  $G = 17$  dB,  $\mathcal{E}_s/N_0 = 14$  dB, and  $GS/I = 10$  dB. The performance advantage of sinusoidal pulses is apparent, but their realization in a transmitted PSK waveform is difficult because of the distortion introduced

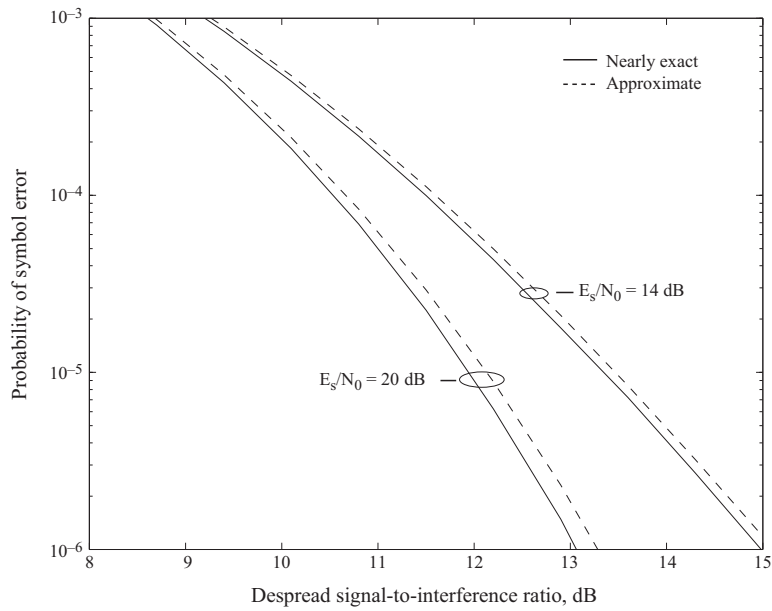


Figure 15. Symbol error probability of binary direct-sequence system with tone interference at carrier frequency and  $G = 17$  dB.

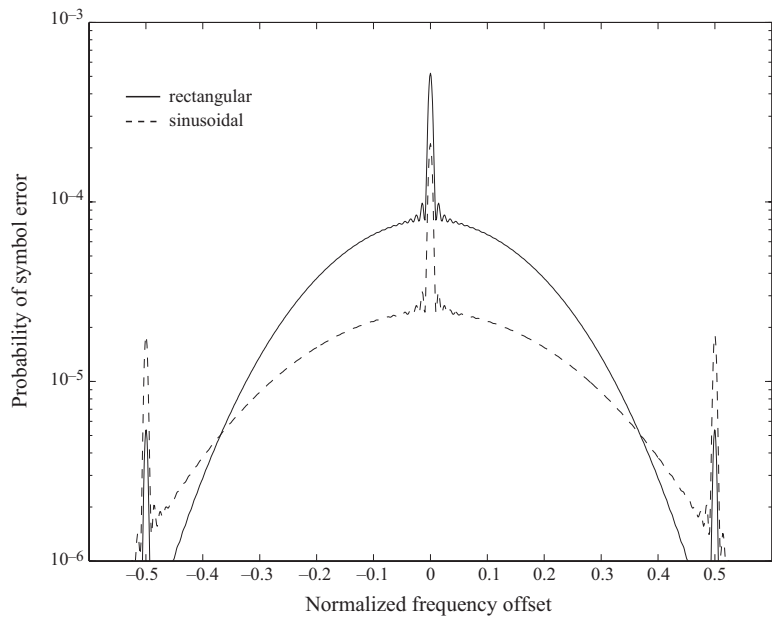


Figure 16. Symbol error probability for direct-sequence system with PSK, rectangular and sinusoidal chip waveforms,  $G = 17$  dB,  $E_s/N_0 = 14$  dB, and  $GS/I = 10$  dB in the presence of tone interference.

by a nonlinear power amplifier in the transmitter when the signal does not have a constant envelope.

### 3.3 Gaussian Interference

*Gaussian interference* is interference that approximates a zero-mean, stationary Gaussian process. If  $i(t)$  is modeled as Gaussian interference and  $f_c \gg 1/T_c$ , then (3-8), a trigonometric expansion, the dropping of a negligible double integral, and a change of variables give

$$E [J_i^2] = \frac{1}{2} \int_0^{T_c} \int_0^{T_c} R_j(t_1 - t_2) \psi(t_1) \psi(t_2) \cos [2\pi f_c (t_1 - t_2)] dt_1 dt_2 \quad (3-40)$$

where  $R_j(t)$  is the autocorrelation of  $i(t)$ . Since  $E[J_i^2]$  does not depend on the index  $i$ , (3-17) gives

$$\text{var}(V_1) = GE [J_i^2] \quad (3-41)$$

Assuming that  $\psi(t)$  is rectangular, we change variables in (3-40) by using  $\tau = t_1 - t_2$  and  $s = t_1 + t_2$ . The Jacobian of this transformation is 2. Evaluating one of the resulting integrals and substituting the result into (3-41) yields

$$\text{var}(V_1) = \frac{1}{2} T_s \int_{-T_c}^{T_c} R_j(\tau) \Lambda\left(\frac{\tau}{T_c}\right) \cos 2\pi f_c \tau d\tau \quad (3-42)$$

The limits in this equation can be extended to  $\pm\infty$  because the integrand is truncated. Since  $R_j(\tau) \Lambda\left(\frac{\tau}{T_c}\right)$  is an even function, the cosine function may be replaced by a complex exponential. Then the convolution theorem and the known Fourier transform of  $\Lambda(t)$  yield the alternative form

$$\text{var}(V_1) = \frac{1}{2} T_s T_c \int_{-\infty}^{\infty} S_j(f) \text{sinc}^2 [(f - f_c) T_c] df \quad (3-43)$$

where  $S_j(f)$  is the power spectral density of the interference after passage through the initial wideband filter of the receiver.

Since  $i(t)$  is a zero-mean Gaussian process, the  $\{J_i\}$  are zero-mean and jointly Gaussian. Therefore, if the  $\{p_i\}$  are given, then  $(V_1)$  is conditionally zero-mean and Gaussian. Since  $\text{var}(V_1)$  does not depend on the  $\{p_i\}$ ,  $V_1$  without conditioning is a zero-mean Gaussian random variable. The independence of the thermal noise and the interference imply that  $V = V_1 + V_2$  is a zero-mean Gaussian random variable. Thus, a standard derivation yields the symbol error probability:

$$P_s = Q\left(\sqrt{\frac{2\mathcal{E}_s}{N_{0e}}}\right) \quad (3-44)$$

where

$$N_{0e} = N_0 + 2T_c \int_{-\infty}^{\infty} S_j(f) \text{sinc}^2 [(f - f_c) T_c] df \quad (3-45)$$

If  $S'_j(f)$  is the interference power spectral density at the input and  $H(f)$  is the transfer function of the initial wideband filter, then  $S_j(f) = S'_j(f)|H(f)|^2$ . Suppose that the interference has a flat spectrum over a band within the passband of the wideband filter so that

$$S_j(f) = \begin{cases} \frac{I}{2W_1}, & |f - f_1| \leq \frac{W_1}{2}, \quad |f + f_1| \leq \frac{W_1}{2} \\ 0, & \text{otherwise} \end{cases} \quad (3-46)$$

If  $f_c \gg 1/T_c$ , the integration over negative frequencies in (3-45) is negligible and

$$N_{0e} = N_0 + \frac{IT_c}{W_1} \int_{f_1 - W_1/2}^{f_1 + W_1/2} \text{sinc}^2 [(f - f_c) T_c] df \quad (3-47)$$

This equation shows that  $f_1 = f_c$  or  $f_d = 0$  coupled with a narrow bandwidth increases the impact of the interference power. Since the integrand is upper-bounded by unity,  $N_{0e} \leq N_0 + IT_c$ . This upper bound is intuitively reasonable because  $IT_c \approx I/B = I_0$ , where  $B \approx 1/T_c$  is the bandwidth of narrowband interference after the despreading, and  $I_0$  is its power spectral density. Equation (3-44) yields

$$P_s \leq Q \left( \sqrt{\frac{2\mathcal{E}_s}{N_0 + IT_c}} \right) \quad (3-48)$$

This upper bound is tight if  $f_d \approx 0$  and the Gaussian interference is narrowband. A plot of (3-48) with the parameter values of Figure 15 indicates that roughly 2 dB more interference power is required for worst-case Gaussian interference to degrade  $P_s$  as much as tone interference at the carrier frequency.

---

## 4. Quaternary Systems with Random Spreading Sequences

---

A received *quaternary direct-sequence signal* with ideal carrier synchronization and a chip waveform of duration  $T_c$  can be represented by

$$s(t) = \sqrt{S}d_1(t)p_1(t) \cos 2\pi f_c t + \sqrt{S}d_2(t + t_0)p_2(t + t_0) \sin 2\pi f_c t \quad (4-1)$$

where two spreading waveforms,  $p_1(t)$  and  $p_2(t)$ , and two data signals,  $d_1(t)$  and  $d_2(t)$ , are used with two quadrature carriers, and  $t_0$  is the relative delay between the in-phase and quadrature components of the signal. For a *quadrature direct-sequence system*, which uses quadrature phase-shift keying (QPSK),  $t_0 = 0$ . For a direct-sequence system with offset QPSK or minimum-shift keying (MSK),  $t_0 = T_c/2$ . For *offset QPSK*, the chip waveforms are

rectangular; for MSK, they are sinusoidal. The use of MSK limits the spectral sidelobes of the direct-sequence signal, which may interfere with other signals.

Consider the *classical* or *dual* quaternary system in which  $d_1(t)$  and  $d_2(t)$  are independent. Let  $T_s$  denote the duration of the data symbols before the generation of (4-1), and let  $T_{s1} = 2T_s$  denote the duration of the channel symbols, which are transmitted in pairs. Let  $T_c$  denote the common chip duration of  $p_1(t)$  and  $p_2(t)$ . The number of chips per channel symbol is  $2G$ , where  $G = T_s/T_c$ . It is assumed that the synchronization is perfect in the receiver, which is shown in Figure 17. Consequently, if the received signal is given by (4-1), then the upper decision variable applied to the decision device at the end of a symbol interval during which  $d_1(t) = d_{10}$  is

$$V = d_{10}\sqrt{S} T_s + \sum_{i=0}^{2G-1} p_{1i}J_i + \sum_{i=0}^{2G-1} p_{1i}N_i \quad (4-2)$$

where  $J_i$  and  $N_i$  are given by (3-8) and (3-9), respectively. The term representing crosstalk,

$$V_c = \sum_{i=0}^{2G-1} p_{1i} \frac{\sqrt{S}}{2} \int_{iT_c}^{(i+1)T_c} d_2(t+t_0) p_2(t+t_0) \psi(t-iT_c) \sin 4\pi f_c t dt \quad (4-3)$$

is negligible if  $f_c \gg 1/T_c$  so that the sinusoid in (4-3) varies much more rapidly than the other factors. Similarly, the lower decision variable at the end of a channel-symbol interval during which  $d_2(t) = d_{20}$  is

$$U = d_{20}\sqrt{S}T_s + \sum_{i=0}^{2G-1} p_{2i}J'_i + \sum_{i=0}^{2G-1} p_{2i}N'_i \quad (4-4)$$

where

$$J'_i = \int_{iT_c}^{(i+1)T_c} i(t)\psi(t-iT_c) \sin 2\pi f_c t dt \quad (4-5)$$

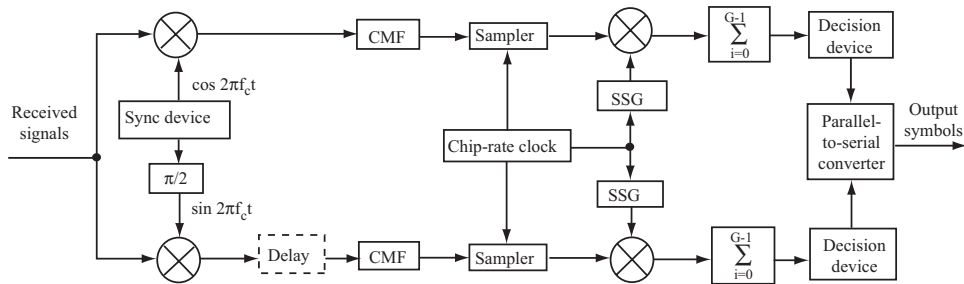


Figure 17. Receiver for direct-sequence signal with dual quaternary modulation; CMF = chip-matched filter; SSG = spreading sequence generator. Delay = 0 for QPSK; delay =  $T_c/2$  for OQPSK and MSK.

$$N'_i = \int_{iT_c}^{(i+1)T_c} n(t)\psi(t - iT_c) \sin 2\pi f_c t \, dt \quad (4-6)$$

Of the available desired-signal power  $S$ , half is in each of the two components of (4-1). Since  $T_{s1} = 2T_s$ , the energy per channel symbol is  $\mathcal{E}_s = ST_s$ , the same as for a direct-sequence system with PSK, and

$$E[V] = d_{10}\sqrt{S} T_s, \quad E[U] = d_{20}\sqrt{S} T_s \quad (4-7)$$

A derivation similar to the one leading to (3-14) gives the variances of the noise terms  $V_2$  and  $U_2$  in (4-2) and (4-4):

$$\text{var}(V_2) = \text{var}(U_2) = \frac{1}{2}N_0T_s \quad (4-8)$$

Using the tone-interference model of Section 3.2, and averaging the error probabilities for the two parallel symbol streams, we obtain the conditional symbol error probability:

$$P_s(\phi) = \frac{1}{2}Q \left[ \sqrt{\frac{2\mathcal{E}_s}{N_{0e}^{(0)}(\phi)}} \right] + \frac{1}{2}Q \left[ \sqrt{\frac{2\mathcal{E}_s}{N_{0e}^{(1)}(\phi)}} \right] \quad (4-9)$$

where  $N_{0e}^{(0)}(\phi)$  and  $N_{0e}^{(1)}(\phi)$  arise from the upper and lower branches of Figure 17, respectively. For rectangular chip waveforms (QPSK and OQPSK signals),

$$N_{0e}^{(l)}(\phi) = N_0 + IT_c \text{sinc}^2(f_d T_c) \left[ 1 + \frac{\text{sinc}(4f_d T_s)}{\text{sinc}(2f_d T_c)} \cos(2\phi + l\pi) \right] \quad (4-10)$$

and for sinusoidal chip waveforms,

$$N_{0e}^{(l)}(\phi) = N_0 + IT_c \left( \frac{8}{\pi^2} \right) \left( \frac{\cos \pi f_d T_c}{1 - 4f_d^2 T_c^2} \right)^2 \left[ 1 + \frac{\text{sinc}(4f_d T_s)}{\text{sinc}(2f_d T_c)} \cos(2\phi + l\pi) \right] \quad (4-11)$$

where  $l = 0, 1$ , and we have used  $T_{s1} = 2T_s$  and

$$\phi = \theta_1 + 2\pi f_d T_s \quad (4-12)$$

These equations indicate that  $P_s(\phi)$  for a quaternary direct-sequence system and the worst value of  $\phi$  is usually lower than  $P_s(\phi)$  for a binary direct-sequence system with the same chip waveform and the worst value of  $\phi$ . The symbol error probability is determined by integrating  $P_s(\phi)$  over the distribution of  $\phi$ . For a uniform distribution, the two integrals are equal. Using the periodicity of  $\cos 2\phi$  to shorten the integration interval, we obtain

$$P_s = \frac{2}{\pi} \int_0^{\pi/2} Q \left[ \sqrt{\frac{2\mathcal{E}_s}{N_{0e}^{(0)}(\phi)}} \right] d\phi \quad (4-13)$$

The quaternary system provides a slight advantage relative to the binary system against tone interference. Both systems provide the same  $P_s$  when  $f_d = 0$  and nearly the same  $P_s$  when  $f_d > 1/T_s$ . Figure 18 illustrates  $P_s$  versus the normalized frequency offset  $f_d T_c$  for quaternary and binary systems,  $G = 17$  dB,  $\mathcal{E}_s/N_0 = 14$  dB, and  $GS/I = 10$  dB.

In another version of the quaternary direct-sequence system, the same data symbols are carried by both the in-phase and quadrature components, which implies that the received direct-sequence signal has the form given by (4-1) with  $d_1(t) = d_2(t) = d(t)$ . Thus, although the spreading is done by quadrature carriers, the data modulation may be regarded as binary PSK. A receiver for this *balanced quaternary system* is shown in Figure 19. The synchronization system is assumed to operate perfectly in the subsequent analysis. If  $f_c \gg 1/T_c$ , the crosstalk terms similar to (4-3) are negligible. If the transmitted symbol is  $d_{10} = d_{20} = d_0$ , then the input to the decision device is

$$V = d_0 \sqrt{S} T_s + \sum_{i=0}^{G-1} p_{1i} J_i + \sum_{i=0}^{G-1} p_{2i} J'_i + \sum_{i=0}^{G-1} p_{1i} N_i + \sum_{i=0}^{G-1} p_{2i} N'_i \quad (4-14)$$

where  $T_s$  is the duration of both a data symbol and a channel symbol. If  $p_1(t)$  and  $p_2(t)$ , are approximated by independent random binary sequences, then the last four terms of (4-14) are zero-mean uncorrelated random variables. Therefore, the variance of  $V$  is equal

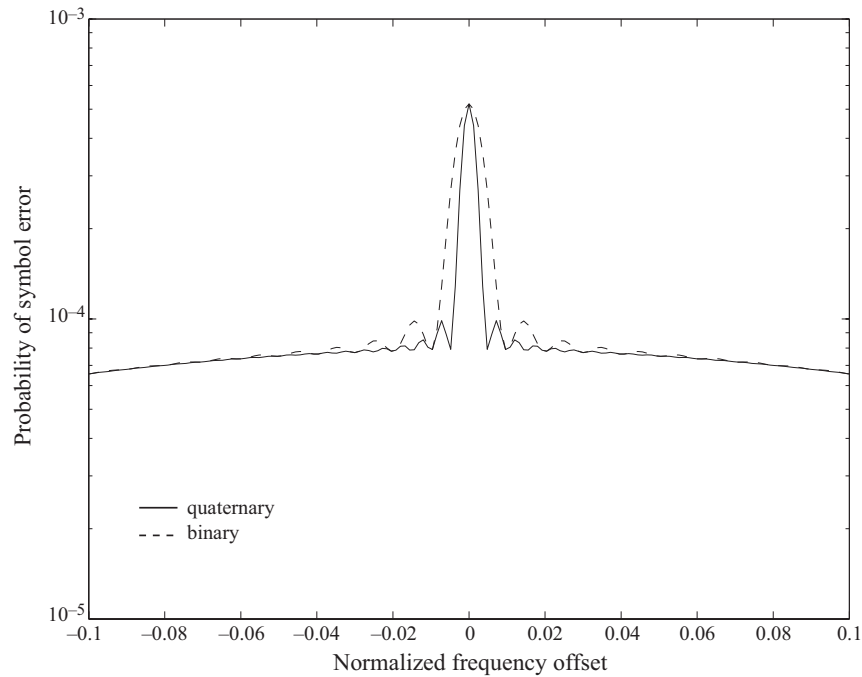


Figure 18. Symbol error probability for quaternary and binary direct-sequence systems with  $G = 17$  dB,  $\mathcal{E}_s/N_0 = 14$  dB, and  $GS/I = 10$  dB in the presence of tone interference.

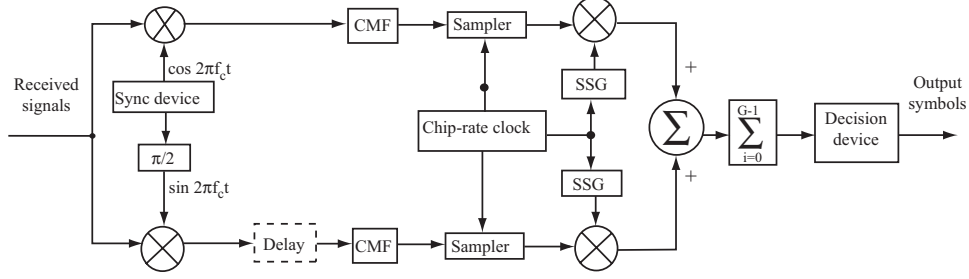


Figure 19. Receiver for direct-sequence signal with balanced quaternary modulation (delay = 0 for QPSK and delay =  $T_c/2$  for OQPSK and MSK); CMF = chip-matched filter; SSG = spreading sequence generator.

to the sum of the variances of these four random variables, and

$$E[V] = d_0 \sqrt{ST_s} \quad (4-15)$$

It is easily verified that *both types of quaternary signals provide the same performance against Gaussian interference as direct-sequence signals with PSK.*

Consider a *balanced QPSK system*, for which  $t_0 = 0$ . If  $i(t)$  is a tone, then a straightforward extension of the preceding analysis for general tone interference (Section 3.2) yields a  $P_s(\phi)$  that is independent of  $\phi$ . Therefore,

$$P_s = P_s(\phi) = Q\left(\sqrt{\frac{2\mathcal{E}_s}{N_{0e}}}\right) \quad (4-16)$$

where for rectangular pulses,

$$N_{0e} = N_0 + IT_c \text{sinc}^2(f_d T_c) \quad (4-17)$$

and for sinusoidal pulses,

$$N_{0e} = N_0 + IT_c \left(\frac{8}{\pi^2}\right) \left(\frac{\cos \pi f_d T_c}{1 - 4f_d^2 T_c^2}\right)^2 \quad (4-18)$$

If  $f_d = 0$ , a nearly exact model similar to the one in Section 3.1 implies that the conditional symbol error probability is

$$P_s(\phi) = \sum_{k_1=0}^G \sum_{k_2=0}^G \binom{G}{k_1} \binom{G}{k_2} \left(\frac{1}{2}\right)^{2G} \left[ \frac{1}{2} P_s(\phi, k_1, k_2, +1) + \frac{1}{2} P_s(\phi, k_1, k_2, -1) \right] \quad (4-19)$$

where  $k_1$  and  $k_2$  are the number of chips in a symbol for which  $p_1(t) = +1$  and  $p_2(t) = +1$ , respectively, and  $P_s(\phi, k_1, k_2, d_0)$  is the conditional symbol error probability given the

values of  $\phi$ ,  $k_1$ , and  $k_2$  and that  $d(t) = d_0$ . A derivation analogous to that of (3-25) yields

$$P_s(\phi, k_1, k_2, d_0) = Q \left\{ \sqrt{\frac{2\mathcal{E}_s}{N_0}} + d_0 \sqrt{\frac{IT_c \kappa}{GN_0}} [(2k_1 - G) \cos \phi - (2k_2 - G) \sin \phi] \right\} \quad (4-20)$$

If  $\phi$  is uniformly distributed over  $[0, 2\pi)$ , then

$$P_s = \frac{1}{2\pi} \int_0^{2\pi} P_s(\phi) d\phi \quad (4-21)$$

Numerical comparisons of the nearly exact model with the approximate results given by (4-16) for  $f_d = 0$  indicate that the approximate results typically introduce an insignificant error if  $G \geq 50$ .

If  $g(x)$  is a convex function over an interval containing the range of a random variable  $X$ , then Jensen's inequality (Appendix A) states that

$$g(E[X]) \leq E[g(X)] \quad (4-22)$$

provided that the indicated expected values exist. Suppose that  $g(x)$  has the form

$$g(x) = Q \left( \sqrt{\frac{1}{a + bx}} \right) \quad (4-23)$$

Since the second derivative of  $g(x)$  is nonnegative over the interval such that  $0 < a + bx \leq 1/3$ ,  $g(x)$  is a convex function over that interval, and Jensen's inequality is applicable.

The application of this result to (4-13) with  $X = \cos 2\phi$  and the fact that  $E[\cos 2\phi] = 0$  yields a lower bound identical to the right-hand side of (4-16). Thus, the *balanced QPSK* system, for which  $d_1(t) = d_2(t)$ , provides a lower symbol error probability against tone interference than the dual quaternary or QPSK system for which  $d_1(t) \neq d_2(t)$ . A sufficient convexity condition for all  $f_d$  is

$$\mathcal{E}_s \geq \frac{3}{2} (N_0 + 2IT_c) \quad (4-24)$$

Figure 20 illustrates the performance advantage of the balanced QPSK system of Figure 19 against tone interference when  $f_d < 1/T_s$ . Equations (4-9) to (4-13) and (4-16) to (4-18) are used for the dual quaternary and the balanced QPSK systems, respectively, and  $G = 17$  dB,  $\mathcal{E}_s/N_0 = 14$  dB, and  $GS/I = 10$  dB. The normalized frequency offset is  $f_d T_c$ . The advantage of the balanced QPSK system when  $f_d$  is small exists because a tone at the carrier frequency cannot have a phase that causes desired-signal cancellation simultaneously in both branches of Figure 19.

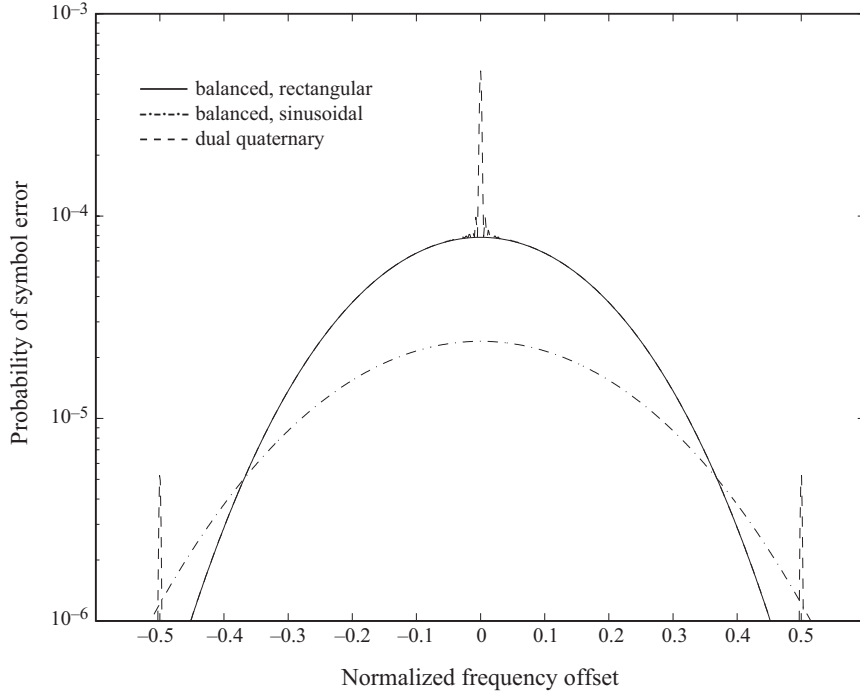


Figure 20. Symbol error probability for direct-sequence systems with balanced QPSK and dual quaternary modulations, rectangular and sinusoidal chip waveforms,  $G = 17$  dB,  $\mathcal{E}_s/N_0 = 14$  dB, and  $GS/I = 10$  dB in the presence of tone interference.

---

## 5. Pulsed Interference

---

*Pulsed interference* is interference that occurs periodically or sporadically for brief durations. Whether it is generated unintentionally or by an opponent, pulsed interference can cause a substantial increase in the bit error rate of a communication system relative to the rate caused by continuous interference with the same average power. Pulsed interference may be produced in a receiver by a signal with a variable center frequency that sweeps over a frequency range that intersects or includes the receiver passband.

Consider a direct-sequence system with binary PSK that operates in the presence of pulsed interference. Let  $\mu$  denote either the pulse duty cycle, which is the ratio of the pulse duration to the repetition period, or the probability of pulse occurrence if the pulses occur randomly. During a pulse, the interference is modeled as Gaussian interference with power  $I/\mu$ , where  $I$  is the average interference power. According to (3-47), the equivalent noise-power spectral density may be decomposed as

$$N_{0e} = N_0 + I_0 \tag{5-1}$$

where the power spectral density of continuous interference ( $\mu = 1$ ) is

$$I_0 = \frac{IT_c}{W_1} \int_{f_1 - W_1/2}^{f_1 + W_1/2} \text{sinc}^2[(f - f_c) T_c] df \quad (5-2)$$

In the absence of a pulse,  $N_{0e} = N_0$ , whereas  $N_{0e} = N_0 + I_0/\mu$  in the presence of a pulse. If the interference pulse duration approximately equals or exceeds the channel-symbol duration, then (3-44) implies that

$$P_s \cong \mu Q \left( \sqrt{\frac{2\mathcal{E}_s}{N_0 + I_0/\mu}} \right) + (1 - \mu) Q \left( \sqrt{\frac{2\mathcal{E}_s}{N_0}} \right), \quad 0 \leq \mu \leq 1 \quad (5-3)$$

If  $\mu$  is treated as a continuous variable over  $[0, 1]$  and  $I_0 \gg N_0$ , calculus gives the value of  $\mu$  that maximizes  $P_s$ :

$$\mu_0 \cong \begin{cases} 0.7 \left( \frac{\mathcal{E}_s}{I_0} \right)^{-1}, & \frac{\mathcal{E}_s}{I_0} > 0.7 \\ 1, & \frac{\mathcal{E}_s}{I_0} \leq 0.7 \end{cases} \quad (5-4)$$

Thus, worst-case pulsed interference is more damaging than continuous interference if  $\mathcal{E}_s/I_0 > 0.7$ .

By substituting  $\mu = \mu_0$  into (5-3), we obtain an approximate expression for the worst-case  $P_s$  when  $I_0 \gg N_0$ :

$$P_s \cong \begin{cases} 0.083 \left( \frac{\mathcal{E}_s}{I_0} \right)^{-1}, & \frac{\mathcal{E}_s}{I_0} > 0.7 \\ Q \left( \sqrt{\frac{2\mathcal{E}_s}{I_0}} \right), & \frac{\mathcal{E}_s}{I_0} \leq 0.7 \end{cases} \quad (5-5)$$

This equation indicates that the worst-case  $P_s$  varies inversely, rather than exponentially, with  $\mathcal{E}_s/I_0$  if this ratio is sufficiently large. To restore a nearly exponential dependence on  $\mathcal{E}_s/I_0$ , an error-correcting code and symbol interleaving are necessary.

Decoding metrics that are effective against white Gaussian noise are not necessarily effective against worst-case pulsed interference. We examine the performance of five different metrics against pulsed interference when the direct-sequence system uses PSK, ideal symbol interleaving, a binary convolutional code, and Viterbi decoding [7]. The results are the same when either dual or balanced QPSK is the modulation.

Let  $B(l)$  denote the total information weight of the paths at Hamming distance  $l$  from the correct path over an unmerged segment in the trellis diagram of the convolutional code. Let  $P_2(l)$  denote the probability of an error in comparing the correct path segment with a path segment that differs in  $l$  symbols. The information-bit error rate satisfies the union bound [1]

$$P_b \leq \sum_{l=d_f}^{\infty} B(l)P_2(l) \quad (5-6)$$

where  $d_f$  is the minimum free distance. If  $r$  is the code rate,  $\mathcal{E}_b$  is the energy per information bit,  $T_b$  is the bit duration, and  $G_u$  is the processing gain of the uncoded system, then

$$\mathcal{E}_s = r\mathcal{E}_b, \quad T_s = rT_b, \quad G = rG_u. \quad (5-7)$$

The decrease in the processing gain is compensated by the coding gain. An upper bound on  $P_b$  for worst-case pulsed interference is obtained by maximizing the right-hand side of (5-6) with respect to  $\mu$ , where  $0 \leq \mu \leq 1$ . The maximizing value of  $\mu$ , which depends on the decoding metric, is not necessarily equal to the actual worst-case  $\mu$  because a bound rather than an equality is maximized. However, the discrepancy is small when the bound is tight.

The simplest practical metric to implement is provided by hard-decision decoding. When the correct path segment is compared to an incorrect one, correct decoding results if the number of incorrect symbols in the decoder input is less than half the number of symbols in which the two segments differ. If the number of symbol errors is exactly half the number of differing symbols, then either of the two segments is chosen with equal probability. Assuming that the deinterleaving ensures the independence of symbol errors, it follows that

$$P_2(l) = \begin{cases} \sum_{i=(l+1)/2}^l \binom{l}{i} P_s^i (1 - P_s)^{l-i}, & l \text{ is odd} \\ \sum_{i=l/2+1}^l \binom{l}{i} P_s^i (1 - P_s)^{l-i} + \frac{1}{2} \binom{l}{l/2} [P_s (1 - P_s)]^{l/2}, & l \text{ is even} \end{cases} \quad (5-8)$$

Since  $\mu = \mu_0$  approximately maximizes  $P_s$ , it also approximately maximizes the upper bound on  $P_b$  for hard-decision decoding given by (5-6) to (5-8).

Figure 21 depicts the upper bound on  $P_b$  as a function of  $\mathcal{E}_b/I_0$  for worst-case pulsed interference,  $\mathcal{E}_b/N_0 = 20$  dB, and binary convolutional codes with several constraint lengths and rates. Tabulated values [8] of  $B(l)$  are used, and the series in (5-6) is truncated after the first 7 terms. This truncation gives reliable results only if  $P_b \leq 10^{-3}$  because the series converges very slowly. However, the truncation error is partially offset by the error incurred by the use of the union bound because the latter error is in the opposite direction. Figure 21 indicates the significant advantage of raising the constraint length  $K$  and reducing  $r$  at the cost of increased implementation complexity and synchronization requirements, respectively.

Let  $N_{0i}$  denote the equivalent one-sided noise-power spectral density in output sample  $y_i$  of a coherent PSK demodulator. For convenience,  $y_i$  is assumed to have the form of the right-hand side of (3-10) normalized by multiplying the latter by  $\sqrt{2/T_s}$ . Thus,  $y_i$  has variance  $N_{0i}/2$ . Given that code symbol  $i$  of sequence  $j$  has value  $x_{ji}$ , the conditional probability density function of  $y_i$  is determined from the Gaussian character of the

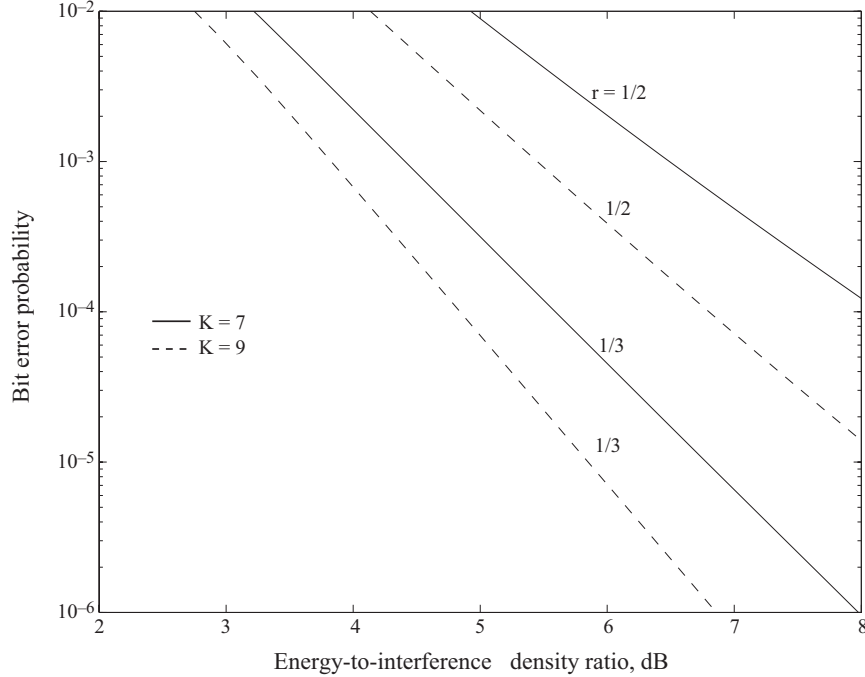


Figure 21. Worst-case performance against pulsed interference for convolutional codes of constraint length  $K$ , rate  $r$ ,  $\mathcal{E}_b/N_0 = 20$  dB, and hard decisions.

interference and noise. For a sequence of  $L$  code symbols, the density is

$$f(y_i|x_{ji}) = \frac{1}{\sqrt{\pi N_{0i}}} \exp \left[ -\frac{(y_i - x_{ji})^2}{N_{0i}} \right], \quad i = 1, 2, \dots, L \quad (5-9)$$

From the log-likelihood function and the statistical independence of the samples, it follows that when the values of  $N_{01}, N_{02}, \dots, N_{0L}$  are known, the *maximum-likelihood metric* for optimal decoding of the sequence is

$$U(j) = \sum_{i=1}^L \frac{x_{ji}y_i}{N_{0i}} \quad (5-10)$$

This metric weights each output sample  $y_i$  according to the level of the equivalent noise. Since each  $y_i$  is assumed to be an independent Gaussian random variable,  $U(j)$  is a Gaussian random variable.

Without loss of generality, let  $j = 1$  label the correct sequence and  $j = 2$  label an incorrect one at distance  $l$ . We assume that there is no quantization of the sample values or that the quantization is infinitely fine. Therefore, the probability that  $U(2) = U(1)$  is zero, and the probability of an error in comparing a correct sequence with an incorrect one that differs in  $l$  symbols,  $P_2(l)$ , is equal to probability that  $M_0 = U(2) - U(1) > 0$ . The symbols that are

the same in both sequences are irrelevant to the calculation of  $P_2(l)$  and are ignored subsequently. Let  $P_2(l|\nu)$  denote the conditional probability that  $M_0 > 0$  given that an interference pulse occurs during  $\nu$  out of  $l$  differing symbols and does not occur during  $l - \nu$  symbols. Because of the interleaving, the probability that a symbol is interfered is statistically independent of the rest of the sequence and equals  $\mu$ . Thus, (5-6 ) yields

$$P_b \leq \sum_{l=d_f}^{\infty} B(l) \sum_{\nu=0}^l \binom{l}{\nu} \mu^\nu (1 - \mu)^{l-\nu} P_2(l|\nu) \quad (5-11)$$

Since  $M_0$  is a Gaussian random variable,  $P_2(l|\nu)$  is determined from the conditional mean and variance. A straightforward calculation gives

$$P_2(l|\nu) = Q \left( \frac{-E[M_0|\nu]}{\sqrt{\text{var}[M_0|\nu]}} \right) \quad (5-12)$$

where  $E[M_0|\nu]$  is the conditional mean and  $\text{var}[M_0|\nu]$  is the conditional variance. When an interference pulse occurs,  $N_{0i} = N_0 + I_0$ ; otherwise,  $N_{0i} = N_0$ . Reordering the symbols for calculative simplicity and observing that  $x_{2i} = -x_{1i}$ ,  $x_{1i}^2 = \mathcal{E}_s$ , and  $E[y_i] = x_{1i}$ , we obtain

$$\begin{aligned} E[M_0|\nu] &= \sum_{i=1}^{\nu} \frac{(x_{2i} - x_{1i}) E[y_i]}{N_0 + I_0/\mu} + \sum_{i=\nu+1}^l \frac{(x_{2i} - x_{1i}) E[y_i]}{N_0} \\ &= \sum_{i=1}^{\nu} \frac{-2\mathcal{E}_s}{N_0 + I_0/\mu} + \sum_{i=\nu+1}^l \frac{-2\mathcal{E}_s}{N_0} \\ &= -2\mathcal{E}_s \left[ \frac{\nu}{N_0 + I_0/\mu} + \frac{l - \nu}{N_0} \right] \end{aligned} \quad (5-13)$$

Using the statistical independence of the samples and observing that  $\text{var}[y_i] = N_{0i}/2$ , we find similarly that

$$\text{var}[M_0|\nu] = 2\mathcal{E}_s \left[ \frac{\nu}{N_0 + I_0/\mu} + \frac{l - \nu}{N_0} \right] \quad (5-14)$$

Substituting (5-13) and (5-14) into (5-12), we obtain

$$P_2[l|\nu] = Q \left\{ \sqrt{\frac{2\mathcal{E}_s}{N_0}} \left[ l - \nu \left( 1 + \frac{\mu N_0}{I_0} \right)^{-1} \right]^{1/2} \right\} \quad (5-15)$$

The substitution of this equation into (5-11) gives the upper bound on  $P_b$  for the maximum-likelihood metric.

The upper bound on  $P_b$  versus  $\mathcal{E}_b/I_0$  for worst-case pulsed interference,  $\mathcal{E}_b/N_0 = 20$  dB, and several binary convolutional codes is shown in Figure 22. Although the worst value of  $\mu$

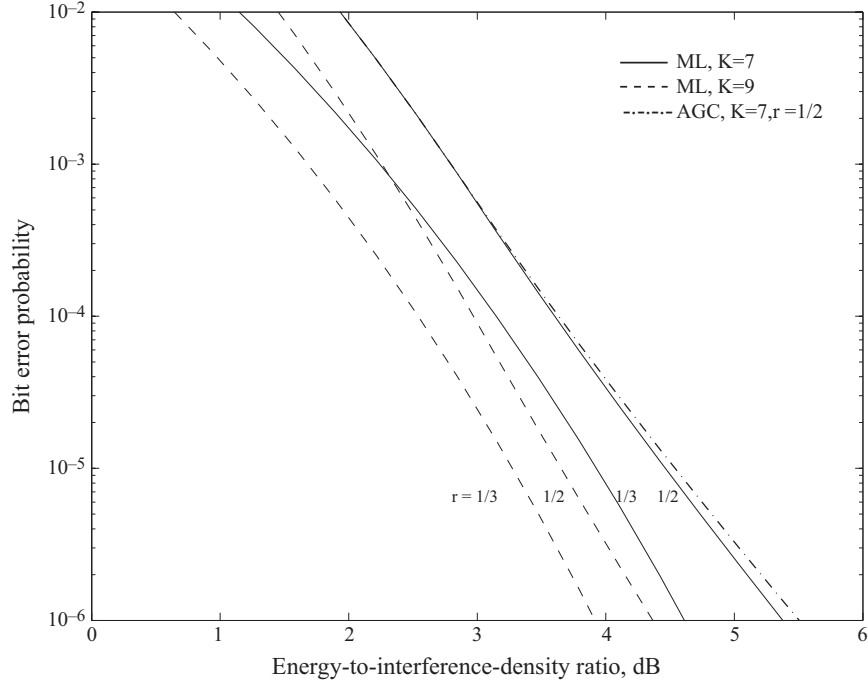


Figure 22. Worst-case performance against pulsed interference for convolutional codes of constraint length  $K$ , rate  $r$ ,  $\mathcal{E}_b/N_0 = 20$  dB and maximum-likelihood (ML) and AGC metrics.

varies with  $\mathcal{E}_b/I_0$ , it is found that worst-case pulsed interference causes very little degradation relative to continuous interference. When  $K = 9$  and  $r = 1/2$ , the *maximum-likelihood metric* provides a performance that is more than 4 dB superior at  $P_b = 10^{-5}$  to that provided by hard-decision decoding; when  $K = 9$  and  $r = 1/3$ , the advantage is approximately 2.5 dB. However, the implementation of the maximum-likelihood metric entails knowledge of not only the presence of interference, but also its density level. Estimates of the  $N_{0i}$  might be based on power measurements in adjacent frequency bands only if the interference spectral density is fairly uniform over the desired-signal and adjacent bands. Any measurement of the power within the desired-signal band is contaminated by the presence of the desired signal, the average power of which is usually unknown *a priori* because of the fading.

Consider an *automatic gain control* (AGC) device that measures the average power at the demodulator output before sampling and then weights the sampled demodulator output  $y_i$  in proportion to the inverse of the measured power to form the *AGC metric*. The average power during channel-symbol  $i$  is  $N_{0i}B + \mathcal{E}_s/T_s$ , where  $B$  is the equivalent bandwidth of the demodulator and  $T_s$  is the channel-symbol duration. If the power measurement is

perfect and  $BT_s \approx 1$ , then the AGC metric is

$$U(j) = \sum_{i=1}^L \frac{x_{ji}y_i}{N_{0i} + \mathcal{E}_s} \quad (5-16)$$

which is a Gaussian random variable. This metric and (5-12) yield

$$P_2(l|\nu) = Q \left\{ \sqrt{\frac{2\mathcal{E}_s}{N_0}} \frac{l(N_0 + \mathcal{E}_s + I_0/\mu) - \nu I_0/\mu}{[l(N_0 + \mathcal{E}_s + I_0/\mu)^2 - \nu(N_0 + I_0/\mu - \mathcal{E}_s^2/N_0)I_0/\mu]^{1/2}} \right\} \quad (5-17)$$

This equation and (5-11) give the upper bound on  $P_b$  for the AGC metric.

The upper bound on  $P_b$  versus  $\mathcal{E}_b/I_0$  for worst-case pulsed interference, the AGC metric, the rate-1/2 binary convolutional code with  $K = 7$ , and  $\mathcal{E}_b/N_0 = 20$  dB is plotted in Figure 22. The figure indicates that the potential performance of the AGC metric is nearly as good as that of the maximum-likelihood metric.

The measurement of  $N_{0i}BT_s + \mathcal{E}_s$  may be performed by a *radiometer*, which is a device that measures the energy at its input. An ideal radiometer (Section 9.2) provides an unbiased estimate of the energy received during a symbol interval. The radiometer outputs are accurate estimates only if the standard deviation of the output is much less than its expected value. This criterion and theoretical results for  $BT_s = 1$  indicate that the energy measurements over a symbol interval will be unreliable if  $\mathcal{E}_s/N_{0i} \leq 10$  during interference pulses. Thus, the potential performance of the AGC metric is expected to be significantly degraded in practice unless each interference pulse extends over many channel symbols and its energy is measured over the corresponding interval.

The maximum-likelihood metric for continuous interference ( $N_{0i}$  is constant for all  $i$ ) is the *white-noise metric*:

$$U(j) = \sum_{i=1}^L x_{ji}y_i \quad (5-18)$$

which is much simpler to implement than the AGC metric. For the white-noise metric, calculations similar to the preceding ones yield

$$P_2(l|\nu) = Q \left\{ \sqrt{\frac{2\mathcal{E}_s}{N_0}} l \left( l + \nu \frac{I_0}{\mu N_0} \right)^{-1/2} \right\} \quad (5-19)$$

This equation and (5-11) give the upper bound on  $P_b$  for the white-noise metric. Figure 23 illustrates the upper bound on  $P_b$  versus  $\mathcal{E}_b/I_0$  for  $K = 7$ ,  $r = 1/2$ ,  $\mathcal{E}_b/N_0 = 20$  dB, and several values of  $\zeta = \mu/\mu_0$ . The figure demonstrates the vulnerability of soft-decision decoding with the white-noise metric to short high-power pulses if interference power is conserved. The high values of  $P_b$  for  $\zeta < 1$  are due to the domination of the metric by a

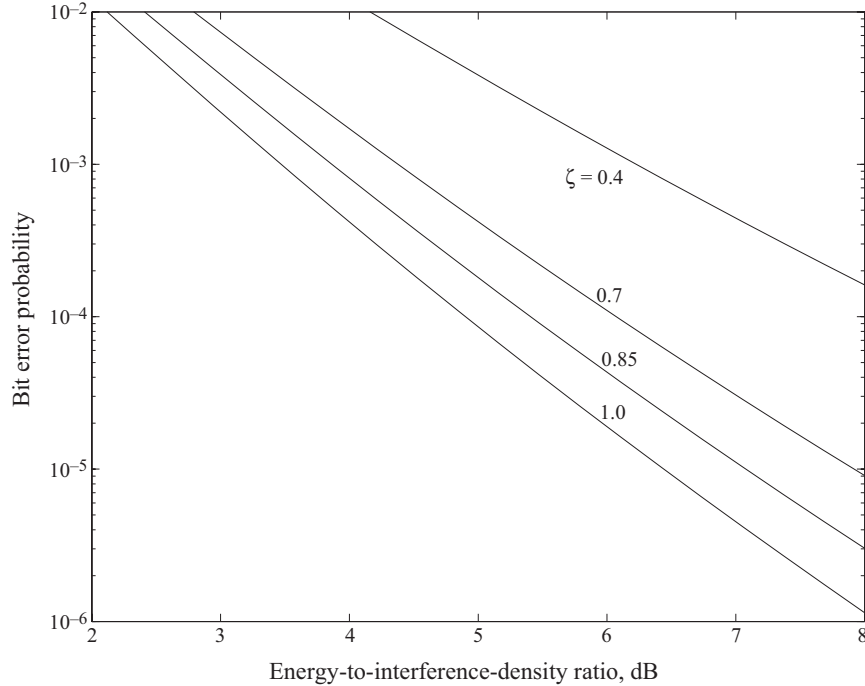


Figure 23. Performance against pulsed interference for convolutional code with white-noise metric, and  $K = 7$ ,  $r = 1/2$ , and  $\mathcal{E}_b/N_0 = 20$  dB.

few degraded symbol metrics. Consider a coherent PSK demodulator that *erases* its output and, hence, a received symbol whenever an interference pulse occurs. The presence of the pulse might be detected by examining a sequence of the demodulator outputs and determining which ones have inordinately large magnitudes compared to the others. Alternatively, the demodulator might decide that a pulse has occurred if an output has a magnitude that exceeds a known upper bound for the desired signal. Consider an ideal demodulator that unerringly detects the pulses and erases the corresponding received symbols. Following the deinterleaving of the demodulated symbols, the decoder processes symbols that have a probability of being erased equal to  $\mu$ . The unerased symbols are decoded by using the white-noise metric. The erasing of  $\nu$  symbols causes two sequences that differ in  $l$  symbols to be compared on the basis of  $l - \nu$  symbols where  $0 \leq \nu \leq l$ . Therefore, we find that

$$P_2(l|\nu) = Q \left[ \sqrt{\frac{2\mathcal{E}_s}{N_0}(l - \nu)} \right] \quad (5-20)$$

This equation and (5-11) give the upper bound on  $P_b$  for the erasures.

The upper bound on  $P_b$  is illustrated in Figure 24 for  $K = 7$ ,  $r = 1/2$ ,  $\mathcal{E}_b/N_0 = 20$  dB, and several values of  $\zeta = \mu/\mu_0$ . In this example, erasures provide no advantage over the white-noise metric in reducing the required  $\mathcal{E}_b/I_0$  for  $P_b = 10^{-5}$  if  $\zeta > 0.85$ , but are increasingly useful as  $\zeta$  decreases. Consider an ideal demodulator that activates erasures only when  $\mu$  is

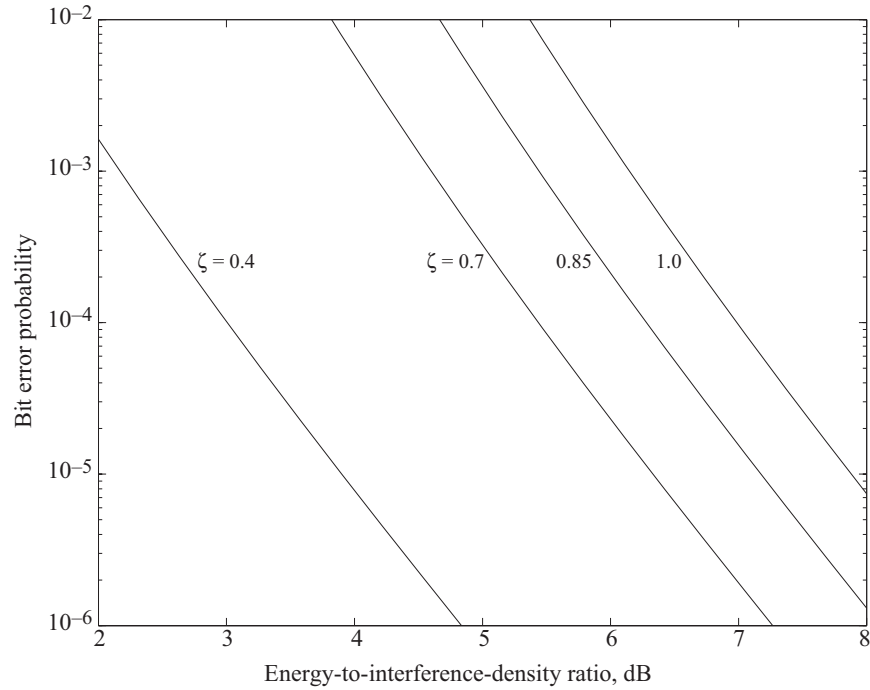


Figure 24. Performance against pulsed interference for convolutional code with erasures,  $K = 7$ ,  $r = 1/2$ , and  $\mathcal{E}_b/N_0 = 20$  dB.

small enough that the erasures are more effective than the white-noise metric. When this condition does not occur, the white-noise metric is used. The upper bound on  $P_b$  for this *ideal erasure decoding*, worst-case pulsed interference,  $\mathcal{E}_b/N_0 = 20$  dB, and several binary convolutional codes is illustrated in Figure 25. The required  $\mathcal{E}_b/I_0$  at  $P_b = 10^{-5}$  is roughly 2 dB less than for worst-case hard-decision decoding. However, a practical demodulator will sometimes erroneously make erasures or fail to erase, and its performance advantage may be much more modest.

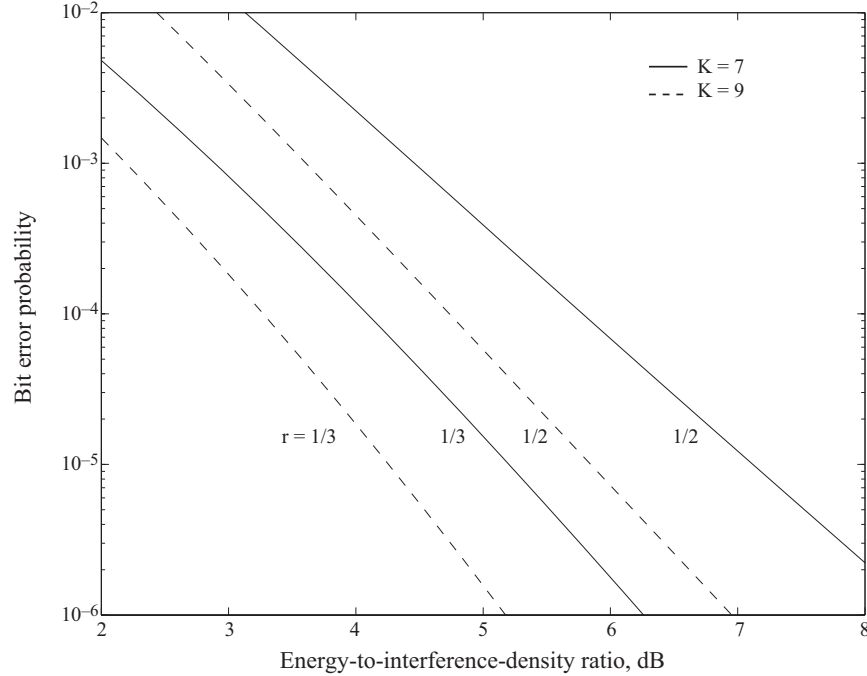


Figure 25. Worst-case performance against pulsed interference for convolutional codes with ideal erasure decoding, constraint length  $K$ , rate  $r$ , and  $\mathcal{E}_b/N_0 = 20$  dB.

---

## 6. Despreading with Matched Filters

---

If the security requirements are mild enough that a short spreading sequence is adequate, then simple direct-sequence systems can use matched filters as despreaders that provide inherent code synchronization. When a short sequence is used, the spreading waveform may be expressed as

$$p(t) = \sum_{i=-\infty}^{\infty} p_1(t - iT) \quad (6-1)$$

where  $p_1(t)$  is one period of the spreading waveform and  $T$  is its period. If the short spreading sequence has length  $N$ , then

$$p_1(t) = \begin{cases} \sum_{i=0}^{N-1} p_i \psi(t - iT_c), & 0 \leq t \leq T \\ 0, & \text{otherwise} \end{cases} \quad (6-2)$$

where  $p_i = \pm 1$ , and  $T = NT_c$ .

## 6.1 Matched Filters

A filter is said to be *matched* to a signal  $x(t)$  that is zero outside the interval  $[0, T]$  if the impulse response of the filter is  $h(t) = x(T - t)$ . When  $x(t)$  is the input to a filter matched to it, the filter output is

$$\begin{aligned} y(t) &= \int_{-\infty}^{\infty} x(u)h(t-u)du = \int_{-\infty}^{\infty} x(u)x(u+T-t)du \\ &= \int_{\max(t-T,0)}^{\min(t,T)} x(u)x(u+T-t)du \end{aligned} \quad (6-3)$$

The *aperiodic autocorrelation* of a deterministic signal with finite energy is defined as

$$R_x(\tau) = \int_{-\infty}^{\infty} x(u)x(u+\tau)du = \int_{-\infty}^{\infty} x(u)x(u-\tau)du \quad (6-4)$$

Therefore, the response of a matched filter to the matched signal is

$$y(t) = R_x(t - T) \quad (6-5)$$

If this output is sampled at  $t = T$ , then  $y(T) = R_x(0)$ , the signal energy.

Consider a *bandpass matched filter* that is matched to

$$x(t) = \begin{cases} p_1(t) \cos(2\pi f_c t + \theta_1), & 0 \leq t \leq T \\ 0, & \text{otherwise} \end{cases} \quad (6-6)$$

where  $p_1(t)$  is one period of a spreading waveform and  $f_c$  is the desired carrier frequency. We evaluate the filter response to the received signal corresponding to a single data symbol:

$$s(t) = \begin{cases} 2Ap_1(t - t_0) \cos(2\pi f_1 t + \theta), & t_0 \leq t \leq t_0 + T \\ 0, & \text{otherwise} \end{cases} \quad (6-7)$$

where  $t_0$  is a measure of the unknown arrival time, the polarity of  $A$  is determined by the data symbol, and  $f_1$  is the received carrier frequency, which differs from  $f_c$  because of oscillator instabilities and the Doppler shift. The matched-filter output is

$$y_s(t) = \int_{t-T}^t s(u)p_1(u+T-t) \cos[2\pi f_c(u+T-t) + \theta_1] du \quad (6-8)$$

If  $f_c \gg 1/T$ , then substituting (6-7) into (6-8) yields

$$y_s(t) = A \int_{\max(t-T, t_0)}^{\min(t, t_0+T)} p_1(u-t_0)p_1(u-t+T) \cos(2\pi f_d u + 2\pi f_c t + \theta_2) du \quad (6-9)$$

where  $\theta_2 = \theta - \theta_1 - 2\pi f_c T$  is the phase mismatch and  $f_d = f_1 - f_c$ . If  $f_d \ll 1/T$ , the carrier-frequency error is inconsequential, and

$$y_s(t) \approx A_s(t) \cos(2\pi f_c t + \theta_2) \quad (6-10)$$

where

$$A_s(t) = A \int_{\max(t-T, t_0)}^{\min(t, t_0+T)} p_1(u - t_0) p_1(u - t + T) du \quad (6-11)$$

In the absence of noise, the matched-filter output is a sinusoidal spike with a polarity determined by  $A$ . Assuming that (3-3) is applicable, the peak magnitude, which occurs at  $t = t_0 + T$ , equals  $|A|T$ . However, if  $f_d > 0.1/T$ , then (6-9) is not well-approximated by (6-10), and the matched-filter output is significantly degraded.

If  $f_c \gg 1/T$ , the response of the matched filter to the interference plus noise, denoted by  $N(t) = i(t) + n(t)$ , may be expressed as

$$\begin{aligned} y_n(t) &= \int_{t-T}^t N(u) p_1(u + T - t) \cos [2\pi f_c(u + T - t) + \theta_1] du \\ &= N_1(t) \cos (2\pi f_c t + \theta_2) + N_2(t) \sin (2\pi f_c t + \theta_2) \end{aligned} \quad (6-12)$$

where

$$N_1(t) = \int_{t-T}^t N(u) p_1(u + T - t) \cos (2\pi f_c u + \theta) du \quad (6-13)$$

$$N_2(t) = \int_{t-T}^t N(u) p_1(u + T - t) \sin (2\pi f_c u + \theta) du \quad (6-14)$$

These equations exhibit the spreading of the interference spectrum.

The envelope of the matched-filter output  $y(t) = y_s(t) + y_n(t)$  is

$$E(t) = \{ [A_s(t) + N_1(t)]^2 + N_2^2(t) \}^{1/2} \quad (6-15)$$

Define  $\epsilon$  such that  $2\pi f_c(t_0 + \epsilon) + \theta - \theta_1$  is an integer times  $2\pi$ . If  $f_c$  is sufficiently large that  $\epsilon \ll t_0 + T$ , then (6-10) and (6-12) imply that if  $y(t)$  is sampled at  $t = t_0 + T + \epsilon$ ,

$$\begin{aligned} y(t_0 + T + \epsilon) &= y_s(t_0 + T + \epsilon) + y_n(t_0 + T + \epsilon) \\ &= A_s(t_0 + T + \epsilon) + N_1(t_0 + T + \epsilon) \\ &\approx AT + N_1(t_0 + T + \epsilon) \end{aligned} \quad (6-16)$$

where  $A_s(t_0 + T) = AT$ . If

$$|AT + N_1(t_0 + T)| \gg |N_2(t_0 + T)| \quad (6-17)$$

then (6-15) implies that

$$E(t_0 + T) \approx |AT + N_1(t_0 + T)| \quad (6-18)$$

A comparison of this equation with (6-16) indicates that there is relatively little degradation in using an envelope detector after the matched filter rather than directly

detecting the peak magnitude of the matched-filter output. The latter procedure would be much more difficult to implement.

A *passive matched filter* can be implemented as an analog or digital transversal filter that essentially stores a replica of the underlying spreading sequence and waits for the received sequence to align itself with the replica. Figure 26 illustrates the basic form of a *surface-acoustic-wave* (SAW) *transversal filter*. The SAW delay line consists primarily of a piezoelectric substrate, which serves as the acoustic propagation medium, and interdigital transducers, which serve as the taps and the input transducer. The transversal filter is matched to one period of the spreading waveform, the propagation delay between taps is  $T_c$ , and  $f_c T_c$  is an integer. The chip matched filter following the summer is matched to  $\psi(t) \cos(2\pi f_c t + \theta)$ . It is easily verified that the impulse response of the transversal filter is that of a filter matched to  $p_1(t) \cos(2\pi f_c t + \theta)$ .

A *convolver* is an *active matched filter* that produces the convolution of the received signal with a local reference [9]. When used as a direct-sequence matched filter, a convolver uses a recirculating, time-reversed replica of the spreading waveform as a reference waveform. In a *SAW elastic convolver*, which is depicted in Figure 27, the received signal and the reference are applied to interdigital transducers that generate acoustic waves at opposite ends of the substrate. The acoustic waves travel in opposite directions with speed  $v$ , and the acoustic terminations suppress reflections. The signal wave is launched at position  $x = 0$  and the reference wave at  $x = L$ . The signal wave travels to the right in the substrate and has the form

$$F(t, x) = f\left(t - \frac{x}{v}\right) \cos\left[2\pi f_c\left(t - \frac{x}{v}\right) + \theta\right] \quad (6-19)$$

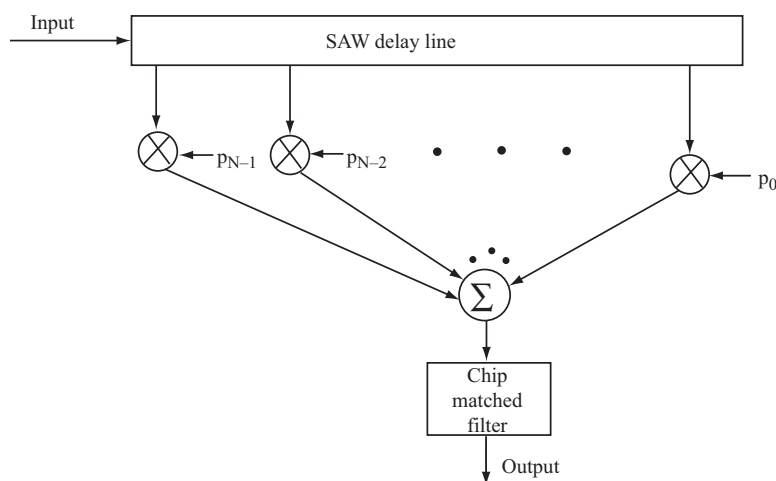


Figure 26. Matched filter that uses a SAW transversal filter.

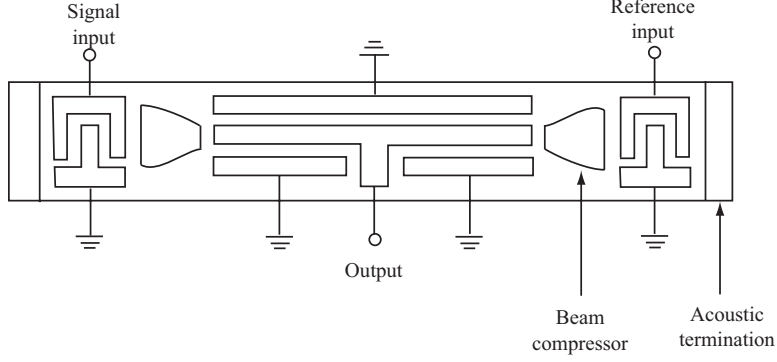


Figure 27. SAW elastic convolver.

where  $f(t)$  is the modulation at position  $x = 0$ . The reference wave travels to the left and has the form

$$G(t, x) = g\left(t + \frac{x}{v} - \frac{L}{v}\right) \cos\left[2\pi f_c\left(t + \frac{x}{v} - \frac{L}{v}\right) + \theta_1\right] \quad (6-20)$$

where  $g(t)$  is the modulation at position  $x = L$ . Both  $f(t)$  and  $g(t)$  are assumed to have bandwidths much smaller than  $f_c$ . The beam compressors, which consist of thin metallic strips, focus the acoustic energy to increase the convolver's efficiency. When the acoustic waves overlap beneath the central electrode, a nonlinear piezoelectric effect causes a surface charge distribution that is spatially integrated by the electrode. The convolver output has the primary component

$$y(t) = \int_0^L \alpha [F(t, x) + G(t, x)]^2 dx \quad (6-21)$$

where  $\alpha$  is a constant. Substituting (6-19) and (6-20) into (6-21) and using trigonometry, we find that  $y(t)$  is the sum of a number of terms, some of which are negligible if  $f_c L/v \gg 1$ . Others are slowly varying and are easily blocked by a filter. The most useful component of the convolver output is

$$y_s(t) = \left[ \alpha \int_0^L f\left(t - \frac{x}{v}\right) g\left(t + \frac{x}{v} - \frac{L}{v}\right) dx \right] \cos(4\pi f_c t + \theta_2) \quad (6-22)$$

where  $\theta_2 = \theta + \theta_1 - 2\pi f_c L/v$ . Changing variables, we find that the amplitude is proportional to

$$A_s(t) = \int_{t-L/v}^t f(y)g(2t - y - L/v)dy \quad (6-23)$$

where the factor  $2t$  results from the counterpropagation of the two acoustic waves.

Suppose that an acquisition pulse is a single period of the spreading waveform. Then  $f(t) = Ap_1(t - t_0)$  and  $g(t) = p(T - t)$ , where  $t_0$  is the uncertainty in the arrival time of an acquisition pulse relative to the launching of the reference signal at  $x = L$ . The periodicity

of  $g(t)$  allows the time origin to be selected so that  $0 \leq t_0 \leq T$ . Equations (6-23) and (6-1) and a change of variables yield

$$A_s(t) = A \sum_{i=-\infty}^{\infty} \int_{t-t_0-L/v}^{t-t_0} p_1(y) p_1(y + iT + t_0 - 2t + L/v) dy \quad (6-24)$$

Since  $p_1(t) = 0$  unless  $0 \leq t < T$ ,  $A_s(t) = 0$  unless  $t_0 < t < t_0 + T + L/v$ . For every positive integer  $k$ , let

$$\tau_k = \frac{kT + t_0 + L/v}{2}, \quad k = 1, 2, \dots \quad (6-25)$$

Only one term in (6-24) can be nonzero when  $t = \tau_k$ , and

$$A_s(\tau_k) = A \int_{\tau_k - t_0 - L/v}^{\tau_k - t_0} p_1^2(y) dy \quad (6-26)$$

The maximum possible magnitude of  $A_s(\tau_k)$  is produced if  $\tau_k - t_0 \geq T$  and  $\tau_k - t_0 - L/v \leq 0$ ; that is, if

$$t_0 + T \leq \tau_k \leq t_0 + \frac{L}{v} \quad (6-27)$$

Since (6-25) indicates that  $\tau_{k+1} - \tau_k = T/2$ , there is some  $\tau_k$  that satisfies (6-27) if

$$L \geq \frac{3}{2}vT \quad (6-28)$$

Thus, if  $L$  is large enough, then there is some  $k$  such that  $A_s(\tau_k) = AT$ , and the envelope of the convolver output at  $t = \tau_k$  has the maximum possible magnitude  $|A|T$ . If  $L = 3vT/2$  and  $t_0 \neq T/2$ , only one peak value occurs in response to the single received pulse.

As an example, let  $t_0 = 0$ ,  $L/v = 6T_c$ , and  $T = 4T_c$ . The chips propagating in the convolver for three separate time instants  $t = 4T_c, 5T_c$ , and  $6T_c$  are illustrated in Figure 28. The top diagrams refer to the counterpropagating periodic reference signal, whereas the bottom diagrams refer to the single received pulse of four chips. The chips are numbered consecutively. The received pulse is completely contained within the convolver during  $4T_c \leq t \leq 6T_c$ . The maximum magnitude of the output occurs at time  $t = 5T_c$ , which is the instant of perfect alignment of the reference signal and the received chips.

## 6.2 Noncoherent Systems

In a noncoherent direct-sequence system with binary *code-shift keying* (CSK), one of two orthogonal spreading sequences is transmitted, as shown in Figure 29(a). One sequence represents the symbol 1, and the other represents the symbol 0. The receiver uses two matched filters, each matched to a different sequence and followed by an envelope detector, as shown in Figure 29(b). In the absence of noise and interference, each sequence causes

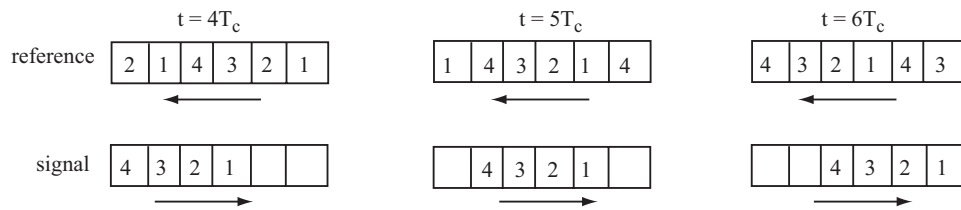


Figure 28. Chip configurations within convolver at time instants  $t = 4T_c$ ,  $5T_c$ , and  $6T_c$  when  $t_0 = 0$ ,  $L/v = T_c$ , and  $T = 4T_c$ .

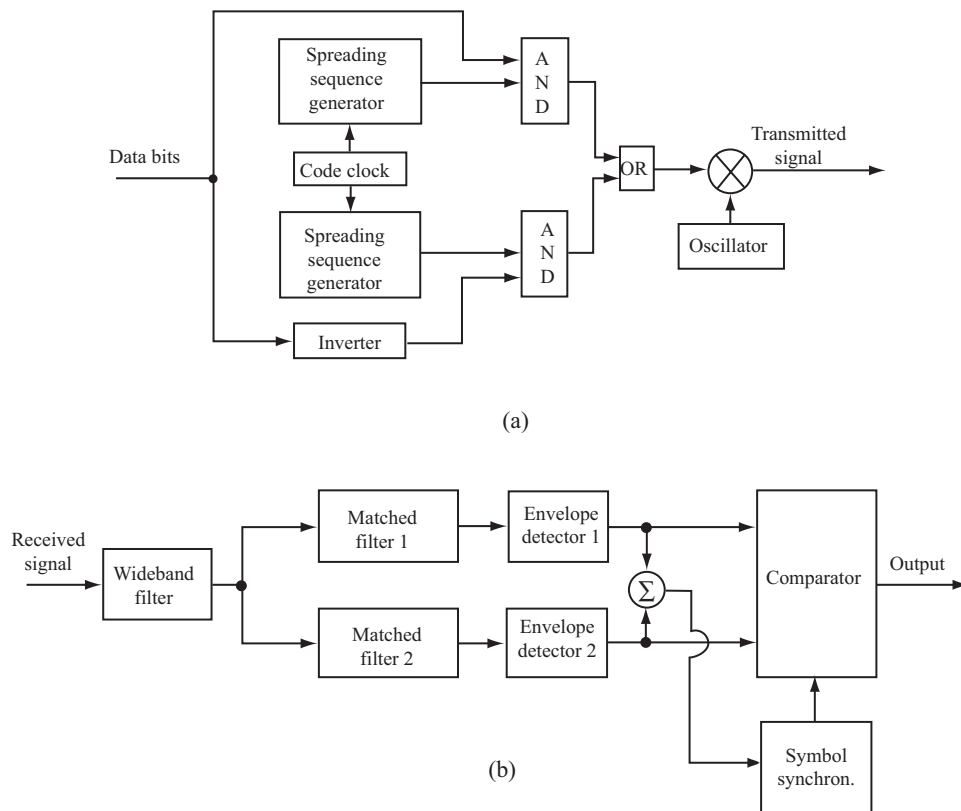


Figure 29. Direct-sequence system with binary code-shift keying: (a) transmitter and (b) receiver.

only one envelope detector to produce a significant output. The data is recovered by comparing the two detector outputs every symbol period. Since each of the two orthogonal sequences has a period equal to the symbol duration, symbol or bit synchronization is identical to code synchronization. The *symbol synchronizer*, which provides timing pulses to the comparator or decision device, must lock onto the autocorrelation spikes appearing in the envelope-detector outputs. Ideally, these spikes have a triangular shape. The symbol synchronizer must be impervious to the autocorrelation sidelobe peaks and any cross-correlation peaks. A simple implementation with a single threshold detector would result in an unacceptable number of false alarms, premature detections, or missed detections when the received signal amplitude is unknown and has a wide dynamic range. Limiting or automatic gain control only exacerbates the problem when the signal power level is below that of the interference plus noise. More than one threshold detector with precedence given to the highest threshold crossed will improve the accuracy of the decision timing or sampling instants produced by the symbol synchronizer [10]. Another approach is to use peak detection based on a differentiator and a zero-crossing detector. Finally, a phase-locked or feedback loop of some type could be used in the symbol synchronizer. A preamble may be transmitted to initiate accurate synchronization so that symbols are not incorrectly detected while synchronization is being established.

Consider the detection of a symbol represented by (6-7), where  $p_1(t)$  is the CSK waveform to which filter 1 is matched. Assuming perfect symbol synchronization, the channel symbol is received during the interval  $0 \leq t \leq T_s$ . From (6-10) to (6-15) with  $T = T_s$  and  $t_0 = 0$ , we find that the output of envelope detector 1 at  $t = T_s$  is

$$R_1 = (Z_1^2 + Z_2^2)^{1/2} \quad (6-29)$$

where

$$Z_1 = AT_s + \int_0^{T_s} N(u)p_1(u) \cos(2\pi f_c u + \theta) du \quad (6-30)$$

$$Z_2 = \int_0^{T_s} N(u)p_1(u) \sin(2\pi f_c u + \theta) du \quad (6-31)$$

Similarly, if filter 2 is matched to sequence  $p_2(t)$ , then the output of envelope detector 2 at  $t = T_s$  is

$$R_2 = (Z_3^2 + Z_4^2)^{1/2} \quad (6-32)$$

where

$$Z_3 = \int_0^{T_s} N(u)p_2(u) \cos(2\pi f_c u + \theta) du \quad (6-33)$$

$$Z_4 = \int_0^{T_s} N(u)p_2(u) \sin(2\pi f_c u + \theta) du \quad (6-34)$$

and the response to the transmitted symbol at  $t = T_s$  is zero because of the orthogonality of the sequences.

Suppose that the interference plus noise  $N(t)$  is modeled as zero-mean, Gaussian interference, and the spreading sequences are modeled as deterministic and orthogonal. Then  $E[Z_1] = AT_s$  and  $E[Z_i] = 0, i = 2, 3, 4$ . If  $N(t)$  is assumed to be wideband enough that its autocorrelation is approximated by (3-13), then straightforward calculations using  $f_c T_s \gg 1$  and the orthogonality of  $p_1(t)$  and  $p_2(t)$  indicate that  $Z_1, Z_2, Z_3$ , and  $Z_4$  are all uncorrelated with each other. The jointly Gaussian character of the random variables then implies that they are statistically independent of each other, and hence  $R_1$  and  $R_2$  are independent. Analogous results can be obtained when the transmitted symbol is represented by CSK waveform  $p_2(t)$ . A straightforward derivation similar to the classical one for orthogonal signals then yields the symbol error probability:

$$P_s = \frac{1}{2} \exp\left(-\frac{\mathcal{E}_s}{2N_{0e}}\right) \quad (6-35)$$

where  $N_{0e}$  is given by (3-47). A comparison of (6-35) with (3-44) indicates that the performance of the direct-sequence system with noncoherent binary CSK in the presence of wideband Gaussian interference is approximately 4 dB worse than that of a direct-sequence system with coherent binary PSK. This difference arises because binary CSK uses orthogonal rather than antipodal signaling. A much more complicated coherent version of Figure 29 would only recover roughly 1 dB of the disparity.

A direct-sequence system with  $q$ -ary CSK encodes each group of  $m$  binary symbols as one of  $q = 2^m$  sequences chosen to have negligible cross correlations. Suppose that bandwidth constraints limit the chip rate of a binary CSK system to  $G$  chips per data bit. For a fixed data-bit rate, the  $q$ -ary CSK system produces  $mG$  chips to represent each group of  $m$  bits, which may be regarded as a single  $q$ -ary symbol. Thus, the processing gain relative to a data symbol is  $mG$ , which indicates an enhanced ability to suppress interference. In the presence of wideband Gaussian interference, the performance improvement of quaternary CSK is more than 2 dB relative to binary CSK, but four filters matched to four double-length sequences are required. When the chip rate is fixed,  $q$ -ary CSK provides a means of increasing the data-bit or code-symbol rate without sacrificing the processing gain.

Elimination of the lower branch in Figure 29(b) leaves a system that uses a single CSK sequence and a minimum amount of hardware. The symbol 1 is signified by the transmission of the sequence, whereas the symbol 0 is signified by the absence of a transmission. Decisions are made after comparing the envelope-detector output with a threshold. One problem with this system is that the optimal threshold is a function of the amplitude of the received signal, which must somehow be estimated. Another problem is the degraded performance of the symbol synchronizer when many consecutive zeros are transmitted. Thus, a system with binary CSK is much more practical.

A direct-sequence system with *differential phase-shift keying* (DPSK) signifies the symbol 1 by the transmission of a spreading sequence without any change in the carrier phase; the symbol 0 is signified by the transmission of the same sequence after a phase shift of  $\pi$  radians in the carrier phase or multiplication of the signal by  $-1$ . A matched filter despreads the received direct-sequence signal, as illustrated in Figure 30. The filter output is applied to a standard DPSK demodulator that makes symbol decisions. An analysis of this system in the presence of wideband Gaussian interference indicates that it is more than 2 dB superior to the system with binary CSK. However, the system with DPSK is more sensitive to Doppler shifts and is more than 1 dB inferior to a system with coherent binary PSK.

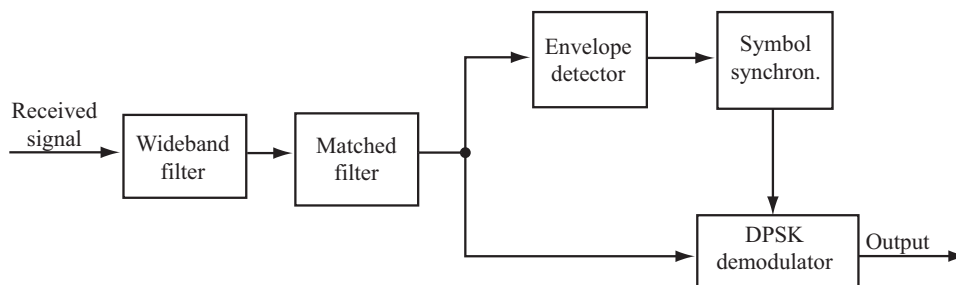


Figure 30. Receiver for direct-sequence system with differential phase-shift keying.

### 6.3 Multipath-Resistant Coherent System

Carrier synchronization is essential for the coherent demodulation of a direct-sequence signal. Prior to despreading, the signal-to-interference-plus-noise ratio (SINR) may be too low for the received signal to serve as the input to a phase-locked loop that produces a phase-coherent carrier. Although the despread matched-filter output has a large SINR near the autocorrelation peak, the average SINR may be insufficient for a phase-locked loop. An alternative approach is to use a recirculation loop to produce a synchronized carrier during the main lobe of the matched-filter output.

A *recirculation loop*, is designed to reinforce a periodic input signal by positive feedback. As illustrated in Figure 31, the feedback elements are an attenuator of gain  $K$  and a delay line with delay  $\hat{T}_s$  approximating a symbol duration  $T_s$ . The basic concept behind this architecture is that successive signal pulses are coherently added while the interference and noise are noncoherently added, thereby producing an output pulse with an improved SINR. The periodic input consists of  $N$  symbol pulses such that

$$s_0(t) = \sum_{i=0}^{N-1} g(t - iT_s) \quad (6-36)$$

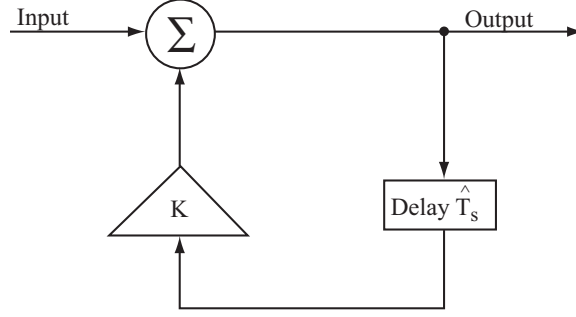


Figure 31. Recirculation loop.

where  $g(t) = 0$  for  $t < 0$  or  $t \geq T_s$ . The figure indicates that the loop output is

$$s_1(t) = s_0(t) + K s_1(t - \hat{T}_s) \quad (6-37)$$

Substitution of this equation into itself yields

$$s_1(t) = s_0(t) + K s_0(t - \hat{T}_s) + K^2 s_1(t - 2\hat{T}_s) \quad (6-38)$$

Repeating this substitution process  $n$  times leads to

$$s_1(t) = \sum_{m=0}^n K^m s_0(t - m\hat{T}_s) + K^{n+1} s_1[t - (n+1)\hat{T}_s] \quad (6-39)$$

which indicates that  $s_1(t)$  increases with  $n$  if  $K \geq 1$  and enough input pulses are available. To prevent an eventual loop malfunction,  $K < 1$  is a design requirement that is assumed henceforth.

During the interval  $[n\hat{T}_s, (n+1)\hat{T}_s]$ ,  $n$  or fewer recirculations of the symbols have occurred. Since  $s_1(t) = 0$  for  $t < 0$ , the substitution of (6-36) into (6-39) yields

$$s_1(t) = \sum_{m=0}^n \sum_{i=0}^N K^m g(t - m\hat{T}_s - iT_s), \quad n\hat{T}_s \leq t < (n+1)\hat{T}_s \quad (6-40)$$

This equation indicates that if  $\hat{T}_s$  is not exactly equal to  $T_s$ , then the pulses do not add coherently, and may combine destructively. However, since  $K < 1$ , the effect of a particular pulse decreases as  $m$  increases and will eventually be negligible. The delay  $\hat{T}_s$  is designed to match  $T_s$ . Suppose that the design error is small enough that

$$N |\hat{T}_s - T_s| \ll \hat{T}_s \quad (6-41)$$

Since  $t - m\hat{T}_s - iT_s = t - (m+i)T_s - m(\hat{T}_s - T_s)$  and  $g(t)$  is time-limited, (6-41) and  $n \leq N$  imply that only the term in (6-40) with  $i = n - m$  contributes appreciably to the output. Therefore,

$$s_1(t) \approx \sum_{m=0}^n K^m g[t - nT_s - m(\hat{T}_s - T_s)], \quad nT_s \leq t < (n+1)T_s \quad (6-42)$$

Let  $\nu$  denote a positive integer such that  $K^m$  is negligible if  $m > \nu$ . Consider an input pulse of the form

$$g(t) = A(t) \cos 2\pi f_c t, \quad 0 \leq t < \min(T_s, \hat{T}_s) \quad (6-43)$$

which implies that each of the  $N$  pulses in (6-36) has the same initial phase. Assume that the amplitude  $A(t)$  varies slowly enough that

$$A \left[ t - nT_s - m \left( \hat{T}_s - T_s \right) \right] \approx A(t - nT_s), \quad 0 \leq m \leq \nu \quad (6-44)$$

and that the design error is small enough that

$$\nu f_c \left| \hat{T}_s - T_s \right| \ll 1 \quad (6-45)$$

Then (6-42) to (6-45) yield

$$\begin{aligned} s_1(t) &\approx g(t - nT_s) \sum_{m=0}^n K^m \\ &= g(t - nT_s) \left( \frac{1 - K^{n+1}}{1 - K} \right), \quad nT_s \leq t \leq (n+1)T_s \end{aligned} \quad (6-46)$$

This equation indicates that the average power in an output pulse during the interval  $nT_s \leq t < (n+1)T_s$  is approximately

$$S_n = \left( \frac{1 - K^{n+1}}{1 - K} \right)^2 S, \quad K < 1 \quad (6-47)$$

where  $S$  is the average power in an input pulse.

Let  $\sigma^2$  denote the average thermal noise power at the output. If  $\hat{T}_s$  is large enough that the recirculated noise is uncorrelated with the input noise, then the noise power after  $n$  recirculations is

$$\begin{aligned} \sigma_n^2 &= \sigma^2 \sum_{m=0}^n (K^2)^m \\ &= \sigma^2 \left( \frac{1 - K^{2n+2}}{1 - K^2} \right), \quad K < 1 \end{aligned} \quad (6-48)$$

The improvement in the signal-to-noise ratio due to the presence of the recirculation loop is

$$\begin{aligned} I(n, K) &= \frac{S_n / \sigma_n^2}{S / \sigma^2} = \frac{(1 - K^{n+1})(1 + K)}{(1 + K^{n+1})(1 - K)} \\ &\leq \frac{1 + K}{1 - K}, \quad K < 1 \end{aligned} \quad (6-49)$$

Since it was assumed that  $K^m$  is negligibly small when  $m > \nu$ , the maximum improvement is nearly attained when  $n \geq \nu$ . However, the upper bound on  $\nu$  for the validity of (6-45)

decreases as the loop phase error  $2\pi f_c |\hat{T}_s - T_s|$  increases. Thus,  $K$  must be decreased as the phase error increases. The phase error of a practical SAW recirculation loop may be caused by a temperature fluctuation, a Doppler shift, oscillator instability, or an imprecise delay-line length. Various other loop imperfections limit the achievable value of  $K$  and, hence, the improvement provided by the recirculation loop [11]. Figure 32 illustrates a *coherent decision-directed demodulator* for a direct-sequence signal with binary PSK and the same carrier phase at the beginning of each symbol. The bandpass matched filter removes the spreading waveform and produces compressed sinusoidal pulses, as indicated by (6-10) and (6-11) when  $A$  is bipolar. A compressed pulse due to a direct-path signal may be followed by one or more compressed pulses due to multipath signals, as illustrated conceptually in Figure 33(a) for pulses corresponding to the transmitted symbols 101. Each compressed pulse is delayed by one symbol and then mixed with the demodulator's output symbol. If this symbol is correct, it coincides with the same data symbol that is modulated onto the compressed pulse. Consequently, the mixer removes the data modulation and produces a phase-coherent reference pulse that is independent of the data symbol, as illustrated in Figure 33(b), where the middle pulses are inverted in phase relative to the corresponding pulses in Figure 33(a). The reference pulses are amplified by a recirculation loop. The loop output and the matched-filter output are applied to a mixer that produces the baseband integrator input illustrated in Figure 33(c). The length of the integration interval is equal to a symbol duration. The integrator output is sampled and applied to a decision device that produces the data output. Since multipath components are coherently integrated, the demodulator provides an improved performance in a fading environment.

Even if the desired-signal multipath components are absent, the coherent decision-directed receiver suppresses interference approximately as much as the correlator of Figure 14. The decision-directed receiver is much simpler to implement because code acquisition and tracking systems are unnecessary, but it requires a short spreading sequence. More efficient exploitation of multipath components is possible with rake combining (Section 10.7).

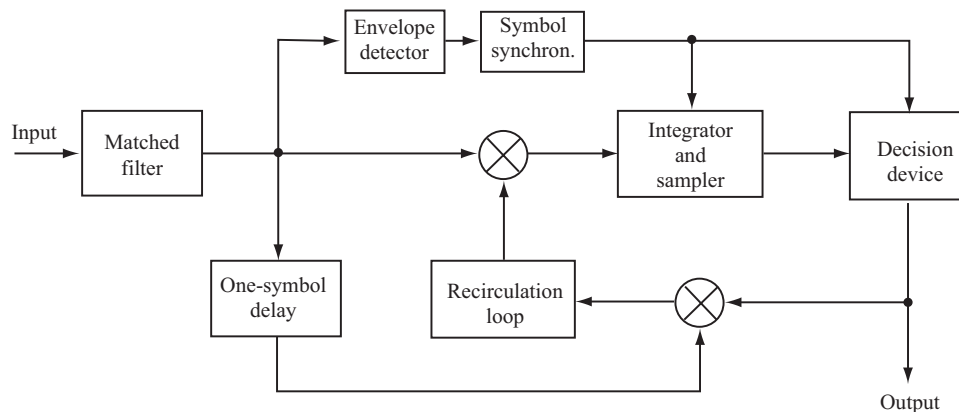


Figure 32. Coherent decision-directed demodulator.

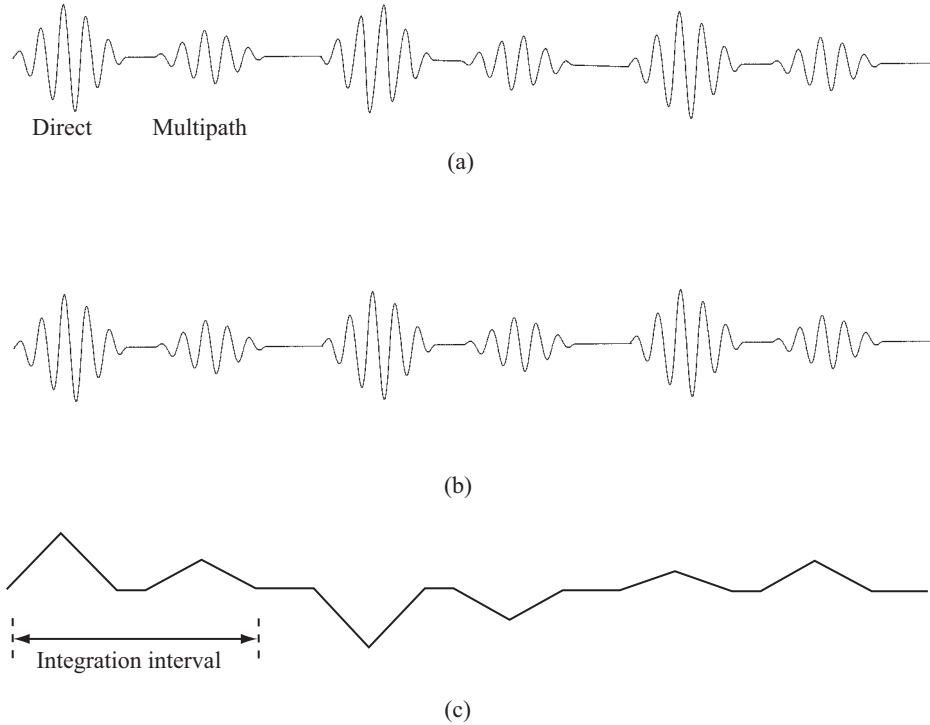


Figure 33. Conceptual waveforms of demodulator: (a) matched-filter output, (b) recirculation loop input or output, and (c) baseband integrator input.

---

## 7. Code Synchronization

---

A spread-spectrum receiver must generate a spreading sequence that is synchronized with the received sequence; that is, the corresponding chips must precisely or nearly coincide. Any misalignment causes the signal amplitude at the demodulator output to fall in accordance with the autocorrelation or partial autocorrelation function. Range uncertainty, clock drifts, and the Doppler shift are the primary sources of synchronization errors. Code synchronization might be obtained from separately transmitted pilot or timing signals. However, to reduce the cost in power and overhead, most direct-sequence receivers acquire code synchronization from the received direct-sequence signal.

In deriving the maximum-likelihood estimate of the *code phase* or timing offset of the spreading sequence, several assumptions are made. Since the presence of the data modulation impedes code synchronization, the transmitter is assumed to assist the synchronization by transmitting the spreading sequence without any data modulation. In nearly all applications, *noncoherent code synchronization* must precede carrier synchronization because the signal energy is spread over a wide spectral band. Prior to despreading, which requires code synchronization, it is difficult to establish a high enough

signal-to-noise ratio in a phase-locked loop for successful carrier tracking. The received signal is

$$r(t) = s(t) + n(t) \quad (7-1)$$

where  $s(t)$  is the desired signal and  $n(t)$  is the additive white Gaussian noise. For a direct-sequence system with PSK modulation, the desired signal is

$$s(t) = \sqrt{2S}p(t - \tau) \cos(2\pi f_c t + 2\pi f_d t + \theta) \quad (7-2)$$

where  $S$  is the average power,  $p(t)$  is the spreading waveform,  $f_c$  is the carrier frequency,  $\theta$  is the random carrier phase, and  $\tau$  and  $f_d$  are the unknown code phase and frequency offset, respectively, that must be estimated. The frequency offset is due to a Doppler shift or to a drift or instability in the transmitter oscillator.

The coefficients in the expansion of the observed waveform in terms of orthonormal basis functions constitute the vector  $\mathbf{r} = [r_1 \ r_2 \ \dots \ r_N]$ . The *likelihood function* for the unknown  $\tau$  and  $f_d$  is the conditional density function of  $\mathbf{r}$  given the values of  $\tau$  and  $f_d$ . Since  $\theta$  is a random variable, the likelihood function is

$$\Lambda(\mathbf{r}) = E_\theta [f(\mathbf{r}|\tau, f_d, \theta)] \quad (7-3)$$

where  $f(\mathbf{r}|\tau, f_d, \theta)$  is the conditional density function of  $\mathbf{r}$  given the values of  $\tau$ ,  $f_d$ , and  $\theta$ , and  $E_\theta$  is the expectation with respect to  $\theta$ . The maximum-likelihood estimates are those values of  $\tau$  and  $f_d$  that maximize  $\Lambda(\mathbf{r})$ .

The coefficients in the expansion of  $r(t)$  in terms of the orthonormal basis functions are statistically independent. Since each coefficient is Gaussian with variance  $N_0/2$ ,

$$f(\mathbf{r}|\tau, f_d, \theta) = \prod_{i=1}^N \frac{1}{\sqrt{\pi N_0}} \exp \left[ -\frac{(r_i - s_i)^2}{N_0} \right] \quad (7-4)$$

where the  $\{s_i\}$  are the coefficients of the signal  $s(t)$  when  $\tau$ ,  $f_d$ , and  $\theta$  are given. Substituting this equation into (7-3) and eliminating factors irrelevant to the maximum-likelihood estimation, we obtain

$$\Lambda(\mathbf{r}) = E_\theta \left\{ \exp \left[ \frac{2}{N_0} \sum_{i=1}^N r_i s_i - \frac{1}{N_0} \sum_{i=1}^N s_i^2 \right] \right\} \quad (7-5)$$

Expansions in the orthonormal basis functions indicate that if  $N \rightarrow \infty$ , the likelihood function may be expressed in terms of the signal waveforms as

$$\Lambda[r(t)] = E_\theta \left\{ \exp \left[ \frac{2}{N_0} \int_0^T r(t)s(t)dt - \frac{\mathcal{E}}{N_0} \right] \right\} \quad (7-6)$$

where  $\mathcal{E}$  is the energy in the signal waveform over the observation interval of duration  $T$ . Assuming that  $\mathcal{E}$  does not vary significantly over the ranges of  $\tau$  and  $f_d$  considered, the

factor involving  $\mathcal{E}$  may be dropped from further consideration. The substitution of  $s(t)$  in (7-2) into (7-6) then yields

$$\Lambda[r(t)] = E_{\theta} \left\{ \exp \left[ \frac{2\sqrt{2S}}{N_0} \int_0^T r(t)p(t-\tau) \cos(2\pi f_c t + 2\pi f_d t + \theta) dt \right] \right\} \quad (7-7)$$

For noncoherent estimation, the received carrier phase  $\theta$  is assumed to be uniformly distributed over  $[0, 2\pi)$ . A trigonometric expansion followed by an integration of (7-7) over  $\theta$  gives (cf. (9-13))

$$\Lambda[r(t)] = I_0 \left( \frac{2\sqrt{2SR(\tau, f_d)}}{N_0} \right) \quad (7-8)$$

where  $I_0(\cdot)$  is the modified Bessel function of the first kind and order zero given by (B-30), and

$$R(\tau, f_d) = \left[ \int_0^T r(t)p(t-\tau) \cos(2\pi f_c t + 2\pi f_d t) dt \right]^2 + \left[ \int_0^T r(t)p(t-\tau) \sin(2\pi f_c t + 2\pi f_d t) dt \right]^2 \quad (7-9)$$

Since  $I_0(x)$  is a monotonically increasing function of  $x$ , (7-8) implies that  $R(\tau, f_d)$  is a sufficient statistic for maximum-likelihood estimation. Ideally, the estimates are determined by considering all possible values of  $\tau$  and  $f_d$ , and then choosing those values that maximize (7-9). A device that implements (7-9) is called a *noncoherent correlator*.

A practical implementation of maximum-likelihood estimation or other type of estimation is greatly facilitated by dividing synchronization into the two operations of acquisition and tracking. *Acquisition* provides coarse synchronization by limiting the choices of the estimated values to a finite number of quantized candidates. Following the acquisition, *tracking* provides and maintains fine synchronization.

One method of acquisition is to use a parallel array of processors, each matched to candidate quantized values of the timing and frequency offsets. The largest processor output then indicates which candidates are to be selected as the estimates. An alternative method of acquisition, which is much less complex, but significantly increases the time needed to make a decision, is to serially search over the candidate offsets. Since the frequency offset is usually negligible or requires only a few candidate values, the remainder of this section analyzes code synchronization in which only the timing offset  $\tau$  is estimated. Search methods rather than parallel processing are examined. *Code acquisition* is the operation by which the phase of the receiver-generated sequence is brought to within a fraction of a chip of the phase of the received sequence. After this condition is detected and verified, the tracking system is activated. *Code tracking* is the operation by which

synchronization errors are further reduced or at least maintained within certain bounds. Both the acquisition and tracking devices regulate the clock rate. Changes in the clock rate adjust the phase or timing offset of the receiver-generated or *local sequence* relative to the phase or timing offset of the received sequence. In a benign environment, *sequential estimation* methods provide rapid acquisition [12]. Successive received chips are demodulated and then loaded into the receiver's code generator to establish its initial state. The tracking system then ensures that the code generator maintains synchronization. However, because chip demodulation is required, the usual despreading mechanism cannot be used to suppress interference during acquisition. Since an acquisition failure completely disables a communication system, an acquisition system must be capable of rejecting the anticipated level of interference. To meet this requirement, *matched-filter acquisition* and *serial-search acquisition* are the most effective techniques in general.

## 7.1 Acquisition with Matched Filter

Matched-filter acquisition provides potentially rapid acquisition when short programmable sequences give adequate security. The matched filter in an acquisition system is matched to one period of the spreading waveform (Section 6.2), which is usually transmitted without modulation during acquisition. The sequence length or integration time of the matched filter is limited by frequency offsets and chip-rate errors. The output envelope, which ideally comprises triangular autocorrelation spikes, is compared with one or more thresholds, one of which is close to the peak value of the spikes. If the data-symbol boundaries coincide with the beginning and end of a spreading sequence, the occurrence of a threshold crossing provides timing information used for both symbol synchronization and acquisition. A major application of matched-filter acquisition is for *burst communications*, which are short and infrequent communications that do not require a long spreading sequence.

A *digital matched filter* that generates  $R(\tau, 0)$  for noncoherent acquisition of a binary spreading waveform is illustrated in Figure 34. The digital matched filter offers great flexibility, but is limited in the bandwidth it can accommodate. The received spreading waveform is decomposed into in-phase and quadrature baseband components, each of which is applied to a separate branch. The outputs of each digitizer are applied to a transversal filter. Tapped outputs of each transversal filter are multiplied by stored weights and summed. The two sums are squared and added together to produce the final matched-filter output.

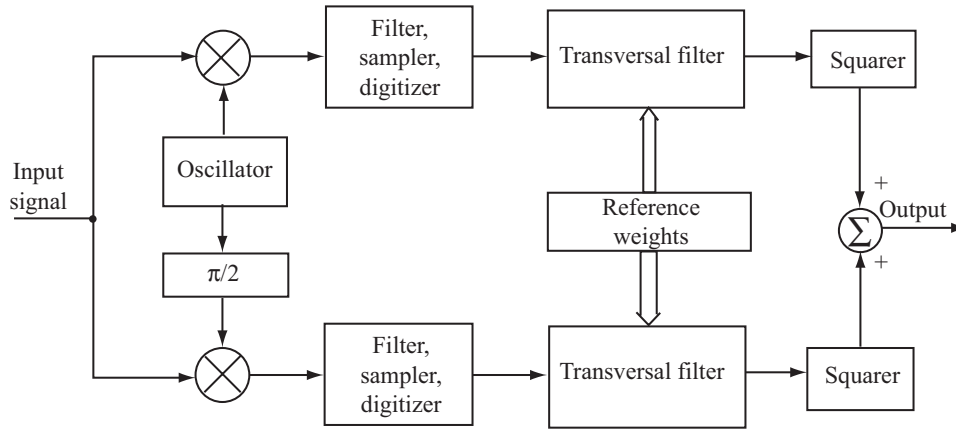


Figure 34. Digital matched filter.

A *one-bit digitizer* makes hard decisions on the received chips by observing the polarities of the sample values. Each transversal filter is a shift register, and the reference weights are sequence chips stored in shift-register stages. The transversal filter contains  $G$  successive received spreading-sequence chips and a correlator that computes the number of received and stored chips that match. The correlator outputs are applied to the squarers.

Matched-filter acquisition for continuous communications is useful when serial-search acquisition with a long sequence fails or takes too long. The transmission of the short sequence may be concealed by embedding it within the long sequence. The short sequence may be a subsequence of the long sequence that is presumed to be ahead of the received sequence and is stored in the programmable matched filter. Figure 35 depicts the configuration of a matched filter for short-sequence acquisition and a serial-search system for long-sequence acquisition. The control signal provides the short sequence that is stored or recirculated in the matched filter. The control signal activates the matched filter when it is needed and deactivates it otherwise. The short sequence is detected when the envelope of the matched-filter output crosses a threshold. The threshold-detector output starts a long-sequence generator in the serial-search system at a predetermined initial state. The long sequence is used for verifying the acquisition and for despreading the received direct-sequence signal. A number of matched filters in parallel can be used to expedite the process.

## 7.2 Serial-Search Acquisition

*Serial-search acquisition* consists of a search, usually in discrete steps, of the possible time alignments of a local sequence relative to a received spreading sequence. The timing uncertainty region is quantized into a finite number of *cells*, which are search positions of relative code phases or timing alignments. The cells are serially tested until it is determined

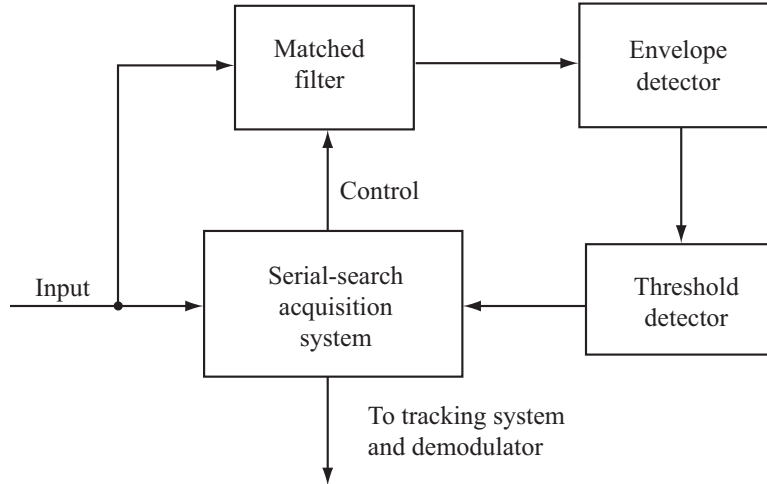


Figure 35. Configuration of a serial-search acquisition system enabled by a matched filter.

that a particular cell corresponds to the alignment of the two sequences to within a fraction of a chip. The *step size* or separation between cells is typically one chip or a half chip.

Figure 36 depicts the principal components of a serial-search acquisition system. The received direct-sequence signal and a local spreading sequence are applied to a noncoherent correlator that produces the statistic (7-9). If the received and local spreading sequences are not aligned, the sampled correlator output is low. Therefore, the threshold is not exceeded, the cell under test is rejected, and the phase of the local sequence is retarded or advanced, possibly by generating an extra clock pulse or by blocking one. A new cell is then tested. If the sequences are nearly aligned, the sampled correlator output is high, the threshold is exceeded, the search is stopped, and the two sequences run in parallel at some fixed phase offset. Subsequent tests verify that the correct cell has been identified. If a cell fails the verification tests, the search is resumed. If a cell passes, the two sequences are assumed to be coarsely synchronized, demodulation begins, and the tracking system is activated. The threshold-detector output continues to be monitored so that any subsequent loss of synchronization activates the serial search.

There may be several cells that potentially provide a valid acquisition. However, if none of these cells corresponds to perfect synchronization, the detected energy is reduced below its potential peak value. If the step size is one-half of a chip, then one of the cells corresponds to an alignment within one-fourth of a chip. On the average, the misalignment of this cell is one-eighth of a chip, which may cause a negligible degradation. As the step size is decreased, the average detected energy during acquisition increases, but the number of cells to be searched increases.

The *dwell time* is the amount of time required for testing a cell and is approximately equal to the length of the integration interval in the noncoherent correlator (Section 7.3). An

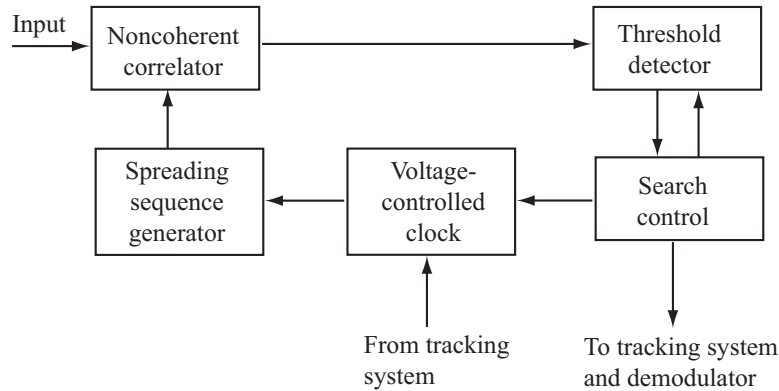


Figure 36. Serial-search acquisition system.

acquisition system is called a *single-dwell system* if a single test determines whether a cell is accepted as the correct one. If verification testing occurs before acceptance, the system is called a *multiple-dwell system*. The dwell times may be either fixed or variable but bounded by some maximum value. The dwell time for the initial test of a cell is usually designed to be much shorter than the dwell times for verification testing. This approach expedites the acquisition by quickly eliminating the bulk of the incorrect cells. In any serial-search system, the dwell time allotted to a test is limited by the Doppler shift, which causes the received and local chip rates to differ. As a result, an initial close alignment of the two sequences may disappear by the end of the test unless the dwell time is much smaller than the inverse of the maximum difference between the chip rates.

A multiple-dwell system may use a *consecutive-count strategy*, in which a failed test causes a cell to be immediately rejected, or an *up-down strategy*, in which a failed test causes a repetition of a previous test. Figures 37 and 38 depict the flow graphs of the consecutive-count and up-down strategies, respectively, that require  $D$  tests to be passed before acquisition is declared. If the threshold is not exceeded during test 1, the cell fails the test, and the next cell is tested. If it is exceeded, the cell passes the test, the search is stopped, and the system enters the *verification mode*. The same cell is tested again, but the dwell time and the threshold may be changed. Once all the verification tests have been passed, the code tracking is activated, and the system enters the *lock mode*. In the lock mode, the lock detector continually verifies that code synchronization is maintained. If the lock detector decides that synchronization has been lost, *reacquisition* begins in the search mode.

The order in which the cells are tested is determined by the general search strategy. Figure 39(a) depicts a *uniform search* over the  $q$  cells of the *timing uncertainty region*. The broken lines represent the discontinuous transitions of the search from the one part of the uncertainty region to another. The *broken-center Z search*, illustrated in Figure 39(b), is appropriate when *a priori* information makes part of the uncertainty region more likely to

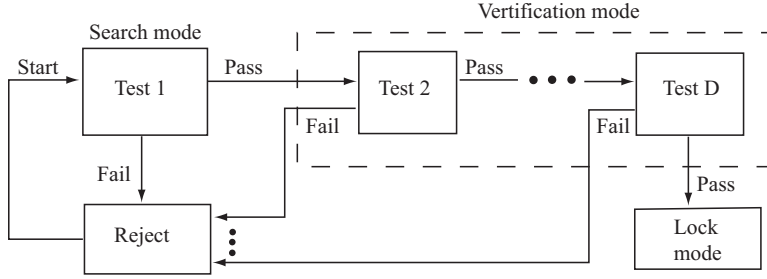


Figure 37. Flow graph of multiple-dwell system with consecutive-count strategy.

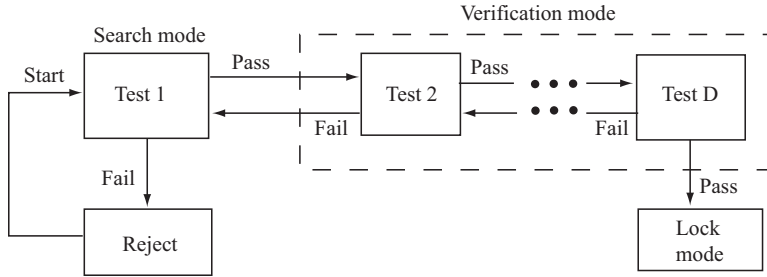


Figure 38. Flow graph of multiple-dwell system with up-down strategy.

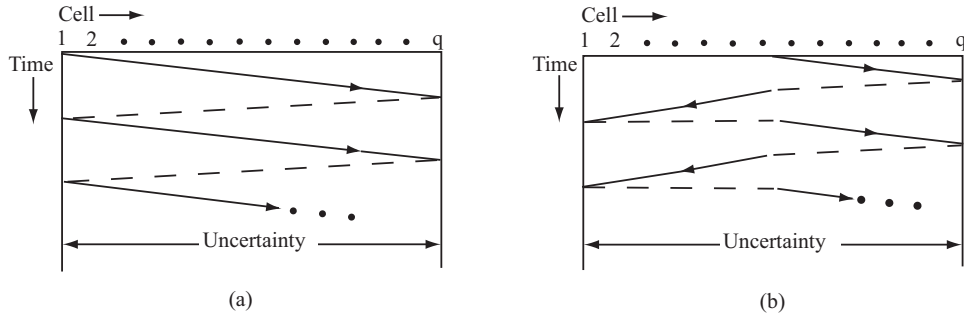


Figure 39. Trajectories of search positions: (a) uniform search and (b) broken-center  $Z$  search.

contain the correct cell than the rest of the region. *A priori* information may be derived from the detection of a short preamble. If the sequences are synchronized with the time of day, then the receiver's estimate of the transmitter range combined with the time of day provide the *a priori* information.

The *acquisition time* is the amount of time required for an acquisition system to locate the correct cell and initiate the code tracking system. To derive the statistics of the acquisition time [13], one of the  $q$  possible cells is considered the correct cell, and the other  $(q - 1)$  cells are incorrect. The difference in timing offsets among cells is  $\Delta T_c$ , where the *step size*  $\Delta$  is usually either 1 or  $1/2$ . However, it is convenient to allow the correct cell to include two or more timing offsets or code phases. Let  $L$  denote the number of times the correct cell is tested before it is accepted and acquisition terminates. Let  $C$  denote the number of the

correct cell and  $\pi_j$  denote the probability that  $C = j$ . Let  $\nu(L, C)$  denote the number of incorrect cells tested during the acquisition process. The functional dependence is determined by the search strategy. Let  $T_r(L, C)$  denote the total *rewinding time* it takes the search to move discontinuously within the uncertainty region. Since an incorrect cell is always ultimately rejected, there are only three types of events that occur during a serial search. Either the  $n$ th incorrect cell is dismissed after  $T_{11}(n)$  seconds, a correct cell is falsely dismissed for the  $m$ th time after  $T_{12}(m)$  seconds, or a correct cell is accepted after  $T_{22}$  seconds, where the first subscript is 1 if dismissal occurs, and 2 otherwise; the second subscript is 1 if the cell is incorrect, and 2 otherwise. Each of these decision times is a random variable assumed to be identically distributed for each cell to which it applies. If an incorrect cell is accepted, the receiver eventually recognizes the mistake and reinitiates the search at the next cell. The wasted time expended in code tracking is called the *penalty time*.

From the preceding definitions, it follows that the acquisition time is the random variable given by

$$T_a = \sum_{n=1}^{\nu(L,C)} T_{11}(n) + \sum_{m=1}^{L-1} T_{12}(m) + T_{22} + T_r(L, C) \quad (7-10)$$

The most important performance measures of the serial search are the mean and variance of  $T_a$ . Given  $L = i$  and  $C = j$ , the conditional expected value of  $T_a$  is

$$E [T_a | i, j] = \nu(i, j) \bar{T}_{11} + (i - 1) \bar{T}_{12} + \bar{T}_{22} + T_r(i, j) \quad (7-11)$$

where  $\bar{T}_{11}$ ,  $\bar{T}_{12}$ , and  $\bar{T}_{22}$  are the expected values of each  $T_{11}(n)$ ,  $T_{12}(m)$ , and  $T_{22}$ , respectively. Therefore, the mean acquisition time is

$$\bar{T}_a = \bar{T}_{22} + \sum_{i=1}^{\infty} P_L(i) \sum_{j=1}^q \pi_j [\nu(i, j) \bar{T}_{11} + (i - 1) \bar{T}_{12} + T_r(i, j)] \quad (7-12)$$

where  $P_L(i)$  is the probability that  $L = i$ . We assume that the test statistics are independent and identically distributed. Therefore,

$$P_L(i) = P_D (1 - P_D)^{i-1} \quad (7-13)$$

where  $P_D$  is the probability that the correct cell is detected when it is tested during a scan of the uncertainty region.

After calculating the conditional expected value of  $T_a^2$  given that  $L = i$  and  $C = j$ , and using the identity  $\overline{x^2} = \text{var}(x) + \bar{x}^2$ , we obtain

$$\begin{aligned} \overline{T_a^2} &= \sum_{i=1}^{\infty} P_L(i) \sum_{j=1}^q \pi_j \{ [\nu(i, j) \bar{T}_{11} + (i - 1) \bar{T}_{12} + \bar{T}_{22} + T_r(i, j)]^2 \\ &\quad + \nu(i, j) \text{var}(T_{11}) + (i - 1) \text{var}(T_{12}) + \text{var}(T_{22}) \} \end{aligned} \quad (7-14)$$

The variance of  $T_a$  is

$$\sigma_a^2 = \overline{T_a^2} - \bar{T}_a^2 \quad (7-15)$$

In some applications, the serial-search acquisition must be completed within a specified period of duration  $T_{max}$ . If the acquisition time exceeds  $T_{max}$ , the serial search is terminated, and special measures are undertaken. For example, matched-filter acquisition of a short sequence. The probability that  $T_a \leq T_{max}$  can be bounded by using Chebyshev's inequality (Appendix A):

$$\begin{aligned} P(T_a \leq T_{max}) &\geq P(|T_a - \bar{T}_a| \leq T_{max} - \bar{T}_a) \\ &\geq 1 - \frac{\sigma_a^2}{(T_{max} - \bar{T}_a)^2} \end{aligned} \quad (7-16)$$

where  $P(A)$  denotes the probability of the event  $A$ .

### Uniform search with uniform *a priori* distribution

As an important application, we consider the uniform search of Figure 39(a) and a uniform *a priori* distribution for the location of the correct cell given by

$$\pi_j = \frac{1}{q}, \quad 1 \leq j \leq 1. \quad (7-17)$$

If the cells in Figure 39(a) are labeled consecutively from left to right, then

$$\nu(i, j) = (i - 1)(q - 1) + j - 1 \quad (7-18)$$

If the rewinding time associated with each broken line is  $T_r$ , then

$$T_r(i, j) = T_r(i) = (i - 1)T_r \quad (7-19)$$

If the uncertainty region covers an entire sequence period, then the cells at the two edges are actually adjacent and  $T_r = 0$ .

To evaluate  $\bar{T}_a$  and  $\overline{T_a^2}$ , we substitute (7-13), (7-17), (7-18), and (7-19) into (7-12) and (7-14) and use the following identities:

$$\begin{aligned} \sum_{i=0}^{\infty} r^i &= \frac{1}{1-r}, & \sum_{i=1}^{\infty} ir^i &= \frac{r}{(1-r)^2}, & \sum_{i=1}^{\infty} i^2 r^i &= \frac{r(1+r)}{(1-r)^3} \\ \sum_{i=1}^n i &= \frac{n(n+1)}{2}, & \sum_{i=1}^n i^2 &= \frac{n(n+1)(2n+1)}{6} \end{aligned} \quad (7-20)$$

where  $0 \leq |r| < 1$ . Defining

$$\alpha = (q - 1)\bar{T}_{11} + \bar{T}_{12} + T_r \quad (7-21)$$

we obtain

$$\bar{T}_a = (q-1) \left( \frac{2-P_D}{2P_D} \right) \bar{T}_{11} + \left( \frac{1-P_D}{P_D} \right) (\bar{T}_{12} + T_r) + \bar{T}_{22} \quad (7-22)$$

and

$$\begin{aligned} \overline{T}_a^2 &= (q-1) \left( \frac{2-P_D}{2P_D} \right) \text{var}(T_{11}) + \left( \frac{1-P_D}{P_D} \right) \text{var}(T_{12}) + \text{var}(T_{22}) \\ &+ \frac{(2q+1)(q+1)}{6} \bar{T}_{11}^2 + \frac{\alpha^2(1-P_D)(2-P_D)}{P_D^2} + (q+1)\alpha \left( \frac{1-P_D}{P_D} \right) \\ &+ (q+1)\bar{T}_{11}(\bar{T}_{22} - \bar{T}_{11}) + 2\alpha \left( \frac{1-P_D}{P_D} \right) (\bar{T}_{22} - \bar{T}_{11}) + (\bar{T}_{22} - \bar{T}_{11})^2 \end{aligned} \quad (7-23)$$

In most applications, the number of cells to be searched is large, and simpler *asymptotic forms* for the mean and variance of the acquisition time are applicable. As  $q \rightarrow \infty$ , (7-22) gives

$$\bar{T}_a \rightarrow q \left( \frac{2-P_D}{2P_D} \right) \bar{T}_{11}, \quad q \rightarrow \infty \quad (7-24)$$

Similarly, (7-23) and (7-15) yield

$$\sigma_a^2 \rightarrow q^2 \left( \frac{1}{P_D^2} - \frac{1}{P_D} + \frac{1}{12} \right) \bar{T}_{11}^2, \quad q \rightarrow \infty \quad (7-25)$$

These equations must be modified in the presence of an uncorrected Doppler shift. The fractional change in the received chip rate of the spreading sequence is equal to the fractional change in the carrier frequency due to the Doppler shift. If the chip rate changes from  $1/T_c$  to  $1/T_c + \delta$ , then the average change in the code or sequence phase during the test of an incorrect cell is  $\delta\bar{T}_{11}$ . The change relative to the step size is  $\delta\bar{T}_{11}/\Delta$ . The number of cells that are actually tested in a sweep of the timing uncertainty region becomes  $q(1 + \delta\bar{T}_{11}/\Delta)^{-1}$ . Since incorrect cells predominate, the substitution of the latter quantity in place of  $q$  in (7-24) and (7-25) gives approximate asymptotic expressions for  $\bar{T}_a$  and  $\sigma_a^2$  when the Doppler shift is significant.

### Consecutive-count double-dwell system

For further specialization, consider the consecutive-count double-dwell system described by Figure 37 with  $D = 2$ . Assume that the *correct cell* actually subsumes two consecutive cells with detection probabilities  $P_a$  and  $P_b$ , respectively. If the test results are assumed to be statistically independent, then

$$P_D = P_a + (1 - P_a)P_b \quad (7-26)$$

Let  $\tau_1, P_{F1}, P_{a1}$ , and  $P_{b1}$  denote the search-mode dwell time, false-alarm probability, and successive detection probabilities, respectively. Let  $\tau_2, P_{F2}, P_{a2}$ , and  $P_{b2}$  denote the

verification-mode dwell time, false-alarm probability, and successive detection probabilities, respectively. Let  $\bar{T}_p$  denote the mean penalty time, which is incurred by the incorrect activation of the tracking mode. The flow graph indicates that since each cell must pass two tests,

$$P_a = P_{a1}P_{a2}, \quad P_b = P_{b1}P_{b2} \quad (7-27)$$

and

$$\bar{T}_{11} = \tau_1 + P_{F1} (\tau_2 + P_{F2}\bar{T}_p) \quad (7-28)$$

Equations (7-26) to (7-28) are all that is needed to evaluate the asymptotic values of the mean and variance given by (7-24) and (7-25). For a more accurate evaluation of the mean acquisition time, expressions for the conditional means  $\bar{T}_{22}$  and  $\bar{T}_{12}$  are needed. Expressing  $\bar{T}_{22}$  as the conditional expectation of the correct-cell test duration given cell detection, enumerating the possible durations and their conditional probabilities, and then simplifying, we obtain

$$\bar{T}_{22} = \tau_1 + \tau_2 + \tau_1 \frac{(1 - P_a) P_b}{P_D} + \tau_2 \frac{P_{a1} (1 - P_{a2}) P_b}{P_D} \quad (7-29)$$

Similarly,

$$\bar{T}_{12} = 2\tau_1 + \tau_2 \left[ \frac{P_{a1} (1 - P_{a2}) (1 - P_b) + (1 - P_a) P_{b1} (1 - P_{b2})}{1 - P_D} \right] \quad (7-30)$$

### Single-dwell and matched-filter systems

Results for a single-dwell system are obtained by setting

$P_{a2} = P_{b2} = P_{F2} = 1, \tau_2 = 0, P_a = P_{a1}, P_b = P_{b1}, P_{F1} = P_F$ , and  $\tau_1 = \tau_d$  in (7-28) to (7-30).

We obtain

$$\bar{T}_{11} = \tau_d + P_F \bar{T}_p, \quad \bar{T}_{22} = \tau_d \left[ 1 + \frac{(1 - P_a) P_b}{P_D} \right], \quad \bar{T}_{12} = 2\tau_d \quad (7-31)$$

Thus, (7-22) yields

$$\bar{T}_a = \frac{(q - 1) (2 - P_D) (\tau_d + P_F \bar{T}_p) + 2\tau_d (2 - P_a) + 2 (1 - P_D) T_r}{2P_D} \quad (7-32)$$

Since the single-dwell system may be regarded as a special case of the double-dwell system, the latter can provide a better performance by appropriate setting of its additional parameters.

The approximate mean acquisition time for a matched filter can be derived in a similar manner. Suppose that many periods of a short spreading sequence with  $N$  chips per period is received, and the matched-filter output is sampled  $m$  times per chip. Then the number of cells that are tested is  $q = mN$  and  $T_r = 0$ . Each sampled output is compared to a threshold so  $\tau_d = T_c/m$  is the time duration associated with a test. For  $m = 1$  or  $2$ , it is reasonable to regard two of the cells as the correct ones. These cells are effectively tested

when a signal period fills or nearly fills the matched filter. Thus, (7-26) is applicable with  $P_a \approx P_b$ , and (7-32) yields

$$\bar{T}_a \approx NT_c \left( \frac{2 - P_D}{2P_D} \right) (1 + mKP_F), \quad q \gg 1 \quad (7-33)$$

where  $K = \bar{T}_p/T_c$ . Ideally, the threshold is exceeded once per period, and the threshold crossing provides the timing marker that initiates the tracking system.

### Up-down double-dwell system

For the up-down double-dwell system with two correct cells, the flow graph of Figure 38 with  $D = 2$  indicates that

$$P_a = P_{a1}P_{a2} \sum_{i=0}^{\infty} [P_{a1}(1 - P_{a2})]^i = \frac{P_{a1}P_{a2}}{1 - P_{a1}(1 - P_{a2})} \quad (7-34)$$

Similarly,

$$P_b = \frac{P_{b1}P_{b2}}{1 - P_{b1}(1 - P_{b2})} \quad (7-35)$$

and  $P_D$  is given by (7-26). If an incorrect cell passes the initial test but fails the verification test, then the cell begins the testing sequence again without any memory of the previous testing. Therefore, for an up-down double-dwell system, a recursive evaluation gives

$$\begin{aligned} \bar{T}_{11} &= (1 - P_{F1})\tau_1 + P_{F1}P_{F2}(\tau_1 + \tau_2 + \bar{T}_p) + P_{F1}(1 - P_{F2})(\tau_1 + \tau_2 + \bar{T}_{11}) \\ &= \frac{\tau_1 + P_{F1}(\tau_2 + P_{F2}\bar{T}_p)}{1 - P_{F1}(1 - P_{F2})} \end{aligned} \quad (7-36)$$

Substitution of (7-34) to (7-36) into (7-24) to (7-26) gives the asymptotic values of the mean and variance of the acquisition time.

From the possible durations and their conditional probabilities, we obtain

$$\begin{aligned} \bar{T}_{22} &= \tau_1 + \tau_2 + P_{a1}(1 - P_{a2})\bar{T}_{22} + \frac{(1 - P_{a1})P_{b1}P_{b2}}{P_D}\tau_1 \\ &\quad + \frac{(1 - P_{a1})P_{b1}(1 - P_{b2})P_b}{P_D}(\tau_1 + \bar{T}'_{22}) \end{aligned} \quad (7-37)$$

where  $\bar{T}'_{22}$  is the expected delay for the detection of the correct cell given that the testing begins at the second correct cell. A recursive evaluation gives

$$\begin{aligned} \bar{T}'_{22} &= \tau_1 + \tau_2 + P_{b1}(1 - P_{b2})\bar{T}'_{22} \\ &= \frac{\tau_1 + \tau_2}{1 - P_{b1}(1 - P_{b2})} \end{aligned} \quad (7-38)$$

Similarly,  $\bar{T}_{12}$  is determined by the recursive equation

$$\begin{aligned}\bar{T}_{12} = & \tau_1 + \frac{(1 - P_{a1})(1 - P_{a2})}{1 - P_D} \tau_1 + P_{a1}(1 - P_{a2})(\tau_2 + \bar{T}_{12}) \\ & + \frac{(1 - P_{a1})P_{b1}(1 - P_{b2})(1 - P_b)}{1 - P_D} (\tau_1 + \tau_2 + \bar{T}'_{12})\end{aligned}\quad (7-39)$$

with

$$\bar{T}'_{12} = \frac{\tau_1 + P_{b1}(1 - P_{b2})\tau_2}{1 - P_{b1}(1 - P_{b2})}\quad (7-40)$$

## Penalty time

The *lock detector* that monitors the code synchronization in the lock mode performs tests to verify the lock condition. The time that elapses before the system incorrectly leaves the lock mode is called the *holding time*. It is desirable to have a large mean holding time and a small mean penalty time, but the realization of one of these goals tends to impede the realization of the other. As a simple example, suppose that each test has a fixed duration  $\tau$  and that code synchronization is actually maintained. A single missed detection, which occurs with probability  $1 - P_{DL}$ , causes the lock detector to assume a loss of lock and to initiate a search. Assuming the statistical independence of the lock-mode tests, the mean holding time is

$$\begin{aligned}\bar{T}_h &= \sum_{i=1}^{\infty} i\tau (1 - P_{DL}) P_{DL}^{i-1} \\ &= \frac{\tau}{1 - P_{DL}}\end{aligned}\quad (7-41)$$

This result may also be derived by recognizing that  $\bar{T}_h = \tau + P_{DL}\bar{T}_h$  because once the lock mode is verified, the testing of the same cell is renewed without any memory of the previous testing. If the locally generated code phase is incorrect, the penalty time expires unless false alarms, each of which occurs with probability  $P_{FL}$ , continue to occur every  $\tau$  seconds. A derivation similar to that of (7-41) yields the mean penalty time for a single-dwell lock detector:

$$\bar{T}_p = \frac{\tau}{1 - P_{FL}}\quad (7-42)$$

A tradeoff between a high  $\bar{T}_h$  and a low  $\bar{T}_p$  exists because increasing  $P_{DL}$  tends to increase  $P_{FL}$ .

When a single test verifies the lock condition, the synchronization system is vulnerable to deep fades and pulsed interference. A preferable strategy is for the lock mode to be maintained until a number of consecutive or cumulative misses occur during a series of tests. The performance analysis is analogous to that of serial-search acquisition.

## Other search strategies

In a *Z search*, no cell is tested more than once until all cells in the timing uncertainty region have been tested. Both strategies of Figure 39 are *Z searches*. A characteristic of the *Z search* is that

$$\nu(i, j) = (i - 1)(q - 1) + \nu(1, j) \quad (7-43)$$

where  $\nu(1, j)$  is the number of incorrect cells tested when  $P_D = 1$  and, hence,  $L = 1$ . For simplicity, we assume that  $q$  is even. For the broken-center *Z search*, the search begins with cell  $q/2 + 1$ , and

$$\nu(1, j) = \begin{cases} j - \frac{q}{2} - 1, & j \geq \frac{q}{2} + 1 \\ q - j, & j \leq \frac{q}{2} \end{cases} \quad (7-44)$$

whereas  $\nu(1, j) = j - 1$  for the uniform search. If the rewinding time is negligible, then (7-12), (7-13), and (7-43) yield

$$\bar{T}_a = \frac{1 - P_D}{P_D} [(q - 1)\bar{T}_{11} + \bar{T}_{12}] + \bar{T}_{22} + \bar{T}_{11}\nu(1) \quad (7-45)$$

where  $\nu(1)$  is the average number of incorrect cells tested when  $P_D = 1$ :

$$\nu(1) = \sum_{j=1}^q \nu(1, j)\pi_j \quad (7-46)$$

If  $C$  has a uniform distribution, then  $\nu(1)$  and, hence,  $\bar{T}_a$  are the same for both strategies. If the distribution of  $C$  is symmetrical about a pronounced central peak and  $P_D \approx 1$ , then a uniform search gives  $\nu(1) \approx q/2$ . Since a broken-center *Z search* usually ends almost immediately or after slightly more than  $q/2$  tests,

$$\nu(1) \approx 0 \left( \frac{1}{2} \right) + \frac{q}{2} \left( \frac{1}{2} \right) = \frac{q}{4} \quad (7-47)$$

which indicates that for large values of  $q$  and  $P_D$  close to unity, the broken-center *Z search* reduces  $\bar{T}_a$  approximately by a factor of 2 relative to its value for the uniform search.

An *expanding-window search* attempts to exploit the information in the distribution of  $C$  by continually retesting cells with high *a priori* probabilities of being the correct cell. Tests are performed on all cells within a radius  $R_1$  from the center. If the correct cell is not found, then tests are performed on all cells within an increased radius  $R_2$ . The radius is increased successively until the boundaries of the uncertainty region are reached. The expanding-window search then becomes a *Z search*. If the rewinding time is negligible and  $C$  is centrally peaked, then the broken-center search of Figure 40(a) is preferable to the continuous-center search of Figure 40(b) because the latter retests cells before testing all the cells near the center of the uncertainty region. In an *equiexpanding search*, the radii have the form

$$R_n = \frac{nq}{2N} \quad , \quad n = 1, 2, \dots, N \quad (7-48)$$

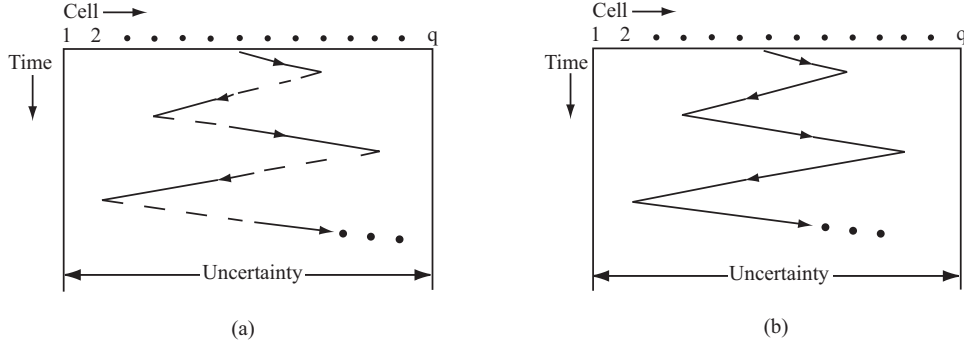


Figure 40. Trajectories of expanding-window search positions: (a) broken-center and (b) continuous-center search.

where  $N$  is the number of sweeps before the search becomes a Z search. If the rewinding time is negligible, then it can be shown [14] that the broken-center equiexpanding-window search is optimized for  $P_D \leq 0.8$  by choosing  $N = 2$ . For this optimized search,  $\bar{T}_a$  is moderately reduced relative to its value for the broken-center Z search.

When  $T_r(i, j) = 0$  and  $P_D = 1$ , the optimal search, which is called a *uniform alternating search*, tests the cells in order of decreasing *a priori* probability. For a symmetric, unimodal, centrally peaked distribution of  $C$ , this optimal search has the trajectory depicted in Figure 41(a). Once all the cells in the uncertainty region have been tested, the search repeats the same pattern. Equations (7-43) and (7-45) are applicable. If  $P_D \approx 1$  and the distribution of  $C$  has a pronounced central peak, then  $\nu(1)$  is small, and (7-47) indicates that the uniform alternating search has an advantage over the broken-center expanding-window search when  $q \gg 4$  and the rewinding time for any discontinuous transition is much smaller than  $\bar{T}_{11}$ . However, computations show that this advantage dissipates as  $P_D$  decreases [14], which occurs because all cells are tested with the same

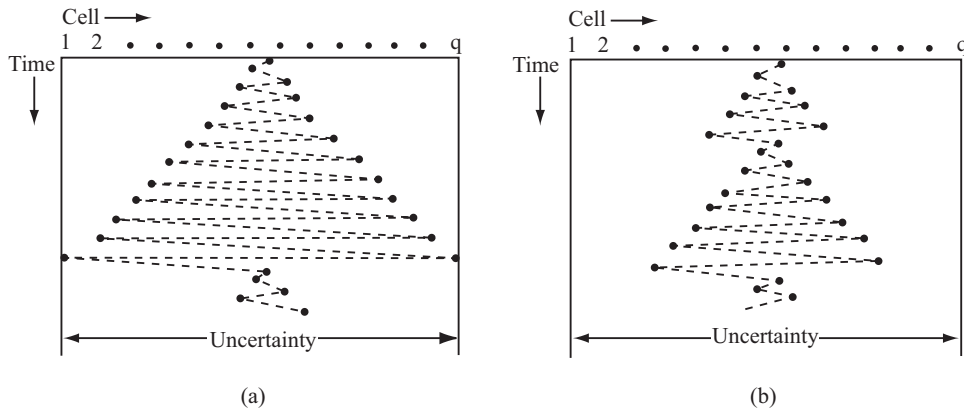


Figure 41. Trajectories of alternating search positions: (a) uniform search and (b) nonuniform search.

frequency without accounting for the distribution of  $C$ . In the *nonuniform alternating search*, illustrated in Figure 41(b), a uniform search is performed until a radius  $R_1$  is reached. Then a second uniform search is performed within a larger radius  $R_2$ . This process continues until the boundaries of the time uncertainty region are reached and the search becomes a uniform alternating search. Computations show that for a centrally peaked distribution of  $C$ , the nonuniform alternating search can give a significant improvement over the uniform alternating search if  $P_D < 0.8$ , and the radii  $R_n, n = 1, 2, \dots$ , are optimized [14]. However, if the radii are optimized for  $P_D < 1$ , then the nonuniform search becomes inferior to the uniform search as  $P_D \rightarrow 1$ .

### Density function of the acquisition time

The density function of  $T_a$  is needed to accurately calculate  $P(T_a \leq T_{max})$  and other probabilities. However, the exact calculation of the density [15] is complicated because the penalty time is, in general, a random variable that depends on the method of lock detection. The density function of  $T_a$  may be decomposed as

$$f_a(t) = P_D \sum_{i=1}^{\infty} (1 - P_D)^{i-1} \sum_{j=1}^q \pi_j f_a(t|i, j) \quad (7-49)$$

where  $f_a(t|i, j)$  is the conditional density of  $T_a$  given that  $L = i$  and  $C = j$ . Let  $*$  denote the convolution operation,  $[f(t)]^{*n}$  denote the  $n$ -fold convolution of the density  $f(t)$  with itself,  $[f(t)]^{*0} = 1$ , and  $[f(t)]^{*1} = f(t)$ . Using this notation, we obtain

$$f_a(t|i, j) = [f_{11}(t)]^{*\nu(i, j)} * [f_{12}(t)]^{*(i-1)} * [f_{22}(t)] \quad (7-50)$$

where  $f_{11}(f)$ ,  $f_{12}(t)$ , and  $f_{22}(t)$  are the densities associated with  $T_{11}$ ,  $T_{12}$ , and  $T_{22}$ , respectively. If one of the decision times is a constant, then the associated density is a delta function.

Since the acquisition time conditioned on  $L = i$  and  $C = j$  is the sum of independent random variables, it is reasonable to approximate  $f_a(t|i, j)$  by a truncated Gaussian density with mean

$$\mu_{ij} = \nu(i, j)\bar{T}_{11} + (i - 1)\bar{T}_{12} + \bar{T}_{22} + T_r(i) \quad (7-51)$$

and variance

$$\sigma_{ij}^2 = \nu(i, j)var(T_{11}) + (i - 1)var(T_{12}) + var(T_{22}) \quad (7-52)$$

The truncation is such that  $f_a(t|i, j) \neq 0$  only if  $0 \leq t \leq T_{max}$  or  $0 \leq t \leq \mu_{ij} + 3\sigma_{ij}$ . When  $P_D$  is large, the infinite series in (7-49) converges rapidly enough that the series can be accurately approximated by its first few terms.

## Alternative analysis

An alternative method of analyzing acquisition relies on transfer functions [16]. Each phase offset of the local code defines a *state* of the system. Of the total number of  $q$  states,  $q - 1$  are states that correspond to offsets (cells) that equal or exceed a chip duration. One state is a *collective state* that corresponds to all phase offsets that are less than a chip duration and, hence, cause acquisition to be terminated and code tracking to begin. The serial-search acquisition process is represented by its *circular state diagram*, a segment of which is illustrated in Figure 42. The *a priori* probability distribution  $\pi_j, j = 1, 2, \dots, q$ , gives the probability that the search begins in state  $j$ . The rewinding time is assumed to be negligible.

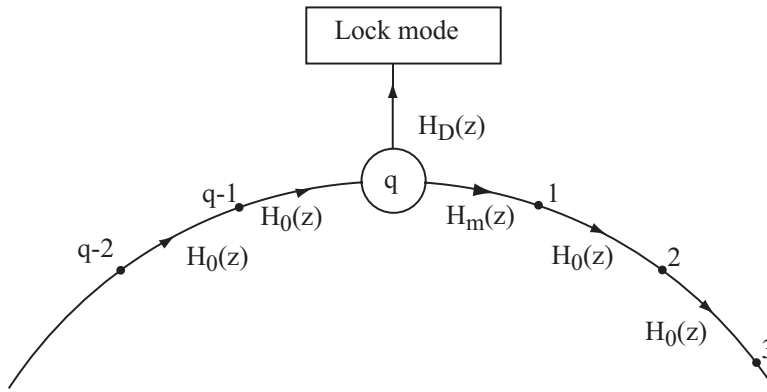


Figure 42. Circular state diagram for serial-search acquisition.

The branch labels between two states are transfer functions that contain information about the delays that may occur during the transition between the two states. Let  $z$  denote the unit-delay variable and let the power of  $z$  denote the time delay. A single-dwell system with dwell  $\tau$ , false-alarm probability  $P_F$ , and constant penalty time  $T_p$  has transfer function  $H_0(z) = (1 - P_F) z^\tau + P_F z^{\tau+T_p}$  for all branches that do not originate in collective state  $q$  because the transition delay is  $\tau$  with probability  $1 - P_F$  and  $\tau + T_p$  with probability  $P_F$ . For a multiple-dwell system,  $H_0(z)$  is determined by first drawing a subsidiary state diagram representing intermediate states and transitions that may occur as the system progresses from one state to the next one in the original circular state diagram. For example, Figure 43 illustrates the subsidiary state diagram for a consecutive-count double-dwell system with false alarms  $P_{F1}$  and  $P_{F2}$  and delays  $\tau_1$  and  $\tau_2$  for the initial test and the verification test, respectively. Examination of all possible paths between the initial state and the next state indicates that

$$\begin{aligned} H_0(z) &= (1 - P_{F1}) z^{\tau_1} + P_{F1} z^{\tau_1} [(1 - P_{F2}) z^{\tau_2} + P_{F2} z^{\tau_2+T_p}] \\ &= (1 - P_{F1}) z^{\tau_1} + P_{F1} (1 - P_{F2}) z^{\tau_1+\tau_2} + P_{F1} P_{F2} z^{\tau_1+\tau_2+T_p} \end{aligned} \quad (7-53)$$

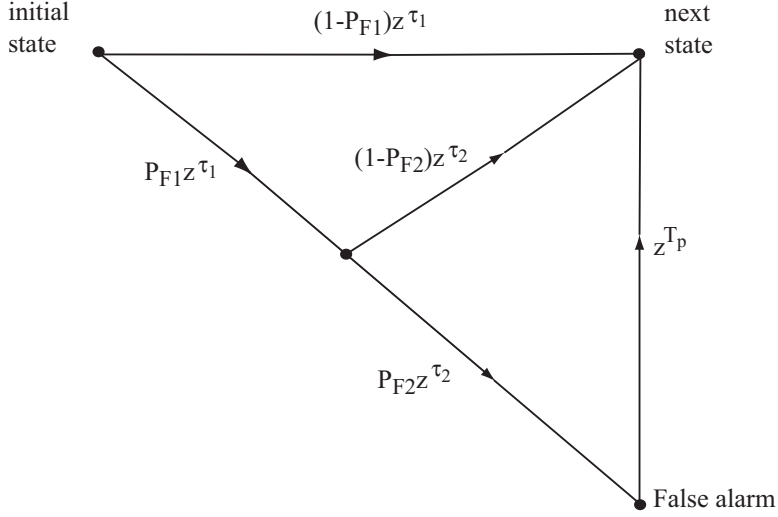


Figure 43. Subsidiary state diagram for determination of  $H_0(z)$  for consecutive-count double-dwell system.

Let  $H_D(z)$  denote the transfer function between the collective state  $q$  and the lock mode. Let  $H_M(z)$  denote the transfer function between state  $q$  and state 1, which represents the failure to recognize code-phase offsets that are less than a chip duration. These transfer functions may be derived in the same manner as  $H_0(z)$ . For example, consider a consecutive-count, double-dwell system with a collective state that comprises two states. Figure 44 depicts the subsidiary state diagram representing intermediate states and transitions that may occur as the system progresses from state  $q$  (with subsidiary states  $a$  and  $b$ ) to either the lock mode or state 1. Examination of all possible paths yields

$$\begin{aligned}
 H_D(z) = & P_{a1}P_{a2}z^{\tau_1+\tau_2} + P_{a1}(1 - P_{a2})P_{b1}P_{b2}z^{2\tau_1+2\tau_2} \\
 & + (1 - P_{a1})P_{b1}P_{b2}z^{2\tau_1+\tau_2}
 \end{aligned} \tag{7-54}$$

$$\begin{aligned}
 H_M(z) = & (1 - P_{a1})(1 - P_{b1})z^{2\tau_1} + (1 - P_{a1})P_{b1}(1 - P_{b2})z^{2\tau_1+\tau_2} \\
 & + P_{a1}(1 - P_{a2})(1 - P_{b1})z^{2\tau_1+\tau_2} \\
 & + P_{a1}(1 - P_{a2})P_{b1}(1 - P_{b2})z^{2\tau_1+2\tau_2}
 \end{aligned} \tag{7-55}$$

For a single-dwell system with a collective state that comprises  $N$  states,

$$H_D(z) = P_1z^\tau + \sum_{j=2}^N P_j \left[ \prod_{i=1}^{j-1} (1 - P_j) \right] z^{j\tau} \tag{7-56}$$

$$H_M(z) = \left[ \prod_{j=1}^N (1 - P_j) \right] z^{N\tau} \tag{7-57}$$

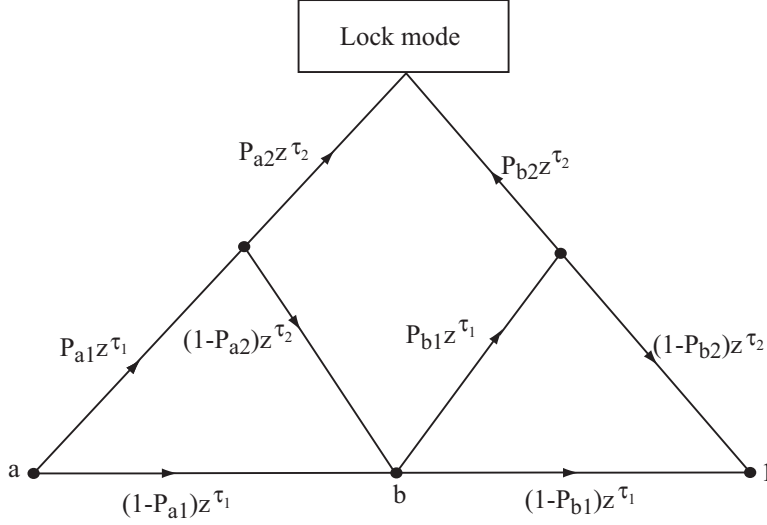


Figure 44. Subsidiary state diagram for calculation of  $H_D(z)$  and  $H_M(z)$  for consecutive-count double-dwell system with two-state collective state.

$$H_0(z) = (1 - P_F) z^\tau + P_F z^{\tau+T_p} \quad (7-58)$$

where  $\tau$  is the dwell time,  $P_F$  is the false-alarm probability, and  $P_j$  is the detection probability of state  $j$  within the collective state. To calculate the statistics of the acquisition time, we seek the *generating function* defined as the polynomial

$$H(z) = \sum_{i=0}^{\infty} p_i(\tau_i) z^{\tau_i} \quad (7-59)$$

where  $p_i(\tau_i)$  is the probability that the acquisition process will terminate in the lock mode after  $\tau_i$  seconds. If  $H(z)$  is known, then the mean acquisition time is

$$\bar{T}_a = \sum_{i=0}^{\infty} \tau_i p_i(\tau_i) = \left. \frac{dH(z)}{dz} \right|_{z=1} \quad (7-60)$$

The second derivative of  $H(z)$  gives

$$\left. \frac{d^2 H(z)}{dz^2} \right|_{z=1} = \sum_{i=0}^{\infty} \tau_i (\tau_i - 1) p_i(\tau_i) = \bar{T}_a^2 - \bar{T}_a \quad (7-61)$$

Therefore, the variance of the acquisition time is

$$\sigma_a^2 = \left\{ \left. \frac{d^2 H(z)}{dz^2} + \frac{dH(z)}{dz} - \left[ \frac{dH(z)}{dz} \right]^2 \right\} \right|_{z=1} \quad (7-62)$$

To derive  $H(z)$ , we observe that it may be expressed as

$$H(z) = \sum_{j=1}^q \pi_j H_j(z) \quad (7-63)$$

where  $H_j(z)$  is the transfer function from an initial state  $j$  to the lock mode. Since the circular state diagram of Figure 42 may be traversed an indefinite number of times during the acquisition process,

$$\begin{aligned} H_j(z) &= H_0^{q-j}(z)H_D(z) \sum_{i=0}^{\infty} [H_M(z)H_0^{q-1}(z)]^i \\ &= \frac{H_0^{q-j}(z)H_D(z)}{1 - H_M(z)H_0^{q-1}(z)} \end{aligned} \quad (7-64)$$

Substitution of this equation into (7-63) yields

$$H(z) = \frac{H_D(z)}{1 - H_M(z)H_0^{q-1}(z)} \sum_{j=1}^q \pi_j H_0^{q-j}(z) \quad (7-65)$$

The generating function may be expressed as the polynomial in (7-59) by means of polynomial long division.

For the uniform *a priori* distribution given by (7-17),

$$H(z) = \frac{H_D(z) [1 - H_0^q(z)]}{q [1 - H_M(z)H_0^{q-1}(z)] [1 - H_0(z)]} \quad (7-66)$$

Since the progression from one state to another is inevitable until the lock mode is reached,  $H_0(1) = 1$ . Since  $H_D(1) + H_M(1) = 1$ , (7-65) and (7-60) yield

$$\bar{T}_a = \frac{1}{H_D(1)} \left\{ H'_D(1) + H'_M(1) + (q-1)H'_0(1) \left[ 1 - \frac{H_D(1)}{2} \right] \right\} \quad (7-67)$$

where the prime indicates differentiation with respect to  $z$ . As an example, consider a single-dwell system with a two-state collective state. The evaluation of (7-67) using (7-56) to (7-58) with  $N = 2$  yields (7-32) with  $T_r = 0$  if we set  $P_1 = P_a, P_2 = P_b, T_p = \bar{T}_p, \tau = \tau_d$ , and define  $P_D$  by (7-26).

### 7.3 Acquisition Correlator

The noncoherent correlator of Figure 36 provides the approximate maximization of  $V(\tau) = R(\tau, 0)$  given by (7-9). It is assumed that chip synchronization is established by one of the standard methods of symbol synchronization. Consequently, the test interval can be defined with boundaries that coincide with chip boundaries, and we test code phases such that  $\tau = \nu T_c$ , where  $\nu$  is an integer. Let  $MT_c$  denote the duration of the test interval, where  $M$  is a positive integer. If the Doppler shift is not estimated,  $f_d$  may be absorbed into  $f_c$  in (7-9). If the test interval begins with chip  $\nu$  of the local spreading sequence, then (3-2) and (7-9) imply that the decision variable for one test of a specific code phase  $\nu T_c$  is

$$V = V_c^2 + V_s^2 \quad (7-68)$$

where

$$V_c = \sum_{k=0}^{M-1} p_{k-\nu} x_k, \quad V_s = \sum_{k=0}^{M-1} p_{k-\nu} y_k \quad (7-69)$$

$$x_k = \int_{kT_c}^{(k+1)T_c} r(t) \psi(t - kT_c) \cos 2\pi f_c t \, dt \quad (7-70)$$

$$y_k = \int_{kT_c}^{(k+1)T_c} r(t) \psi(t - kT_c) \sin 2\pi f_c t \, dt \quad (7-71)$$

The sequences  $\{x_k\}$  and  $\{y_k\}$  can be obtained by an in-phase and quadrature downconversions followed by chip-matched filters sampled at times  $t = kT_c$ . Thus, the acquisition correlator has the form depicted in Figure 45. The decision variable  $V$  is applied to a threshold detector to determine whether or not a test of a particular code phase is passed. If a quaternary data modulation is used instead of PSK, then the only modification necessary is that separate spreading sequence generators are assigned to the two parallel branches of the correlator.

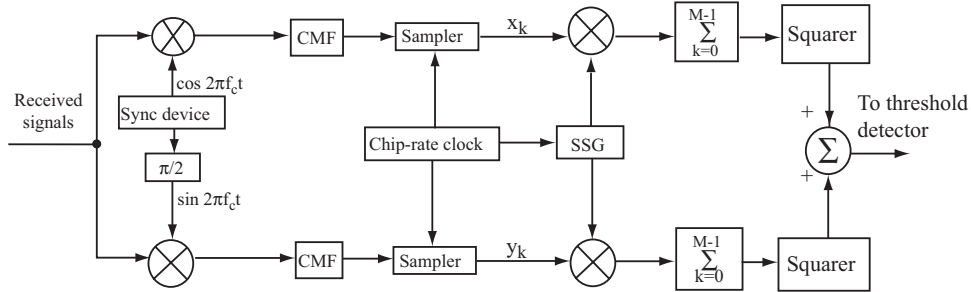


Figure 45. Noncoherent correlator for acquisition system. CMF = chip matched filter. SSG = spreading sequence generator.

The sequences  $\{x_k\}$  and  $\{y_k\}$  can be applied to multiple parallel inner products with different values of  $\nu$  simultaneously. This procedure allows a parallel search of various code phases with a moderate amount of additional hardware or software. Since  $p_k = \pm 1$ , each inner product may be computed by either adding or subtracting each component of  $\{x_k\}$  or  $\{y_k\}$ .

To analyze the performance of the acquisition correlator under fading conditions, we assume that the received signal is

$$r(t) = \sqrt{2S}\alpha p(t - \tau) \cos(2\pi f_c t + \theta) + n(t) \quad (7-72)$$

where  $\alpha$  is the attenuation due to fading,  $S$  is the average power when  $\alpha = 1$ ,  $p(t)$  is the spreading waveform,  $f_c$  is the carrier frequency,  $\theta$  is the random carrier phase,  $\tau$  is the delay due to the unknown code phase, and  $n(t)$  is the interference plus noise modeled as

additive white Gaussian noise. The data modulation  $d(t)$  is omitted because either it is not transmitted during acquisition or the test duration  $MT_c$  is much smaller than a symbol duration  $T_s = GT_c$ . In the latter case, the probability that a symbol transition occurs during a test is negligible, and the squaring operations eliminate the symbol value from  $V$ . Let  $\hat{\tau} = \nu T_c$  denote the delay associated with the code phase of the local spreading sequence. The difference between  $\hat{\tau}$  and  $\tau$  may be expressed in the form  $\hat{\tau} - \tau = NT_c + \epsilon T_c$ , where  $N$  is an integer and  $0 < \epsilon < 1$ . For a rectangular chip waveform, (7-69), (7-70), and (7-72),  $f_c T_c \gg 1$ , and the definition of chip  $\nu$  yield

$$V_c = \sqrt{\frac{S}{2}} \alpha T_c \cos \theta \sum_{k=0}^{M-1} p_{k-\nu} [(1-\epsilon) p_{k-\nu+N} + \epsilon p_{k-\nu+N+1}] + \sum_{k=0}^{M-1} p_{k-\nu} n_k \quad (7-73)$$

where

$$n_k = \int_{kT_c}^{(k+1)T_c} n(t) \psi(t - kT_c) \cos 2\pi f_c t \, dt \quad (7-74)$$

The alignment of the received and local spreading sequences is close enough for acquisition if  $N = -1$  or  $N = 0$ . If  $N \neq -1$  and  $N \neq 0$ , then the cell may be considered incorrect. The equation for  $V_s$  is the same as (7-74) except that  $-\sin \theta$  replaces  $\cos \theta$ , and  $n_k$  is given by (7-74) with  $\sin 2\pi f_c t$  replacing  $\cos 2\pi f_c t$ . The first term of  $V_c$  in (7-73) contributes *self-interference* that may cause a false alarm. The self-interference is small if the autocorrelation of the spreading sequence is sharply peaked. In a network of similar systems, interfering sequences are substantially suppressed if the cross-correlations among sequences are small, as they are if all the sequences are Gold or Kasami sequences (Section 9.2).

In the performance analysis, the spreading sequence  $\{p_k\}$  is modeled as a random binary sequence and  $\epsilon$  is modeled as a random variable. Thus, given the values of  $\alpha$  and  $\theta$ , the self-interference varies with respect to its mean value and, hence, degrades acquisition even when the noise term is negligible. If the variable part the self-interference is negligible, then (7-73) can be approximated by

$$V_c = E[V_c] + N_{gc} \quad (7-75)$$

where  $N_{gc}$  is the second term in (7-73). Since  $n(t)$  is zero-mean, white Gaussian noise,  $n_k$  is a zero-mean Gaussian random variable. Since  $p_{k-\nu} = \pm 1$  and is independent of  $n_k$ , the product  $p_{k-\nu} n_k$  is zero-mean and Gaussian. The independence of the terms in the sum then indicates that  $N_{gc}$  is a zero-mean Gaussian random variable. Similarly, we obtain the approximation

$$V_s = E[V_s] + N_{gs} \quad (7-76)$$

where  $N_{gs}$  is a zero-mean, Gaussian random variable. Straightforward calculations using  $f_c T_c \gg 1$  indicate that  $N_{gc}$  and  $N_{gs}$  are statistically independent with the same variance:

$$\sigma^2 = \text{var}(N_{gc}) = \text{var}(N_{gs}) = \frac{N_0 M T_c}{4} \quad (7-77)$$

To determine the condition under which the self-interference is well-approximated by its mean value, we calculate  $var(V_c)$ . Given  $\alpha, \theta$ , and  $\epsilon$ , (7-73) yields

$$var(V_c) = \frac{S\alpha^2 MT_c^2 \cos^2 \theta}{2} (2\epsilon^2 - 2\epsilon + 1) + \frac{N_0 MT_c}{4} \quad (7-78)$$

where  $g(\epsilon) = \epsilon^2$  if  $N = 0$ ,  $g(\epsilon) = (1 - \epsilon)^2$  if  $N = -1$ , and  $g(\epsilon) = 2\epsilon^2 - 2\epsilon + 1$  if  $N \neq 0, -1$ . The first term is much smaller than the second term if  $\mathcal{E}_c/N_0 \ll 1$ , where  $\mathcal{E}_c = S\alpha^2 T_c$  is the energy per chip. This condition is satisfied with high probability in most practical systems, especially if  $N_0$  incorporates the power spectral densities due to multiple-access interference and multipath signals. Accordingly, we proceed with the analysis using the approximations (7-75) and (7-76). Without these approximations, alternative approximations and assumptions are necessary or the analysis becomes much more complicated [17]. A common approximation is that  $\epsilon \approx 0$ . If  $\hat{\tau} - \tau \geq T_c$ , then a cell is incorrect and (7-73) with  $N \neq -1, 0$  implies that  $E[V_c] = E[V_s] = 0$ . If  $\hat{\tau} - \tau < T_c$ , the values of  $E[V_c]$  and  $E[V_s]$  depend on the step size of the serial search, which is denoted by  $\Delta$ . When  $\Delta = 1$ , two consecutive cells are considered correct. If  $\hat{\tau} - \tau$  is increasing, then the cell corresponding to  $N = -1$  occurs first and is followed by the cell corresponding to  $N = 0$ . If  $\epsilon$  is assumed to be uniformly distributed over  $(0,1)$  and  $N_1 = -1$  or  $0$ , then (7-73) and the similar equation for  $V_s$  yield the conditional means given  $\alpha$  and  $\theta$ :

$$E[V_c] = \sqrt{\frac{S}{2}} \frac{\alpha MT_c \cos \theta}{2}, \quad E[V_s] = -\sqrt{\frac{S}{2}} \frac{\alpha MT_c \sin \theta}{2}, \quad \Delta = 1 \quad (7-79)$$

When  $\Delta = 1/2$ , the two consecutive cells with the smallest values of  $\hat{\tau} - \tau$  are considered the two correct cells. For all the others, we assume that  $E[V_c] \approx E[V_s] \approx 0$ . The first correct cell corresponds to  $N = -1$  and  $1/2 \leq \epsilon < 1$ , whereas the second one corresponds to  $N = 0$  and  $0 < \epsilon \leq 1/2$ . If  $\epsilon$  is assumed to be uniformly distributed over the latter intervals, then for both cells, we obtain

$$E[V_c] = \sqrt{\frac{S}{2}} \frac{3\alpha MT_c \cos \theta}{4}, \quad E[V_s] = -\sqrt{\frac{S}{2}} \frac{3\alpha MT_c \sin \theta}{4}, \quad \Delta = \frac{1}{2} \quad (7-80)$$

Let  $V_1$  denote the decision variable  $V$  when the correct cell is tested, and let  $V_0$  denote  $V$  when the incorrect cell is tested. Equations (7-68), (7-75), and (7-76) and the preceding analysis indicate that  $V_0$  is the sum of the squares of two independent, zero-mean Gaussian random variables. The results of Appendix B then indicate that  $V_0$  has a central chi-square distribution with two degrees of freedom and a probability density function

$$f_c(x) = \frac{1}{2\sigma^2} \exp\left(-\frac{x}{2\sigma^2}\right) u(x) \quad (7-81)$$

where  $u(x) = 1, x \geq 0$ , and  $u(x) = 0, x < 0$ , and  $\sigma^2 = var(N_{gc}) = var(N_{gs})$ . The false-alarm probability for a test of an incorrect cell is the probability that  $V_0 > V_t$ , where

$V_t$  is the threshold. The integration of (7-81) gives the false-alarm probability:

$$P_f = \exp\left(-\frac{V_t}{2\sigma^2}\right) \quad (7-82)$$

Similarly, given  $\alpha$  and  $\theta$ ,  $V_1$  is the sum of the squares of two independent Gaussian random variables with nonzero means. The results of Appendix B then indicate that  $V_1$  has a noncentral chi-square distribution with two degrees of freedom and a probability density function

$$f_1(x) = \frac{1}{2\sigma^2} \exp\left(-\frac{\lambda+x}{2\sigma^2}\right) I_0\left(\frac{\sqrt{\lambda x}}{\sigma^2}\right) u(x) \quad (7-83)$$

where

$$\lambda = (E[V_c])^2 + (E[V_s])^2 = \frac{9}{32} f S \alpha^2 M^2 T_c^2 \quad (7-84)$$

and

$$f = \begin{cases} 1, & \Delta = 1/2 \\ 4/9, & \Delta = 1 \end{cases} \quad (7-85)$$

The detection probability for a test of a correct cell is the probability that  $V_1 > V_t$ . The integration of (7-83) and the substitution of (7-84) gives the detection probability

$$P_d = Q_1\left(\sqrt{\xi}\alpha, \frac{\sqrt{V_t}}{\sigma}\right) \quad (7-86)$$

where  $Q_1(\cdot)$  is the generalized  $Q$ -function defined by (B-15),

$$\xi = \frac{9}{8} f M \frac{\mathcal{E}_c}{N_0} \quad (7-87)$$

and  $\mathcal{E}_c = ST_c$  is the signal energy per chip when fading is absent and  $\alpha = 1$ .

Combining (7-86) and (7-82) yields

$$P_d = Q_1\left(\sqrt{\xi}\alpha, \sqrt{-2 \ln P_f}\right) \quad (7-88)$$

Thus, if  $P_f$  is specified,  $P_d$  is given by (7-88). The threshold needed to realize a specified  $P_f$  is

$$V_t = -\frac{N_0 M T_c}{2} \ln P_f \quad (7-89)$$

which requires an accurate estimate of  $N_0$ .

In the presence of fast Rayleigh fading,  $\alpha$  has the Rayleigh probability density (Appendix B-4):

$$f_\alpha(x) = 2x \exp(-x^2)u(x) \quad (7-90)$$

where  $E[\alpha^2] = 1$  so that  $S$  remains the average signal power in (7-72). It is assumed that  $\alpha$  is approximately constant during a test, but independent from test-to-test. Since (7-86) is conditioned on  $\alpha$ , the detection probability in the presence of fast fading is

$$P_d = \int_0^\infty 2x \exp(-x^2) Q_1\left(\sqrt{\xi}x, \sqrt{-2 \ln P_f}\right) dx \quad (7-91)$$

To evaluate this integral, we substitute the integral definition of  $Q_1(\cdot)$  given by (B-15), interchange the order of integration in the resulting double integral, and then use (B-33) to evaluate one of the integrals. The remaining integration over an exponential function is elementary. The final result is

$$P_d = P_f^{2/(2+\xi)} \quad (7-92)$$

For slow Rayleigh fading with a coherence time much larger than the acquisition time, it is appropriate to use (7-86) in calculating the conditional mean acquisition time and then integrate over the Rayleigh density to obtain the mean acquisition time.

Let  $C$  denote the number of chips in the time uncertainty region. The *normalized mean acquisition times* (NMAT) is defined as  $\bar{T}_a/CT_c$ . The *normalized standard deviation* (NSD) is defined as  $\sigma_a/CT_c$ .

### Example 1

As an example of the application of the preceding results, consider a single-dwell system with a uniform search and a uniform *a priori* correct-cell location distribution. Let  $\tau_d = MT_c$ , where  $M$  is the number of chips per test, and  $\bar{T}_p = KT_c$ , where  $K$  is the number of chips in the mean penalty time. It is assumed that there are two independent correct cells with the common detection probability  $P_d = P_a = P_b$ . If  $q \gg 1$ , (7-32) and (7-26) yield the NMAT:

$$\frac{\bar{T}_a}{CT_c} = \left(\frac{2 - P_D}{2P_D}\right) \frac{q}{C} (M + KP_F) \quad (7-93)$$

where

$$P_D = 2P_d - P_d^2 \quad (7-94)$$

In a single-dwell system,  $P_F = P_f$ , which is given by (7-82). For step size  $\Delta = 1, q/C = 1$ ; for  $\Delta = 1/2, q/C = 2$ . In the absence of fading, (7-88) relates  $P_d$  and  $P_f$ , whereas (7-92) relates them in the presence of fast Rayleigh fading

Figure 46 shows the NMAT as a function of  $\mathcal{E}_c/N_0$  for fast Rayleigh fading and no fading. At each value of  $\mathcal{E}_c/N_0$ , the values of  $P_f$  and  $M$  are selected to minimize the NMAT. The figure indicates the advantage of  $\Delta = 1/2$  when  $K \geq 10^5$  and the advantage of  $\Delta = 1$  when  $K \leq 10^4$ . The large increase in the NMAT due to fast Rayleigh fading is apparent. From (7-25), it is found that each plot of the NSD is similar to that of the corresponding NMAT.

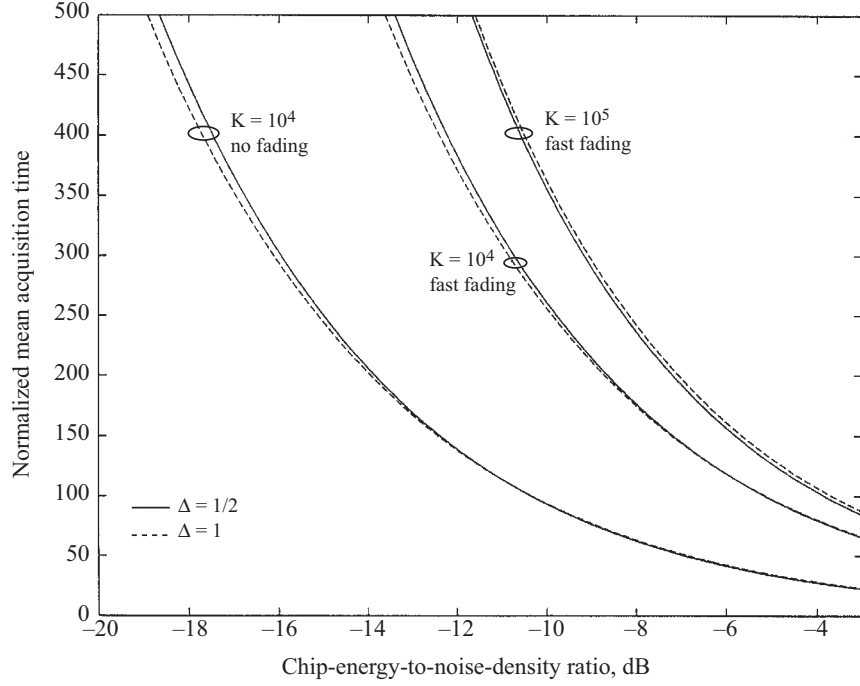


Figure 46. NMAT versus  $\mathcal{E}_c/N_0$  for single-dwell system in presence of fast Rayleigh fading or no fading. Values of  $P_f$  and  $M$  are optimized.

## Example 2

Consider double-dwell systems with a uniform search, a uniform *a priori* correct-cell location distribution, and two independent correct cells with  $P_d = P_a = P_b$ ,  $P_{a1} = P_{b1}$ , and  $P_{a2} = P_{b2}$ . The test durations are  $\tau_1 = M_1 T_c$  and  $\tau_2 = M_2 \tau_c$ . If  $q \gg 1$ , the NMAT is obtained from (7-24) and (7-94), where  $\bar{T}_{11}$  is given by (7-28) for a consecutive-count system and (7-36) for an up-down system. By replacing  $P_d$  with  $P_{ai}$  and  $P_f$  with  $P_{Fi}$ , the probabilities  $P_{ai}$  and  $P_{Fi}$ ,  $i = 1$  or  $2$ , are related through (7-88) with  $\alpha = 1$  for no fading and (7-92) for fast Rayleigh fading.

Figure 47 shows the NMAT as a function of  $\mathcal{E}_c/N_0$  for double-dwell systems in the presence of fast Rayleigh fading. The step size is  $\Delta = 1/2$ , which is found to be advantageous for the parameter values chosen. At each value of  $\mathcal{E}_c/N_0$ , the values of  $P_{F1}$ ,  $P_{F2}$ ,  $M_1$ , and  $M_2$  are selected to minimize the NMAT. The figure illustrates the advantage of the up-down system in most practical applications. From (7-25), it is found that each plot of the NSD is similar to that of the corresponding NMAT. A comparison of Figure 47 with Figure 46 indicates that double-dwell systems are capable of significantly lowering the NMAT relative to a single-dwell system.  $\square$

The existence of two consecutive correct cells can be directly exploited in *joint two-cell detection*, which can be shown to provide a lower NMAT than the conventional cell-by-cell

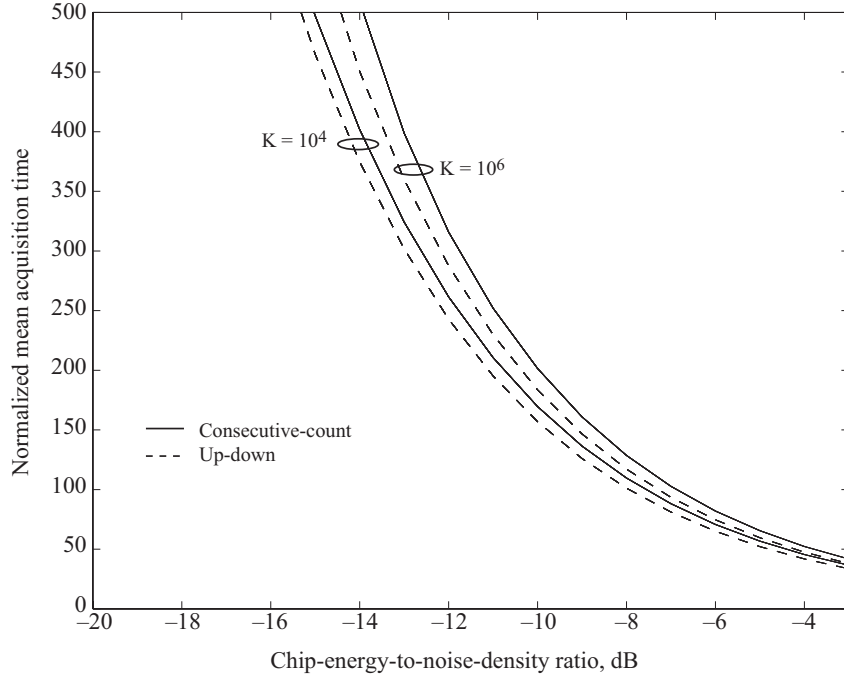


Figure 47. NMAT versus  $\mathcal{E}_c/N_0$  for double-dwell systems in presence of fast Rayleigh fading. Step size is  $\Delta = 1/2$ . Values of  $P_{F1}$ ,  $P_{F2}$ ,  $M_1$ , and  $M_2$  are optimized.

detection [18]. In the presence of frequency-selective fading with a large number of resolvable multipath signals, the NMAT of serial-search acquisition is usually increased because the increased self-interference is more significant than the higher number of nonconsecutive correct cells with correct phases. However, joint two-cell detection is more resistant to multiple-access interference and more robust against variations in the detection threshold, the power level of the desired signal, and the number of multipath signals. The advantage of joint two-cell detection over cell-by-cell detection is the result of the efficient combining of the energy of two adjacent correct-phase samples. The detection threshold of (7-89) depends on an estimate of  $N_0$ , the equivalent noise-power spectral density. An accurate estimate usually requires a long observation interval. However, in mobile communication systems and in the presence of jamming, the instantaneous interference power may be rapidly varying. To cope with this environment, an adaptive threshold may be set by the instantaneous received power [19]. As a result, the mean acquisition time is lowered relative to its value for nonadaptive schemes when Rayleigh fading or pulsed Gaussian noise jamming is present. When a rake receiver (Section 7.8) is used, each finger of the receiver must acquire the timing of a separate multipath signal. Whether matched filtering or a serial search is used, some mechanism is needed to ensure that each finger acquires a distinct multipath signal [20].

An alternative to acquisition tests of fixed dwell time or number of detector samples is *sequential detection*, which uses only the number necessary for a reliable decision. Thus,

some sample sequences may allow a quick decision, while others may warrant using a large number of samples in the evaluation of a single phase of the spreading waveform. The *sequential probability ratio test* [2], [3] entails the recalculation of the likelihood ratio after each new detector sample is produced. This ratio is compared with both upper and lower thresholds to determine if the test is terminated and no more samples need to be extracted. If the upper threshold is exceeded, the receiver declares acquisition and the lock mode is entered. If the likelihood ratio drops below the lower threshold, the test fails, and another code phase is tested. As long as the likelihood ratio lies between the two thresholds, a decision is postponed and the ratio continues to be updated. Although the sequential detector is capable of significantly reducing the mean acquisition time relative to detectors that use a fixed number of detector samples, it has a number of practical limitations. Chief among them is the computational complexity of the calculation of the likelihood ratio or log-likelihood ratio.

#### 7.4 Code Tracking

Coherent code-tracking loops operate at baseband following the coherent removal of the carrier of the received signal. An impediment to their use is that the input signal-to-noise ratio is usually too low for carrier synchronization prior to code synchronization and the subsequent despreading of the received signal. Furthermore, coherent loops cannot easily accommodate the effects of data modulation. Noncoherent loops operate directly on the received signal and are unaffected by the data modulation.

To motivate the design of the noncoherent loop, one may adapt the statistic (7-9). If the maximum-likelihood estimate  $\hat{\tau}$  is assumed to be within the interior of its uncertainty region and  $R(\tau, f_d)$  is a differentiable function of  $\tau$ , then the estimate  $\hat{\tau}$  that maximizes  $R(\tau, f_d)$  may be found by setting

$$\left. \frac{\partial R(\tau, f_d)}{\partial \tau} \right|_{\tau=\hat{\tau}} = 0 \quad (7-95)$$

A major problem with this approach is that  $R(\tau, f_d)$  given by (7-9) is not differentiable if the chip waveform is rectangular. This problem is circumvented by using a difference equation as an approximation of the derivative. Thus, for a positive  $\delta T_c$ , we set

$$\frac{\partial R(\tau, f_d)}{\partial \tau} \approx \frac{R(\tau + \delta T_c, f_d) - R(\tau - \delta T_c, f_d)}{2\delta T_c} \quad (7-96)$$

This equation implies that the solution of (7-95) may be approximately obtained by a device that finds the  $\hat{\tau}$  such that

$$R(\hat{\tau} + \delta T_c, f_d) - R(\hat{\tau} - \delta T_c, f_d) = 0 \quad (7-97)$$

To derive an alternative to this equation, we assume that no noise is present,  $f_d = 0$ , and that the correct timing offset of the received signal is  $\tau = 0$ . Substituting (7-2) with  $\tau = 0$  into (7-9) and using trigonometry, we obtain

$$R(\hat{\tau}, 0) = \frac{S}{2} \left[ \int_0^T p(t)p(t - \hat{\tau})dt \right]^2 \quad (7-98)$$

If  $p(t)$  is modeled as the spreading waveform for a random binary sequence and the interval  $[0, T]$  includes many chips, then the integral is reasonably approximated by its expected value, which is proportional to the autocorrelation

$$R_p(\tau) = \Lambda\left(\frac{\tau}{T_c}\right) \quad (7-99)$$

Substituting this result into (7-97), we find that the maximum-likelihood estimate is approximately obtained by a device that finds the  $\hat{\tau}$  such that

$$R_p^2(\hat{\tau} + \delta T_c) - R_p^2(\hat{\tau} - \delta T_c) = 0 \quad (7-100)$$

The noncoherent *delay-locked loop* [21], which is diagrammed in Figure 48, implements an approximate computation of the difference on the left-hand side of (7-100) and then continually adjusts  $\hat{\tau}$  so that this difference remains near zero. The estimate is used to produce the synchronized local spreading sequence that is used for despreading the received direct-sequence signal. The code generator produces three sequences, one of which is the reference sequence used for acquisition and demodulation. The other two sequences are advanced and delayed, respectively, by  $\delta T_c$  relative to the reference sequence. The product  $\delta T_c$  is usually equal to the acquisition step size, and thus usually  $\delta = 1/2$ , but other values are plausible. The advanced and delayed sequences are multiplied by the received direct-sequence signal in separate branches. The advanced and delayed sequences are multiplied by the received

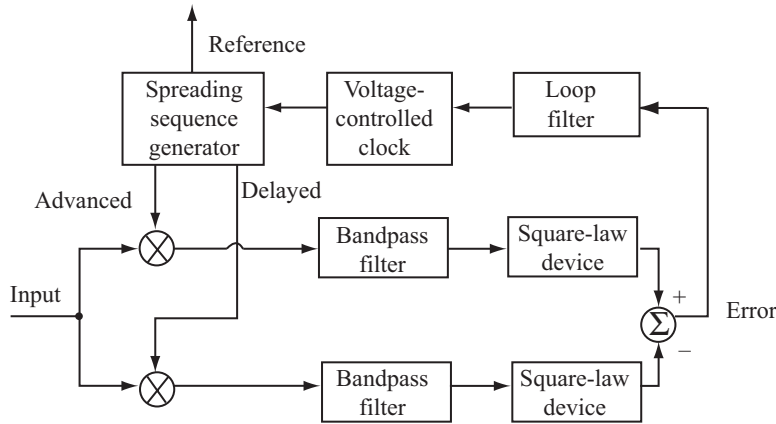


Figure 48. Delay-locked loop.

For the received direct-sequence signal (7-2), the signal portion of the upper-branch mixer output is

$$s_{u1}(t) = Ad(t)p(t)p(t + \delta T_c - \epsilon T_c) \cos(2\pi f_c t + \theta) \quad (7-101)$$

where  $A = \sqrt{2S}$  and  $\epsilon T_c$  is the delay of the reference sequence relative to the received sequence. Although  $\epsilon$  is a function of time because of the loop dynamics, the time dependence is suppressed for notational convenience. Since each bandpass filter has a bandwidth on the order of  $1/T_s$ , where  $T_s$  is the duration of each symbol,  $d(t)$  is not significantly distorted by the filtering. Nearly all spectral components except the slowly varying expected value of  $p(t)p(t + \delta T_c - \epsilon T_c)$  are blocked by the upper-branch bandpass filter. Since this expected value is the autocorrelation of the spreading sequence, the filter output is

$$s_{u2}(t) \approx Ad(t)R_p(\delta T_c - \epsilon T_c) \cos(2\pi f_c t + \theta) \quad (7-102)$$

Any double-frequency component produced by the square-law device is ultimately suppressed by the loop filter and thus is ignored. Since  $d^2(t) = 1$ , the data modulation is removed, and the upper-branch output is

$$s_{u3}(t) \approx \frac{A^2}{2} R_p^2(\delta T_c - \epsilon T_c) \quad (7-103)$$

Similarly, the output of the lower branch is

$$s_{l3}(t) \approx \frac{A^2}{2} R_p^2(-\delta T_c - \epsilon T_c) \quad (7-104)$$

The difference between the outputs of the two branches is the *error signal*:

$$s_e(t) \approx \frac{A^2}{2} [R_p^2(\delta T_c - \epsilon T_c) - R_p^2(-\delta T_c - \epsilon T_c)] \quad (7-105)$$

Since  $R_p(\tau)$  is an even function, the error signal is proportional to the left-hand side of (7-100).

The substitution of (7-99) and (2-8) into (7-105) yields

$$s_e(t) \approx \frac{A^2}{2} S(\epsilon, \delta) \quad (7-106)$$

where  $S(\epsilon, \delta)$  is the *discriminator characteristic* or *S-curve* of the tracking loop. For  $0 \leq \delta \leq 1/2$ ,

$$S(\epsilon, \delta) = \begin{cases} 4\epsilon(1 - \delta), & 0 \leq \epsilon \leq \delta \\ 4\delta(1 - \epsilon), & \delta \leq \epsilon \leq 1 - \delta \\ 1 + (\epsilon - \delta)(\epsilon - \delta - 2), & 1 - \delta \leq \epsilon \leq 1 + \delta \\ 0, & 1 + \delta \leq \epsilon \end{cases} \quad (7-107)$$

For  $1/2 \leq \delta \leq 1$ ,

$$S(\epsilon, \delta) = \begin{cases} 4\epsilon(1 - \delta), & 0 \leq \epsilon \leq 1 - \delta \\ 1 + (\epsilon - \delta)(\epsilon - \delta + 2), & 1 - \delta \leq \epsilon \leq \delta \\ 1 + (\epsilon - \delta)(\epsilon - \delta - 2), & \delta \leq \epsilon \leq 1 + \delta \\ 0, & 1 + \delta \leq \epsilon \end{cases} \quad (7-108)$$

In both cases,

$$S(-\epsilon, \delta) = -S(\epsilon, \delta) \quad (7-109)$$

Figure 49 illustrates the discriminator characteristic for  $\delta = 1/2$ . The filtered error signal is applied to the voltage-controlled clock. Changes in the clock frequency cause the reference sequence to converge toward alignment with the received spreading sequence. When  $0 < \epsilon(t) < 1 + \delta$ , the reference sequence is delayed relative to the received sequence. As shown in Figure 49,  $S(\epsilon, \delta)$  is positive, so the clock rate is increased, and  $\epsilon(t)$  decreases. The figure indicates that  $s_e(t) \rightarrow 0$  as  $\epsilon(t) \rightarrow 0$ . Similarly, when  $\epsilon(t) < 0$ , we find that  $s_e(t) \rightarrow 0$  as  $\epsilon(t) \rightarrow 0$ . Thus, the delay-locked loop tracks the received code timing once the acquisition system has finished the coarse alignment.

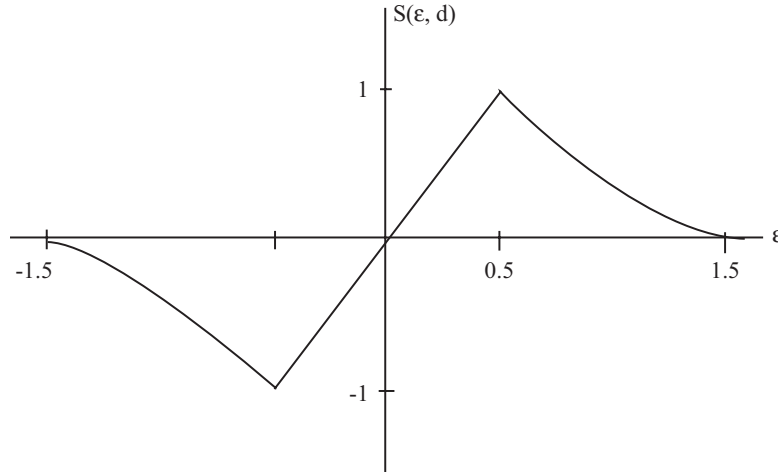


Figure 49. Discriminator characteristic of delay-locked loop for  $\delta = 1/2$ .

The discriminator characteristic of code-tracking loops differs from that of phase-locked loops in that it is nonzero only within a finite range of  $\epsilon$ . Outside that range, code tracking cannot be sustained, the synchronization system loses lock, and a reacquisition search is initiated by the lock detector. Tracking resumes once the acquisition system reduces  $\epsilon$  to within the range for which the discriminator characteristic is nonzero.

When short spreading sequences are used in a synchronous direct-sequence network, the reduced randomness in the multiple-access interference (Section 10) may cause increased

tracking jitter or even an offset in the discriminator characteristic [22]. For orthogonal sequences, the interference is zero when synchronization exists, but becomes large when there is a code-phase error in the local spreading sequence. In the presence of a tracking error, the delay-locked-loop arm with the larger offset relative to the correct code phase receives relatively more noise power than the other arm. This disparity reduces the slope of the discriminator characteristic and, hence, degrades the tracking performance. Moreover, because of the nonsymmetric character of the crosscorrelations among the spreading sequences, the discriminator characteristic may be biased in one direction, which will cause a tracking offset.

The main components of a noncoherent *tau-dither loop* are depicted in Figure 50. The dither generator controls a switch that alternately passes an advanced or delayed local sequence. Let  $D(t)$  denote the *dither signal*, a square wave that alternates between +1 and -1. In the absence of noise, the output of the switch can be represented by

$$s_1(t) = \left[ \frac{1 + D(t)}{2} \right] p(t + \delta T_c - \epsilon T_c) + \left[ \frac{1 - D(t)}{2} \right] p(t - \delta T_c - \epsilon T_c) \quad (7-110)$$

where the two factors within brackets are orthogonal functions of time and alternate between +1 and 0. Only one of the factors is nonzero at any instant. The received direct-sequence signal is multiplied by  $s_1(t)$ , filtered, and then applied to a square-law device. If the bandpass filter has a sufficiently narrow bandwidth, then a derivation similar to that of (7-103) indicates that the device output is

$$s_2(t) \approx \frac{A^2}{2} \left[ \frac{1 + D(t)}{2} \right] R_p^2(\delta T_c - \epsilon T_c) + \frac{A^2}{2} \left[ \frac{1 - D(t)}{2} \right] R_p^2(-\delta T_c - \epsilon T_c) \quad (7-111)$$

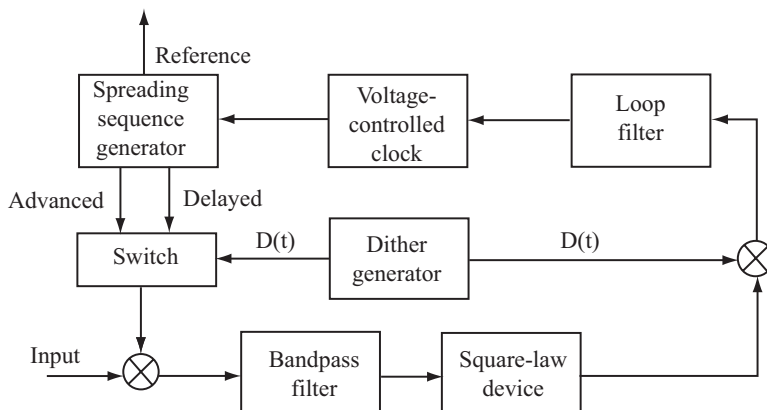


Figure 50. Tau-dither loop.

Since  $D(t)[1 + D(t)] = 1 + D(t)$  and  $D(t)[1 - D(t)] = -[1 - D(t)]$ , the input to the loop filter is

$$s_3(t) \approx \frac{A^2}{2} \left[ \frac{1 + D(t)}{2} \right] R_p^2 (\delta T_c - \epsilon T_c) - \frac{A^2}{2} \left[ \frac{1 - D(t)}{2} \right] R_p^2 (-\delta T_c - \epsilon T_c) \quad (7-112)$$

which is a rectangular wave if the time variation of  $\epsilon$  is ignored. Since the loop filter has a narrow bandwidth relative to that of  $D(t)$ , its output is approximately the direct-current component of  $s_3(t)$ , which is the average value of  $s_3(t)$ . Averaging the two terms of (7-112), we obtain the filter output:

$$s_4(t) \approx \frac{A^2}{4} [R_p^2 (\delta T_c - \epsilon T_c) - R_p^2 (-\delta T_c - \epsilon T_c)] \quad (7-113)$$

The substitution of (7-99) yields the clock input:

$$s_4(t) = \frac{A^2}{4} S(\epsilon, \delta) \quad (7-114)$$

where the discriminator characteristic is given by (7-107) to (7-109). Thus, the tau-dither loop can track the code timing in a manner similar to that of the delay-locked loop. The tau-dither loop requires less hardware than the delay-locked loop and eliminates the need to balance the gains and delays in the two branches of the delay-locked loop. However, a detailed analysis indicates that the tau-dither loop provides less accurate code tracking [2], [3].

In the presence of frequency-selective fading, the discriminator characteristics of tracking loops are severely distorted. Much better performance is potentially available from a noncoherent tracking loop with diversity and multipath-interference cancellation [23], but a large increase in implementation complexity is required.

---

## 8. Rejection of Narrowband Interference

---

Narrowband interference presents a crucial problem for *spread-spectrum overlay systems*, which are systems that have been assigned a spectral band already occupied by narrowband communication systems. Jamming against tactical spread-spectrum communications is another instance of narrowband interference that may exceed the natural resistance of a practical spread-spectrum system, which has a limited processing gain. There are a wide variety of techniques that supplement the inherent ability of a direct-sequence system to reject narrowband interference [24], [25]. All of the techniques directly or indirectly exploit the spectral disparity between the narrowband interference and the wideband direct-sequence signal. The most useful methods can be classified as

time-domain adaptive filtering, transform-domain processing, nonlinear filtering, or code-aided techniques. The general form of a receiver that rejects narrowband interference and demodulates a direct-sequence signal with binary PSK is shown in Figure 51. The processor, which follows the chip-rate sampling of a baseband signal.

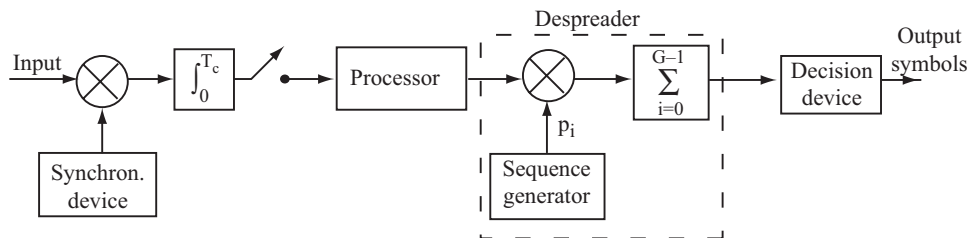


Figure 51. Direct-sequence receiver with processor for rejecting narrowband interference.

## 8.1 Time-Domain Adaptive Filtering

A time-domain *adaptive filter* [26] for interference suppression processes the baseband sample values of a received signal to adaptively estimate the interference. This estimate is subtracted from the sample values, thereby canceling the interference. The adaptive filter is primarily a predictive system that exploits the inherent predictability of a narrowband signal to form an accurate replica of it for the subtraction. Since the wideband desired signal is largely unpredictable, it does not significantly impede the prediction of a narrowband signal. When adaptive filtering is used, the processor in Figure 51 has the form of Figure 52(a). The adaptive filter may be a one-sided or two-sided transversal filter.

The *two-sided adaptive transversal filter* multiplies each tap output by a weight except for the central tap output, as diagrammed in Figure 52(b). This filter is an *interpolator* in that it uses *both* past and future samples to estimate the value to be subtracted. The two-sided filter provides a better performance than the one-sided filter, which is a *predictor*. The adaptive algorithm of the weight-control mechanism is designed to adjust the weights so that the power in the filter output is minimized. The direct-sequence components of the tap outputs, which are delayed by integer multiples of a chip duration, are largely uncorrelated with each other, but the narrowband interference components are strongly correlated. As a result, the adaptive algorithm causes the interference cancellation in the filter output, but the direct-sequence signal is largely unaffected.

An adaptive filter with  $2N + 1$  taps and  $2N$  weights, as shown in Figure 52(b), has input vector at iteration  $k$  given by

$$\mathbf{x}(k) = [x_1(k) \ x_2(k) \ \dots \ x_{2N}(k)]^T \quad (8-1)$$

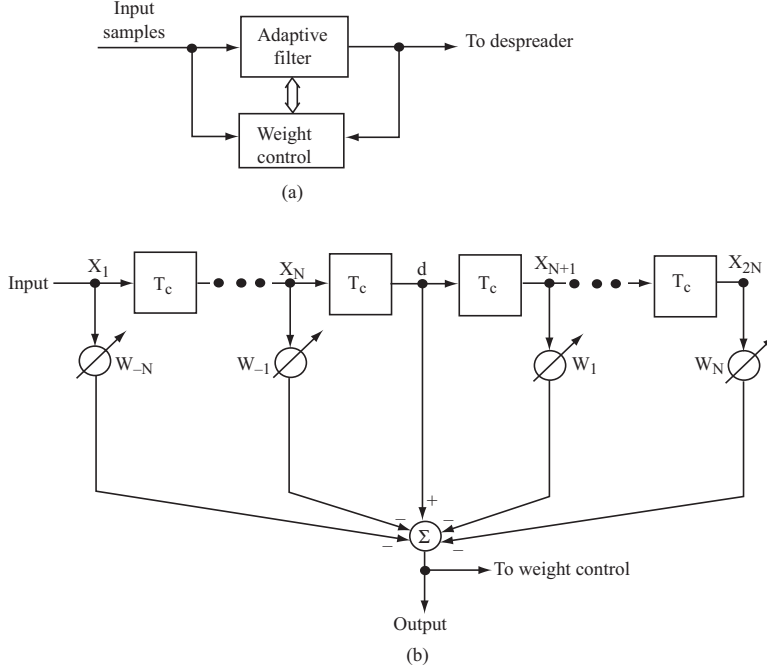


Figure 52. (a) Processor using adaptive filter and (b) two-sided adaptive transversal filter.

and weight vector

$$\mathbf{W}(k) = [W_{-N}(k) \ W_{-N+1}(k) \ \dots \ W_{-1}(k) \ W_1(k) \ \dots \ W_N(k)]^T \quad (8-2)$$

where  $T$  denotes the transpose and the central tap output, which is denoted by  $d$ , has been excluded from  $\mathbf{x}$ . Since coherent demodulation produces real-valued inputs to the adaptive filter,  $\mathbf{x}(k)$  and  $\mathbf{W}(k)$  are assumed to have real-valued components. The symmetric *correlation matrix* of  $\mathbf{x}$  is defined as  $\mathbf{R}_{xx} = E[\mathbf{x}\mathbf{x}^T]$ . The *cross-correlation vector* is defined as  $\mathbf{R}_{xd} = E[\mathbf{x}d]$ . According to the Wiener-Hopf equation (Appendix D), the optimal weight vector is

$$\mathbf{W}_0 = \mathbf{R}_{xx}^{-1} \mathbf{R}_{xd} \quad (8-3)$$

The least-mean-square (LMS) algorithm (Appendix D) computes the weight vector at iteration  $k$  as

$$\mathbf{W}(k) = \mathbf{W}(k-1) + \mu \epsilon_k \mathbf{x}(k) \quad (8-4)$$

where  $\epsilon_k = d - y_k$  is the estimation error,  $y_k = \mathbf{W}^T(k)\mathbf{x}(k)$  is the filter output, and  $\mu$  is the adaptation constant, which controls the rate of convergence of the algorithm. The output of the adaptive filter is  $\epsilon_k$ , which is applied to the despreader. Under certain conditions, the mean weight vector converges to  $\mathbf{W}_0$  after a number of iterations of the adaptive algorithm. If it is assumed that  $\mathbf{W} = \mathbf{W}_0$ , then a straightforward analysis indicates that the adaptive transversal filter provides a substantial suppression of narrowband interference [24]. Although the interference suppression increases with the number of taps, it is always

incomplete if the interference has a nonzero bandwidth because a finite-impulse-response filter can only place a finite number of zeros in the frequency domain.

The adaptive transversal filter is inhibited by the presence of direct-sequence components in the filter input vector  $\mathbf{x}(k)$ . These components can be suppressed by using decision-directed feedback, as shown in Figure 53. Previously detected symbols remodulate the spreading sequence delayed by  $G$  chips (long sequence) or one period of the spreading sequence (short sequence). After an amplitude compensation by a factor  $\eta$ , the resulting sequence provides estimates of the direct-sequence components of previous input samples. A subtraction then provides estimated sample values of the interference plus noise that are largely free of direct-sequence contamination. These samples are then applied to an adaptive transversal filter that has the form of Figure 52 except that it has no central tap. The transversal filter output consists of refined interference estimates that are subtracted from the input samples to produce samples that have relatively small interference components. An erroneous symbol from the decision device causes an enhanced direct-sequence component in samples applied to the transversal filter, and error propagation is possible. However, for moderate values of the signal-to-interference ratio at the input, the performance is not degraded significantly.

Adaptive filtering is only effective after the convergence of the adaptive algorithm, which may not be able to track time-varying interference. In contrast, transform-domain processing suppresses interference almost instantaneously.

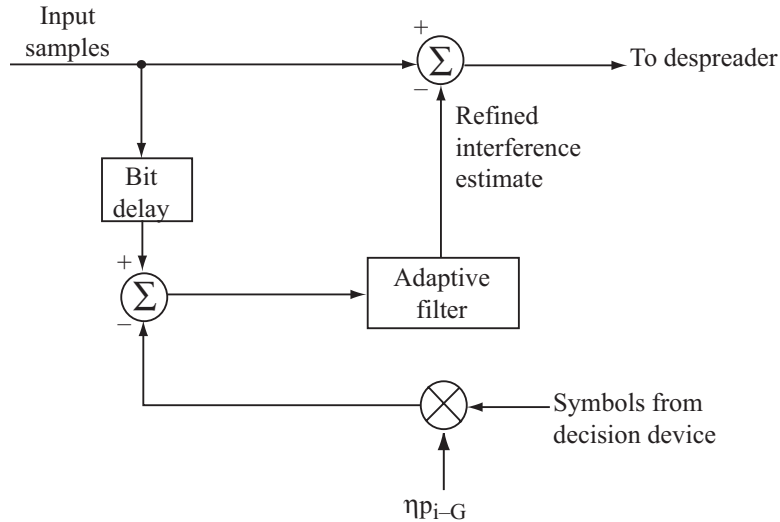


Figure 53. Processor with decision-directed adaptive filter.

## 8.2 Transform-Domain Processing

The input of a *transform-domain processor* could be a continuous-time received signal that feeds a real-time Fourier transformer implemented as a chirp transform processor [1]. In a more versatile implementation, which is depicted in Figure 54 and assumed henceforth, the input consists of the output samples of a chip-matched filter. Blocks of these samples feed a discrete-time Fourier or wavelet transformer. The transform is selected so that the transform-domain forms of the desired signal and interference are easily distinguished. Ideally, the transform produces interference components that are confined to a few transform bins while the desired-signal components have nearly the same magnitude in all the transform bins. A simple exciser can then suppress the interference with little impact on the desired signal by setting to zero the components in bins containing the interference. The decision as to which bins contain interference can be based on the comparison of each component to a threshold. After the excision operation, the desired signal is largely restored by the inverse transformer.

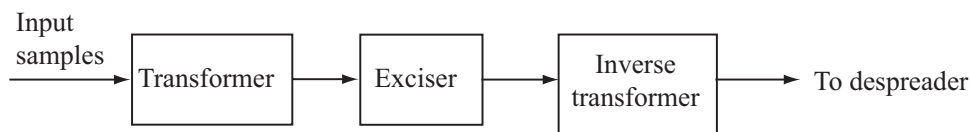


Figure 54. Transform-domain processor.

Much better performance against stationary narrowband interference may be obtained by using a transform-domain adaptive filter as the exciser [27]. This filter adjusts a single nonbinary weight at each transform-bin output. The adaptive algorithm is designed to minimize the difference between the weighted transform and a desired signal that is the transform of the spreading sequence used by the input block of the processor. If the direct-sequence signal uses the same short spreading sequence for each data symbol and each processor input block includes the chips for a single data symbol, then the desired-signal transform may be stored in a read-only memory. However, if a long spreading sequence is used, then the desired-signal transform must be continuously produced from the output of the receiver's code generator. The main disadvantage of the adaptive filter is that its convergence rate may be insufficient to track rapidly time-varying interference.

A transform that operates on disjoint blocks of  $N$  input samples may be defined in terms of  $N$  orthonormal,  $N$ -component basis vectors:

$$\phi_i = [\phi_{i1} \ \phi_{i2} \ \dots \ \phi_{iN}]^T, \quad i = 1, 2, \dots, N \quad (8-5)$$

which span a linear vector space of dimension  $N$ . Since the components may be complex numbers, the orthonormality implies that

$$\phi_i^H \phi_k = \begin{cases} 0, & i \neq k \\ 1, & i = k \end{cases} \quad (8-6)$$

where  $H$  denotes the complex conjugate of the transpose. The input block

$$\mathbf{x} = [x_1 \ x_2 \ \dots \ x_N]^T \quad (8-7)$$

may be expressed in terms of the basis as

$$\mathbf{x} = \sum_{i=1}^N c_i \phi_i \quad (8-8)$$

where

$$c_i = \phi_i^H \mathbf{x}, \quad i = 1, 2, \dots, N \quad (8-9)$$

If the discrete Fourier transform is used, then  $\phi_{ik} = \exp(j2\pi ik/N)$ , where  $j = \sqrt{-1}$ .

The transformer extracts the vector

$$\mathbf{c} = [c_1 \ c_2 \ \dots \ c_N]^T \quad (8-10)$$

by computing

$$\mathbf{c} = \mathbf{B}^H \mathbf{x} \quad (8-11)$$

where  $\mathbf{B}$  is the unitary matrix of basis vectors:

$$\mathbf{B} = [\phi_1 \ \phi_2 \ \dots \ \phi_N] \quad (8-12)$$

The exciser weights each component of the transform  $\mathbf{c}$  by computing

$$\mathbf{e} = \mathbf{W}_d \mathbf{c} \quad (8-13)$$

where  $\mathbf{W}_d$  is the  $N \times N$  diagonal weight matrix with diagonal elements  $W_1, W_2, \dots, W_N$ . The inverse transformer then produces the excised block that is applied to the despreader:

$$\mathbf{z} = [z_1 \ z_2 \ \dots \ z_N]^T = \mathbf{B} \mathbf{e} = \mathbf{B} \mathbf{W}_d \mathbf{c} = \mathbf{B} \mathbf{W}_d \mathbf{B}^H \mathbf{x} \quad (8-14)$$

If there were no weighting, then  $\mathbf{W}_d = \mathbf{I}$ . Since  $\mathbf{B}\mathbf{B}^H = \mathbf{I}$ ,  $\mathbf{z} = \mathbf{x}$  would result, as expected when the transformer and inverse transformer are in tandem. In general, the diagonal elements of  $\mathbf{W}_d$  are either set by a threshold device fed by  $\mathbf{c}$  or they are the outputs of the weight-control mechanism of an adaptive filter. When  $N$  equals the processing gain  $G$  and the input comprises the unmodulated spreading sequence, the despreader correlates its

input block with the appropriate segment of the spreading sequence to form the decision variable:

$$V = \sum_{i=1}^G p_i z_i \quad (8-15)$$

The filtering and despreading can be simultaneously performed in the transform domain. Let

$$\mathbf{p} = [p_1 \ p_2 \ \dots \ p_G]^T \quad (8-16)$$

denote a synchronous replica of the spreading sequence, which is generated by the receiver code generator. Then (8-14) to (8-16) give

$$V = \mathbf{p}^T \mathbf{z} = \mathbf{p}^T \mathbf{B} \mathbf{W}_d \mathbf{c} \quad (8-17)$$

Thus, if the spreading sequence is used to produce the matrix  $\mathbf{p}^T \mathbf{B} \mathbf{W}_d$ , then the product of this matrix and the transform  $\mathbf{c}$  gives  $V$  without the need for an inverse transformer and a separate despreader.

### 8.3 Nonlinear Filtering

By modeling the narrowband interference as part of a dynamical linear system, one can use the Kalman-Bucy filter [26] to extract an optimal linear estimate of the interference. A subtraction of this estimate from the filter input then removes a large part of the interference from the despreader input. However, a superior nonlinear filter can be designed by approximating an extension of the Kalman-Bucy filter.

Consider the estimation of an  $n \times 1$  state vector  $\mathbf{x}_k$  of a dynamical system based on the  $r \times 1$  observation vector  $\mathbf{z}_k$ . Let  $\phi_k$  denote the  $n \times n$  state transition matrix,  $\mathbf{H}_k$  an  $r \times n$  observation matrix, and  $\mathbf{u}_k$  and  $\mathbf{v}_k$  disturbance vectors of dimensions  $n \times 1$  and  $r \times 1$ , respectively. According to the linear dynamical system model, the state and observation vectors satisfy

$$\mathbf{x}_{k+1} = \phi_k \mathbf{x}_k + \mathbf{u}_k, \quad 0 \leq k < \infty \quad (8-18)$$

$$\mathbf{z}_k = \mathbf{H}_k \mathbf{x}_k + \mathbf{v}_k, \quad 0 \leq k < \infty \quad (8-19)$$

It is assumed that the sequences  $\{\mathbf{u}_k\}$ ,  $\{\mathbf{v}_k\}$  are independent sequences of independent, zero-mean random vectors that are also independent of the initial state  $\mathbf{x}_0$ . The covariance of  $\mathbf{u}_k$  is  $E[\mathbf{u}_k \mathbf{u}_k^T] = \mathbf{Q}_k$ . Let  $Z^k = (\mathbf{z}_1, \mathbf{z}_2, \dots, \mathbf{z}_k)$  denote the first  $k$  observation vectors. Let  $f(\mathbf{z}_k | Z^{k-1})$  and  $f(\mathbf{x}_k | Z^{k-1})$  denote the probability density functions of  $\mathbf{z}_k$  and  $\mathbf{x}_k$ , respectively, conditioned on  $Z^{k-1}$ . A fundamental result of estimation theory is that the estimate  $\hat{\mathbf{x}}_k$  that minimizes the mean-norm-squared error  $E[\|\mathbf{x}_k - \hat{\mathbf{x}}_k\|^2]$  is the expectation conditioned on  $Z^k$ :

$$\hat{\mathbf{x}}_k = E[\mathbf{x}_k | Z^k] \quad (8-20)$$

The corresponding conditional covariance is denoted by

$$\mathbf{P}_k = E \left[ (\mathbf{x}_k - \hat{\mathbf{x}}_k) (\mathbf{x}_k - \hat{\mathbf{x}}_k)^T \mid Z^k \right] \quad (8-21)$$

From (8-18), it follows that the expectation of  $\mathbf{x}_k$  conditioned on  $Z^{k-1}$  is

$$\bar{\mathbf{x}}_k = E \left[ \mathbf{x}_k \mid Z^{k-1} \right] = \phi_{k-1} \hat{\mathbf{x}}_{k-1} \quad (8-22)$$

The covariance of  $\mathbf{x}_k$  conditioned on  $Z^{k-1}$  is defined as

$$\mathbf{M}_k = E \left[ (\mathbf{x}_k - \bar{\mathbf{x}}_k) (\mathbf{x}_k - \bar{\mathbf{x}}_k)^T \mid Z^{k-1} \right] \quad (8-23)$$

The following theorem due to Masreliez [28] extends the Kalman-Bucy filter.

**Theorem.** Assume that  $f(\mathbf{x}_k \mid Z^{k-1})$  is a Gaussian density with mean  $\bar{\mathbf{x}}_k$  and  $n \times n$  covariance matrix  $\mathbf{M}_k$ , and that  $f(\mathbf{z}_k \mid Z^{k-1})$  is twice differentiable with respect to the components of  $\mathbf{z}_k$ . Then the conditional expectation  $\hat{\mathbf{x}}_k$  and the conditional covariance  $\mathbf{P}_k$  satisfy

$$\hat{\mathbf{x}}_k = \bar{\mathbf{x}}_k + \mathbf{M}_k \mathbf{H}_k^T \mathbf{g}_k(\mathbf{z}_k) \quad (8-24)$$

$$\mathbf{P}_k = \mathbf{M}_k - \mathbf{M}_k \mathbf{H}_k^T \mathbf{G}_k(\mathbf{z}_k) \mathbf{H}_k \mathbf{M}_k \quad (8-25)$$

$$\mathbf{M}_{k+1} = \phi_k \mathbf{P}_k \phi_k^T + \mathbf{Q}_k \quad (8-26)$$

$$\bar{\mathbf{x}}_{k+1} = \phi_k \hat{\mathbf{x}}_k \quad (8-27)$$

where  $\mathbf{g}_k(\mathbf{z}_k)$  is an  $r \times 1$  vector with components

$$\{\mathbf{g}_k(\mathbf{z}_k)\}_i = -\frac{1}{f(\mathbf{z}_k \mid Z^{k-1})} \frac{\partial f(\mathbf{z}_k \mid Z^{k-1})}{\partial z_{ki}} \quad (8-28)$$

$\mathbf{G}_k(\mathbf{z}_k)$  is an  $r \times r$  matrix with elements

$$\{\mathbf{G}_k(\mathbf{z}_k)\}_{ij} = \frac{\partial \{\mathbf{g}_k(\mathbf{z}_k)\}_i}{\partial z_{kj}} \quad (8-29)$$

and  $z_{kj}$  is the  $j$ th component of  $\mathbf{z}_k$ .

**Proof.** When  $\mathbf{x}_k$  is given, (8-19) indicates that  $\mathbf{z}_k$  is independent of  $Z^{k-1}$ . Therefore, Bayes' rule gives

$$f(\mathbf{x}_k \mid Z^k) = \frac{f(\mathbf{x}_k \mid Z^{k-1}) f(\mathbf{z}_k \mid \mathbf{x}_k)}{f(\mathbf{z}_k \mid Z^{k-1})} \quad (8-30)$$

With the concise notation  $b = [f(\mathbf{z}_k \mid Z^{k-1})]^{-1}$ , (8-20) and the fact that a density is a scalar function yield

$$\begin{aligned} \hat{\mathbf{x}}_k - \bar{\mathbf{x}}_k &= b \int_{R^n} (\mathbf{x}_k - \bar{\mathbf{x}}_k) f(\mathbf{z}_k \mid \mathbf{x}_k) f(\mathbf{x}_k \mid Z^{k-1}) d\mathbf{x}_k \\ &= b \mathbf{M}_k \int_{R^n} f(\mathbf{z}_k \mid \mathbf{x}_k) \mathbf{M}_k^{-1} (\mathbf{x}_k - \bar{\mathbf{x}}_k) f(\mathbf{x}_k \mid Z^{k-1}) d\mathbf{x}_k \end{aligned}$$

Using the Gaussian density  $f(\mathbf{x}_k|Z^{k-1})$ , (8-22), and (8-23), and then integrating by parts, we obtain

$$\begin{aligned}\hat{\mathbf{x}}_k - \bar{\mathbf{x}}_k &= -b\mathbf{M}_k \int_{R^n} f(\mathbf{z}_k|\mathbf{x}_k) \frac{\partial}{\partial \mathbf{x}_k} f(\mathbf{x}_k|Z^{k-1}) d\mathbf{x}_k \\ &= b\mathbf{M}_k \int_{R^n} f(\mathbf{x}_k|Z^{k-1}) \frac{\partial}{\partial \mathbf{x}_k} f(\mathbf{z}_k|\mathbf{x}_k) d\mathbf{x}_k\end{aligned}$$

where the  $n \times 1$  gradient vector  $\partial/\partial \mathbf{x}_k$  has  $\partial/\partial x_{ki}$  as its  $i$ th component. Equation (8-19) implies that

$$\begin{aligned}\frac{\partial}{\partial \mathbf{x}_k} f(\mathbf{z}_k|\mathbf{x}_k) &= \frac{\partial}{\partial \mathbf{x}_k} f_v(\mathbf{z}_k - \mathbf{H}_k \mathbf{x}_k) = -\mathbf{H}_k^T \frac{\partial}{\partial \mathbf{z}_k} f_v(\mathbf{z}_k - \mathbf{H}_k \mathbf{x}_k) \\ &= -\mathbf{H}_k^T \frac{\partial}{\partial \mathbf{z}_k} f(\mathbf{z}_k|\mathbf{x}_k)\end{aligned}$$

where  $f_v(\cdot)$  is the density of  $\mathbf{v}_k$ . Substitution of this equation into the preceding one gives

$$\begin{aligned}\hat{\mathbf{x}}_k - \bar{\mathbf{x}}_k &= -b\mathbf{M}_k \mathbf{H}_k^T \int_{R^n} f(\mathbf{x}_k|Z^{k-1}) \frac{\partial}{\partial \mathbf{z}_k} f(\mathbf{z}_k|\mathbf{x}_k) d\mathbf{x}_k \\ &= -b\mathbf{M}_k \mathbf{H}_k^T \frac{\partial}{\partial \mathbf{z}_k} \int_{R^n} f(\mathbf{x}_k|Z^{k-1}) f(\mathbf{z}_k|\mathbf{x}_k) d\mathbf{x}_k\end{aligned}$$

where the second equality results because  $f(\mathbf{x}_k|Z^{k-1})$  is not a function of  $\mathbf{z}_k$ . Substituting (8-30) into this equation and evaluating the integral, we obtain (8-24).

To derive (8-25), we add and subtract  $\bar{\mathbf{x}}_k$  in (8-21) and simplify, which gives

$$\mathbf{P}_k = E \left[ (\mathbf{x}_k - \bar{\mathbf{x}}_k) (\mathbf{x}_k - \bar{\mathbf{x}}_k)^T | Z^k \right] - (\hat{\mathbf{x}}_k - \bar{\mathbf{x}}_k) (\hat{\mathbf{x}}_k - \bar{\mathbf{x}}_k)^T$$

The second term of this equation may be evaluated by substituting (8-24). The first term may be evaluated in a similar manner as the derivation of (8-24) except that an integration by parts must be done twice. After a tedious calculation, we obtain (8-25). Equation (8-26) is derived by using the definition of  $\mathbf{M}_{k+1}$  given by (8-23) and then substituting (8-18), (8-22), and (8-21). Equation (8-27) follows from (8-22).  $\square$

The filter defined by this theorem is the Kalman-Bucy filter if  $f(\mathbf{z}_k|Z^{k-1})$  is a Gaussian density. Since (8-19) and (8-23) indicate that the covariance of  $\mathbf{z}_k$  conditioned on  $Z^{k-1}$  is  $\mathbf{H}_k \mathbf{M}_k \mathbf{H}_k^T + \mathbf{R}_k$ , where  $\mathbf{R}_k = E[\mathbf{v}_k \mathbf{v}_k^T]$ , a Gaussian density implies that

$$\mathbf{g}_k(\mathbf{z}_k) = (\mathbf{H}_k \mathbf{M}_k \mathbf{H}_k^T + \mathbf{R}_k)^{-1} (\mathbf{z}_k - \mathbf{H}_k \bar{\mathbf{x}}_k) \quad (8-31)$$

$$\mathbf{G}_k(\mathbf{z}_k) = (\mathbf{H}_k \mathbf{M}_k \mathbf{H}_k^T + \mathbf{R}_k)^{-1} \quad (8-32)$$

Substitution of these two equations into (8-24) and (8-25) yields the usual Kalman-Bucy equations.

To apply this theorem to the interference suppression problem, the narrowband interference sequence  $\{i_k\}$  at the filter input is modeled as an autoregressive process that satisfies

$$i_k = \sum_{l=1}^q \phi_l i_{k-l} + e_k \quad (8-33)$$

where  $e_k$  is a white Gaussian process with variance  $\sigma_e^2$  and the  $\{\phi_l\}$  are known to the receiver. The state-space representation of the system is

$$\mathbf{x}_k = \boldsymbol{\phi} \mathbf{x}_{k-1} + \mathbf{u}_k \quad (8-34)$$

$$z_k = \mathbf{H} \mathbf{x}_k + v_k \quad (8-35)$$

where

$$\mathbf{x}_k = [i_k \quad i_{k-1} \quad \dots \quad i_{k-q+1}]^T \quad (8-36)$$

$$\boldsymbol{\phi} = \begin{bmatrix} \phi_1 & \phi_2 & \dots & \phi_{q-1} & \phi_q \\ 1 & 0 & \dots & 0 & 0 \\ 0 & 1 & \dots & 0 & 0 \\ \vdots & \vdots & \dots & \vdots & \vdots \\ 0 & 0 & \dots & 1 & 0 \end{bmatrix} \quad (8-37)$$

$$\mathbf{u}_k = [e_k \quad 0 \quad \dots \quad 0]^T \quad (8-38)$$

$$\mathbf{H} = [1 \quad 0 \quad \dots \quad 0] \quad (8-39)$$

The observation noise  $v_k$  is the sum of the direct-sequence signal  $s_k$  and the white Gaussian noise  $n_k$ :

$$v_k = s_k + n_k \quad (8-40)$$

Since the first component of the state vector  $\mathbf{x}_k$  is the interference  $i_k$ , the state estimate  $\mathbf{H} \hat{\mathbf{x}}_k$  provides an interference estimate that can be subtracted from the received signal to cancel the interference.

For a random spreading sequence,  $s_k = +c$  or  $-c$  with equal probability. If  $n_k$  is zero-mean and Gaussian with variance  $\sigma_n^2$ , then  $v_k$  has the density

$$f_v(v) = \frac{1}{2} N_{\sigma_n^2}(v - c) + \frac{1}{2} N_{\sigma_n^2}(v + c) \quad (8-41)$$

where

$$N_{\sigma^2}(x) = \frac{1}{\sqrt{2\pi}\sigma} \exp\left(-\frac{x^2}{2\sigma^2}\right) \quad (8-42)$$

For this non-Gaussian density, the optimal filter that computes the exact conditional mean given by (8-20) is nonlinear with exponentially increasing complexity and, thus, is impractical. The density  $f(\mathbf{x}_k | Z^{k-1})$  is not Gaussian as required by Masreliez's theorem.

However, by assuming that this density is approximately Gaussian, we can use results of the theorem to derive the *approximate conditional mean* (ACM) filter [29].

Conditioned on  $Z^{k-1}$  and  $s_k$ , the expected value of  $z_k$  is  $\mathbf{H}\bar{\mathbf{x}}_k + s_k$  since  $\mathbf{x}_k$  and  $n_k$  are independent of  $s_k$ . From the definition of  $\mathbf{M}_k$  and (8-35), it follows that the conditional variance of  $z_k$  is

$$\sigma_z^2 = \mathbf{H} \mathbf{M}_k \mathbf{H}^T + \sigma_n^2 \quad (8-43)$$

Since  $f(\mathbf{x}_k|Z^{k-1})$  is approximated by a Gaussian density, we obtain

$$f(z_k | Z^{k-1}) = \frac{1}{2} N_{\sigma_z^2}(z_k - \mathbf{H}\bar{\mathbf{x}}_k - c) + \frac{1}{2} N_{\sigma_z^2}(z_k - \mathbf{H}\bar{\mathbf{x}}_k + c) \quad (8-44)$$

Substitution of this equation into (8-28) and (8-29) yields

$$g_k(z_k) = \frac{1}{\sigma_z^2} \left[ \epsilon_k - c \tanh\left(\frac{c\epsilon_k}{\sigma_z^2}\right) \right] \quad (8-45)$$

$$G_k(z_k) = \frac{1}{\sigma_z^2} \left[ 1 - \frac{c^2}{\sigma_z^2} \operatorname{sech}^2\left(\frac{c\epsilon_k}{\sigma_z^2}\right) \right] \quad (8-46)$$

where the *innovation* or prediction residual is

$$\epsilon_k = z_k - \mathbf{H}\bar{\mathbf{x}}_k = z_k - \bar{z}_k \quad (8-47)$$

and

$$\bar{z}_k = \mathbf{H}\bar{\mathbf{x}}_k \quad (8-48)$$

is the predicted observation based on  $Z^{k-1}$ . The update equations of the ACM filter are given by (8-24) to (8-27) and (8-45) to (8-48). The difference between the ACM filter and the Kalman-Bucy filter is the presence of the nonlinear *tanh* and *sech* functions in (8-45) and (8-46).

### Adaptive ACM filter

In practical applications, the elements of the matrix  $\phi$  in (8-37) are unknown and may vary with time. To cope with these problems, an adaptive algorithm that can track the interference is desirable. The *adaptive ACM filter* receives  $z_k = i_k + s_k + n_k$  and produces the interference estimate denoted by  $\bar{z}_k$ . The output of the filter is denoted by  $\epsilon_k = z_k - \bar{z}_k$  and ideally is  $s_k + n_k$  plus a small residual of  $i_k$ . An adaptive transversal filter is embedded in the adaptive ACM filter. To use the structure of the nonlinear ACM filter, we observe that the second term inside the brackets in (8-45) would be absent if  $s_k$  were absent. Therefore,  $c \tanh(c\epsilon_k/\sigma_z^2)$  may be interpreted as a soft decision on the direct-sequence signal  $s_k$ . The input to the adaptive transversal filter at time  $k$  is taken to be the difference between the observation  $z_k$  and the soft decision:

$$\tilde{z}_k = z_k - c \tanh\left(\frac{c\epsilon_k}{\sigma_z^2}\right) = \bar{z}_k + \rho(\epsilon_k) \quad (8-49)$$

where

$$\rho(\epsilon_k) = \epsilon_k - c \tanh\left(\frac{c\epsilon_k}{\sigma_z^2}\right) \quad (8-50)$$

The input  $\tilde{z}_k$  is a reasonable estimate of the interference that is improved by the adaptive filter. The architecture of the one-sided adaptive ACM filter [30] is shown in Figure 55.

The output of the N-tap transversal filter provides the interference estimate

$$\bar{z}_k = \mathbf{W}^T(k)\tilde{\mathbf{z}}_k \quad (8-51)$$

where  $\mathbf{W}(k)$  is the weight vector and

$$\tilde{\mathbf{z}}_k = [\tilde{z}_{k-1} \ \tilde{z}_{k-2} \ \dots \ \tilde{z}_{k-N}]^T \quad (8-52)$$

which is extracted from the filter taps. When  $\tilde{z}_k$  has only a small component due to  $s_k$ , the filter can effectively track the interference, and  $\bar{z}_k$  is a good estimate of this interference.

A normalized version of the LMS algorithm for the adaptive ACM filter is given by the weight-update equation:

$$\mathbf{W}(k) = \mathbf{W}(k-1) + \frac{\mu_0}{r_k} (\tilde{z}_k - \bar{z}_k) \tilde{\mathbf{z}}_k \quad (8-53)$$

where  $\mu_0$  is the adaptation constant and  $r_k$  is an estimate of the input power iteratively determined by

$$r_k = r_{k-1} + \mu_0 [|\tilde{z}_k|^2 - r_{k-1}] \quad (8-54)$$

The division by  $r_k$  in (8-53) normalizes the algorithm by making the choice of an appropriate  $\mu_0$  for fast convergence and good performance much less dependent on the input power level.

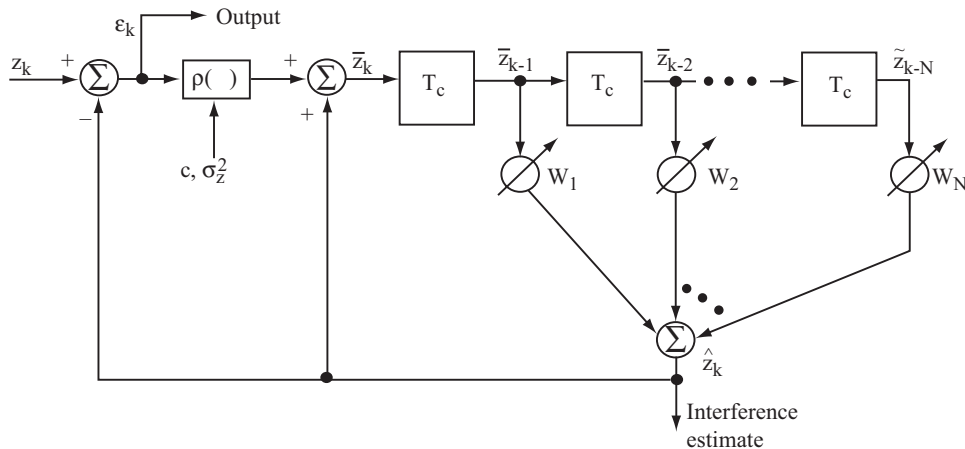


Figure 55. Adaptive ACM filter.

The calculation of  $\rho(\epsilon_k)$  requires the estimation of  $\sigma_z^2$ . If the  $\bar{z}_k$  produced by the adaptive filter approximates the prediction residual of (8-48), then (8-47), (8-35), (8-40), and (8-23) imply that  $\text{var}(\epsilon_k^2) \approx \sigma_z^2 + c^2$ . Therefore, if  $\text{var}(\epsilon_k^2)$  is estimated by computing the sample variance of the filter output, then the subtraction of  $c^2$  from the sample variance gives an estimate of  $\sigma_z^2$ .

A figure of merit for filters is the *SINR improvement*, which is the ratio of the output SINR to the input SINR. Since the filters of concern do not change the signal power, the SINR improvement is

$$R = \frac{E \{|z_k - s_k|^2\}}{E \{|\epsilon_k - s_k|^2\}} \quad (8-55)$$

In terms of this performance measure, the nonlinear adaptive ACM filter has been found to provide much better suppression of narrowband interference than the linear Kalman-Bucy filter if the noise power in  $n_k$  is less than the direct-sequence signal power in  $s_k$ . If the latter condition is not satisfied, the advantage is small or absent. Disadvantages apparent from (8-50) are the requirements to estimate the parameters  $c$  and  $\sigma_z^2$  and to compute or store the *tanh* function. At the cost of additional complexity and delay, a nonlinear *adaptive interpolator* [30] gives a slight performance gain. The preceding linear and nonlinear methods are primarily predictive methods that exploit the inherent predictability of narrowband interference. Further improvements in interference suppression are theoretically possible by using *code-aided methods*, which exploit the predictability of the spread-spectrum signal itself [31]. Most of these methods are based on methods that were originally developed for multiuser detection (Section 11). Some of them can potentially be used to simultaneously suppress both narrowband interference and multiple-access interference. However, code-aided methods require even more computation and parameter estimation than the ACM filter, and the most powerful of the adaptive methods are practical only for short spreading sequences.

---

## 9. Detection of Direct-Sequence Signals

---

In this section, we analyze the possibility of unauthorized detection of a direct-sequence signal, assuming that the spreading sequence is unknown to the detector, which cannot mimic the intended receiver. The results of Section 2.3 indicate that the peak power spectral density of a direct-sequence signal with a random spreading sequence is  $A^2 T_c / 4 = \mathcal{E}_s / 2G$ , where  $\mathcal{E}_s$  is the symbol energy and  $G$  is the processing gain. A spectrum analyzer usually cannot detect a signal with a power spectral density below that of the background noise, which has spectral density  $N_0/2$ . Thus, a received  $\mathcal{E}_s / N_0 > G$  is an approximate necessary, but not sufficient, condition for a spectrum analyzer to detect a

direct-sequence signal. If  $\mathcal{E}_s/N_0 < G$ , detection may still be possible by other means. If not, the direct-sequence signal is said to have a *low probability of interception*.

## 9.1 Ideal Detection

Detection theory provides various detection receivers depending on precisely what is assumed to be known about the signal to be detected. We make the idealized assumptions that the chip timing of the spreading waveform is known and that whenever the signal is present, it is present during the entire observation interval. The spreading sequence is modeled as a random binary sequence, which implies that a time shift of the sequence by a chip duration corresponds to the same stochastic process. Thus, to account for uncertainty in the chip timing, one might partition a chip duration among several parallel detectors each of which implements a different chip timing.

Consider the detection of a direct-sequence signal with PSK modulation:

$$s(t) = \sqrt{2S}p(t) \cos(2\pi f_c t + \phi) \quad (9-1)$$

where  $S$  is the average signal power,  $f_c$  is the known carrier frequency, and  $\phi$  is the carrier phase assumed to be constant over the observation interval  $0 \leq t \leq T$ . To determine whether a signal  $s(t)$  is present based on the observation of the received signal, classical detection theory requires that one choose between the hypothesis  $H_1$  that the signal is present and the hypothesis  $H_0$  that the signal is absent. Over the observation interval  $0 \leq t \leq T$ , the received signal under the two hypothesis is

$$r(t) = \begin{cases} s(t) + n(t), & H_1 \\ n(t), & H_0 \end{cases} \quad (9-2)$$

where  $n(t)$  is zero-mean, white Gaussian noise with two-sided power spectral density  $N_0/2$ . The spreading waveform  $p(t)$ , which subsumes the random data modulation, is given by (3-2) with the  $\{p_i\}$  modeled as a random binary sequence.

The coefficients in the expansion of the observed waveform in terms of orthonormal basis functions constitute the received vector  $\mathbf{r} = [r_1 \ r_2 \ \dots \ r_N]$ . Let  $\boldsymbol{\theta}$  denote the vector of parameter values that characterize the signal to be detected. The *average likelihood ratio* [32], which is compared with a threshold for a detection decision, is

$$\Lambda(\mathbf{r}) = \frac{E_{\boldsymbol{\theta}}[f(\mathbf{r}|H_1, \boldsymbol{\theta})]}{f(\mathbf{r}|H_0)} \quad (9-3)$$

where  $f(\mathbf{r}|H_1, \boldsymbol{\theta})$  is the conditional density function of  $\mathbf{r}$  given hypothesis  $H_1$  and the value of  $\boldsymbol{\theta}$ ,  $f(\mathbf{r}|H_0)$  is the conditional density function of  $\mathbf{r}$  given hypothesis  $H_0$ , and  $E_{\boldsymbol{\theta}}$  is the expectation over the random vector  $\boldsymbol{\theta}$ . The coefficients in the expansion of the Gaussian

process  $n(t)$  in terms of the orthonormal basis functions are uncorrelated and, hence, statistically independent. Since each coefficient is Gaussian with variance  $N_0/2$ ,

$$f(\mathbf{r}|H_1, \boldsymbol{\theta}) = \prod_{i=1}^N \frac{1}{\sqrt{\pi N_0}} \exp \left[ -\frac{(r_i - s_i)^2}{N_0} \right] \quad (9-4)$$

$$f(\mathbf{r}|H_0) = \prod_{i=1}^N \frac{1}{\sqrt{\pi N_0}} \exp \left( -\frac{r_i^2}{N_0} \right) \quad (9-5)$$

where the  $\{s_i\}$  are the coefficients of the signal. Substituting these equations into (9-3) yields

$$\Lambda(\mathbf{r}) = E_{\boldsymbol{\theta}} \left\{ \exp \left[ \frac{2}{N_0} \sum_{i=1}^N r_i s_i - \frac{1}{N_0} \sum_{i=1}^N s_i^2 \right] \right\} \quad (9-6)$$

Expansions in the orthonormal basis functions indicate that if  $N \rightarrow \infty$ , the average likelihood ratio may be expressed in terms of the signal waveforms as

$$\Lambda[r(t)] = E_{\boldsymbol{\theta}} \left\{ \exp \left[ \frac{2}{N_0} \int_0^T r(t)s(t)dt - \frac{\mathcal{E}}{N_0} \right] \right\} \quad (9-7)$$

where  $\mathcal{E}$  is the energy in the signal waveform over the observation interval of duration  $T$ .

If  $N$  is the number of chips, each of duration  $T_c$ , received in the observation interval, then there are  $2^N$  equally likely patterns of the spreading sequence. For *coherent detection*, we set  $\phi = 0$  in (9-1), substitute it into (9-7), and then evaluate the expectation to obtain

$$\Lambda(r(t)) = \exp \left( -\frac{\mathcal{E}}{N_0} \right) \sum_{j=1}^{2^N} \exp \left[ \frac{2\sqrt{2S}}{N_0} \sum_{i=0}^{N-1} p_i^{(j)} r'_i \right] \quad (\text{coherent}) \quad (9-8)$$

where  $p_i^{(j)}$  is the  $i$ th chip of pattern  $j$  and

$$r'_i = \int_{iT_c}^{(i+1)T_c} r(t)\psi(t - iT_c) \cos(2\pi f_c t) dt \quad (9-9)$$

These equations indicate how  $\Lambda(r(t))$  is to be calculated by the ideal coherent detector. The factor  $\exp(-\mathcal{E}/N_0)$  is irrelevant in the sense that it can be merged with the threshold level with which the average likelihood ratio is compared.

For the more realistic *noncoherent detection* of a direct-sequence signal, the received carrier phase is assumed to be uniformly distributed over  $[0, 2\pi)$ . Substituting (9-1) into (9-7), using a trigonometric expansion, dropping the irrelevant factor that can be merged with the threshold level, and then evaluating the expectation over the random spreading sequence, we obtain

$$\Lambda(r(t)) = E_{\phi} \left\{ \sum_{j=1}^{2^N} \exp \left[ \frac{2\sqrt{2S}}{N_0} \sum_{i=0}^{N-1} p_i^{(j)} (r_{ic} \cos \phi - r_{is} \sin \phi) \right] \right\} \quad (9-10)$$

where

$$\begin{aligned} r_{ic} &= \int_{iT_c}^{(i+1)T_c} r(t)\psi(t - iT_c) \cos(2\pi f_c t) dt, \\ r_{is} &= \int_{iT_c}^{(i+1)T_c} r(t)\psi(t - iT_c) \sin(2\pi f_c t) dt \end{aligned} \quad (9-11)$$

and  $E_\phi\{ \}$  denote the expectation with respect to  $\phi$ .

The *modified Bessel function of the first kind and order zero* is given by

$$I_0(x) = \frac{1}{2\pi} \int_0^{2\pi} \exp(x \cos u) du \quad (9-12)$$

Since the cosine is a periodic function and the integration is over the same period, we may replace  $\cos u$  with  $\cos(u + \phi)$  for any  $\phi$  in (9-12). A trigonometric expansion and  $x_1 = x \cos \phi$ ,  $x_2 = x \sin \phi$  then yields

$$I_0(x) = \frac{1}{2\pi} \int_0^{2\pi} \exp(x_1 \cos u - x_2 \sin u) du, \quad x = \sqrt{x_1^2 + x_2^2} \quad (9-13)$$

Using this relation, the average likelihood ratio of (9-10) becomes

$$\Lambda(r(t)) = \sum_{j=1}^{2^N} I_0 \left( \frac{2\sqrt{2SR_j}}{N_0} \right) \quad (\text{noncoherent}) \quad (9-14)$$

where

$$R_j = \left[ \sum_{i=0}^{N-1} p_i^{(j)} r_{ic} \right]^2 + \left[ \sum_{i=0}^{N-1} p_i^{(j)} r_{is} \right]^2 \quad (9-15)$$

Equations (9-14), (9-15), and (9-11) define the optimum noncoherent detector for a direct-sequence signal. The presence of the desired signal is declared if (9-14) exceeds a threshold level.

The implementation of either the coherent or noncoherent optimum detector would be very complicated, and the complexity would grow exponentially with  $N$ , the number of chips in the observation interval. Calculations [33] indicate that the ideal coherent and noncoherent detectors typically provide 3 dB and 1.5 dB advantages, respectively, over the far more practical wideband radiometer, which is analyzed subsequently. The use of four or two wideband radiometers, respectively, can compensate for these advantages with less complexity than the optimum detectors. Furthermore, implementation losses and imperfections in the optimum detectors are likely to be significant.

## 9.2 Wideband Radiometer

Among the many alternatives to the optimum detector, the *wideband radiometer* is notable in that it requires virtually no detailed information about the signals to be detected other than their rough spectral location. Not even whether the modulation is binary or quaternary is required. Suppose that the signal to be detected is approximated by a zero-mean, white Gaussian process. Consider two hypotheses that both assume the presence of a zero-mean, white Gaussian process over an observation interval  $0 \leq t \leq T$ . Under  $H_0$  only noise is present, and the one-sided power spectral density is  $N_0$ , while under  $H_1$  both signal and noise are present, and the power spectral density is  $N_1$ . Using  $N$  orthonormal basis functions as in the derivation of (9-4) and (9-5), we find that the conditional densities are

$$f(\mathbf{r}|H_i) = \prod_{l=1}^N \frac{1}{\sqrt{\pi N_i}} \exp\left(-\frac{r_l^2}{N_i}\right), \quad i = 0, 1 \quad (9-16)$$

Calculating the likelihood ratio, taking the logarithm, and merging constants with the threshold, we find that the decision rule is to compare

$$V = \sum_{l=1}^N r_l^2 \quad (9-17)$$

to a threshold. If we let  $N \rightarrow \infty$  and use the properties of orthonormal basis functions, then we find that the test statistic is

$$V = \int_0^T r^2(t) dt \quad (9-18)$$

which defines an *energy detector* or *radiometer*. Although it was derived for a white Gaussian process, the radiometer is a reasonable configuration for determining the presence of unknown deterministic signals.

A radiometer may have one of the three equivalent forms shown in Figure 56. Consider the system of Figure 56(a), which gives a direct realization of (9-18). The bandpass filter is assumed to be an ideal rectangular filter with center frequency  $f_c$ , bandwidth  $W$ , and input

$$r(t) = s(t) + n(t) \quad (9-19)$$

where  $s(t)$  is a deterministic signal, and  $n(t)$  is bandlimited white Gaussian noise with a two-sided power spectral density equal to  $N_0/2$ . Substituting (9-19) into (9-18), taking the expected value, and observing that  $n(t)$  is a zero-mean process, we obtain

$$\begin{aligned} E[V] &= \int_0^T s^2(t) dt + \int_0^T E[n^2(t)] dt \\ &= \mathcal{E} + N_0 T W \end{aligned} \quad (9-20)$$

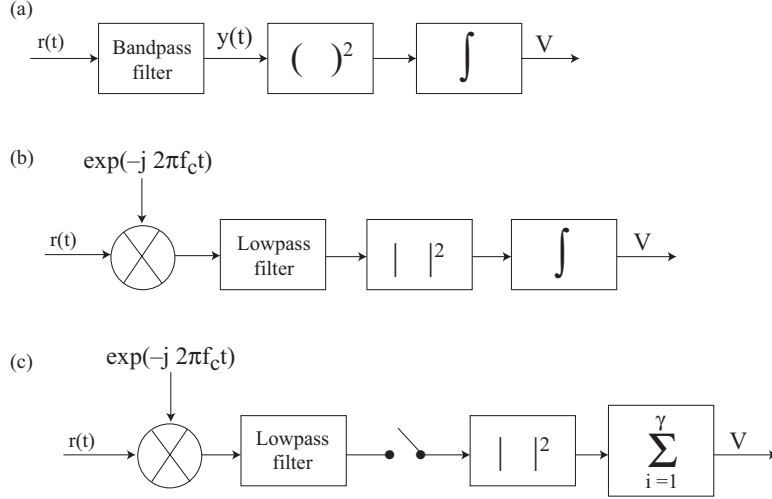


Figure 56. Radiometers: (a) passband, (b) baseband with integration, and (c) baseband with sampling at rate  $1/W$  and summation.

which indicates that the radiometer output is an unbiased estimate of the total energy in  $r(t)$ .

According to the results of Appendix C-1, a bandlimited deterministic signal can be represented as

$$s(t) = s_c(t) \cos 2\pi f_c t - s_s(t) \sin 2\pi f_c t \quad (9-21)$$

Since the spectrum of  $s(t)$  is confined within the filter passband,  $s_c(t)$  and  $s_s(t)$  have frequency components confined to the band  $|f| \leq W/2$ . The Gaussian noise emerging from the bandpass filter can be represented in terms of quadrature components as (Appendix C-2)

$$n(t) = n_c(t) \cos 2\pi f_c t - n_s(t) \sin 2\pi f_c t \quad (9-22)$$

where  $n_c(t)$  and  $n_s(t)$  have flat power spectral densities, each equal to  $N_0$  over  $|f| \leq W/2$ . Substituting (9-22), (9-21), and (9-19) into (9-18) and assuming that  $f_c \gg W$  and  $f_c \gg 1/T$ , we obtain

$$V = \frac{1}{2} \int_0^T [s_c(t) + n_c(t)]^2 dt + \frac{1}{2} \int_0^T [s_s(t) + n_s(t)]^2 dt \quad (9-23)$$

A straightforward calculation verifies that the baseband radiometer of Figure 56(b) also produces this test statistic.

The *sampling theorems* for deterministic and stochastic processes (Appendix C-3) provide expansions of  $s_c(t)$ ,  $s_s(t)$ ,  $n_c(t)$  and  $n_s(t)$  that facilitate a statistical performance analysis. For example,

$$s_c(t) = \sum_{i=-\infty}^{\infty} s_c \left( \frac{i}{W} \right) \text{sinc}(Wt - i) \quad (9-24)$$

where  $\text{sinc } x = (\sin \pi x)/\pi x$ . Since the Fourier transform of the sinc function is a rectangular function, using Parseval's theorem from Fourier analysis and evaluating the resulting integral yields the approximations:

$$\int_0^T \text{sinc}^2(Wt - i)dt \approx \int_{-\infty}^{\infty} \text{sinc}^2(Wt - i)dt = \frac{1}{W}, \quad 0 < i \leq TW \quad (9-25)$$

$$\int_0^T \text{sinc}(Wt - i)\text{sinc}(Wt - j)dt \approx \int_{-\infty}^{\infty} \text{sinc}(Wt - i)\text{sinc}(Wt - j)dt = 0, \quad i \neq j \quad (9-26)$$

The rapid decline of  $\text{sinc } x$  for  $|x| > 1$  implies that

$$\int_0^T \text{sinc}^2(Wt - i)dt \approx 0, \quad i \leq 0 \text{ or } i > TW \quad (9-27)$$

We define  $\gamma = \lfloor TW \rfloor$ , where  $\lfloor x \rfloor$  denotes the integer part of  $x$ . Substituting expansions similar to (9-24) into (9-23) and then using the preceding approximations, we obtain

$$V \approx \frac{1}{2W} \sum_{i=1}^{\gamma} \left[ s_c \left( \frac{i}{W} \right) + n_c \left( \frac{i}{W} \right) \right]^2 + \frac{1}{2W} \sum_{i=1}^{\gamma} \left[ s_s \left( \frac{i}{W} \right) + n_s \left( \frac{i}{W} \right) \right]^2 \quad (9-28)$$

where it is always assumed that  $TW \geq 1$ . The error introduced by (9-27) at  $i = 0$  and the error introduced by (9-25) at  $i = TW$  are both nearly  $1/2W$ . For other values of  $i$ , the errors caused by the approximations are much less than  $1/2W$  and decrease as  $TW$  increases. Equation (9-28) becomes an increasingly accurate approximation of (9-23) as  $\gamma$  increases. A test statistic proportional to (9-28) can be derived for the baseband radiometer of Figure 56(c) and the sampling rate  $1/W$  without invoking the sampling theorems and the accompanying approximations.

Since  $n(t)$  is a zero-mean Gaussian process and has a power spectral density that is symmetrical about  $f_c$ ,  $n_c(t)$  and  $n_s(t)$  are zero-mean, independent Gaussian processes (Appendix C-2). Thus,  $n_c(i/W)$  and  $n_s(j/W)$  are zero-mean, independent Gaussian random variables. Equation (C-40) implies that the power spectral densities of  $n_c(t)$  and  $n_s(t)$  are

$$S_c(f) = S_s(f) = \begin{cases} N_0 & , \quad |f| \leq W/2 \\ 0 & , \quad |f| > W/2 \end{cases} \quad (9-29)$$

The associated autocorrelation functions are

$$R_c(\tau) = R_s(\tau) = N_0 W \text{sinc}(W\tau) \quad (9-30)$$

This expression indicates that  $n_c(i/W)$  is statistically independent of  $n_c(j/W)$ ,  $i \neq j$ , and similarly for  $n_s(i/W)$  and  $n_s(j/W)$ . Therefore, (9-28) becomes

$$V = \frac{N_0}{2} \left\{ \sum_{i=1}^{\gamma} A_i^2 + \sum_{i=1}^{\gamma} B_i^2 \right\} \quad (9-31)$$

where the  $A_i$  and the  $B_i$  are statistically independent Gaussian random variables with unit variances and means

$$m_{1i} = E[A_i] = \frac{1}{\sqrt{N_0 W}} s_c \left( \frac{i}{W} \right) \quad (9-32)$$

$$m_{2i} = E[B_i] = \frac{1}{\sqrt{N_0 W}} s_s \left( \frac{i}{W} \right) \quad (9-33)$$

Thus,  $2V/N_0$  has a *noncentral chi-squared* ( $\chi^2$ ) *distribution* (Appendix B) with  $2\gamma$  degrees of freedom and a noncentral parameter

$$\begin{aligned} \lambda &= \sum_{i=1}^{\gamma} m_{1i}^2 + \sum_{i=1}^{\gamma} m_{2i}^2 = \frac{1}{N_0 W} \sum_{i=1}^{\gamma} s_c^2 \left( \frac{i}{W} \right) + \frac{1}{N_0 W} \sum_{i=1}^{\gamma} s_s^2 \left( \frac{i}{W} \right) \\ &\approx \frac{1}{N_0} \int_0^T [s_c^2(t) + s_s^2(t)] dt \approx \frac{2}{N_0} \int_0^T s^2(t) dt = \frac{2\mathcal{E}}{N_0} \end{aligned} \quad (9-34)$$

The probability density function of  $Z = 2V/N_0$  is

$$f_Z(x) = \frac{1}{2} \left( \frac{x}{\lambda} \right)^{(\gamma-1)/2} \exp \left( -\frac{x + \lambda}{2} \right) I_{\gamma-1} \left( \sqrt{x\lambda} \right) u(x) \quad (9-35)$$

where  $I_n(\cdot)$  is the modified Bessel function of the first kind and order  $n$  (Appendix B), and  $u(x) = 1, x \geq 0$ , and  $u(x) = 0, x < 0$ . Using the series expansion in  $\lambda$  of the Bessel function and then setting  $\lambda = 0$  in (9-35), we obtain the probability density function for  $Z$  in the absence of the signal:

$$f_Z(x) = \frac{1}{2^\gamma \Gamma(\gamma)} x^{\gamma-1} \exp \left( -\frac{x}{2} \right) u(x), \quad \lambda = 0 \quad (9-36)$$

where  $\Gamma(\cdot)$  is the gamma function (Appendix B).

By straightforward calculations using the statistics of Gaussian variables, (9-31) and the subsequent results yield

$$E[V] = \mathcal{E} + N_0 \gamma \quad (9-37)$$

$$\text{var}(V) = 2N_0 \mathcal{E} + N_0^2 \gamma \quad (9-38)$$

Equation (9-37) approaches the exact result of (9-20) as  $TW$  increases.

Let  $V_t$  denote the threshold level to which  $V$  is compared. A false alarm occurs if  $V > V_t$  when the signal is absent. Application of (9-36) yields the probability of a false alarm:

$$\begin{aligned} P_F &= \int_{2V_t/N_0}^{\infty} \frac{1}{2^\gamma \Gamma(\gamma)} v^{\gamma-1} e^{-v/2} dv \\ &= 1 - \Gamma \left( \frac{V_t}{N_0}, \gamma \right) \end{aligned} \quad (9-39)$$

where the *incomplete gamma function* is defined as

$$\Gamma(x, a) = \frac{1}{\Gamma(a)} \int_0^x e^{-t} t^{a-1} dt \quad (9-40)$$

and  $\Gamma(\infty, a) = 1$ . Integrating (9-39) by parts  $\gamma - 1$  times yields the series

$$P_F = \exp\left(-\frac{V_t}{N_0}\right) \sum_{i=0}^{\gamma-1} \frac{1}{i!} \left(\frac{V_t}{N_0}\right)^i \quad (9-41)$$

Since correct detection occurs if  $V > V_t$  when the signal is present, (9-35) indicates that the probability of detection is

$$P_D = \int_{2V_t/N_0}^{\infty} \frac{1}{2} \left(\frac{v}{\lambda}\right)^{(\gamma-1)/2} \exp\left(-\frac{v+\lambda}{2}\right) I_{\gamma-1}(\sqrt{v\lambda}) dv \quad (9-42)$$

The *generalized Marcum Q-function* is defined as

$$Q_m(\alpha, \beta) = \int_{\beta}^{\infty} x \left(\frac{x}{\alpha}\right)^{m-1} \exp\left(-\frac{x^2 + \alpha^2}{2}\right) I_{m-1}(\alpha x) dx \quad (9-43)$$

where  $m$  is a nonnegative integer, and  $\alpha$  and  $\beta$  are nonnegative real numbers. A change of variables in (9-42) yields

$$P_D = Q_{\gamma}(\sqrt{\lambda}, \sqrt{2V_t/N_0}) \quad (9-44)$$

The threshold  $V_t$  is usually set to a value that ensures a specified  $P_F$ . To derive an easily computed closed-form expression for  $V_t$  in terms of  $P_F$ , we first approximate (9-39). When  $TW \gg 1$ ,  $\gamma \approx TW$ , and the central limit theorem for the sum of independent, identically distributed random variables with finite means and variances indicates that the distribution of  $V$  given by (9-31) is approximately Gaussian. Using (9-37) and (9-38) with  $\mathcal{E} = 0$  and the Gaussian distribution, we obtain

$$\begin{aligned} P_F &\approx \frac{1}{(2\pi N_0^2 TW)^{1/2}} \int_{V_t}^{\infty} \exp\left[-\frac{(v - N_0 TW)^2}{2N_0^2 TW}\right] dv \\ &= Q\left[\frac{V_t - N_0 TW}{(N_0^2 TW)^{1/2}}\right], \quad TW \gg 1 \end{aligned} \quad (9-45)$$

where  $Q(x)$  is defined by (3-26). Inverting this equation, we obtain  $V_t$  in terms of  $P_F$  and  $N_0$ . Accordingly, if the estimate of  $N_0$  is  $\hat{N}_0$  and  $P_F$  is specified, then the threshold should be

$$V_t \approx \hat{N}_0 \sqrt{TW} Q^{-1}(P_F) + \hat{N}_0 TW, \quad TW \gg 1 \quad (9-46)$$

where  $Q^{-1}(\cdot)$  denotes the inverse of the function  $Q(\cdot)$ . In the absence of a signal, (9-20) indicates that  $N_0 = E[V]/TW$ . Thus,  $N_0$  can be estimated by averaging sampled radiometer outputs when it is known that no signal is present.

In some applications, one might wish to specify the *false alarm rate*, which is the expected number of false alarms per unit time, rather than  $P_F$ . If successive observation intervals do not overlap each other except possibly at end points, then the false alarms rate is

$$F = \frac{P_F}{T} \quad (9-47)$$

For  $TW > 100$ , the generalized Marcum Q-function is difficult to compute. Thus, we seek an approximation that is easier to compute and to invert. If  $V$  is approximated by a Gaussian random variable, then (9-37) and (9-38) imply that

$$P_D \approx Q \left[ \frac{V_t - N_0 TW - \mathcal{E}}{(N_0^2 TW + 2N_0 \mathcal{E})^{1/2}} \right], \quad TW \gg 1 \quad (9-48)$$

Figure 57 depicts  $P_D$  versus  $\mathcal{E}/N_0$  for a wideband radiometers with  $\hat{N}_0 = N_0$  and  $P_F = 10^{-3}$ . Equations (9-46) and (9-48) are used to calculate  $V_t$  and  $P_D$ , respectively. The figure illustrates the increased energy required to maintain a specified  $P_D$  as  $TW$  increases. The figure also illustrates the impact of the imperfect estimation of  $N_0$  when  $P_F = 10^{-3}$  and  $TW = 10^7$ . When the estimation uncertainty is enough that  $\hat{N}_0 = 1.001 N_0$ , the detection probability is lowered considerably.

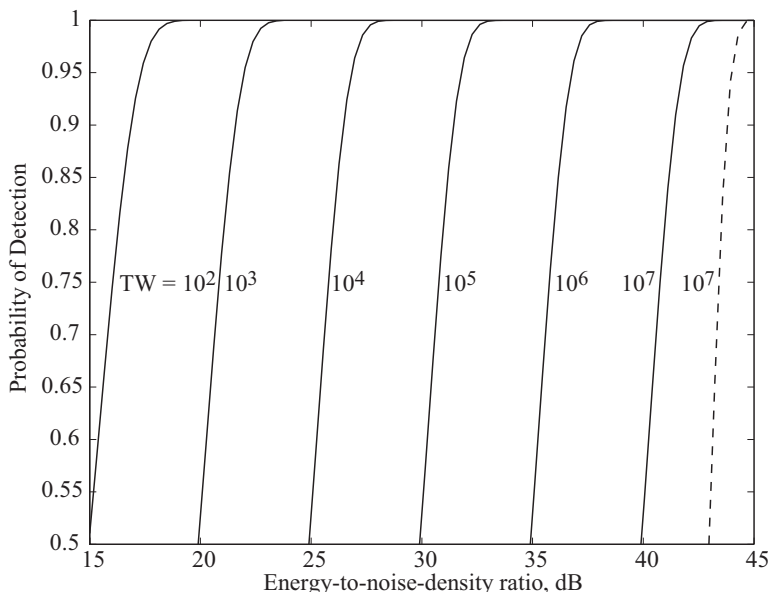


Figure 57. Probability of detection versus  $\mathcal{E}/N_0$  for wideband radiometer with  $P_F = 10^{-3}$  and various values of  $TW$ . Solid curves are the  $\hat{N}_0 = N_0$ ; dashed curve is for  $\hat{N}_0 = 1.001 N_0$ .

The sensitivity of the radiometer to errors in  $\hat{N}_0$  when  $TW$  is large, which has been observed experimentally [34], is due to the fact the  $\mathcal{E}[V]$  contains a bias term equal to  $N_0TW$  and  $\text{var}(V)$  contains a term equal to  $N_0^2 TW$ , as indicated by (9-37) and (9-38). Setting  $\hat{N}_0$  high enough that  $\hat{N}_0 \geq N_0$  is certain ensures that  $V_t$  will be large enough that the required  $P_F$  is achieved regardless of the exact value of  $N_0$ . It is important that  $\hat{N}_0/N_0$  is as close to unity as possible to avoid degrading  $P_D$  when  $TW$  is large. Consequently, the radiometer output due to noise alone, which provides  $\hat{N}_0$ , should be observed often enough that  $\hat{N}_0$  closely tracks the changes in  $N_0$  that might result from small changes in the circuitry or the environmental noise.

When  $V_t$  is specified, the value of  $\mathcal{E}/N_0$  necessary to achieve a specified value of  $P_D$  may be obtained by inverting (9-44), which is computationally difficult but can be closely approximated. Assuming that  $2V_t > N_0TW$ , (9-48) yields the necessary value:

$$\frac{\mathcal{E}}{N_0} \approx [Q^{-1}(P_D)]^2 + \frac{V_t}{N_0} - TW - [Q^{-1}(P_D)] \sqrt{[Q^{-1}(P_D)]^2 + \frac{2V_t}{N_0} - TW}, \quad TW \gg 1 \quad (9-49)$$

According to (9-46), the condition  $2V_t > N_0TW$  is satisfied if  $P_F \leq 1/2$  and  $\hat{N}_0 \approx N_0$ . The substitution of (9-46) into (9-49) and a rearrangement of terms yields

$$\frac{\mathcal{E}}{N_0} \approx h\sqrt{TW}\beta + (h-1)TW + \psi(\beta, \xi, TW, h), \quad TW \gg 1 \quad (9-50)$$

where

$$\beta = Q^{-1}(P_F), \quad \xi = Q^{-1}(P_D), \quad h = \hat{N}_0/N_0 \quad (9-51)$$

$$\psi(\beta, \xi, TW, h) = \xi^2 - \sqrt{TW}\xi \left[ 2h - 1 + \frac{2\beta h}{\sqrt{TW}} + \frac{\xi^2}{TW} \right]^{1/2} \quad (9-52)$$

As  $TW$  increases, the significance of the third term in (9-50) decreases, while that of the second term increases if  $h > 1$ . Figure 58 shows  $\mathcal{E}/N_0$  versus  $TW$  for  $P_D = 0.99$  and various values of  $P_F$  and  $h$ .

Denoting the intercepted signal power by  $S$  and the signal duration by  $T_1$ , we find from (9-50) with  $\mathcal{E} = ST_1$  that the intercepted power necessary to achieve specified values of  $P_D$  and either  $P_F$  or  $F$  is

$$\frac{S}{N_0} \approx \begin{cases} h\frac{\sqrt{TW}}{T_1}\beta + (h-1)W\frac{T}{T_1} + \frac{\psi}{T_1}, & T_1 < T \\ h\sqrt{\frac{W}{T}}\beta + (h-1)W + \frac{\psi}{T}, & T_1 \geq T \end{cases} \quad (9-53)$$

This equation indicates that increasing the observation interval  $T$  decreases the required power only if  $T \leq T_1$ . Although a single wideband radiometer is incapable of determining whether one or more than one signal has been detected, narrowband interference can be rejected by the methods of Section 8.

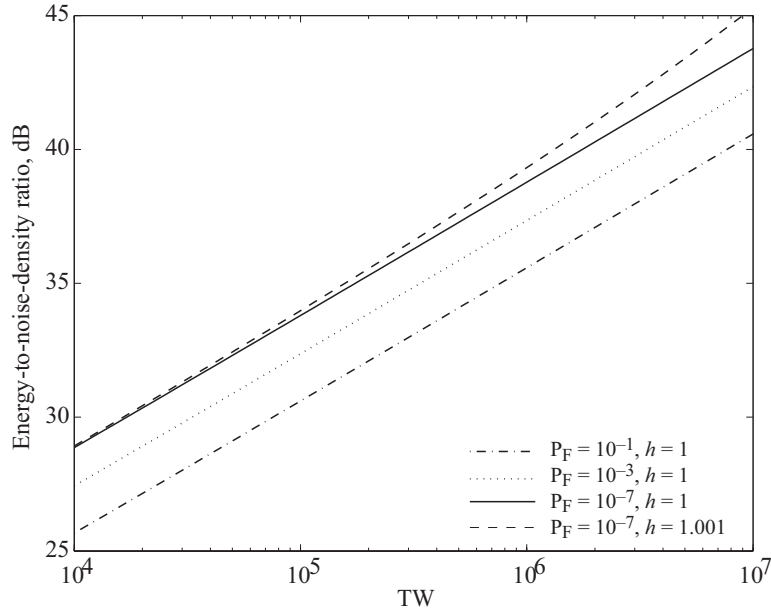


Figure 58. Energy-to-noise-density ratio versus  $TW$  for wideband radiometer with  $P_D = 0.99$  and various values of  $P_F$  and  $h$ .

---

## 10. Direct-Sequence Code-Division Multiple Access

---

*Multiple access* is the ability of many users to communicate with each other while sharing a common transmission medium. Wireless multiple-access communications are facilitated if the transmitted signals are orthogonal or separable in some sense. Signals may be separated in time (*time-division multiple access* or TDMA), frequency (*frequency-division multiple access* or FDMA), or code (*code-division multiple access* or CDMA). CDMA is realized by using spread-spectrum modulation while transmitting signals from multiple users in the same frequency band at the same time. All signals use the entire allocated spectrum, but the spreading sequences differ. Information theory indicates that in an isolated cell, CDMA systems achieve the same spectral efficiency as TDMA or FDMA systems only if optimal multiuser detection is used. However, even with single-user detection, CDMA is advantageous for cellular networks because it eliminates the need for frequency and timeslot coordination among cells and allows carrier-frequency reuse in adjacent cells. Frequency planning is vastly simplified. A major CDMA advantage exists in networks accommodating voice communications. A voice-activity detector activates the transmitter only when the user is talking. Since typically fewer than 40% of the users are talking at any given time, the number of telephone users can be increased while maintaining a specified average interference power. Another major CDMA advantage is the ease with which it can be combined with multibeamed antenna arrays that are either

adaptive or have fixed patterns covering cell sectors. There is no practical means of reassigning time slots in TDMA systems or frequencies in FDMA systems to increase capacity by exploiting intermittent voice signals or multibeamed arrays. Reassignments to accommodate variable data rate are almost always impractical in FDMA or TDMA systems. These general advantages of CDMA, combined with the resistance of spread-spectrum signals to jamming, interception, and multipath interference, make CDMA the most attractive choice for most mobile communications. The two principal types of spread-spectrum CDMA are *direct-sequence* CDMA and *frequency-hopping* CDMA. In direct-sequence CDMA, pulses with a large bandwidth relative to the symbol rate can be generated by using a chip waveform that is modulated by a spreading sequence. In frequency-hopping CDMA, the carrier frequency of a transmission is changed periodically.

Consider a direct-sequence CDMA network with  $K$  users in which every receiver has the form of Figure 14. The multiple-access interference that enters a receiver synchronized to a desired signal is modeled as

$$i(t) = \sum_{i=1}^{K-1} \sqrt{2I_i} d_i(t - \tau) q_i(t - \tau_i) \cos(2\pi f_c t + \phi_i) \quad (10-1)$$

where  $K - 1$  is the number of interfering direct-sequence signals, and  $I_i$  is the average power,  $d_i(t)$  is the code-symbol modulation,  $q_i(t)$  is the spreading waveform,  $\tau_i$  is the relative delay, and  $\phi_i$  is the phase shift of interference signal  $i$  including the effect of carrier time delay. Each spreading waveform has the form

$$q_i(t) = \sum_{j=-\infty}^{\infty} q_j^{(i)} \psi(t - jT_c) \quad (10-2)$$

where the chip waveforms are assumed to be identical throughout the network and  $q_j^{(i)} \in \{-1, 1\}$ . Substituting (10-1) into (3-8) and (3-11) and then using (3-2), we obtain the interference component of the demodulator output due to a received symbol:

$$V_1 = \sum_{i=1}^{K-1} \sqrt{\frac{I_i}{2}} \cos \phi_i \int_0^{T_s} d_i(t - \tau_i) q_i(t - \tau_i) p(t) dt \quad (10-3)$$

where a double-frequency term is neglected and  $p(t)$  is the spreading waveform of the desired signal. In a direct-sequence CDMA network, the spreading sequences are often called *signature sequences*.

## 10.1 Orthogonal Sequences

Suppose that the communication signals are synchronous so that all data symbols have duration  $T_s$ , symbol and chip transitions are aligned at the receiver input, and short

spreading sequences with period  $N = G$  extend over each data symbol. Then  $\tau_i = 0, i = 1, 2, \dots, K - 1$ , and  $d_i(t) = d_i$  is constant over the integration interval  $[0, T_s]$ . The *cross-correlation* between  $q_i(t)$  and  $p(t)$  is defined as

$$C_{pi}(\tau) = \frac{1}{T_s} \int_0^{T_s} p(t)q_i(t - \tau)dt \quad (10-4)$$

Thus, for synchronous communications, (10-3) may be expressed as

$$V_1 = \sum_{i=1}^{K-1} \lambda_i C_{pi}(0) \quad (10-5)$$

where

$$\lambda_i = \sqrt{\frac{I_i}{2}} d_i T_s \cos \phi_i \quad (10-6)$$

Substituting (10-2) and (3-2) into (10-4) and then using (3-3) and (3-4), we obtain

$$C_{pi}(0) = \frac{1}{G} \sum_{j=1}^G p_j q_j^{(i)} \quad (10-7)$$

where the right-hand side is the *periodic cross-correlation* between the sequences  $\{q_j^{(i)}\}$  and  $\{p_j\}$ . Let  $\mathbf{a}$  and  $\mathbf{b}_i$  denote the binary sequences with components  $a_j, b_j^{(i)} \in GF(2)$ , respectively, that map into the binary antipodal sequences with components  $p_j = (-1)^{a_j+1}$  and  $q_j^{(i)} = (-1)^{b_j^{(i)}+1}$ . Then a derivation similar to that in (2-28) gives

$$C_{pi}(0) = \frac{A_i - D_i}{G} \quad (10-8)$$

where  $A_i$  denotes the number of agreements in the corresponding bits of  $\mathbf{a}$  and  $\mathbf{b}_i$ , and  $D_i$  denotes the number of disagreements. The sequences are *orthogonal* if  $C_{pi}(0) = 0$ . If the spreading sequence  $\mathbf{a}$  is orthogonal to all the spreading sequences  $\mathbf{b}_i, i = 1, 2, \dots, K$ , then  $V_1 = 0$  and the multiple-access interference  $i(t)$  is suppressed at the receiver. A large number of multiple-access interference signals can be suppressed in a network if each such signal has its chip transitions aligned and the spreading sequences are mutually orthogonal.

Two binary sequences, each of length two, are orthogonal if each sequence is described by one of the rows of the  $2 \times 2$  matrix

$$\mathbf{H}_1 = \begin{bmatrix} 0 & 0 \\ 0 & 1 \end{bmatrix} \quad (10-9)$$

because  $A = D = 1$ . A set of  $2^n$  sequences, each of length  $2^n$ , is obtained by using the rows of the matrix

$$\mathbf{H}_n = \begin{bmatrix} \mathbf{H}_{n-1} & \mathbf{H}_{n-1} \\ \mathbf{H}_{n-1} & \bar{\mathbf{H}}_{n-1} \end{bmatrix}, \quad n = 2, 3, \dots \quad (10-10)$$

where  $\bar{\mathbf{H}}_{n-1}$  is the *complement* of  $\mathbf{H}_{n-1}$ , obtained by replacing each 1 and 0 by 0 and 1, respectively, and  $\mathbf{H}_1$  is defined by (10-9). Any pair of rows in  $\mathbf{H}_n$  differ in exactly  $2^{n-1}$  columns, thereby ensuring orthogonality of the corresponding sequences. The  $2^n \times 2^n$  matrix  $\mathbf{H}_n$ , which is called a *Hadamard* matrix, can be used to generate  $2^n$  spreading sequences for synchronous direct-sequence communications. These spreading sequences are often called *Walsh sequences*.

As an alternative to the Walsh sequences, consider the set of  $2^m - 1$  maximal sequences generated by a primitive polynomial of degree  $m$  and the  $2^m - 1$  different initial states of the shift register. Equation (2-28) implies that by appending a 0 at the end of each period of each sequence, we obtain a set of  $2^m - 1$  orthogonal sequences of period  $2^m$ . Without the appending of symbols, a set of nearly orthogonal sequences for a synchronous network may be generated from different time displacements of a single maximal sequence because its autocorrelation, which is given by (2-29), determines the cross-correlations among the sequences of the set. The low values of the autocorrelation for nonzero delay causes the rejection of multipath signals. In contrast, the Walsh sequences do not have such favorable autocorrelation functions.

## 10.2 Sequences with Small Cross-Correlations

The symbol transitions of *asynchronous* multiple-access signals at a receiver are not simultaneous, usually because of changing path-length differences among the various communication links. Since the spreading sequences are shifted relative to each other, sets of periodic sequences with small cross-correlations for any relative shifts are desirable to limit the effect of multiple-access interference. Maximal sequences, which have the longest periods of sequences generated by a linear feedback shift register of fixed length, are often inadequate. Let  $\mathbf{a} = (\dots, a_0, a_1, \dots)$  and  $\mathbf{b} = (\dots, b_0, b_1, \dots)$  denote binary sequences with components in  $GF(2)$ . The sequences  $\mathbf{a}$  and  $\mathbf{b}$  are mapped into antipodal sequences  $\mathbf{p}$  and  $\mathbf{q}$ , respectively, with components in  $\{-1, +1\}$  by means of the transformation

$$p_i = (-1)^{a_i+1}, \quad q_i = (-1)^{b_i+1} \quad (10-11)$$

The *periodic cross-correlation* of periodic binary sequences  $\mathbf{a}$  and  $\mathbf{b}$  with the same period  $N$  is defined as the periodic cross-correlation of the antipodal sequences  $\mathbf{p}$  and  $\mathbf{q}$ , which is defined as

$$\theta_{pq}(j) = \frac{1}{N} \sum_{i=0}^{N-1} p_i q_{i+j}, \quad j = 1, 2, \dots, N-1 \quad (10-12)$$

A calculation similar to that in (2-28) yields the periodic cross-correlation

$$\theta_{pq}(j) = \frac{A_j - D_j}{N} \quad (10-13)$$

where  $A_j$  denotes the number of agreements in the corresponding components of  $\mathbf{a}$  and the shift sequence  $\mathbf{b}(j) = (\dots, b_j, b_{j+1}, \dots, b_{j+N-1}, \dots)$ , and  $D_j$  denotes the number of disagreements.

In the presence of asynchronous multiple-access interference for which  $\tau_i \neq 0$ , the interference component of the correlator output is given by (10-3). If we assume that the data modulation is absent so that we may set  $d_i(t) = 1$  in (10-3), then it is observed that interference signal  $i$  produces a term in  $V_1$  that is proportional to  $C_{pi}(\tau_i)$ . Let  $\tau_i = N_i T_c + \epsilon_i$ , where  $N_i$  is a nonnegative integer and  $0 \leq \epsilon_i < T_c$ . A derivation similar to the one leading to (2-34) gives

$$C_{pi}(N_i T_c + \epsilon_i) = \left(1 - \frac{\epsilon_i}{T_c}\right) \theta_{pi}(N_i) + \frac{\epsilon_i}{T_c} \theta_{pi}(N_i + 1) \quad (10-14)$$

where  $\theta_{pi}(N_i)$  is the periodic cross-correlation of the sequence  $\mathbf{p}$  and  $\mathbf{q}_i$  and is given by (10-13). Thus, ensuring that the periodic cross-correlations are always small is a critical *necessary* condition for the success of asynchronous multiple-access communications. Although the data modulation may be absent during acquisition, it will be present during data transmission, and  $d_i(t)$  may change polarity during an integration interval. Thus, the effect of asynchronous multiple-access interference (Section 10.3) will exceed that predicted from (10-14).

For a set  $S$  of  $M$  periodic antipodal sequences of length  $N$ , let  $\theta_{\max}$  denote the peak magnitude of the cross-correlations or autocorrelations:

$$\theta_{\max} = \max \{|\theta_{pq}(k)| : 0 \leq k \leq N - 1; \mathbf{p}, \mathbf{q} \in S; p \neq q \text{ or } k \neq 0\} \quad (10-15)$$

**Theorem.** *A set  $S$  of  $M$  periodic antipodal sequences of length  $N$  has*

$$\theta_{\max} \geq \sqrt{\frac{M-1}{MN-1}} \quad (10-16)$$

**Proof.** Consider an extended set  $S_e$  of  $MN$  sequences  $\mathbf{p}^{(i)}$ ,  $i = 1, 2, \dots, MN$ , that comprises the  $N$  distinct shifted sequences derived from each of the sequences in  $S$ . The cross-correlation of sequences  $\mathbf{p}^{(i)}$  and  $\mathbf{p}^{(j)}$  in  $S_e$  is

$$\psi_{ij} = \frac{1}{N} \sum_{n=1}^N p_n^{(i)} p_n^{(j)} \quad (10-17)$$

and

$$\theta_{\max} = \max \{|\psi_{ij}|, p^{(i)} \in S_e, p^{(j)} \in S_e, i \neq j\} \quad (10-18)$$

Define the double summation

$$Z = \sum_{i=1}^{MN} \sum_{j=1}^{MN} \psi_{ij}^2 \quad (10-19)$$

Separating the  $MN$  terms for which  $\psi_{ii} = 1$  and then bounding the remaining  $MN(MN - 1)$  terms yields

$$Z \leq MN + MN(MN - 1)\theta_{\max}^2 \quad (10-20)$$

Substituting (10-17) into (10-19), interchanging summations, and omitting the terms for which  $m \neq n$ , we obtain

$$\begin{aligned} Z &= \frac{1}{N^2} \sum_{n=1}^N \sum_{m=1}^N \sum_{i=1}^{MN} p_n^{(i)} p_m^{(i)} \sum_{j=1}^{MN} p_n^{(j)} p_m^{(j)} \\ &= \frac{1}{N^2} \sum_{n=1}^N \sum_{m=1}^N \left( \sum_{i=1}^{MN} p_n^{(i)} p_m^{(i)} \right)^2 \\ &\geq \frac{1}{N^2} \sum_{n=1}^N \left[ \sum_{i=1}^{MN} (p_n^{(i)})^2 \right]^2 = M^2 N \end{aligned} \quad (10-21)$$

Combining this inequality with (10-20) gives (10-16).  $\square$

The lower bound in (10-16) is known as the *Welch bound*. It approaches  $1/\sqrt{N}$  for large values of  $M$  and  $N$ . Only small subsets of maximal sequences can be found with  $\theta_{\max}$  close to this lower bound. The same is true for Walsh sequences.

Large sets of sequences with  $\theta_{\max}$  approaching the Welch bound can be obtained by combining maximal sequences with sampled versions of these sequences. If  $q$  is a positive integer, the new binary sequence  $\mathbf{b}$  formed by taking every  $q$ th bit of binary sequence  $\mathbf{a}$  is known as a *decimation* of  $\mathbf{a}$  by  $q$ , and the components of the two sequences are related by  $b_i = a_{qi}$ . Let  $\gcd(x, y)$  denote the greatest common divisor of  $x$  and  $y$ . If the original sequence  $\mathbf{a}$  has a period  $N$  and the new sequence  $\mathbf{b}$  is not identically zero, then  $\mathbf{b}$  has period  $N/\gcd(N, q)$ . If  $\gcd(N, q) = 1$ , then the decimation is called a *proper decimation*. Following a proper decimation, the bits of  $\mathbf{b}$  do not repeat themselves until every bit of  $\mathbf{a}$  has been sampled. Therefore,  $\mathbf{b}$  and  $\mathbf{a}$  have the same period  $N$ , and it can be shown that if  $\mathbf{a}$  is maximal, then  $\mathbf{b}$  is a maximal sequence [35]. A *preferred pair* of maximal sequences with period  $2^m - 1$  are a pair with a periodic cross-correlation that takes only the three values  $-t(m)/N$ ,  $-1/N$ , and  $[t(m) - 2]/N$ , where

$$t(m) = 2^{\lfloor (m+2)/2 \rfloor} + 1 \quad (10-22)$$

and  $\lfloor x \rfloor$  denotes the integer part of the real number  $x$ . The *Gold sequences* are a large set of sequences with period  $N = 2^m - 1$  that may be generated by the modulo-2 addition of preferred pairs when  $m$  is odd or  $m = 2$  modulo-4 [35]. One sequence of the preferred pair is a decimation by  $q$  of the other sequence. The positive integer  $q$  is either  $q = 2^k + 1$  or  $q = 2^{2k} - 2^k + 1$ , where  $k$  is a positive integer such that  $\gcd(m, k) = 1$  when  $m$  is odd and  $\gcd(m, k) = 2$  when  $m = 2$  modulo-4.

Since the cross-correlation between any two Gold sequences in a set can take only three values, the peak magnitude of the periodic cross-correlation between any two Gold sequences of period  $N = 2^m - 1$  is

$$\theta_{\max} = \frac{t(m)}{2^m - 1} \quad (10-23)$$

For large values of  $m$ ,  $\theta_{\max}$  for Gold sequences exceeds the Welch bound by a factor of  $\sqrt{2}$  for  $m$  odd and a factor of 2 for  $m$  even.

One form of a Gold sequence generator is shown in Figure 59. If each maximal sequence generator has  $m$  stages, different Gold sequences in a set are generated by selecting the initial state of one maximal sequence generator and then shifting the initial state of the other generator. Since any shift from 0 to  $2^m - 2$  results in a different Gold sequence,  $2^m - 1$  different Gold sequences can be produced by the system of Figure 59. Gold sequences identical to maximal sequences are produced by setting the state of one of the maximal sequence generators to zero. Altogether, there are  $2^m + 1$  different Gold sequences, each with a period of  $2^m - 1$ , in the set.

An example of a set of Gold sequences is the set generated by the preferred pair specified by the primitive characteristic polynomials

$$f_1(x) = 1 + x^3 + x^7, \quad f_2(x) = 1 + x + x^2 + x^3 + x^7 \quad (10-24)$$

Since  $m = 7$ , there are 129 Gold sequences of period 127 in this set, and (10-23) gives  $\theta_{\max} = 0.134$ . Equation (2-57) indicates that there are only 18 maximal sequences with  $m = 7$ . For this set of 18 sequences, calculations [35] indicate that  $\theta_{\max} = 0.323$ . If  $\theta_{\max} = 0.134$  is desired for a set of maximal sequences with  $m = 7$ , then one finds that the

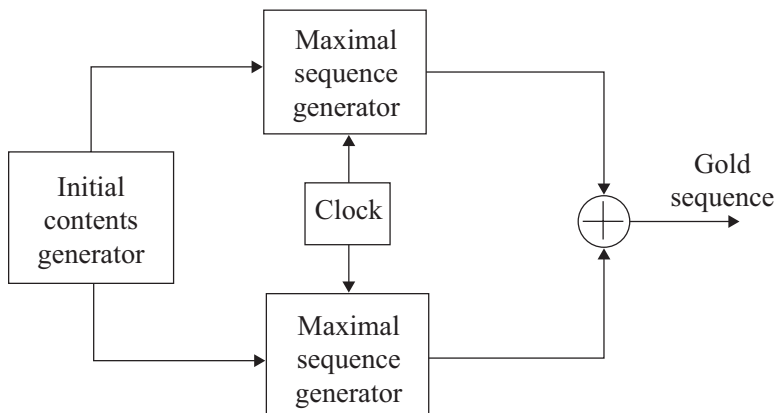


Figure 59. Gold sequence generator.

set has only 6 sequences. This result illustrates the much greater utility of Gold sequences in CDMA networks with many subscribers.

Consider a Gold sequence generated by using the characteristic functions  $f_1(x)$  and  $f_2(x)$  of degree  $m$ . The generating function for the Gold sequence is

$$\begin{aligned} G(x) &= \frac{\phi_1(x)}{f_1(x)} + \frac{\phi_2(x)}{f_2(x)} \\ &= \frac{\phi_1(x)f_2(x) + \phi_2(x)f_1(x)}{f_1(x)f_2(x)} \end{aligned} \quad (10-25)$$

where  $\phi_1(x)$  and  $\phi_2(x)$  have the form specified by the numerator of (2-54). Since the degrees of both  $\phi_1(x)$  and  $\phi_2(x)$  are less than  $m$ , the degree of the numerator of  $G(x)$  must be less than  $2m$ . Since the product  $f_1(x)f_2(x)$  has the form of a characteristic function of degree  $2m$  given by (2-50), this product defines the feedback coefficients of a single linear feedback shift register with  $2m$  stages that can generate the Gold sequences. The initial state of the register for any particular sequence can be determined by equating each coefficient in the numerator of (10-25) with the corresponding coefficient in (2-54) and then solving  $2m$  linear equations.

A *small set of Kasami sequences* comprises  $2^{m/2}$  sequences with period  $2^m - 1$  if  $m$  is even [35]. To generate a set, a maximal sequence  $\mathbf{a}$  with period  $N = 2^m - 1$  is decimated by  $q = 2^{m/2} + 1$  to form a binary sequence  $\mathbf{b}$  with period  $N/\gcd(N, q) = 2^{m/2} - 1$ . The modulo-2 addition of  $\mathbf{a}$  and any cyclic shift of  $\mathbf{b}$  from 0 to  $2^{m/2} - 2$  provides a Kasami sequence. By including  $\mathbf{a}$ , we obtain a set of  $2^{m/2}$  Kasami sequences with period  $2^m - 1$ . The periodic cross-correlation between any two Kasami sequences in a set can only take the values  $-s(m)/N$ ,  $-1/N$ , or  $[s(m) - 2]/N$ , where

$$s(m) = 2^{m/2} + 1 \quad (10-26)$$

The peak magnitude of the periodic cross-correlation between any two Kasami sequences is

$$\theta_{\max} = \frac{s(m)}{N} = \frac{2^{m/2} + 1}{2^m - 1} = \frac{1}{2^{m/2} - 1} \quad (10-27)$$

For  $m \geq 2$  and  $M = 2^{m/2}$ , the use of  $NM - 1 > NM - N$  in the Welch bound gives  $\theta_{\max} > 1/\sqrt{N}$ . Since  $N = 2^m - 1$ ,

$$N\theta_{\max} > \sqrt{2^m - 1} > 2^{m/2} - 1 \quad (10-28)$$

Since  $N$  is an odd integer,  $A_j - D_j$  in (10-13) must be an odd integer. Therefore, the definition of  $\theta_{\max}$  and (10-13) indicate that  $N\theta_{\max}$  must be an odd integer. Inequality (10-28) then implies that for  $M = 2^{m/2}$ ,  $N = 2^m - 1$ , and even values of  $m$ ,

$$N\theta_{\max} \geq 2^{m/2} + 1 \quad (10-29)$$

A comparison of this result with (10-27) indicates that the Kasami sequences are optimal in the sense that  $\theta_{\max}$  has the minimum value for any set of sequences of the same size and period.

As an example, let  $m = 10$ . There are 60 maximal sequences, 1025 Gold sequences, and 32 Kasami sequences with period 1023. The peak cross-correlations are 0.37, 0.06, and 0.03, respectively.

A large set of Kasami sequences comprises  $2^{m/2}(2^m + 1)$  sequences if  $m = 2$  modulo-4 and  $2^{m/2}(2^m + 1) - 1$  sequences if  $m = 0$  modulo-4 [35]. The sequences have period  $2^m - 1$ . To generate a set, a maximal sequence  $\mathbf{a}$  with period  $N = 2^m - 1$  is decimated by  $q = 2^{m/2} + 1$  to form a binary sequence  $\mathbf{b}$  and then decimated by  $q = 2^{(m+2)/2} + 1$  to form another binary sequence  $\mathbf{c}$ . The modulo-2 addition of  $\mathbf{a}$ , a cyclic shift of  $\mathbf{b}$ , and a cyclic shift of  $\mathbf{c}$  provides a Kasami sequence with period  $N$ . The periodic cross-correlations between any two Kasami sequences in a set can only take the values  $-1/N$ ,  $-t(m)/N$ ,  $[t(m) - 2]/N$ ,  $-s(m)/N$ , or  $[s(m) - 2]/N$ . A large set of Kasami sequences includes both a small set of Kasami sequences and a set of Gold sequences as subsets. Since  $t(m) \geq s(m)$ , the value of  $\theta_{\max}$  for a large set is the same as that for Gold sequences (10-23). This value is suboptimal, but the large size of these sets makes them an attractive option for asynchronous CDMA networks.

### 10.3 Symbol Error Probability for Direct-Sequence Systems

Let  $\mathbf{d}_i = (d_{-1}^{(i)}, d_0^{(i)})$  denote the vector of the two symbols of asynchronous multiple-access interference signal  $i$  that are received during the detection of a symbol of the desired signal. A straightforward evaluation of (10-3) gives

$$V_1 = \sum_{i=1}^{K-1} \sqrt{\frac{I_i}{2}} \cos \phi_i \left[ d_{-1}^{(i)} R_{pi}(\tau_i) + d_0^{(i)} \hat{R}_{pi}(\tau_i) \right] \quad (10-30)$$

where the *continuous-time partial cross-correlation functions* are

$$R_{pi}(\tau) = \int_0^\tau p(t)q_i(t - \tau)dt \quad (10-31)$$

$$\hat{R}_{pi}(\tau) = \int_\tau^T p(t)q_i(t - \tau)dt \quad (10-32)$$

For rectangular chip waveforms and spreading sequences of period  $N$ , straightforward calculations yield

$$R_{pi}(\tau) = A_{pi}(l - N)T_c + [A_{pi}(l + 1 - N) - A_{pi}(l - N)](\tau - lT_c) \quad (10-33)$$

$$\hat{R}_{pi}(\tau) = A_{pi}(l)T_c + [A_{pi}(l + 1) - A_{pi}(l)](\tau - lT_c) \quad (10-34)$$

where  $l = \lfloor \tau/T_c \rfloor$  and the *aperiodic cross-correlation function* is defined by

$$A_{pi}(l) = \begin{cases} \sum_{j=0}^{N-1-l} p_j q_{j+l}^{(i)}, & 0 \leq l \leq N-1 \\ \sum_{j=0}^{N-1+l} p_j q_j^{(i)}, & 1-N \leq l < 0 \end{cases} \quad (10-35)$$

and  $A_{pi}(l) = 0$  for  $|l| \geq N$ . These equations indicate that the aperiodic cross-correlations are more important than the related periodic cross-correlations defined by (10-12) in determining the interference level and, hence, the symbol error probability. Without careful selection of the sequences, the aperiodic cross-correlations may be much larger than the periodic cross-correlation. If all the spreading sequences are short with  $N = G$ , and  $S = I_i, i = 1, 2, \dots, K-1$ , then the symbol error probability can be approximated and bounded [36], [37], but the process is complicated. An alternative approach is to model the spreading sequences as random binary sequences, as is done for long sequences.

In a network with multiple-access interference, code acquisition depends on both the periodic and aperiodic cross-correlations. In the absence of data modulations,  $V_c$  in (7-73) has additional terms, each of which is proportional to the periodic cross-correlation between the desired signal and an interference signal. When data modulations are present, some or all of these terms entail aperiodic cross-correlations.

#### 10.4 Complex-Valued Quaternary Sequences

Quaternary direct-sequence system (Section 4) may use pairs of short binary sequences, such as Gold or Kasami sequences, to exploit the favorable periodic autocorrelation and cross-correlation functions. However, Gold sequences do not attain the Welch bound, and Kasami sequences that do are limited in number. To support many users and to facilitate the unambiguous synchronization to particular signals in a CDMA network, one might consider complex-valued quaternary sequences that are not derived from pairs of standard binary sequences but have better periodic correlation functions.

For  $q$ -ary PSK modulation, sequence symbols are powers of the complex  $q$ th root of unity, which is

$$\Omega = \exp\left(j \frac{2\pi}{q}\right) \quad (10-36)$$

where  $j = \sqrt{-1}$ . The complex spreading or signature sequence  $\mathbf{p}$  of period  $N$  has symbols given by

$$p_i = \Omega^{a_i} e^{j\phi_r}, \quad a_i \in Z_q = \{0, 1, 2, \dots, q-1\}, \quad i = 1, 2, \dots, N \quad (10-37)$$

where  $\phi_r$  is an arbitrary phase chosen for convenience. If  $p_i$  is specified by the exponent  $a_i$  and  $q_i$  is specified by the exponent  $b_i$ , then the periodic cross-correlation between sequences  $\mathbf{p}$  and  $\mathbf{q}$  is defined as

$$\theta_{pq}(k) = \frac{1}{N} \sum_{i=0}^{N-1} p_{i+k} q_i^* = \frac{1}{N} \sum_{i=0}^{N-1} \Omega^{a_{i+k} - b_i} \quad (10-38)$$

The maximum magnitude  $\theta_{max}$  defined by (10-15) must satisfy the Welch bound of (10-16). For a positive integer  $m$ , a family  $\mathcal{A}$  of  $M = N + 2$  quaternary or  $Z_4$  sequences, each of period  $N = 2^m - 1$ , with  $\theta_{max}$  that asymptotically approaches the Welch bound has been identified [38]. In contrast, a small set of binary Kasami sequences has only  $\sqrt{N+1}$  sequences

The sequences in a family  $\mathcal{A}$  are determined by the *characteristic polynomial*, which is defined as

$$f(x) = 1 + \sum_{i=0}^m c_i x^i \quad (10-39)$$

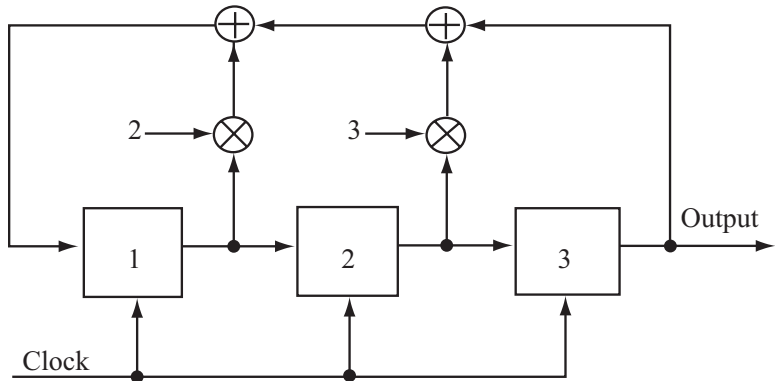
where coefficients  $c_i \in Z_4$  and  $c_m = 1$ . The output sequence satisfies the linear recurrence relation of (2-14). For example, the characteristic polynomial  $f(x) = 1 + 2x + 3x^2 + x^3$  has  $m = 3$  and generates a family with period  $N = 7$ . A feedback shift register that implements the sequence of the family is depicted in Figure 60(a), where all operations are modulo-4. The generation of a particular sequence is illustrated in Figure 60(b). Different sequences may be generated by loading the shift register with any nonzero initial contents and then cycling the shift register through its full period  $N = 2^m - 1$ . Since the shift register has  $4^m - 1$  nonzero states, there are  $M = (4^m - 1)/(2^m - 1) = 2^m + 1$  *cyclically distinct* members of the family. Each family member may be generated by loading the shift register with any nonzero triple that is not a state occurring during the generation of another family member.

A complex-valued symbol in the family  $\mathcal{A}$  may be represented by  $d = d_1 + jd_2$ , where  $d_1$  and  $d_2$  are antipodal symbols with values  $\pm 1/\sqrt{2}$  and  $\phi_r = \pi/4$  in (10-37). If a complex-valued symbol of the spreading sequence is  $p = p_1 + jp_2$ , then the complex multiplication of the data and spreading sequences produces the complex-valued sequence  $y = y_1 + jy_2 = dp$ . The implementation of this product is shown in Figure 61, in which real-valued inputs  $d_1, d_2, p_1$  and  $p_2$  produce the two real-valued outputs  $y_1$  and  $y_2$ . The equation  $y = dp$  gives a compact complex-variable representation of the real variable equations:

$$y_1 = d_1 p_1 - d_2 p_2, \quad y_2 = d_2 p_1 + d_1 p_2 \quad (10-40)$$

Each chip  $y_1$  modulates the in-phase carrier, and each chip  $y_2$  modulates the quadrature carrier. The transmitted signal may be represented as

$$s(t) = \Re \{ Ad(t)p(t)e^{j2\pi f_c t} \} \quad (10-41)$$



(a)

Shift	Contents		
	Stage 1	Stage 2	Stage 3
Initial	0	0	1
1	1	0	0
2	2	1	0
3	3	2	1
4	1	3	2
5	1	1	3
6	0	1	1
7	0	0	1

(b)

Figure 60. (a) Feedback shift register for a quaternary sequence and (b) contents after successive shifts.

where  $\Re\{x\}$  denotes the real part of  $x$ ,  $A$  is the amplitude, and  $d(t)$  and  $p(t)$  are waveforms modulated by the data and spreading sequences.

A representation of the receiver in terms of complex variables is illustrated in Figure 61. If  $f_c T_c \gg 1$ , two cross-correlation terms are negligible, and the actual implementation can be done by the architectures of Figures 17 and 19 except that the final multiplications in the two branches are replaced by a complex multiplication. Thus,  $y$  is extracted by separate in-phase and quadrature demodulation. Since the complex quaternary symbols have unity magnitude, the despreading entails the complex multiplication of  $y$  by  $p^*$  to produce  $d|p|^2 = d$  along with the residual interference and noise. As illustrated in Figure 62, the summation of  $G$  multiplications produces the decision variable, where  $G$  is the number of chips per bit.

Although some complex-valued quaternary sequences have more favorable periodic autocorrelations and cross-correlations than pairs of standard binary sequences, they do not provide significantly smaller error probabilities in multiple-access systems [39]. The reason is that system performance is determined by the complex aperiodic functions analogous to those of Section 10.3. However, complex sequences have the potential to provide better acquisition performance than the Gold or Kasami sequences because of their superior periodic autocorrelations.

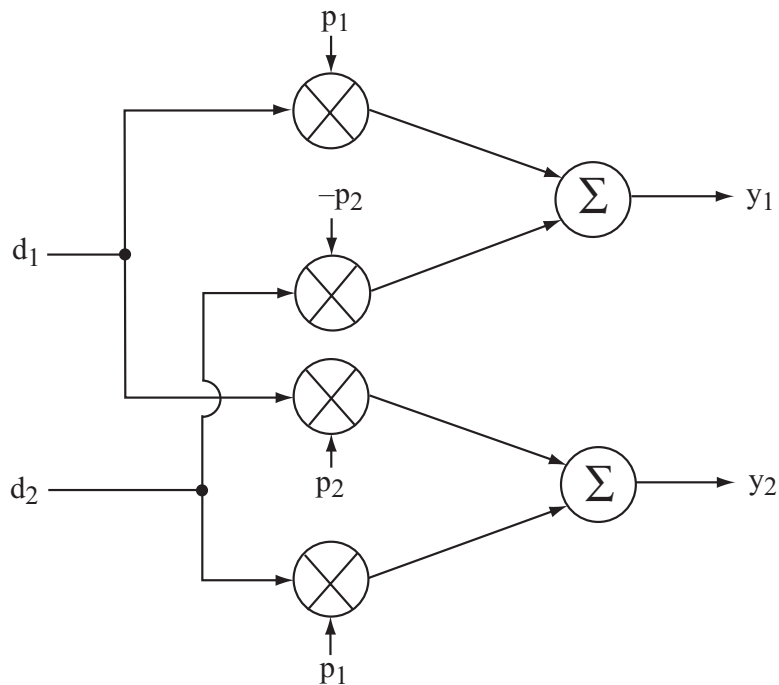


Figure 61. Product of quaternary data and spreading sequences.

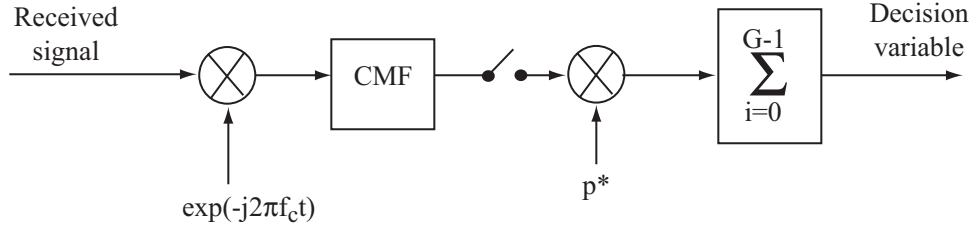


Figure 62. Receiver for direct-sequence system with complex quaternary spreading sequences. CMF is chip-matched filter.

## 10.5 Direct-Sequence Systems with PSK and Random Sequences

If all the spreading sequences in a network of asynchronous CDMA systems have a common period equal to the data-symbol duration, then by the proper selection of the sequences and their relative phases, one can obtain a system performance better than that theoretically attainable with random sequences. However, the number of suitable sequences is too small for many applications, and long sequences that extend over many data symbols provide more system security. Furthermore, long sequences ensure that successive data symbols are covered by different sequences, thereby limiting the time duration of an unfavorable cross-correlation due to multiple-access interference. Even if short sequences are used, the random-sequence model gives fairly accurate performance predictions.

Consider the direct-sequence receiver of Figure 14 when multiple-access interference is present. If the spreading sequence of the desired signal is modeled as a random binary sequence and the chip waveform confined to  $[0, T_c]$ , then (3-15) indicates that an input  $V$  to the decision device has mean value

$$E[V] = d_0 \sqrt{\frac{S}{2}} T_s \quad (10-42)$$

for the direct-sequence system with coherent PSK. The interference component is

$$V_1 = \sum_{\nu=0}^{G-1} p_\nu J_\nu \quad (10-43)$$

where

$$J_\nu = \int_{\nu T_c}^{(\nu+1)T_c} i(t) \psi(t - \nu T_c) \cos 2\pi f_c t \, dt \quad (10-44)$$

and  $i(t)$  is given by (10-1). Since the data modulation  $d_i(t)$  in an interference signal is modeled as a random binary sequence, it can be subsumed into  $q_i(t)$  given by (10-2) with no loss of generality. Since  $q_i(t)$  is determined by an independent, random spreading sequence, only time delays modulo- $T_c$  are significant and, thus, we can assume that  $0 \leq \tau_i < T_c$  in (10-1) without loss of generality.

Since  $\psi(t)$  is confined to  $[0, T_c]$  and  $f_c T_c \gg 1$ , the substitution of (10-1) and (10-2) into (10-44) yields

$$J_\nu = \sum_{i=1}^{K-1} \sqrt{\frac{I_i}{2}} \cos \phi_i \left\{ q_{\nu-1}^{(i)} \int_{\nu T_c}^{\nu T_c + \tau_i} \psi(t - \nu T_c) \psi[t - (\nu - 1)T_c - \tau_i] dt \right. \\ \left. + q_\nu^{(i)} \int_{\nu T_c + \tau_i}^{(\nu+1)T_c} \psi(t - \nu T_c) \psi(t - \nu T_c - \tau_i) dt \right\} \quad (10-45)$$

The *partial autocorrelation* for the chip waveform is defined as

$$R_\psi(s) = \int_0^s \psi(t) \psi(t + T_c - s) dt, \quad 0 \leq s < T_c \quad (10-46)$$

Substitution into (10-45) and appropriate changes of variables in the integrals yield

$$J_\nu = \sum_{i=1}^{K-1} \sqrt{\frac{I_i}{2}} \cos \phi_i \left[ q_{\nu-1}^{(i)} R_\psi(\tau_i) + q_\nu^{(i)} R_\psi(T_c - \tau_i) \right] \quad (10-47)$$

For rectangular pulses in the spreading waveform,

$$\psi(t) = \begin{cases} 1 & , \quad 0 \leq t \leq T_c \\ 0 & , \quad \text{otherwise.} \end{cases} \quad (10-48)$$

Consequently,

$$R_\psi(s) = s, \quad \text{rectangular pulse} \quad (10-49)$$

For sinusoidal pulses in the spreading waveform,

$$\psi(t) = \begin{cases} \sqrt{2} \sin\left(\frac{\pi}{T_c} t\right) & , \quad 0 \leq t \leq T_c \\ 0 & , \quad \text{otherwise.} \end{cases} \quad (10-50)$$

Substituting this equation into (10-46), using a trigonometric identity, and performing the integrations, we obtain

$$R_\psi(s) = \frac{T_c}{\pi} \sin\left(\frac{\pi}{T_c} s\right) - s \cos\left(\frac{\pi}{T_c} s\right), \quad \text{sinusoidal pulse} \quad (10-51)$$

Since both  $J_\nu$  and  $J_{\nu+1}$  contain the same random variable  $q_\nu^{(i)}$ , it does not appear at first that the terms in (10-47) are statistically independent even when  $\boldsymbol{\phi} = (\phi_1, \phi_2, \dots, \phi_{K-1})$  and  $\boldsymbol{\tau} = (\tau_1, \tau_2, \dots, \tau_{K-1})$  are given. The following lemma [40] resolves this issue.

**Lemma.** Suppose that  $\{\alpha_i\}$  and  $\{\beta_i\}$  are statistically independent, random binary sequences. Let  $x$  and  $y$  denote arbitrary constants. Then  $\alpha_i \beta_j x$  and  $\alpha_i \beta_k y$  are statistically independent random variables when  $j \neq k$ .

*Proof.* Let  $P(\alpha_i\beta_jx = a, \alpha_i\beta_ky = b)$  denote the joint probability that  $\alpha_i\beta_jx = a$  and  $\alpha_i\beta_ky = b$  where  $|a| = |x|$  and  $|b| = |y|$ . From the theorem of total probability, it follows that

$$\begin{aligned} & P(\alpha_i\beta_jx = a, \alpha_i\beta_ky = b) \\ &= P(\alpha_i\beta_jx = a, \alpha_i\beta_ky = b, \alpha_i = 1) + P(\alpha_i\beta_jx = a, \alpha_i\beta_ky = b, \alpha_i = -1) \\ &= P(\beta_jx = a, \beta_ky = b, \alpha_i = 1) + P(\beta_jx = -a, \beta_ky = -b, \alpha_i = -1) \end{aligned}$$

From the independence of  $\{\alpha_i\}$  and  $\{\beta_j\}$  and the fact that they are random binary sequences, we obtain the further simplification for  $j \neq k$ ,  $x \neq 0$ , and  $y \neq 0$ :

$$\begin{aligned} & P(\alpha_i\beta_jx = a, \alpha_i\beta_ky = b) \\ &= P(\beta_jx = a)P(\beta_ky = b)P(\alpha_i = 1) + P(\beta_jx = -a)P(\beta_ky = -b)P(\alpha_i = -1) \\ &= \frac{1}{2}P\left(\beta_j = \frac{a}{x}\right)P\left(\beta_k = \frac{b}{y}\right) + \frac{1}{2}P\left(\beta_j = -\frac{a}{x}\right)P\left(\beta_k = -\frac{b}{y}\right) \end{aligned}$$

Since  $\beta_j$  equals  $+1$  or  $-1$  with equal probability,  $P(\beta_j = a/x) = P(\beta_j = -a/x)$  and thus

$$\begin{aligned} P(\alpha_i\beta_jx = a, \alpha_i\beta_ky = b) &= P\left(\beta_j = \frac{a}{x}\right)P\left(\beta_k = \frac{b}{y}\right) \\ &= P(\beta_jx = a)P(\beta_ky = b) \end{aligned}$$

A similar calculation gives

$$P(\alpha_i\beta_jx = a)P(\alpha_i\beta_ky = b) = P(\beta_jx = a)P(\beta_ky = b)$$

Therefore,

$$P(\alpha_i\beta_jx = a, \alpha_i\beta_ky = b) = P(\alpha_i\beta_jx = a)P(\alpha_i\beta_ky = b)$$

which satisfies the definition of statistical independence of  $\alpha_i\beta_jx$  and  $\alpha_i\beta_ky$ . The same relation is trivial to establish for  $x = 0$  or  $y = 0$ .  $\square$

The lemma indicates that when  $\phi$  and  $\tau$  are given, the terms in (10-43) are statistically independent. Since  $p_\nu^2 = 1$ , the conditional variance is

$$\text{var}(V_1) = \sum_{\nu=0}^{G-1} \text{var}(J_\nu) \quad (10-52)$$

The independence of the  $K$  spreading sequences, the independence of successive terms in each random binary sequence, and (10-47) imply that the conditional variance of  $J_\nu$  is independent of  $\nu$  and, therefore,

$$\text{var}(V_1) = \sum_{i=1}^{K-1} \frac{1}{2}GI_i \cos^2 \phi_i [R_\psi^2(\tau_i) + R_\psi^2(T_c - \tau_i)] \quad (10-53)$$

Since the terms of  $V_1$  in (10-43) are independent, zero-mean random variables that are uniformly bounded and  $\text{var}(V_1) \rightarrow \infty$  as  $G \rightarrow \infty$ , the central limit theorem [6] implies that  $V_1/\sqrt{\text{var}(V_1)}$  converges in distribution to a Gaussian random variable with mean 0 and variance 1. Thus, when  $\phi$  and  $\tau$  are given, the conditional distribution of  $V_1$  is approximately Gaussian when  $G$  is large. Since the noise component  $V_2$  in (3-10) has a Gaussian distribution and is independent of  $V_1$ ,  $V$  has an approximate Gaussian distribution with mean given by (10-42), and  $\text{var}(V) = \text{var}(V_1) + \text{var}(V_2)$ .

A straightforward derivation using the Gaussian distribution of the decision statistic  $V$  indicates that the conditional symbol error probability given  $\phi$  and  $\tau$  is

$$P_s(\phi, \tau) = Q\left(\sqrt{\frac{2\mathcal{E}_s}{N_{0e}(\phi, \tau)}}\right) \quad (10-54)$$

where  $\mathcal{E}_s = ST_s$  is the *energy per symbol* in  $d(t)$ , and the *equivalent noise power spectral density* is defined as

$$N_{0e}(\phi, \tau) = N_0 + \sum_{i=1}^{K-1} 2\frac{I_i}{T_c} \cos^2 \phi_i [R_\psi^2(\tau_i) + R_\psi^2(T_c - \tau_i)] \quad (10-55)$$

For rectangular pulses, this equation simplifies to

$$N_{0e}(\phi, \tau) = N_0 + \sum_{i=1}^{K-1} 2I_i T_c \cos^2 \phi_i \left(1 - 2\frac{\tau_i}{T_c} + 2\frac{\tau_i^2}{T_c^2}\right) \quad (10-56)$$

Numerical evaluations [40] give strong evidence that the error in (10-54) due to the Gaussian approximation is negligible if  $G \geq 50$ . For an asynchronous network, it is assumed that the time delays are independent and uniformly distributed over  $[0, T_c)$  and that the phase angles  $\theta_i, i = 1, 2, \dots, K-1$ , are uniformly distributed over  $[0, 2\pi)$ . Therefore, the symbol error probability is

$$P_s = \left(\frac{2}{\pi T_c}\right)^{K-1} \int_0^{\pi/2} \dots \int_0^{\pi/2} \int_0^{T_c} \dots \int_0^{T_c} P_s(\phi, \tau) d\phi d\tau \quad (10-57)$$

where the fact that  $\cos^2 \phi_i$  takes all its possible values over  $[0, \pi/2)$  has been used to shorten the integration intervals. The absence of sequence parameters ensures that the amount of computation required for (10-57) is much less than the amount required to compute  $P_s$  when the spreading sequence is short. Nevertheless, the computational requirements are large enough that it is highly desirable to find an accurate approximation that entails less computation. The conditional symbol error probability given  $\phi$  is defined as

$$P_s(\phi) = \left(\frac{1}{T_c}\right)^{K-1} \int_0^{T_c} \dots \int_0^{T_c} P_s(\phi, \tau) d\tau \quad (10-58)$$

A closed-form approximation to  $P_s(\boldsymbol{\phi})$  greatly simplifies the computation of  $P_s$ , which reduces to

$$P_s = \left(\frac{2}{\pi}\right)^{K-1} \int_0^{\pi/2} \dots \int_0^{\pi/2} P_s(\boldsymbol{\phi}) d\boldsymbol{\phi} \quad (10-59)$$

To approximate  $P_s(\boldsymbol{\phi})$ , we first obtain upper and lower bounds on it.

For either rectangular or sinusoidal pulses, elementary calculus establishes that

$$R_{\psi}^2(\tau_i) + R_{\psi}^2(T_c - \tau_i) \leq T_c^2 \quad (10-60)$$

Using this upper bound successively in (10-55), (10-54), and (10-58), and performing the trivial integrations that result, we obtain

$$P_s(\boldsymbol{\phi}) \leq Q\left(\sqrt{\frac{2\mathcal{E}_s}{N_{0u}(\boldsymbol{\phi})}}\right) \quad (10-61)$$

where

$$N_{0u}(\boldsymbol{\phi}) = N_0 + \sum_{i=1}^{K-1} 2I_i T_c \cos^2 \phi_i \quad (10-62)$$

To apply Jensen's inequality (4-22), the successive integrals in (10-57) are interpreted as the evaluation of expected values. Consider the random variable

$$X = R_{\psi}^2(\tau_i) + R_{\psi}^2(T_c - \tau_i). \quad (10-63)$$

Since  $\tau_i$  is uniformly distributed over  $[0, T_c]$ , straightforward calculations using (10-49) and (10-51) give

$$E[X] = \frac{1}{T_c} \int_0^{T_c} [R_{\psi}^2(\tau_i) + R_{\psi}^2(T_c - \tau_i)] d\tau_i = hT_c^2 \quad (10-64)$$

where

$$h = \begin{cases} \frac{2}{3}, & \text{rectangular pulse} \\ \frac{1}{3} + \frac{5}{2\pi^2}, & \text{sinusoidal pulse.} \end{cases} \quad (10-65)$$

The function (10-54) has the form given by (4-23). Therefore, (10-55), (10-60), and  $\cos^2 \phi_i \leq 1$  yield a sufficient condition for convexity:

$$\mathcal{E}_s \geq \frac{3}{2} \left[ N_0 + \sum_{i=1}^{K-1} 2I_i T_c \right] \quad (10-66)$$

Application of Jensen's inequality successively to each component of  $\boldsymbol{\tau}$  in (10-58) yields

$$P_s(\boldsymbol{\phi}) \geq Q\left(\sqrt{\frac{2\mathcal{E}_s}{N_{0l}(\boldsymbol{\phi})}}\right) \quad (10-67)$$

where

$$N_{0l}(\phi) = N_0 + \sum_{i=1}^{K-1} 2hI_iT_c \cos^2 \phi_i \quad (10-68)$$

If  $N_0$  is negligible, then (10-68) and (10-62) give  $N_{0l}/N_{0u} = h$ . Thus, a good approximation is provided by

$$P_s(\phi) \approx Q\left(\sqrt{\frac{2\mathcal{E}_s}{N_{0a}(\phi)}}\right) \quad (10-69)$$

where

$$N_{0a}(\phi) = N_0 + \sum_{i=1}^{K-1} 2\sqrt{h}I_iT_c \cos^2 \phi_i \quad (10-70)$$

If  $N_0$  is negligible, then  $N_{0u}/N_{0a} = N_{0a}/N_{0l} = 1/\sqrt{h}$ . Therefore, in terms of the value of  $\mathcal{E}_s$  needed to ensure a given  $P_s(\phi)$ , the error in using approximation (10-69) instead of (10-58) is bounded by  $10 \log_{10}(1/\sqrt{h})$  in decibels, which equals 0.88 dB for rectangular pulses and 1.16 dB for sinusoidal pulses. In practice, the error is expected to be only a few tenths of a decibel because  $N_0 \neq 0$  and  $P_s$  coincides with neither the upper nor the lower bound.

As an example, suppose that rectangular pulses are used,  $\mathcal{E}_s/N_0 = 15$  dB, and  $K = 2$ . Figure 63 illustrates four different evaluations of  $P_s$  as a function of  $G\mathcal{E}_s/IT_s = GS/I$ , the *despread signal-to-interference ratio*, which is the signal-to-interference ratio after taking into account the beneficial results from the despreading in the receiver. The accurate approximation is computed from (10-54) and (10-57), the upper bound from (10-61) and (10-59), the lower bound from (10-67) and (10-59), and the simple approximation from (10-69) and (10-59). The figure shows that the accurate approximation moves from the lower bound toward the simple approximation as the symbol error probability decreases. For  $P_s = 10^{-5}$ , the simple approximation is less than 0.3 dB in error relative to the accurate approximation. Figure 64 compares the symbol error probabilities for  $K = 2$  to  $K = 4$ , rectangular pulses and  $\mathcal{E}_s/N_0 = 15$  dB. The simple approximation is used for  $P_s$ , and the abscissa shows  $GS/I$  where  $I$  is the interference power of each equal-power interfering signal. The figure shows that  $P_s$  increases with  $K$ , but the shift in  $P_s$  is mitigated somewhat because the interference signals tend to partially cancel each other.

The preceding bounding methods can be extended to the bounds on  $P_s(\phi)$  by observing that  $\cos^2 \phi_i \leq 1$  and setting  $X = \cos^2 \phi_i$  during the successive applications of Jensen's inequality, which is applicable if (10-66) is satisfied. After evaluating (10-59), we obtain

$$Q\left(\sqrt{\frac{2\mathcal{E}_s}{N_0 + hI_tT_c}}\right) \leq P_s \leq Q\left(\sqrt{\frac{2\mathcal{E}_s}{N_0 + 2I_tT_c}}\right) \quad (10-71)$$

where

$$I_t = \sum_{i=1}^{K-1} I_i \quad (10-72)$$

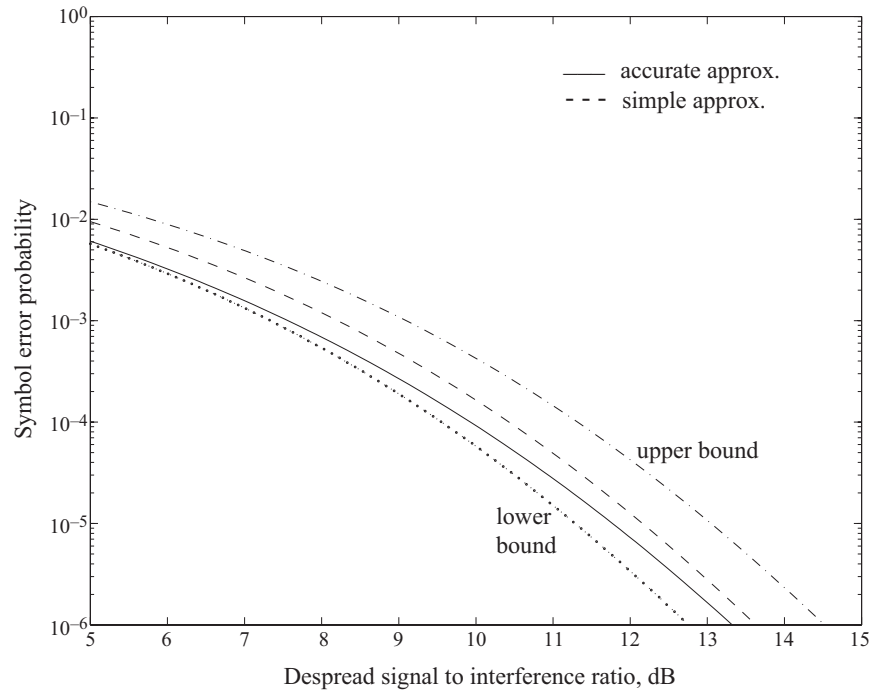


Figure 63. Symbol error probability of direct-sequence system with PSK in presence of single multiple-access interference signal and  $\mathcal{E}_s/N_0 = 15$  dB.

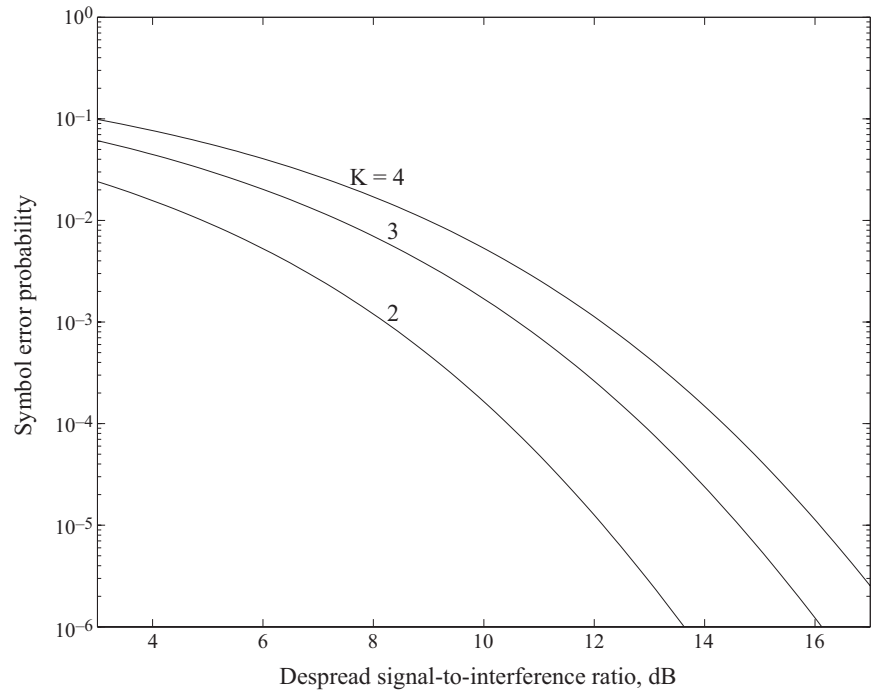


Figure 64. Symbol error probability of direct-sequence system with PSK in presence of  $K - 1$  equal-power multiple-access interference signals and  $\mathcal{E}_s/N_0 = 15$  dB.

A simple approximation is provided by

$$P_s \approx Q\left(\sqrt{\frac{2\mathcal{E}_s}{N_0 + \sqrt{2h} I_t T_c}}\right) \quad (10-73)$$

If  $P_s$  is specified, then the error in the required  $\mathcal{E}_s/I_t$  caused by using (10-73) instead of (10-57) is bounded by  $10 \log_{10} \sqrt{2/h}$  in decibels. Thus, the error is bounded by 2.39 dB for rectangular pulses and 2.66 dB for sinusoidal pulses.

The lower bound in (10-71) gives the same result as that often called the *standard Gaussian approximation*, in which  $V_1$  in (10-43) is assumed to be approximately Gaussian, each  $\phi_i$  in (10-47) is assumed to be uniformly distributed over  $[0, 2\pi)$ , and each  $\tau_i$  is assumed to be uniformly distributed over  $[0, T_c)$ . This approximation, gives an optimistic result for  $P_s$  that can be as much as 4.77 dB in error for rectangular pulses according to (10-71). The substantial improvement in accuracy provided by (10-69) or (10-54) is due to the application of the Gaussian approximation only after conditioning  $V_1$  on given values of  $\phi$  and  $\tau$ . The accurate approximation given by (10-54) is a version of what is often called the *improved Gaussian approximation*.

Figure 65 illustrates the symbol error probability for 3 interferers, each with power  $I$ , rectangular pulses, and  $\mathcal{E}_s/N_0 = 15$  dB as a function of  $GS/I$ . The graphs show the standard Gaussian approximation of (10-71), the simple approximation of (10-73), and the upper and lower bounds given by (10-61), (10-67), and (10-59). The large error in the standard Gaussian approximation is evident. The simple approximation is reasonably accurate if  $10^{-6} \leq P_s \leq 10^{-2}$ .

For *synchronous* networks, (10-54) and (10-55) can be simplified because the  $\{\tau_i\}$  are all zero. For either rectangular or sinusoidal pulses, we obtain

$$P_s(\phi) = Q\left(\sqrt{\frac{2\mathcal{E}_s}{N_{0e}(\phi)}}\right) \quad (10-74)$$

where

$$N_{0e}(\phi) = N_0 + \sum_{i=1}^{K-1} 2I_i T_c \cos^2 \phi_i \quad (10-75)$$

A comparison with (10-61) and (10-62) indicates that  $P_s$  for a synchronous network equals or exceeds  $P_s$  for a similar asynchronous network when random spreading sequences are used. This phenomenon is due to the increased bandwidth of a despread asynchronous interference signal, which allows increased filtering in the receiver.

The accurate approximation of (10-54) follows from the standard central limit theorem, which is justified by the lemma. This lemma depends on the restriction of the chip

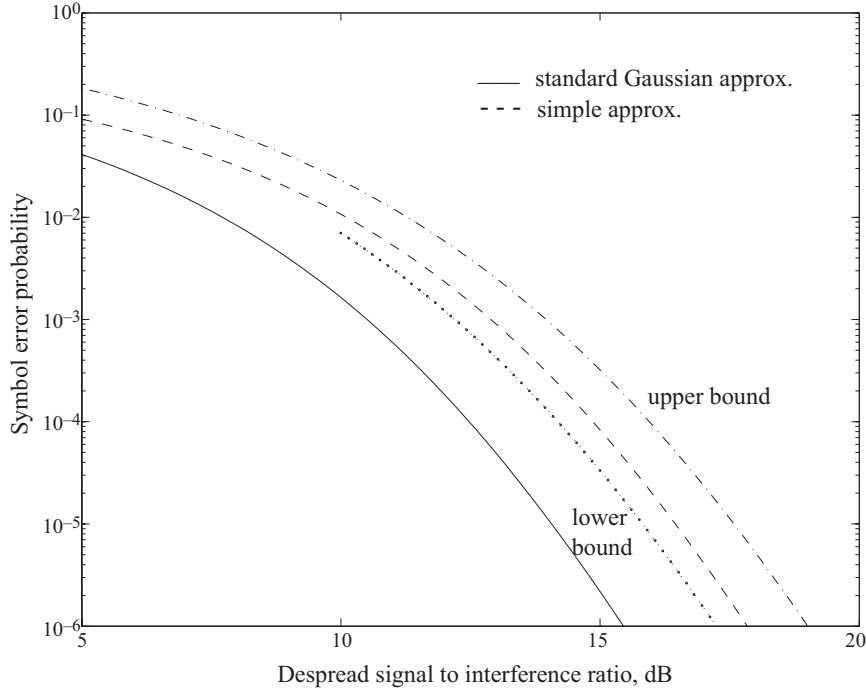


Figure 65. Symbol error probability of direct-sequence system with PSK in presence of 3 equal-power multiple-access interference signals and  $\mathcal{E}_s/N_0 = 15$  dB.

waveform to the interval  $[0, T_c]$ . If the chip waveform extends beyond this interval but is time-limited, as is necessary for implementation with digital hardware, then an extension of the central limit theorem for  $m$ -dependent sequences can be used to derive an improved Gaussian approximation [41]. Alternatives to the analysis in this section and the next one abound in the literature (e.g., [41], [42]), but they are not as amenable to comparisons among systems.

## 10.6 Quadriphase Direct-Sequence Systems with Random Sequences

Consider a network of quadriphase direct-sequence systems, each of which uses dual QPSK and random spreading sequences. Each direct-sequence signal is given by (4-1) with  $t_0 = 0$ . A suitable model for multiple-access interference is

$$i(t) = \sum_{i=1}^{K-1} [\sqrt{I} q_{1i}(t - \tau_i) \cos(2\pi f_c t + \phi_i) + \sqrt{I} q_{2i}(t - \tau_i) \sin(2\pi f_c t + \phi_i)] \quad (10-76)$$

where  $q_{1i}(t)$  and  $q_{2i}(t)$  both have the form of (10-2) and incorporate the data modulation. The decision variables are given by (4-2) and (4-4) with  $G = T_s/T_c$ . A straightforward

calculation using (10-44) indicates that

$$J_\nu = \sum_{i=1}^{K-1} \sqrt{I_i} \{ \cos \phi_i [q_{\nu-1}^{(1i)} R_\psi(\tau_i) + q_\nu^{(1i)} R_\psi(T_c - \tau_i)] \\ - \sin \phi_i [q_{\nu-1}^{(2i)} R_\psi(\tau_i) + q_\nu^{(2i)} R_\psi(T_c - \tau_i)] \} \quad (10-77)$$

The statistical independence of the two sequences, the lemma of Section 10.5, and analogous results for  $J'_\nu$  yield the variances of the interference terms of the decision variables:

$$\text{var}(V_1) = \text{var}(U_1) = \sum_{i=1}^{K-1} \frac{1}{2} \frac{T_s}{T_c} I_i [R_\psi^2(\tau_i) + R_\psi^2(T_c - \tau_i)] \quad (10-78)$$

The noise variances and the means are given by (4-8) and (4-7). Since all variances and means are independent of  $\phi$ , the Gaussian approximation yields a  $P_s(\phi, \boldsymbol{\tau})$  that is independent of  $\phi$ :

$$P_s = \left( \frac{1}{T_c} \right)^{K-1} \int_0^{T_c} \cdots \int_0^{T_c} Q \left( \sqrt{\frac{2\mathcal{E}_s}{N_{0e}(\boldsymbol{\tau})}} \right) d\boldsymbol{\tau} \quad (10-79)$$

where

$$N_{0e}(\boldsymbol{\tau}) = N_0 + \sum_{i=1}^{K-1} \frac{I_i}{T_c} [R_\psi^2(\tau_i) + R_\psi^2(T_c - \tau_i)] \quad (10-80)$$

Since a similar analysis for direct-sequence systems with balanced QPSK yields (10-80) again, *both quadriphase systems perform equally well against multiple-access interference*. Application of the previous bounding and approximation methods to (10-79) yields

$$Q \left( \sqrt{\frac{2\mathcal{E}_s}{N_0 + hI_t T_c}} \right) \leq P_s \leq Q \left( \sqrt{\frac{2\mathcal{E}_s}{N_0 + I_t T_c}} \right) \quad (10-81)$$

where the total interference power  $I_t$  is defined by (10-72). A sufficient condition for the validity of the lower bound is

$$\mathcal{E}_s \geq \frac{3}{2} (N_0 + I_t T_c) \quad (10-82)$$

A simple approximation that limits the error in the required  $\mathcal{E}_s/I_t$  for a specified  $P_s$  to  $10 \log_{10}(1/\sqrt{h})$  is

$$P_s \approx Q \left( \sqrt{\frac{2\mathcal{E}_s}{N_0 + \sqrt{h} I_t T_c}} \right) \quad (10-83)$$

This approximation introduces errors bounded by 0.88 dB and 1.16 dB for rectangular and sinusoidal pulses, respectively, which are much less than the maximum errors for (10-73). In (10-81) and (10-83), only the total interference power is relevant, not how it is distributed among the individual interference signals.

Figure 66 illustrates  $P_s$  for a quadriphase direct-sequence system in the presence of 3 interferers, each with power  $I$ , rectangular pulses, and  $\mathcal{E}_s/N_0 = 15$  dB. The graphs plot the

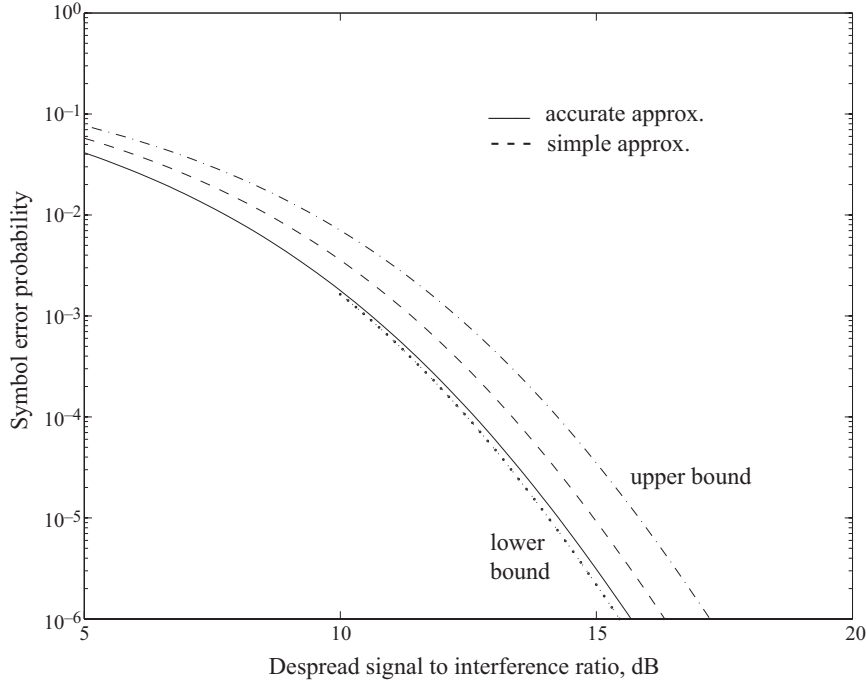


Figure 66. Symbol error probability of quadriphase direct-sequence system in presence of 3 equal-power multiple-access interference signals and  $\mathcal{E}_s/N_0 = 15$  dB.

accurate approximation of (10-79), the simple approximation of (10-83), and the bounds of (10-81) as functions of  $GS/I$ . A comparison of Figures 66 and 65 indicates the advantage of a quadriphase system.

For *synchronous networks* with either rectangular or sinusoidal pulses, we set the  $\{\tau_i\}$  equal to zero in (10-79) and obtain

$$P_s = Q\left(\sqrt{\frac{2\mathcal{E}_s}{N_0 + I_t T_c}}\right) \quad (10-84)$$

Since this equation coincides with the upper bound in (10-81), we conclude that asynchronous networks accommodate more multiple-access interference than similar synchronous networks using quadriphase direct-sequence signals with random spreading sequences. To compare asynchronous quadriphase direct-sequence systems with asynchronous systems using binary PSK, we find a lower bound on  $P_s$  for direct-sequence systems with PSK. Substituting (10-54) into (10-57) and applying Jensen's inequality successively to the integrations over  $\phi_i, i = 1, 2, \dots, K - 1$ , we find that a lower bound on  $P_s$  is given by the right-hand side of (10-79) if (10-82) is satisfied. This result implies that asynchronous quadriphase direct-sequence systems are more resistant to multiple-access interference than asynchronous direct-sequence systems with binary PSK. The equations for  $P_s$  allow the evaluation of the information-bit error probability  $P_b$  for error-correcting codes with hard-decision decoders. To facilitate the analysis of soft-decision decoding, two

assumptions are necessary. Assume that there is enough symbol interleaving that symbol errors are independent of each other and that  $K$  is large enough that the multiple-access interference after despreading is approximately Gaussian rather than conditionally Gaussian. Since the equivalent power spectral density  $N_{0e}$  is derived from the variance of a zero-mean process, it can be obtained by averaging  $N_{0e}(\boldsymbol{\phi}, \boldsymbol{\tau})$  over the distributions of  $\boldsymbol{\phi}$  and  $\boldsymbol{\tau}$ . With the application of (10-64), (10-72) and (10-80) yield

$$N_{0e} = N_0 + hI_tT_c \quad (10-85)$$

Thus, for a binary convolutional code with rate  $r$ , constraint length  $K$ , and minimum free distance  $d_f$ ,  $P_b$  is upper-bounded by (5-6) with

$$P_2(l) = Q\left(\sqrt{\frac{2\mathcal{E}_s l}{N_{0e}}}\right) = Q\left(\sqrt{\frac{2r\mathcal{E}_b l}{N_0 + hI_tT_c}}\right) \quad (10-86)$$

The *system capacity* is the number of equal-power users that can be accommodated while achieving a specified  $P_b$ . For equal-power users,  $I_t = (K - 1)\mathcal{E}_s/T_s$ . Let  $\gamma_1$  denote the value of  $\mathcal{E}_s/N_{0e}$  necessary for a specific error correcting code to achieve the specified  $P_b$ . Equation (10-85) implies that the system capacity is

$$K = \left\lceil 1 + \frac{G}{h} \left( \frac{1}{\gamma_1} - \frac{1}{\gamma_0} \right) \right\rceil, \quad \gamma_0 \geq \gamma_1 \quad (10-87)$$

where  $\lfloor x \rfloor$  is the integer part of  $x$ ,  $\gamma_0 = \mathcal{E}_s/N_0$ ,  $G = T_s/T_c$  is the processing gain, and the requirement  $\gamma_0 \geq \gamma_1$  is necessary to ensure that the specified  $P_b$  can be achieved for some value of  $K$ . Since  $h < 1$  in general, the factor  $G/h$  reflects the increased gain due to the random distributions of interference phases and delays. If they are not random but  $\boldsymbol{\phi} = \boldsymbol{\tau} = \mathbf{0}$ , then  $h = 1$  and the number of users accommodated is reduced.

As an example, consider a system that resembles the downlink of the IS-95 CDMA network. The data modulation is balanced QPSK and  $G = 64$ . The error-correcting code is a rate-1/2 binary convolutional code with constraint length 9. The chip waveform is approximately sinusoidal so that  $h = 1/3 + 5/2\pi^2 = 0.587$ . If  $P_b = 10^{-5}$  or better is desired, the performance curves for convolutional codes indicate that  $\gamma_1 \cong 3$  dB is required. Equation (10-87) then indicates that the system capacity is  $K = 44$  if  $\gamma_0 = 10$  dB and  $K = 54$  if  $\gamma_0 = 20$  dB.

## 10.7 Wideband Direct-Sequence CDMA

A direct-sequence CDMA system is called *wideband* if it uses a spectral band with a bandwidth that exceeds the coherence bandwidth of a frequency-selective fading channel. The two most commonly proposed types of wideband systems are single-carrier and

multicarrier systems. A single-carrier direct-sequence CDMA system uses a single carrier frequency to transmit signals. A multicarrier direct-sequence CDMA system partitions the available spectral band among multiple direct-sequence signals, each of which has a distinct carrier frequency. The main attractions of the multicarrier system are its potential ability to operate over disjoint, noncontiguous spectral regions and its ability to avoid transmissions in spectral regions with strong interference or where the multicarrier signal might interfere with other signals. These features have counterparts in frequency-hopping CDMA systems.

A single-carrier system provides diversity by using a rake receiver that combines several multipath signals. A multicarrier system provides diversity by the maximal-ratio combining of the parallel correlator outputs, each of which is associated with a different carrier. Bit error probabilities are determined subsequently for ideal multicarrier and single-carrier systems with lossless diversity combining in the presence of white Gaussian noise and Rayleigh fading.

### **Multicarrier Direct-Sequence CDMA**

A typical multicarrier system divides a spectral band of bandwidth  $W$  into  $L$  regions, each of bandwidth  $W/L$  approximately equal to the coherence bandwidth [43]. In the transmitter, the product  $d(t)p(t)$  of the data modulation  $d(t)$  and the spreading waveform  $p(t)$  simultaneously modulates  $L$  carriers, each of which has its frequency in the center of one of the  $L$  spectral regions, as illustrated in Figure 67(a). The receiver comprises  $L$  parallel demodulators, one for each carrier, the outputs of which are suitably combined, as indicated in Figure 67(b). The total signal power is divided equally among the  $L$  carriers. The chip rate and, hence, the processing gain for each carrier of a multicarrier direct-sequence system is reduced by the factor  $L$ . However, if strong interference exists in a spectral region, the associated carrier can be omitted and the saved power redistributed among the remaining carriers. Error correcting codes and interleaving can be used to provide both time diversity and coding gain.

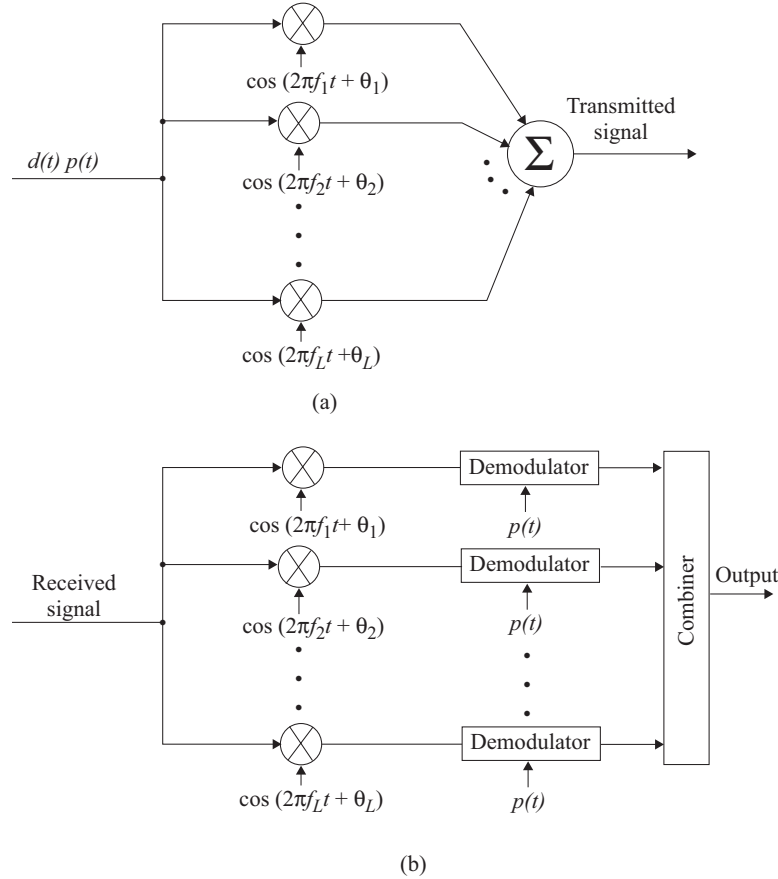


Figure 67. Multicarrier direct-sequence CDMA system: (a) transmitter and (b) receiver.

Since the spectral regions are defined so that the fading in each of them is independent and frequency nonselective, rake combining is not possible, but the frequency diversity provided by the regions can be exploited in a diversity combiner. Whether or not the diversity gain exceeds that of a single-carrier system using the entire spectral band and rake combining depends on the multipath intensity profile of the single-carrier system.

Consider a multicarrier system that uses binary PSK to modulate each carrier. Each received signal copy with a different carrier frequency experiences independent Rayleigh fading that is constant during a symbol interval. The received signal for a symbol in branch  $i$  is

$$r_i(t) = \text{Re} [\alpha_i e^{j\theta_i} x \psi(t) e^{j2\pi f_i t}] + n_i(t), \quad 0 \leq t \leq T_s, \quad i = 1, 2, \dots, L \quad (10-88)$$

where  $x = +1$  or  $-1$  depending on the transmitted symbol, each  $\alpha_i$  is a fading amplitude, each  $\theta_i$  is a phase shift,  $f_i$  is the carrier frequency,  $T_s$  is the symbol duration, and  $n_i(t)$  is the noise. Assume that either the interference is absent or, more generally, that the received interference plus noise in each diversity branch can be modeled as independent, zero-mean, white Gaussian noise with the same two-sided power spectral density  $N_0/2$ .

Ideal lossless power splitting among the  $L$  carriers is assumed. Let  $\mathcal{E} = \mathcal{E}_s/L$  denote the received symbol energy per carrier in the absence of fading, where  $\mathcal{E}_s$  is the total received energy per symbol. Assume that the spectral division among the carriers prevents significant interference among them in the receiver. For coherent detection, a classical analysis [44] indicates that the conditional symbol error probability given the  $\{\alpha_i\}$  is

$$P_{s|\alpha}(\gamma_s) = Q\left(\sqrt{2\gamma_s}\right) \quad (10-89)$$

where

$$\gamma_s = \frac{\mathcal{E}}{N_0} \sum_{i=1}^L \alpha_i^2 \quad (10-90)$$

The symbol error probability is determined by averaging  $P_{s|\alpha}(\gamma_s)$  over the distribution of  $\gamma_s$ , which depends on the  $\{\alpha_i\}$  and embodies the statistics of the fading channel.

Suppose that independent Rayleigh fading occurs so that each of the  $\{\alpha_i\}$  is independent with the identical Rayleigh distribution and  $E\{\alpha_i^2\} = \bar{\alpha}^2$ . Since  $\alpha_i^2$  is exponentially distributed,  $\gamma_s$  is the sum of  $L$  independent, identically and exponentially distributed random variables. It follows that (Appendix B-5) the probability density function of  $\gamma_s$  is

$$f_\gamma(x) = \frac{1}{(L-1)!\bar{\gamma}^L} x^{L-1} \exp\left(-\frac{x}{\bar{\gamma}}\right) u(x) \quad (10-91)$$

where  $u(x) = 1$  if  $x \geq 0$  and  $u(x) = 0$  if  $x < 0$ , and the average signal-to-noise ratio (SNR) per branch is

$$\bar{\gamma} = \frac{\mathcal{E}}{N_0} \bar{\alpha}^2 = \frac{\mathcal{E}_s \bar{\alpha}^2}{LN_0} \quad (10-92)$$

The symbol error probability is determined by averaging (10-89) over the density given by (10-91). Thus,

$$P_s(L) = \int_0^\infty Q\left(\sqrt{2x}\right) \frac{1}{(L-1)!\bar{\gamma}^L} x^{L-1} \exp\left(-\frac{x}{\bar{\gamma}}\right) dx \quad (10-93)$$

Direct calculations verify that since  $L$  is an integer,

$$\frac{d}{dx} Q\left(\sqrt{2x}\right) = -\frac{1}{2\sqrt{\pi}} \frac{\exp(-x)}{\sqrt{x}} \quad (10-94)$$

$$\frac{d}{dx} \left[ e^{-x/\bar{\gamma}} \sum_{i=0}^{L-1} \frac{(x/\bar{\gamma})^i}{i!} \right] = -\frac{1}{(L-1)!\bar{\gamma}^L} x^{L-1} \exp\left(-\frac{x}{\bar{\gamma}}\right) \quad (10-95)$$

Applying integration by parts to (10-93), and using (10-94), (10-95), and  $Q(0) = 1/2$ , we obtain

$$P_s(L) = \frac{1}{2} - \sum_{i=0}^{L-1} \frac{1}{i!\bar{\gamma}^i 2\sqrt{\pi}} \int_0^\infty \exp[-x(1 + \bar{\gamma}^{-1})] x^{i-1/2} dx \quad (10-96)$$

This integral can be evaluated in terms of the gamma function  $\Gamma(\cdot)$ . A change of variable in (10-96) yields

$$P_s(L) = \frac{1}{2} - \frac{1}{2} \sqrt{\frac{\bar{\gamma}}{1 + \bar{\gamma}}} \sum_{i=0}^{L-1} \frac{\Gamma(i + 1/2)}{\sqrt{\pi} i! (1 + \bar{\gamma})^i} \quad (10-97)$$

Since  $\Gamma(1/2) = \sqrt{\pi}$ , the symbol error probability for no diversity or a single branch is

$$p = P_s(1) = \frac{1}{2} \left( 1 - \sqrt{\frac{\bar{\gamma}}{1 + \bar{\gamma}}} \right) \quad (\text{PSK, QPSK}) \quad (10-98)$$

Since  $\Gamma(x) = (x - 1)\Gamma(x - 1)$ , it follows that

$$\Gamma(k + 1/2) = \frac{\sqrt{\pi}\Gamma(2k)}{2^{2k-1}\Gamma(k)} = \frac{\sqrt{\pi}k!}{2^{2k-1}} \binom{2k-1}{k}, \quad k \geq 1 \quad (10-99)$$

Solving (10-98) to determine  $\bar{\gamma}$  as a function of  $p$  and then using this result and (10-99) in (10-97) gives

$$P_s(L) = p - (1 - 2p) \sum_{i=1}^{L-1} \binom{2i-1}{i} [p(1-p)]^i \quad (10-100)$$

This expression explicitly shows the change in the symbol error probability as the number of diversity branches increases. Equations (10-98) and (10-99) are valid for quadriphase-shift keying (QPSK) because the latter can be transmitted as two independent binary PSK waveforms in phase quadrature.

An alternative expression for  $P_s(L)$ , which may be obtained by a far more complicated calculation entailing the use of the properties of the Gauss hypergeometric function, is [44], [45]

$$P_s(L) = p^L \sum_{i=0}^{L-1} \binom{L+i-1}{i} (1-p)^i \quad (10-101)$$

By using mathematical induction, this equation can be derived from (10-100) without invoking the hypergeometric function.

Figure 68 plots  $P_s(L)$  for multicarrier systems as a function of  $\mathcal{E}_s \bar{\alpha}^2 / N_0$ , the average symbol signal-to-noise ratio (SNR). The diminishing returns as the diversity level  $L$  increases is apparent. If the required bit error probability is  $10^{-6}$  or more, than increasing  $L$  beyond  $L = 32$  is not likely to be useful because of the hardware requirements and the losses entailed in the power division in the transmitter.

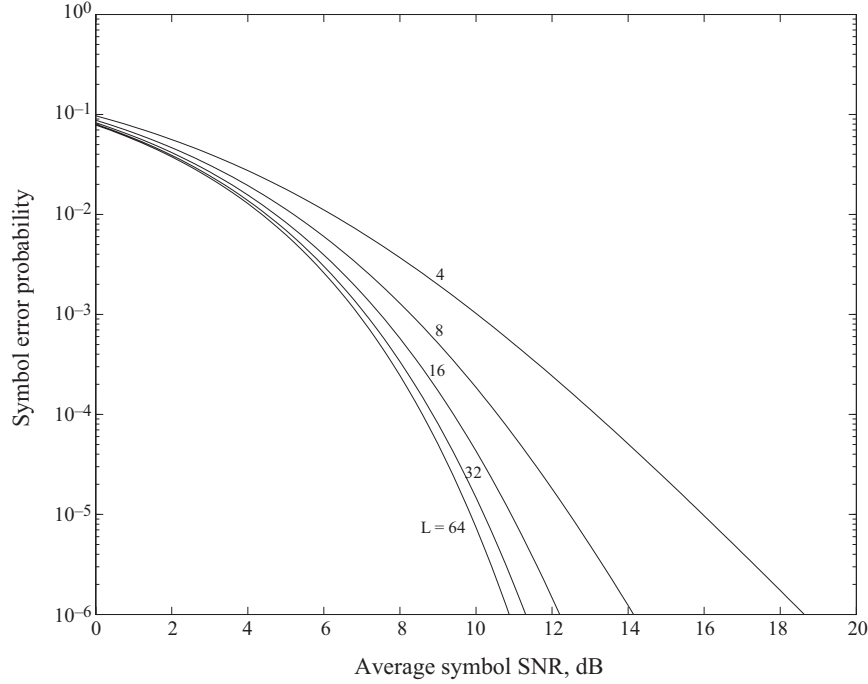


Figure 68. Symbol error probability for multicarrier systems with  $L$  carriers.

### Rake Receiver for Single-Carrier Direct-Sequence CDMA

Consider a direct-sequence signal that has a random spreading sequence and is accompanied by multipath components in addition to the direct-path signal. If the multipath components are delayed by more than one chip, then the independence of the chips ensures that the multipath interference is suppressed by at least the processing gain. However, since multipath signals carry information, they are a potential resource to be exploited rather than merely rejected. A *rake receiver* [44] provides *path diversity* by coherently combining the resolvable multipath components present during frequency-selective fading, which occurs when the chip rate of the spreading sequence exceeds the coherence bandwidth. Consider a multipath channel with frequency-selective fading slow enough that its time variations are negligible over a signaling interval. To harness the energy in all the multipath components, a receiver should decide which signal was transmitted among  $M$  candidates,  $s_1(t), s_2(t), \dots, s_M(t)$  only after processing all the received multipath components of the signal. Thus, the receiver selects among the  $M$  baseband signals or complex envelopes

$$\nu_k(t) = \sum_{i=1}^L c_i s_k(t - \tau_i) , \quad k = 1, 2, \dots, M, \quad 0 \leq t \leq T + T_d \quad (10-102)$$

where  $T$  is the duration of the transmitted signal,  $T_d$  is the multipath delay spread,  $L$  is the number of multipath components,  $\tau_i$  is the delay of component  $i$ , and the channel

parameter  $c_i$  is a complex number representing the attenuation and phase shift of component  $i$ .

When the data modulation is binary PSK, only a single symbol waveform  $s_1(t)$  and its associated decision variable are needed. Assume the presence of zero-mean, white Gaussian noise with two-sided power spectral density  $N_0/2$ . If  $\alpha_i = |c_i|$ , then it can be shown [44] that for a rake receiver with perfect tap weights, the conditional bit error probability given the  $\{\alpha_i\}$  is provided by (10-89). However, for a rake receiver, each of the  $\{\alpha_i\}$  is associated with a different multipath component, and hence each  $E[\alpha_i^2]$  has a different value in general. Since there is only a single carrier, we may set  $\mathcal{E} = \mathcal{E}_s$  in (10-90), which may be expressed as

$$\gamma_s = \sum_{i=1}^L \gamma_i, \quad \gamma_i = \frac{\mathcal{E}_s}{N_0} \alpha_i^2 \quad (10-103)$$

If each  $\alpha_i$  has a Rayleigh distribution then each  $\gamma_i$  has the exponential probability density function

$$f_{\gamma_i} = \frac{1}{\bar{\gamma}_i} \exp\left(-\frac{x}{\bar{\gamma}_i}\right) u(x), \quad i = 1, 2, \dots, L \quad (10-104)$$

where the average SNR for a symbol in branch  $i$  is

$$\bar{\gamma}_i = \frac{\mathcal{E}_s}{N_0} E[\alpha_i^2], \quad i = 1, 2, \dots, L \quad (10-105)$$

If each multipath component fades independently so that each of the  $\{\gamma_i\}$  is statistically independent, then  $\gamma_s$  is the sum of independent, exponentially distributed random variables. Therefore, if  $\bar{\gamma}_i \neq \bar{\gamma}_j, j \neq k$ , then the probability density function of  $\gamma_s$  is (Appendix B-5)

$$f_{\gamma}(x) = \sum_{i=1}^L \frac{A_i}{\bar{\gamma}_i} \exp\left(-\frac{x}{\bar{\gamma}_i}\right) u(x) \quad (10-106)$$

where

$$A_i = \begin{cases} \prod_{\substack{k=1 \\ k \neq i}}^L \frac{\bar{\gamma}_i}{\bar{\gamma}_i - \bar{\gamma}_k}, & L \geq 2 \\ 1, & L = 1 \end{cases} \quad (10-107)$$

The symbol error probability is determined by averaging the conditional symbol error probability of (10-89) over the density given by (10-106). A derivation similar to that leading to (10-97) yields

$$P_s(L) = \frac{1}{2} \sum_{i=1}^L A_i \left(1 - \sqrt{\frac{\bar{\gamma}_i}{1 + \bar{\gamma}_i}}\right) \quad (10-108)$$

Since only white Gaussian noise is present, the processing gain of the system is irrelevant.

To assess the potential performance of the rake receiver, it is assumed that the largest multipath component has  $\bar{\gamma}_1 = \bar{\gamma}$  and that  $L \leq 4$  components are received. The other three or fewer minor multipath components have relative average symbol SNRs specified by the *multipath intensity vector*

$$\Gamma = \left( \frac{\bar{\gamma}_2}{\bar{\gamma}}, \frac{\bar{\gamma}_3}{\bar{\gamma}}, \frac{\bar{\gamma}_4}{\bar{\gamma}} \right) \quad (10-109)$$

Figure 69 plots the symbol error probability as a function of  $\bar{\gamma} = \mathcal{E}_s \overline{a_1^2} / N_0$ , the average symbol SNR of the main component, for representative multipath intensity vectors. This figure and other numerical data establish two basic features of single-carrier systems with rake receivers.

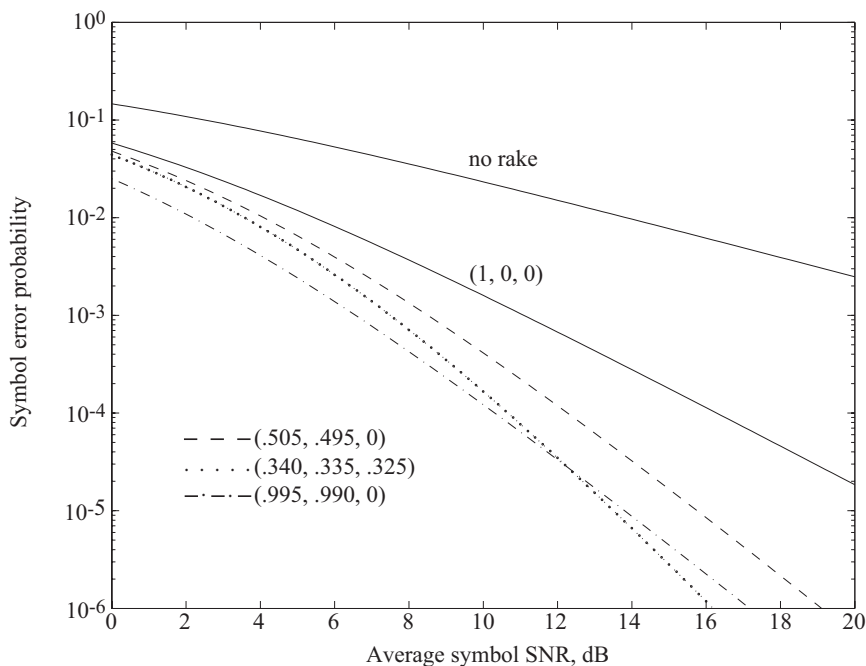


Figure 69. Symbol error probability for single-carrier systems and  $L \leq 4$  multipath components with different multipath intensity vectors.

1. System performance improves as the total energy in the minor multipath components increases.
2. When the total energy in the minor multipath components is fixed, the system performance improves as the number of resolved multipath components  $L$  increases and as the energy becomes uniformly distributed among these components.

The improvement as  $L$  increases depends on the assumption that ideal channel estimation is available to the rake receiver. However, when a practical channel estimator is used, measurements indicate that only three or fewer components are likely to have a sufficient signal-to-interference ratio to be useful in the rake combining [46]. An increase in  $L$  due to an increase in the bandwidth  $W$  is not always beneficial for a practical system. Although new components provide additional diversity and may exhibit the more favorable Ricean fading rather than Rayleigh fading, the average power per multipath component decreases because some composite components fragment into more numerous but weaker components. Hence, the estimation of the channel parameters becomes more difficult, and the fading of some multipath components may be highly correlated rather than independent.

In mobile CDMA networks, typically three significant multipath components for which  $\bar{\gamma}_2 + \bar{\gamma}_3$  has a value between  $\bar{\gamma}$  and  $2\bar{\gamma}$  are potentially available. Thus, the graphs with  $\Gamma = (.505, .495, 0)$  and  $\Gamma = (.995, .990, 0)$  represent reasonable approximations of relatively unfavorable and favorable multipath intensity vectors, respectively.

A comparison of Figures 68 and 69 indicates that a multicarrier system with diversity  $L = 32$  outperforms single-carrier systems with diversity  $L = 4$  if  $\bar{\gamma}$  is sufficiently large. However, this value  $\bar{\gamma}$  is much larger than is required in practical systems. To make a more realistic comparison, we assume that an error-correcting code with ideal channel-symbol interleaving is used. For a loosely packed, binary block code and hard-decision decoding with a bounded-distance decoder, the information-bit error probability is [47]

$$P_b \approx \sum_{i=t+1}^n \binom{n-1}{i-1} P_s^i (1 - P_s)^{n-1} \quad (10-110)$$

where  $n$  is the code length,  $t$  is the number of symbol errors that the decoder can correct, and  $P_s$  is the channel-symbol error probability. The signal energy per channel symbol is  $\mathcal{E}_s = r\mathcal{E}_b$ , where  $r = k/n$  is the code rate,  $k$  is the number of information bits per codeword, and  $\mathcal{E}_b$  is the energy per information bit. We may evaluate  $P_s$  by using the expressions for  $P_s(L)$  with  $\bar{\gamma} = r\bar{\gamma}_b$ , where  $\bar{\gamma}_b$  is the average bit SNR.

As an example, we assume that a BCH(63, 36) code with  $n = 63$ ,  $k = 36$ , and  $t = 5$  is used. Figure 70 plots  $P_b$  for a multicarrier system with  $L = 32$  and single-carrier systems with  $\Gamma_1 = (.505, .495, 0)$  and  $\Gamma_2 = (.995, .990, 0)$ . If the required  $P_b$  exceeds  $10^{-5}$ , then the rake combining provides more than a 0.5 dB advantage when the multipath intensity vector is  $\Gamma_1$  and more than a 2.1 dB advantage when it is  $\Gamma_2$ .

The preceding results imply that in a benign environment, devoid of partial-band interference, a multicarrier system suffers a potential performance loss relative to the less costly single-carrier system. The underlying reason is that the rake receiver of the single-carrier system harnesses energy that would otherwise be unavailable. In contrast, the multicarrier receiver recovers energy that has been redistributed among the  $L$  carriers but

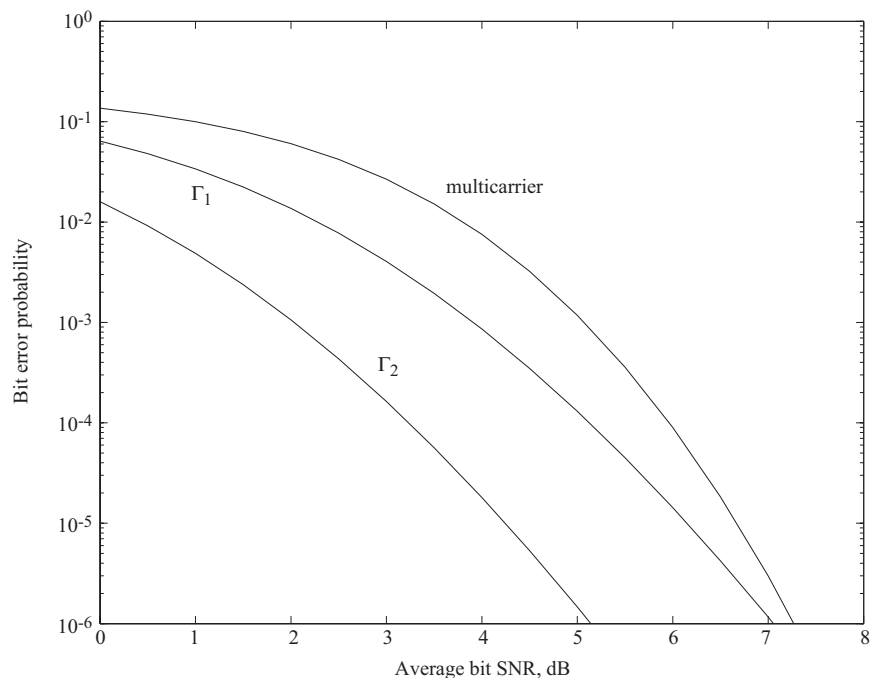


Figure 70. Information-bit error probability for multicarrier system with  $L = 32$  and for single-carrier systems with  $\Gamma_1 = (.505, .495, 0)$  and  $\Gamma_2 = (.995, .990, 0)$ . Error-correcting code is BCH(63, 36).

is available to the single-carrier system even without rake combining. Despite its potential disadvantage in a benign environment, a multicarrier direct-sequence CDMA system will often be preferable to single-carrier systems because of its substantially superior performance against partial-band interference [43].

## 10.8 Cellular Networks and Power Control

In a *cellular network*, a geographic region is partitioned into cells, as illustrated in Figure 71. A base station that includes a transmitter and receiver is located at the center of each cell. Ideally, the cells have equal hexagonal areas. Each *mobile* (user or subscriber) in the network transmits omnidirectionally and communicates with the base station from which it receives the largest average power. Typically, most of the mobiles in a cell communicate with the base station at the center of the cell, and only a few communicate with more distant ones. The base stations act as switching centers for the mobiles and communicate among themselves by wirelines in most applications. Cellular networks with direct-sequence CDMA allow universal frequency reuse in that the same carrier frequency and spectral band is shared by all the cells. Distinctions among the direct-sequence signals are possible because each signal is assigned a unique spreading sequence.

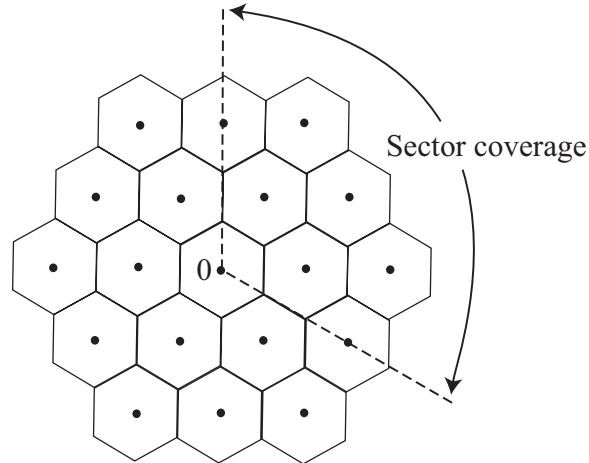


Figure 71. Geometry of cellular network with base station at center of each hexagon. Two concentric tiers of cells surrounding a central cell are shown.

Cells may be divided into *sectors* by using several directional sector antennas or arrays at the base stations. Only mobiles in the directions covered by a sector antenna can cause multiple-access interference on the *reverse link* or *uplink* from a mobile to its associated sector antenna. Only a sector antenna serving a cell sector oriented toward a mobile can cause multiple-access interference on the *forward link* or *downlink* from the mobile's associated sector antenna to the mobile. Thus, the numbers of interfering signals on both the uplink and the downlink are reduced approximately by a factor equal to the number of sectors.

To facilitate the identification of a base station controlling communications with a mobile, each spreading sequence for a downlink is formed as the product or concatenation of two sequences often called the scrambling and channelization codes. A *scrambling code* is a sequence that identifies a particular base station when the code is acquired by mobiles associated with the base station and its cell or sector. A long sequence is preferable to minimize the possibility of a prolonged outage. If the set of base stations use the Global Positioning System or some other common timing source, then each scrambling code may be a known phase shift of a common long pseudonoise sequence. If a common timing source is not used, then at the cost of increased acquisition time or complexity, the scrambling codes may comprise a set of long Gold sequences that approximate random binary sequences. Walsh or other orthogonal sequences are suitable as *channelization codes* that allow each mobile to extract its messages while blocking messages to other mobiles within the same cell or sector. For the uplinks, channelization codes are not strictly necessary, and the scrambling codes that identify the mobiles may be drawn from a set of long Gold sequences.

The principal difficulty of direct-sequence CDMA is called the *near-far problem*. If all mobiles transmit at the same power level, then the received power at a base station is higher for transmitters near the receiving antenna. There is a near-far problem because transmitters that are far from the receiving antenna may be at a substantial power disadvantage, and the spread-spectrum processing gain may not be enough to allow satisfactory reception of their signals. A similar problem may also result from large differences in received power levels due to differences in the shadowing experienced by signals traversing different paths or due to independent fading. In cellular communication networks, the near-far problem is critical only on the uplink because on the downlink, the base station transmits orthogonal signals synchronously to each mobile associated with it. For cellular networks, the usual solution to the near-far problem of uplinks is *power control*, whereby all mobiles regulate their power levels. By this means, power control potentially ensures that the power arriving at a common receiving antenna is almost the same for all transmitters. Since solving the near-far problem is essential to the viability of a direct-sequence CDMA network, the accuracy of the power control is a crucial issue.

In networks with *peer-to-peer communications*, there is no cellular or hierarchical structure. Communications between two mobiles are either direct or are relayed by other mobiles. Since there is no feasible method of power control to prevent the near-far problem, direct-sequence CDMA systems are not as attractive an option as frequency-hopping CDMA systems in these networks.

An *open-loop method* of power control in a cellular network causes a mobile to adjust its transmitted power to be inversely proportional to the received power of a *pilot signal* transmitted by the base station. An open-loop method is used to initiate power control, but its subsequent effectiveness requires that the propagation losses on the forward and reverse links be nearly the same. Whether they are or not depends on the duplexing method used to allow simultaneous or nearly simultaneous transmissions on both links. *Frequency-division duplexing* assigns different frequencies to an uplink and its corresponding downlink. *Time-division duplexing* assigns closely spaced but distinct time slots to the two links. When frequency-division duplexing is used, as in the IS-95 and Global System for Mobile (GSM) standards, the frequency separation is generally wide enough that the channel transfer functions of the uplink and downlink are different. This lack of *link reciprocity* implies that power measurements over the downlink do not provide reliable information for subsequent uplink transmissions. When time-division duplexing is used, the received local-mean power levels for the uplink and the downlink will usually be nearly equal when the transmitted powers are the same, but the Rayleigh fading may subvert link reciprocity. For these reasons, a *closed-loop method* of power control, which is more flexible than an open-loop method, is desirable. A closed-loop method requires the base station to transmit power-control information to each mobile based on the power level received from the mobile or the signal-to-interference power ratio.

When closed-loop power control is used, each base station attempts to either directly or indirectly track the received power of a desired signal from a mobile and dynamically transmit a power-control signal. The effect of increasing the carrier frequency or the mobile speeds is to increase the fading rate. As the fading rate increases, the tracking ability and, hence, the power-control accuracy decline. This problem and an analysis of intercell and intracell interference are presented in references [48] and [49].

---

## 11. Multiuser Detectors

---

The conventional single-user direct-sequence receiver of Figure 14 is optimal against multiple-access interference only if the spreading sequences of all the interfering signals and the desired signal are orthogonal (Section 10.1). Orthogonality is possible in a synchronous communication network, but in an asynchronous network, it is not possible to find sequences that remain orthogonal for all relative delays. Thus, the conventional single-user receiver, which only requires knowledge of the spreading sequence of the desired signal, is suboptimal against asynchronous multiple-access interference. The price of the suboptimality might be minor if the spreading sequences are carefully chosen and the noise is relatively high, especially if an error-correcting code and a sector antenna or adaptive array are used. If a potential near-far problem exists (Section 10.8), power control may be used to limit its impact. However, power control is imperfect, entails a substantial overhead cost, and is not feasible for peer-to-peer communication networks. Even if the power control is perfect, the remaining interference causes a nonzero *error floor*, which is a minimum bit error probability that exists when the thermal noise is zero. Thus, an alternative to the conventional receiver is desirable.

A *multiuser detector* is a receiver that exploits the deterministic structure of multiple-access interference or uses joint processing of a set of multiple-access signals. An optimum multiuser detector almost completely eliminates the multiple-access interference and, hence, the near-far problem, thereby rendering power control unnecessary. A more practical multiuser detector alleviates but does not eliminate the power-control requirements of a cellular network on its uplinks. Even if a multiuser detector rejects *intracell interference* from mobiles within a cell, it cannot reject *intercell interference*, which arrives from mobiles associated with different base stations than the one receiving a desired signal. Since intercell interference is typically more than one-third of the total interference on an uplink, even ideal multiuser detection will increase network capacity by a factor less than three. Multipath components can be accommodated as separate interference signals or rake combining may precede the multiuser detection.

## 11.1 Optimum Detectors

Consider a direct-sequence CDMA network with  $K$  users, each of which uses PSK to transmit a block of  $N$  binary symbols. A *jointly optimum* detector makes collective symbol decisions for  $K$  received signals based on the *maximum a posteriori* (MAP) criterion. The *individually optimum* detector selects the most probable set of symbols of a single desired signal from one user based on the MAP criterion, thereby providing the minimum symbol error probability. In nearly all applications, jointly optimum decisions would be preferable because of their lower complexity and because both types of decisions will agree with very high probability unless the symbol error probability is very high. Assuming equally likely symbols are transmitted, the jointly optimum MAP detector is the same as the jointly optimum maximum-likelihood detector, which is henceforth referred to as the *optimum detector*.

For synchronous communications in the presence of white Gaussian noise, the symbols are aligned in time, and the detection of each symbol of the desired signal is independent of the other symbols. Thus, the optimum detector can be determined by considering a single symbol interval  $0 \leq t \leq T_s$ . Let  $d_k$  denote the symbol transmitted by user  $k$ . The customary (highly idealized) assumption is that a perfect carrier synchronization enables the receiver to remove a common carrier frequency and phase. Thus, the composite baseband received signal is

$$r(t) = \sum_{k=1}^K A_k d_k p_k(t) + n(t) \quad 0 \leq t \leq T_s \quad (11-1)$$

where  $A_k$  is the received symbol amplitude from user  $k$ ,  $p_k(t)$  is the unit-energy spreading waveform of user  $k$ ,  $d_k = \pm 1$ , and  $n(t)$  is the baseband Gaussian noise. If it is assumed that each of the  $K$  signals has a common carrier frequency but a distinct phase relative to the phase of the receiver-generated synchronization signal, then each  $A_k$  in (11-1) is replaced by  $A_k \cos \phi_k$ , where  $\phi_k$  is the relative phase of the signal from mobile  $k$ .

Assuming that all possible values of the symbol vector  $\mathbf{d} = [d_1 \dots d_K]^T$  are equally likely, the optimum detector is the *maximum-likelihood detector* [44], [50], which selects the value of  $\mathbf{d}$  that minimizes the log-likelihood function

$$\Lambda(\mathbf{d}) = \int_0^{T_s} \left[ r(t) - \sum_{k=1}^K A_k d_k p_k(t) \right]^2 dt \quad (11-2)$$

subject to the constraint that  $d_k = +1$  or  $-1$ . The vector of the cross correlations between  $r(t)$  and the spreading sequences is denoted by  $\boldsymbol{\theta} = [r_1 \ r_2 \ \dots \ r_K]^T$ , where

$$r_k = \int_0^{T_s} r(t) p_k(t) dt, \quad k = 1, 2, \dots, K \quad (11-3)$$

Let  $\mathbf{A}$  denote the  $K \times K$  diagonal matrix with diagonal components  $A_1, A_2, \dots, A_K$ . Let  $\mathbf{R}$  denote the  $K \times K$  *correlation matrix* with elements

$$R_{ik} = \int_0^{T_s} p_i(t)p_k(t)dt \quad , \quad i, k = 1, 2, \dots, K \quad (11-4)$$

where  $R_{ii} = 1$  and  $|R_{ik}| \leq 1$  because the spreading waveforms are normalized to unit energy. Expanding (11-2), dropping an integral that is irrelevant to the selection of  $\mathbf{d}$ , and then substituting (11-3) and (11-4), we find that the maximum-likelihood detector selects the value of  $\mathbf{d}$  that maximizes the *correlation metric*

$$C = 2\mathbf{d}^T \mathbf{A} \boldsymbol{\theta} - \mathbf{d}^T \mathbf{A} \mathbf{R} \mathbf{A} \mathbf{d} \quad (11-5)$$

subject to the constraint that  $d_k = +1$  or  $-1, k = 1, 2, \dots, K$ .

This equation implies that the optimum detector uses a filter bank of  $K$  parallel correlators. Correlator  $k$  computes  $r_k$  given by (11-3) and can be implemented as the single-user detector of Figure 14. Equation (11-5) also indicates that the  $K$  spreading sequences must be known so that  $\mathbf{R}$  can be calculated, and the  $K$  signal amplitudes must be estimated. Short spreading sequences are necessary or  $\mathbf{R}$  must change with each symbol. The optimum detector is capable of making joint symbol decisions for all  $K$  signals or merely the symbol decisions for a single signal.

As an example, consider synchronous communications with  $K = 2$  and  $R_{12} = \rho$ . After the elimination of terms irrelevant to the selection, (11-5) implies that the optimum detector evaluates  $C = 2A_1d_1\theta_1 + 2A_2d_2\theta_2 - 2\rho A_1A_2d_1d_2$  for the four pairs with  $d_1 = \pm 1$  and  $d_2 = \pm 1$ . The pair that maximizes  $C$  provides the decisions for  $d_1$  and  $d_2$ .

For asynchronous communications over the AWGN channel, the derivation of the maximum-likelihood detector is analogous but more complicated [44], [50]. A major difference is that a desired symbol overlaps two consecutive symbols from each interference signal. The optimum detector uses a filter bank of  $K$  parallel correlators, but  $N$  symbols from each correlator must be processed to make decisions about  $NK$  binary symbols. The vector  $\mathbf{d}$  is  $NK \times 1$  with the first  $N$  elements representing the symbols of signal 1, the second  $N$  elements representing the symbols of signal 2, etc. The detector must estimate the transmission delays of all  $K$  multiple-access signals, and the  $NK \times NK$  correlation matrix  $\mathbf{R}$  has components that are partial cross correlations among the signals. In principle, the detector must compute  $2^{NK}$  correlation metrics and then select  $K$  symbol sequences, each of length  $N$ , corresponding to the largest correlation metric. The Viterbi algorithm simplifies computations by exploiting the fact that each received symbol overlaps at most  $2(K - 1)$  other symbols. Nevertheless, the computational complexity increases exponentially with  $K$ .

In view of both the computational requirements and the parameters that must be estimated, it is highly unlikely that the optimum multiuser detector will have practical

applications. Subsequently, alternative suboptimal multiuser detectors are considered. All of them follow carrier removal with a filter bank of correlators.

## 11.2 Decorrelating detector

The decorrelating detector may be derived by maximizing the correlation metric of (11-5) without any constraint on  $\mathbf{d}$ . For this purpose, the gradient of  $f$  with respect to the  $n$ -dimensional, real-valued vector  $\mathbf{x}$  is defined as the column vector  $\nabla_{\mathbf{x}}f$  with components  $\partial f/\partial x_i$ ,  $i = 1, 2, \dots, n$ . From this definition, it follows that for column vectors  $\mathbf{x}$  and  $\mathbf{y}$

$$\nabla_{\mathbf{x}} (\mathbf{x}^T \mathbf{y}) = \nabla_{\mathbf{x}} (\mathbf{y}^T \mathbf{x}) = \mathbf{y} \quad (11-6)$$

If  $\mathbf{A}$  is an  $n \times n$  symmetric matrix, then expressing  $\mathbf{x}^T \mathbf{A} \mathbf{x}$  in component form and using the chain rule yields

$$\nabla_{\mathbf{x}} (\mathbf{x}^T \mathbf{A} \mathbf{x}) = 2\mathbf{A} \mathbf{x} \quad (11-7)$$

Applying (11-6) and (11-7) to the correlation metric, we find that  $\nabla_{\mathbf{x}} C = \mathbf{0}$  implies that  $C$  is maximized by  $\mathbf{d} = \mathbf{d}'$ , where

$$\mathbf{A} \mathbf{d}' = \mathbf{R}^{-1} \boldsymbol{\theta} \quad (11-8)$$

provided that  $\mathbf{R}$  is invertible. Since each component of the vector  $\mathbf{A} \mathbf{d}'$  is a positive multiple of the corresponding component of  $\mathbf{d}'$ , there is no need to solve for  $\mathbf{d}'$ . A suitable estimate of the transmitted bits is

$$\hat{\mathbf{d}} = \text{sgn} (\mathbf{R}^{-1} \boldsymbol{\theta}) \quad (11-9)$$

where each component of the vector  $\text{sgn}(\mathbf{x})$  is the signum function of the corresponding component of the vector  $\mathbf{x}$ . The *signum function* is defined as  $\text{sgn}(x) = 1, x \geq 0$ , and  $\text{sgn}(x) = -1, x < 0$ . The *decorrelating detector*, which implements (11-9), has the form diagrammed in Figure 72. For asynchronous communications, each of the  $K$  correlators in the filter bank produces  $N$  bits. The accumulator constructs the  $NK$ -dimensional vector  $\boldsymbol{\theta}$  and the linear transformer computes  $\mathbf{R}^{-1} \boldsymbol{\theta}$ . The decision devices evaluate (11-9) to produce  $\hat{\mathbf{d}}$ .

A second derivation of the decorrelating detector assumes that the detector has the filter bank as its first stage. If (11-1) gives the input, then the output of this stage is

$$\boldsymbol{\theta} = \mathbf{R} \mathbf{A} \mathbf{d} + \mathbf{n} \quad (11-10)$$

where  $\mathbf{n}$  is the  $NK$ -dimensional noise vector. This equation indicates that the coupling among components of  $\mathbf{d}$ , which causes the correlation among components of  $\boldsymbol{\theta}$ , is due solely to the presence of the matrix  $\mathbf{R}$ . The effect of this matrix is removed by computing

$$\mathbf{R}^{-1} \boldsymbol{\theta} = \mathbf{A} \mathbf{d} + \mathbf{R}^{-1} \mathbf{n} \quad (11-11)$$

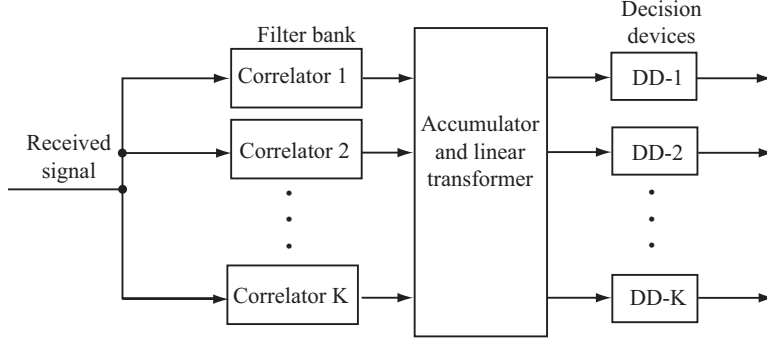


Figure 72. Architecture of decorrelating detector and MMSE detector. Filter bank comprises parallel correlators.

If (11-9) is used to determine the  $NK$  transmitted bits, the multiple-access interference is completely decorrelated from  $\hat{\mathbf{d}}$ .

A third derivation assumes the presence of the filter bank. If zero-mean, white Gaussian noise with two-sided power spectral density  $N_0/2$  enters each correlator, then a straightforward calculation indicates that the  $NK \times NK$  covariance matrix of  $\boldsymbol{\theta}$  is

$$E[\mathbf{nn}^T] = \frac{N_0}{2} \mathbf{R} \quad (11-12)$$

The probability density function of  $\boldsymbol{\theta}$  given  $\mathbf{A} \mathbf{d}$  is

$$f(\boldsymbol{\theta} | \mathbf{A} \mathbf{d}) = (N_0 \pi \det \mathbf{R})^{-K/2} \exp \left[ -N_0^{-1} (\boldsymbol{\theta} - \mathbf{R} \mathbf{A} \mathbf{d})^T \mathbf{R}^{-1} (\boldsymbol{\theta} - \mathbf{R} \mathbf{A} \mathbf{d}) \right] \quad (11-13)$$

The maximum-likelihood estimate of  $\mathbf{A} \mathbf{d}$  is the vector that maximizes (11-13) or, equivalently, minimizes the log-likelihood function

$$\Lambda(\mathbf{A} \mathbf{d}) = (\boldsymbol{\theta} - \mathbf{R} \mathbf{A} \mathbf{d})^T \mathbf{R}^{-1} (\boldsymbol{\theta} - \mathbf{R} \mathbf{A} \mathbf{d}) \quad (11-14)$$

Using (11-6) and (11-7), we again obtain the estimate given by (11-8), which leads to  $\hat{\mathbf{d}}$  given by (11-9).

Although the decorrelating detector eliminates the multiple-access interference, it increases the noise by changing  $\mathbf{n}$  to  $\mathbf{R}^{-1} \mathbf{n}$ . From (11-12), and the symmetric character of  $\mathbf{R}$ , it follows that the covariance matrix of the noise vector  $\mathbf{R}^{-1} \mathbf{n}$  entering the decision devices is

$$E[\mathbf{R}^{-1} \mathbf{nn}^T \mathbf{R}^{-1}] = \frac{N_0}{2} \mathbf{R}^{-1} \quad (11-15)$$

The variance of the noise that accompanies one of the symbols of user  $k$  is  $(N_0/2)(\mathbf{R}^{-1})_{kk}$ . Therefore, the symbol error probability is

$$P_s(k) = Q \left( \sqrt{\frac{2\mathcal{E}_k}{N_0 (\mathbf{R}^{-1})_{kk}}} \right), \quad k = 1, 2, \dots, K \quad (11-16)$$

where  $\mathcal{E}_k = A_k^2$  is the symbol energy. The symbol error probability for single-user detection by user  $k$  in the absence of multiple access interference is

$$P_s(k) = Q\left(\sqrt{\frac{2\mathcal{E}_k}{N_0}}\right), \quad k = 1, 2, \dots, K \quad (11-17)$$

Thus, the presence of multiple-access interference requires an increase of energy by the factor  $(\mathbf{R}^{-1})_{kk}$  when the decorrelating detector is used if a specified  $P_s$  is to be maintained.

As an example, consider synchronous communications with  $K = 2$  and  $R_{12} = R_{21} = \rho$ . The correlation matrix and its inverse are

$$\mathbf{R} = \begin{bmatrix} 1 & \rho \\ \rho & 1 \end{bmatrix}, \quad \mathbf{R}^{-1} = \frac{1}{1 - \rho^2} \begin{bmatrix} 1 & -\rho \\ -\rho & 1 \end{bmatrix} \quad (11-18)$$

Equation (11-9) indicates that the symbol estimates are  $\hat{d}_1 = \text{sgn}(r_1 - \rho r_2)$  and  $\hat{d}_2 = \text{sgn}(r_2 - \rho r_1)$ . Since  $(\mathbf{R}^{-1})_{11} = (\mathbf{R}^{-1})_{22} = (1 - \rho^2)^{-1}$ ,

$$P_s(k) = Q\left(\sqrt{\frac{2\mathcal{E}_k(1 - \rho^2)}{N_0}}\right), \quad k = 1, 2 \quad (11-19)$$

If  $\rho \leq 1/2$ , the required energy increase or shift in each  $P_s$  curve is less than 1.25 dB.

To demonstrate analytically the advantage of the decorrelating detector, consider synchronous communications and a receiver with a filter bank of  $K$  conventional detectors. Each conventional detector is a single-user matched filter. If perfect carrier synchronization removes a common phase shift of all the signals and produces the baseband received signal of (11-1), then (11-3) implies, that the output of detector  $k$  is

$$r_k = d_k A_k + \sum_{\substack{i=1 \\ i \neq k}}^K d_i A_i R_{ik} + \int_0^{T_s} n(t) p_k(t) dt \quad (11-20)$$

The set of  $K$  symbols is estimated by

$$\hat{d} = \text{sgn}(\theta) \quad (11-21)$$

By symmetry, we can assume that  $d_k = 1$  in the evaluation of the symbol error probability. Let  $\mathbf{D}_k$  denote the  $(K - 1)$ -dimensional vector of all the  $d_i, i \neq k$ . Conditioning on  $\mathbf{D}_k$  and calculating that  $\text{var}(r_k) = N_0/2$ , we find that the conditional symbol error probability for user  $k$  is

$$P_s(k|\mathbf{D}_k) = Q\left(\sqrt{\frac{2\mathcal{E}_k}{N_0}} B_k\right) \quad (11-22)$$

where

$$B_k = 1 + \sum_{\substack{i=1 \\ i \neq k}}^K d_i R_{ik} \frac{A_i}{A_k} \quad (11-23)$$

If all symbol sets are equally likely, then the symbol error probability for user  $k$  is

$$P_s(k) = 2^{-(K-1)} \sum_{j=1}^{2^{K-1}} P_s(k | \mathbf{D}_{kj}) \quad (11-24)$$

where  $\mathbf{D}_{kj}$  is the  $j$ th choice of the vector  $\mathbf{D}_k$ , which can take  $2^{K-1}$  values.

For  $K = 2$  with  $R_{12} = R_{21} = \rho$  and  $A_2/A_1 = \sqrt{\mathcal{E}_2}/\sqrt{\mathcal{E}_1}$ , (11-22) to (11-24) yield the symbol error probability for user 1:

$$\begin{aligned} P_s(1) &= \frac{1}{2}Q \left( \sqrt{\frac{2\mathcal{E}_1}{N_0}} \left( 1 - \rho \sqrt{\frac{\mathcal{E}_2}{\mathcal{E}_1}} \right) \right) + \frac{1}{2}Q \left( \sqrt{\frac{2\mathcal{E}_1}{N_0}} \left( 1 + \rho \sqrt{\frac{\mathcal{E}_2}{\mathcal{E}_1}} \right) \right) \\ &= \frac{1}{2}Q \left( \sqrt{\frac{2\mathcal{E}_1}{N_0}} \left( 1 - |\rho| \sqrt{\frac{\mathcal{E}_2}{\mathcal{E}_1}} \right) \right) + \frac{1}{2}Q \left( \sqrt{\frac{2\mathcal{E}_1}{N_0}} \left( 1 + |\rho| \sqrt{\frac{\mathcal{E}_2}{\mathcal{E}_1}} \right) \right) \end{aligned} \quad (11-25)$$

The symbol error probability for user 2 is given by (11-25) with the roles of  $\mathcal{E}_1$  and  $\mathcal{E}_2$  interchanged. The second term in (11-25) is usually negligible compared with the first one if  $\rho \neq 0$ . Thus, if

$$\rho^2 \mathcal{E}_2 / \mathcal{E}_1 > \left( 1 - \sqrt{1 - \rho^2} \right)^2 \quad (11-26)$$

then a comparison of (11-25) with (11-19) indicates that decorrelating detector usually outperforms the conventional detector. However, if  $\mathcal{E}_2$  is sufficiently small, then the conventional detector gives a lower  $P_s$  than the decorrelating detector.

In a more realistic model of the decorrelating and conventional detectors, the received signal in Figure 72 is passband. Correlator  $k$  uses a synchronized carrier to remove carrier  $k$  at the common frequency  $f_c$ . Since each carrier has a distinct phase  $\phi_k$ , the elements of the correlation matrix are

$$R_{ik} = \cos(\phi_k - \phi_i) \int_0^{T_c} p_i(t) p_k(t) dt, \quad i, k = 1, 2, \dots, K \quad (11-27)$$

if  $f_c T_c \gg 1$ . For synchronous communications with  $K = 2$ , (11-19) and (11-25) with  $\rho = R_{12} = R_{21}$  then represent the *conditional* symbol error probability given the value of  $\phi = \phi_k - \phi_i$ . Averaging over  $\phi$  is necessary to obtain  $P_s(1)$  and  $P_s(2)$ .

Compared with the optimum detector, the decorrelating detector offers greatly reduced, but still formidable, computational requirements. There is no need to estimate the signal

amplitudes, but the transmission delays of asynchronous signals must still be estimated. The inversion of the correlation matrix  $\mathbf{R}$  in real time is not possible for asynchronous signals with practical values of  $NK$ . Suboptimal partitioning and short spreading sequences are generally necessary and degrade the theoretical performance given by (11-16).

### 11.3 MMSE Detector

The *minimum mean-square-error* (MMSE) detector is the receiver that results from a linear transformation of  $\boldsymbol{\theta}$  by the  $K \times K$  matrix  $\mathbf{L}$  such that the metric

$$M = E [\|\mathbf{d} - \mathbf{L}\boldsymbol{\theta}\|^2] \quad (11-28)$$

is minimized. Let  $\mathbf{L}_0$  denote the solution of the equation

$$E [(\mathbf{d} - \mathbf{L}_0\boldsymbol{\theta}) \boldsymbol{\theta}^T] = \mathbf{0} \quad (11-29)$$

Let  $tr(\mathbf{B})$  denote the trace of the matrix  $\mathbf{B}$ . Since  $\|\mathbf{x}\|^2 = tr(\mathbf{x}\mathbf{x}^T)$  for a vector  $\mathbf{x}$ ,

$$\begin{aligned} \|\mathbf{d} - \mathbf{L}\boldsymbol{\theta}\|^2 &= tr \left\{ [\mathbf{d} - \mathbf{L}_0\boldsymbol{\theta} + (\mathbf{L}_0 - \mathbf{L}) \boldsymbol{\theta}] [\mathbf{d} - \mathbf{L}_0\boldsymbol{\theta} + (\mathbf{L}_0 - \mathbf{L}) \boldsymbol{\theta}]^T \right\} \\ &= \|\mathbf{d} - \mathbf{L}_0\boldsymbol{\theta}\|^2 + \|(\mathbf{L}_0 - \mathbf{L}) \boldsymbol{\theta}\|^2 + 2tr \left[ (\mathbf{d} - \mathbf{L}_0\boldsymbol{\theta}) \boldsymbol{\theta}^T (\mathbf{L}_0 - \mathbf{L})^T \right] \end{aligned} \quad (11-30)$$

Substitution of this equation into (11-28) and the application of (11-29) yields

$$M = E [\|\mathbf{d} - \mathbf{L}_0\boldsymbol{\theta}\|^2] + E [\|(\mathbf{L}_0 - \mathbf{L}) \boldsymbol{\theta}\|^2] \geq E [\|\mathbf{d} - \mathbf{L}_0\boldsymbol{\theta}\|^2] \quad (11-31)$$

which proves that  $\mathbf{L}_0$  minimizes  $M$ . If the data symbols are independent and equally likely to be  $+1$  or  $-1$ , then  $E[\mathbf{d}\mathbf{d}^T] = \mathbf{I}$ , where  $\mathbf{I}$  is the identity matrix. Using this result, (11-10), (11-12),  $E[\mathbf{n}] = \mathbf{0}$ , and the independence of  $\mathbf{d}$  and  $\mathbf{n}$ , we obtain

$$E [\mathbf{d}\boldsymbol{\theta}^T] = \mathbf{A} \mathbf{R} \quad , \quad E [\boldsymbol{\theta}\boldsymbol{\theta}^T] = \mathbf{R} \mathbf{A}^2 \mathbf{R} + \frac{N_0}{2} \mathbf{R} \quad (11-32)$$

Substitution of these equations into (11-29) yields

$$\mathbf{L}_0 = \left( \mathbf{R}\mathbf{A} + \frac{N_0}{2} \mathbf{A}^{-1} \right)^{-1} = \mathbf{A}^{-1} \left( \mathbf{R} + \frac{N_0}{2} \mathbf{A}^{-2} \right)^{-1} \quad (11-33)$$

provided that the inverses exist. Since  $\mathbf{A}$  and, hence,  $\mathbf{A}^{-1}$  are diagonal matrices with positive diagonal components if all signals are active, (11-33) may be simplified to the linear transformation matrix

$$\mathbf{L}_0 = \left( \mathbf{R} + \frac{N_0}{2} \mathbf{A}^{-2} \right)^{-1} \quad (11-34)$$

without any change in the MMSE estimate of the transmitted symbols:

$$\hat{d} = \text{sgn}(\mathbf{L}_0 \boldsymbol{\theta}) \quad (11-35)$$

The MMSE detector has the structure of Figure 72.

The MMSE and decorrelating detectors have almost the same computational requirements, and they both have equalizer counterparts, but they differ in several ways. The MMSE detector is near-far resistant, but does not obliterate the multiple-access interference and, hence, does not completely eliminate the near-far problem. However, it does not accentuate the noise to the degree that the decorrelating detector does. As  $N_0 \rightarrow 0$ ,  $\mathbf{L}_0 \rightarrow \mathbf{R}^{-1}$  and the MMSE estimate approaches the decorrelating detector estimate. As  $N_0$  increases, the MMSE estimate approaches that of the conventional detector given by (11-21), and the symbol error probability generally tends to be lower than that provided by the decorrelating detector. A disadvantage of the MMSE detector is that the signal amplitudes must be estimated so that  $\mathbf{A}$  in (11-34) can be computed.

For either the MMSE or decorrelating linear detectors to be practical, it is necessary for the spreading sequences to be short. Short sequences ensure that the correlation matrix  $\mathbf{R}$  is approximately constant for significant time durations if the communication channel and the amplitudes of the interference signals are slowly varying. The price of short sequences is a security loss and the occasional but sometimes persistent performance loss due to a particular set of relative signal delays. Even with short spreading sequences, adaptive versions of the MMSE detector are much more practical than the nonadaptive versions of either linear detector.

An *adaptive multiuser detector* [50] is one that does not require explicit knowledge of either the spreading sequences or the timing of the multiple-access interference signals. The receiver samples the output of a wideband filter at the chip rate. The use of short spreading sequences affords the opportunity for the adaptive detector to essentially learn the sequence cross-correlations and thereby to suppress the interference. The learning is accomplished by processing a known *training sequence* of symbols for the desired signal during a *training phase*. This operational phase is followed by a *decision-directed phase* that continues the adaptation by feeding back symbol decisions. Adaptive detectors potentially can achieve much better performance than conventional ones at least if the transmission channel is time-invariant, but coping with fast fading and interference changes requires elaborate modifications. A *blind adaptive detector* [51] is one that does not require training sequences. These detectors are desirable for applications such as system recovery but entail some performance loss and complexity increase relative to other adaptive detectors. Long sequences do not possess the cyclostationarity that makes possible many of the advanced signal processing techniques used for blind multiuser detection and adaptive channel estimation.

## 11.4 Interference Cancellers

An *interference canceller* is a multiuser detector that explicitly estimates the interference signals and then subtracts them from the received signal to produce the desired signal. Interference cancellers may be classified as *successive interference cancellers* in which the subtractions are done sequentially, *parallel interference cancellers* in which the subtractions are done simultaneously, or hybrids of these types. Only the basic structures and features of the successive and parallel cancellers are presented subsequently. A large number of alternative versions, some of them hybrids, adaptive, or blind, have been proposed in the literature [50]. Some type of interference canceller is by far the most practical multiuser detector for an asynchronous direct-sequence CDMA network, especially if long spreading sequences are planned [52].

## 11.5 Successive Interference Canceller

Figure 73 is a functional block diagram of a successive interference canceller, which uses nonlinear replica generations and subtractions to produce estimates of the symbol streams  $\hat{\mathbf{d}}_1, \hat{\mathbf{d}}_2, \dots, \hat{\mathbf{d}}_K$  transmitted by the  $K$  users. The input may be the sampled outputs of a chip-matched filter for PSK modulation or the complex-valued samples derived from a quadrature demodulator for quaternary modulation. Detector-generator  $i$  produces a replica of the signal transmitted by user  $i$ . Its basic structure is depicted in Figure 74. The correlator, which comprises a multiplier and summer as in Figure 14, despreads signal  $i$ . The channel estimate is a stream of complex numbers that are applied to the correlator output to remove the effects of the propagation channel. The decision device produces the estimated symbols transmitted by user  $i$ . These symbols are remodulated and modified to account for the effects of the channel. After a respreading, the replica of signal  $i$  is generated and sent to the corresponding subtracter. The input or output of the decision device may produce the estimated symbol stream, depending on whether the decoder uses soft or hard decisions. The channel estimator uses known pilot or training symbols to determine the effect of the channel. Hard decisions are used in the replica generation, but may not be appropriate if the channel estimate is inaccurate because a symbol error doubles the amplitude of the interference that enters the next stage of the canceller of Figure 73. The enhanced interference adversely affects subsequent symbol estimates and replicas.

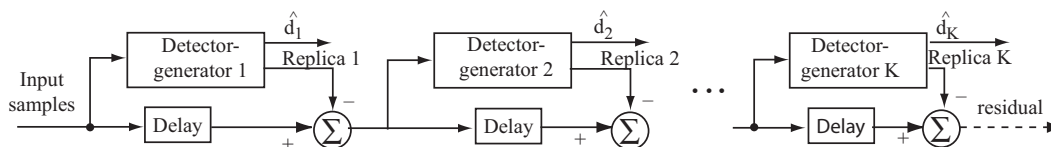


Figure 73. Successive interference canceller with  $K$  detector-generators to produce signal estimates for subtraction.

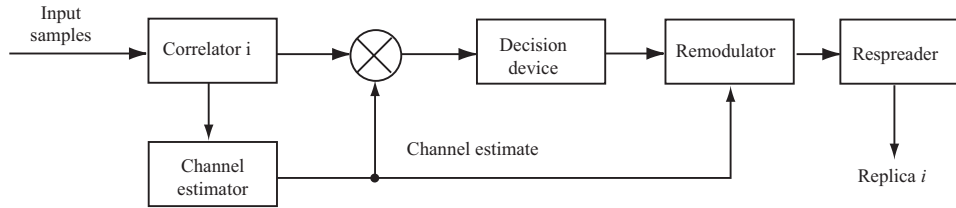


Figure 74. Structure of detector-generator for signal  $i$ .

The outputs of a set of  $K$  correlators and level detectors are applied to a device that orders the  $K$  received signals according to their power levels. This ordering determines the placement of the detector-generators in Figure 73. Detector-generator  $i, i = 1, 2, \dots, K$ , corresponds to the  $i$ th strongest signal.

The first canceller stage eliminates the strongest signal, thereby immediately alleviating the near-far problem while exploiting the superior detectability of the strongest signal. The first difference signal is applied to the detector-generator for the second strongest received signal, etc. The amount of interference removal from a signal tends to increase from the strongest received signal to the weakest one. The delay introduced, the impact of cancellation errors, and the implementation complexity may limit the number of canceller stages to fewer than  $K$ , and a set of conventional detectors may be needed to estimate some of the symbol streams. At a low signal-to-noise ratio, inaccurate cancellations may cause the canceller to lose its advantage over the conventional detector. The successive interference canceller of Figure 73 requires known spreading sequences and timing of all signals.

A *multistage canceller* comprising more than one successive interference canceller potentially improves performance by repeated cancellations if the delay and complexity can be accommodated. The second canceller or stage of a multistage canceller is illustrated in Figure 75. The input is the residual of canceller 1, which is shown in Figure 73. Replica 1 of canceller 1 is added to the input and then an improved replica of signal 1 is subtracted. Subsequently, other replicas from canceller 1 are added and corresponding improved replicas are subtracted. The symbol streams are produced by the final canceller. Rake combining of multipath components may be incorporated into a multistage or single-stage canceller to improve performance in a fading environment [53].

## 11.6 Parallel Interference Canceller

A parallel interference canceller detects, generates, and then subtracts all multiple-access interference signals simultaneously, thereby avoiding the delay inherent in successive interference cancellers. A parallel interference canceller for two signals is diagrammed in

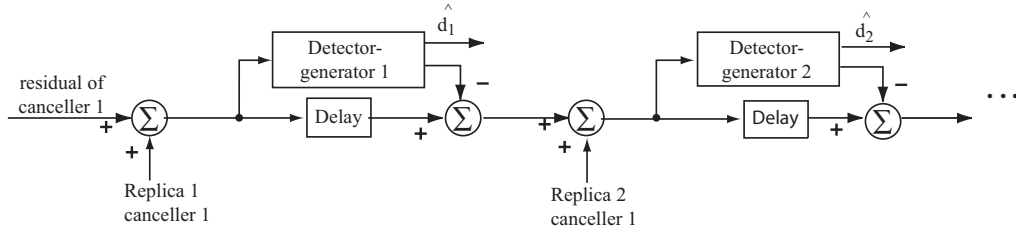


Figure 75. Second canceller of multistage canceller using successive interference cancellers.

Figure 76. Each detector-generator pair may be implemented as shown in Figure 74. Each of the final detectors includes a digital matched filter and a decision device that produce soft or hard decisions, which are applied to the decoder. Since all signals are processed in the same manner and the initial detections influence the final ones, the parallel interference canceller is not as effective in suppressing the near-far problem as the successive interference canceller unless the CDMA network uses power control. Power control also relieves the timing synchronization requirements. A better suppression of the near-far problem is provided by the *multistage parallel interference canceller*, in which each stage is similar but has an improved input that results in an improved output. Figure 77 shows the multistage canceller for two signals. Each stage has the form of Figure 76 without the final detectors.

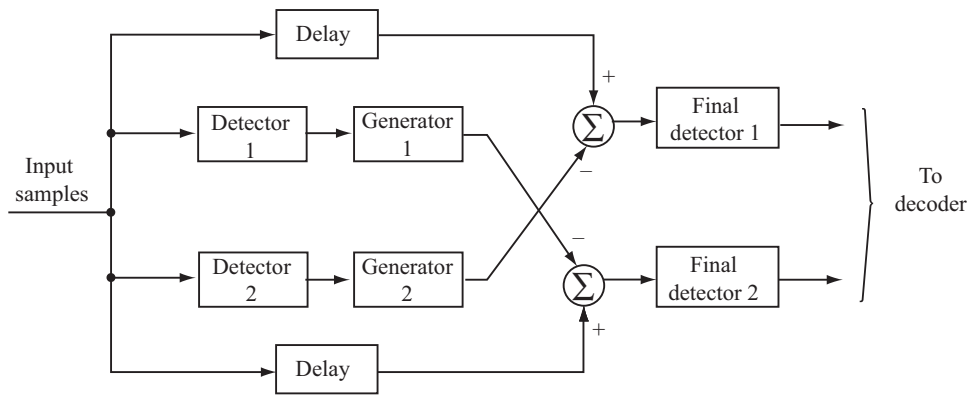


Figure 76. Parallel interference canceller for two signals.

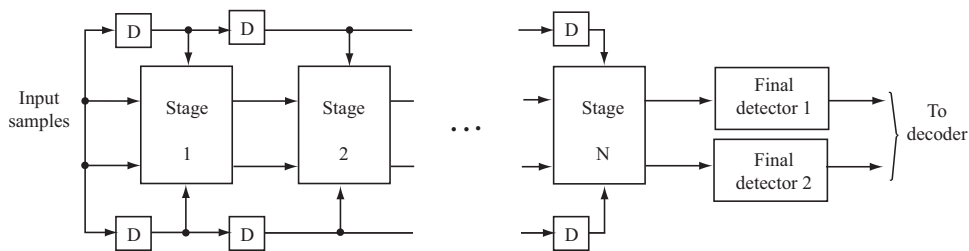


Figure 77. Multistage parallel interference canceller for two signals.  $D$ =delay.

---

## A. Inequalities

---

### A.1 Jensen's Inequality

A function  $g(x)$  defined on an open interval  $I$  is *convex* if

$$g(px + (1-p)y) \leq pg(x) + (1-p)g(y) \quad (\text{A.1})$$

for  $x, y$  in  $I$  and  $0 \leq p \leq 1$ . Suppose that  $g(x)$  has a continuous, nondecreasing derivative  $g'(x)$  on  $I$ . The inequality is valid if  $p = 0$  or  $1$ . If  $x \geq y$  and  $0 \leq p < 1$ ,

$$\begin{aligned} g(px + (1-p)y) - g(y) &= \int_y^{px+(1-p)y} g'(z)dz \leq p(x-y)g'(px + (1-p)y) \\ &\leq \frac{p}{1-p} \int_{px+(1-p)y}^x g'(z)dz \\ &= \frac{p}{1-p} [g(x) - g(px + (1-p)y)] \end{aligned}$$

Simplifying this result, we obtain (A-1). If  $y \geq x$ , a similar analysis again yields (A-1). Thus, if  $g(x)$  has a continuous, nondecreasing derivative on  $I$ , it is convex.

**Lemma.** If  $g(x)$  is a convex function on the open interval  $I$ , then

$$g(y) \geq g(x) + g^-(x)(y-x) \quad (\text{A.2})$$

for all  $y, x$  in  $I$ , where  $g^-(x)$  is the left derivative of  $g(x)$ .

*Proof.* If  $y-x \geq z > 0$ , then substituting  $p = 1 - z/(y-x)$  into (A-1) gives

$$g(x+z) \leq \left(1 - \frac{z}{y-x}\right)g(x) + \frac{z}{y-x}g(y)$$

which yields

$$\frac{g(x+z) - g(x)}{z} \leq \frac{g(y) - g(x)}{y-x}, \quad y-x \geq z > 0 \quad (\text{A.3})$$

If  $v > 0$  and  $z > 0$ , then (A-1) implies that

$$g(x) \leq \frac{z}{v+z}g(x-v) + \frac{v}{v+z}g(x+z)$$

which yields

$$\frac{g(x) - g(x-v)}{v} \leq \frac{g(x+z) - g(x)}{z}, \quad v, z > 0 \quad (\text{A.4})$$

Inequality (A-3) indicates that the ratio  $[g(y) - g(x)]/(y-x)$  decreases monotonically as  $y \rightarrow x$  from above and (A-4) implies that this ratio has a lower bound. Therefore, the right

derivative  $g^+(x)$  exists on  $I$ . If  $x - y \geq v > 0$ , then (A-1) with  $p = 1 - v/(x - y)$  implies that

$$g(x - v) \leq \left(1 - \frac{v}{x - y}\right)g(x) + \frac{v}{x - y}g(y)$$

which yields

$$\frac{g(x) - g(y)}{x - y} \leq \frac{g(x) - g(x - v)}{v}, \quad x - y \geq v > 0 \quad (\text{A.5})$$

This inequality indicates that the ratio  $[g(x) - g(y)]/(x - y)$  increases monotonically as  $y \rightarrow x$  from below and (A-4) implies that this ratio has an upper bound. Therefore, the left derivative  $g^-(x)$  exists on  $I$ , and (A-4) yields

$$g^-(x) \leq g^+(x) \quad (\text{A.6})$$

Taking the limits as  $z \rightarrow 0$  and  $v \rightarrow 0$  in (A-3) and (A-5), respectively, and then using (A-6), we find that (A-2) is valid for all  $y, x$  in  $I$ .  $\square$

**Jensen's inequality.** If  $X$  is a random variable with a finite expected value  $E[X]$ , and  $g(\cdot)$  is a convex function on an open interval containing the range of  $X$ , then

$$E[g(X)] \geq g(E[X])$$

*Proof.* Set  $y = X$  and  $x = E[X]$  in (A-2), which gives  $g(X) \geq g(E[X]) + g^-(E[X])(X - E[X])$ . Taking the expected values of the random variables on both sides of this inequality gives Jensen's inequality.  $\square$

## A.2 Chebyshev's Inequality

Consider a random variable  $X$  with distribution  $F(x)$ . Let  $E[X] = m$  denote the expected value of  $X$  and  $P[A]$  denote the probability of event  $A$ . From elementary probability it follows that

$$\begin{aligned} E[|X - m|^k] &= \int_{-\infty}^{\infty} |x - m|^k dF(x) \geq \int_{|x - m| \geq \alpha} |x - m|^k dF(x) \\ &\geq \alpha^k \int_{|x - m| \geq \alpha} dF(x) = \alpha^k P[|X - m| \geq \alpha] \end{aligned}$$

Therefore,

$$P[|X - m| \geq \alpha] \leq \frac{1}{\alpha^k} E[|X - m|^k] \quad (\text{A.7})$$

Let  $\sigma^2 = E[(X - m)^2]$  denote the variance of  $X$ . If  $k = 2$ , then (D.1.1) becomes *Chebyshev's inequality*:

$$P[|X - m| \geq \alpha] \leq \frac{\sigma^2}{\alpha^2} \quad (\text{A.8})$$

As an application, let  $\alpha = 3\sigma$ . Then

$$P[|X - m| < 3\sigma] \geq \frac{8}{9}$$

This inequality indicates that the probability that a random variable is within three standard deviations of its mean value is at least  $8/9$ .

---

## B. Probability Distributions

---

### B.1 Chi-Square Distribution

Consider the random variable

$$Z = \sum_{i=1}^N A_i^2 \quad (\text{B.1})$$

where the  $\{A_i\}$  are independent Gaussian random variables with means  $\{m_i\}$  and common variance  $\sigma^2$ . The random variable  $Z$  is said to have a *noncentral chi-square* ( $\chi^2$ ) *distribution* with  $N$  degrees of freedom and a *noncentral parameter*

$$\lambda = \sum_{i=1}^N m_i^2 \quad (\text{B.2})$$

To derive the probability density function of  $Z$ , we first note that each  $A_i$  has the density function

$$f_{A_i}(x) = \frac{1}{\sqrt{2\pi}\sigma} \exp\left[-\frac{(x - m_i)^2}{2\sigma^2}\right] \quad (\text{B.3})$$

From elementary probability, the density of  $Y_i = A_i^2$  is

$$f_{Y_i}(x) = \frac{1}{2\sqrt{x}} [f_{A_i}(\sqrt{x}) + f_{A_i}(-\sqrt{x})] u(x) \quad (\text{B.4})$$

where  $u(x) = 1, x \geq 0$ , and  $u(x) = 0, x < 0$ . Substituting (B-3) into (B-4), expanding the exponentials, and simplifying, we obtain the density

$$f_{Y_i}(x) = \frac{1}{\sqrt{2\pi x}\sigma} \exp\left(-\frac{x + m_i^2}{2\sigma^2}\right) \cosh\left(\frac{m_i\sqrt{x}}{\sigma^2}\right) u(x) \quad (\text{B.5})$$

The characteristic function of a random variable  $X$  is defined as

$$C_X(j\nu) = E[e^{j\nu X}] = \int_{-\infty}^{\infty} f_X(x) \exp(j\nu x) dx \quad (\text{B.6})$$

where  $j = \sqrt{-1}$ , and  $f_X(x)$  is the density of  $X$ . Since  $C_X(j\nu)$  is the conjugate Fourier transform of  $f_X(x)$ ,

$$f_X(x) = \frac{1}{2\pi} \int_{-\infty}^{\infty} C_X(j\nu) \exp(-j\nu x) d\nu \quad (\text{B.7})$$

From Laplace or Fourier transform tables, it is found that the characteristic function of  $f_{Y_i}(x)$  is

$$C_{Y_i}(j\nu) = \frac{\exp[jm_i^2\nu/(1 - j2\sigma^2\nu)]}{(1 - j^2\sigma^2\nu)^{1/2}} \quad (\text{B.8})$$

The characteristic function of a sum of independent random variables is equal to the product of the individual characteristic functions. Because  $Z$  is the sum of the  $Y_i$ , the characteristic function of  $Z$  is

$$C_Z(j\nu) = \frac{\exp[j\lambda\nu/(1 - j2\sigma^2\nu)]}{(1 - j^2\sigma^2\nu)^{N/2}} \quad (\text{B.9})$$

where we have used (B-2). From (B-9), (B-7), and Laplace or Fourier transform tables, we obtain the probability density function of *noncentral  $\chi^2$  random variable* with  $N$  degrees of freedom and a noncentral parameter  $\lambda$ :

$$f_Z(x) = \frac{1}{2\sigma^2} \left(\frac{x}{\lambda}\right)^{(N-2)/4} \exp\left[-\frac{x+\lambda}{2\sigma^2}\right] I_{N/2-1}\left(\frac{\sqrt{x\lambda}}{\sigma^2}\right) u(x) \quad (\text{B.10})$$

where  $I_n(\cdot)$  is the modified Bessel function of the first kind and order  $n$ . This function may be represented by

$$I_n(x) = \sum_{i=0}^{\infty} \frac{(x/2)^{n+2i}}{i! \Gamma(n+i+1)} \quad (\text{B.11})$$

where the gamma function is defined as

$$\Gamma(x) = \int_0^{\infty} y^{x-1} \exp(-y) dy, \quad x > 0 \quad (\text{B.12})$$

The probability distribution function of a noncentral  $\chi^2$  random variable is

$$F_Z(x) = \int_0^x \frac{1}{2\sigma^2} \left(\frac{y}{\lambda}\right)^{(N-2)/4} \exp\left(-\frac{y+\lambda}{2\sigma^2}\right) I_{N/2-1}\left(\frac{\sqrt{y\lambda}}{\sigma^2}\right) dy, \quad x \geq 0 \quad (\text{B.13})$$

When  $N$  is even so that  $N/2$  is an integer, then using  $F_Z(\infty) = 1$  and a change of variables in (B-13) yields

$$F_Z(x) = 1 - Q_{N/2}\left(\frac{\sqrt{\lambda}}{\sigma}, \frac{\sqrt{x}}{\sigma}\right), \quad x \geq 0 \quad (\text{B.14})$$

where the *generalized Q-function* is defined as

$$Q_m(\alpha, \beta) = \int_{\beta}^{\infty} x \left(\frac{x}{\alpha}\right)^{m-1} \exp\left(-\frac{x^2 + \alpha^2}{2}\right) I_{m-1}(\alpha x) dx \quad (\text{B.15})$$

and  $m$  is an integer. Since  $Q_m(\alpha, 0) = 1$ , it follows that  $1 - Q_m(\alpha, \beta)$  is an integral with finite limits that can be numerically integrated. However, the numerical computation of the generalized  $Q$ -function is simplified if it is expressed in alternative forms [2].

The mean, variance, and moments of  $Z$  can be easily obtained by using (B-1) and the properties of independent Gaussian random variables. The mean and variance of  $Z$  are

$$E[Z] = N\sigma^2 + \lambda \quad (\text{B.16})$$

$$\sigma_z^2 = 2N\sigma^4 + 4\lambda\sigma^2 \quad (\text{B.17})$$

where  $\sigma^2$  is the common variance of the  $\{A_i\}$ .

From (B-9), it follows that the sum of two independent noncentral  $\chi^2$  random variables with  $N_1$  and  $N_2$  degrees of freedom, noncentral parameters  $\lambda_1$  and  $\lambda_2$ , respectively, and the same parameter  $\sigma^2$  is a noncentral  $\chi^2$  random variable with  $N_1 + N_2$  degrees of freedom and noncentral parameter  $\lambda_1 + \lambda_2$ .

## B.2 Central Chi-Square Distribution

To determine the probability density function of  $Z$  when the  $\{A_i\}$  have zero means, we substitute (B-11) into (B-10) and then take the limit as  $\lambda \rightarrow 0$ . We obtain

$$f_Z(x) = \frac{1}{(2\sigma^2)^{N/2}\Gamma(N/2)} x^{N/2-1} \exp\left(-\frac{x}{2\sigma^2}\right) u(x) \quad (\text{B.18})$$

Alternatively, this equation results if we substitute  $\lambda = 0$  into the characteristic function (B-9) and then use (B-7). Equation (B-18) is the probability density function of a *central*  $\chi^2$  random variable with  $N$  degrees of freedom. The probability distribution function is

$$F_Z(x) = \int_0^x \frac{1}{(2\sigma^2)^{N/2}\Gamma(N/2)} y^{N/2-1} \exp\left(-\frac{y}{2\sigma^2}\right) dy, \quad x \geq 0 \quad (\text{B.19})$$

If  $N$  is even so that  $N/2$  is an integer, then integrating this equation by parts  $N/2 - 1$  times yields

$$F_Z(x) = 1 - \exp\left(-\frac{x}{2\sigma^2}\right) \sum_{i=0}^{N/2-1} \frac{1}{i!} \left(\frac{x}{2\sigma^2}\right)^i, \quad x \geq 0 \quad (\text{B.20})$$

By direct integration using (B-18) and (B-12) or from (B-16) and (B-17), the mean and variance of  $Z$  are

$$E[Z] = N\sigma^2 \quad (\text{B.21})$$

$$\sigma_z^2 = 2N\sigma^4 \quad (\text{B.22})$$

## B.3 Rice Distribution

Consider the random variable

$$R = \sqrt{A_1^2 + A_2^2} \quad (\text{B.23})$$

where  $A_1$  and  $A_2$  are independent Gaussian random variables with means  $m_1$  and  $m_2$ , respectively, and a common variance  $\sigma^2$ . The probability distribution function of  $R$  must satisfy  $F_R(r) = F_Z(r^2)$ , where  $Z = A_1^2 + A_2^2$  is a  $\chi^2$  random variable with two degrees of freedom. Therefore, (??) with  $N = 2$  implies that

$$F_R(r) = 1 - Q_1 \left( \frac{\sqrt{\lambda}}{\sigma}, \frac{r}{\sigma} \right), \quad r \geq 0 \quad (\text{B.24})$$

where  $\lambda = m_1^2 + m_2^2$ . This function is called the *Rice probability distribution function*. The *Rice probability density function*, which may be obtained by differentiation of (B-24), is

$$f_R(r) = \frac{r}{\sigma^2} \exp \left( -\frac{r^2 + \lambda}{2\sigma^2} \right) I_0 \left( \frac{r\sqrt{\lambda}}{\sigma^2} \right) u(r) \quad (\text{B.25})$$

The moments of even order can be derived from (B-23) and the moments of the independent Gaussian random variables. The second moment is

$$E[R^2] = 2\sigma^2 + \lambda \quad (\text{B.26})$$

In general, moments of the Rice distribution are given by an integration over the density in (B-25). Substituting (B-11) into the integrand, interchanging the summation and integration, changing the integration variable, and using (B-12), we obtain a series that is recognized as a special case of the confluent hypergeometric function. Thus,

$$E[R^n] = (2\sigma^2)^{n/2} \exp \left( -\frac{\lambda}{2\sigma^2} \right) \Gamma \left( 1 + \frac{n}{2} \right) {}_1F_1 \left( 1 + \frac{n}{2}, 1; \frac{\lambda}{2\sigma^2} \right), \quad n \geq 0 \quad (\text{B.27})$$

where the *confluent hypergeometric function* is defined as

$${}_1F_1(\alpha, \beta; x) = \sum_{i=0}^{\infty} \frac{\Gamma(\alpha + i)\Gamma(\beta)x^i}{\Gamma(\alpha)\Gamma(\beta + i)i!}, \quad \beta \neq 0, -1, -2, \dots \quad (\text{B.28})$$

The Rice density function often arises in the context of a transformation of variables. Let  $A_1$  and  $A_2$  represent independent Gaussian random variables with common variance  $\sigma^2$  and means  $m$  and zero, respectively. Let  $R$  and  $\Theta$  be implicitly defined by  $A_1 = R \cos \Theta$  and  $A_2 = R \sin \Theta$ . Then (B-23) and  $\Theta = \tan^{-1}(A_2/A_1)$  describes a transformation of variables. A straightforward calculation yields the joint density function of  $R$  and  $\Theta$ :

$$f_{R,\Theta}(r, \theta) = \frac{r}{2\pi\sigma^2} \exp \left( -\frac{r^2 - 2rm \cos \theta + m^2}{2\sigma^2} \right), \quad r \geq 0, \quad |\theta| \leq \pi \quad (\text{B.29})$$

The density function of the envelope  $R$  is obtained by integration over  $\theta$ . Since the *modified Bessel function of the first kind and order zero* satisfies

$$I_0(x) = \frac{1}{2\pi} \int_0^{2\pi} \exp(x \cos u) du \quad (\text{B.30})$$

this density function reduces to the Rice density function of (B-25). The density function of the angle  $\Theta$  is obtained by integrating (B-29) over  $r$ . Completing the square in the argument of (B-29), changing variables, and defining

$$Q(x) = \frac{1}{\sqrt{2\pi}} \int_{-x}^{\infty} \exp\left(-\frac{y^2}{2}\right) dy = \frac{1}{2} \operatorname{erfc}\left(\frac{x}{\sqrt{2}}\right) \quad (\text{B.31})$$

where  $\operatorname{erfc}(\cdot)$  is the complementary error function, we obtain

$$f_{\Theta}(\theta) = \frac{1}{2\pi} \exp\left(-\frac{m^2}{2\sigma^2}\right) + \frac{m \cos \theta}{\sqrt{2\pi}\sigma} \exp\left(-\frac{m^2 \sin^2 \theta}{2\sigma^2}\right) \left[1 - Q\left(\frac{m \cos \theta}{\sigma}\right)\right], \quad |\theta| \leq \pi \quad (\text{B.32})$$

Since (B-29) cannot be written as the product of (B-25) and (B-32), the random variables  $R$  and  $\Theta$  are not independent.

Since the density function of (B-25) must integrate to unity, we find that

$$\int_0^{\infty} r \exp\left(-\frac{r^2}{2b}\right) I_0\left(\frac{r\sqrt{\lambda}}{b}\right) dr = b \exp\left(\frac{\lambda}{2b}\right) \quad (\text{B.33})$$

where  $\lambda$  and  $b$  are positive constants. This equation is useful in calculations involving the Rice density function.

#### B.4 Rayleigh Distribution

A Rayleigh-distributed random variable is defined by (B-23) when  $A_1$  and  $A_2$  are independent Gaussian random variables with zero means and a common variance  $\sigma^2$ . Since  $F_R(r) = F_Z(r^2)$ , where  $Z$  is a central  $\chi^2$  random variable with two degrees of freedom, (B-20) with  $N = 2$  implies that the *Rayleigh probability distribution function* is

$$F_R(r) = 1 - \exp\left(-\frac{r^2}{2\sigma^2}\right), \quad r \geq 0 \quad (\text{B.34})$$

The *Rayleigh probability density function*, which may be obtained by differentiation of (B-34), is

$$f_R(r) = \frac{r}{\sigma^2} \exp\left(-\frac{r^2}{2\sigma^2}\right) u(r) \quad (\text{B.35})$$

By a change of variables in the defining integral, any moment of  $R$  can be expressed in terms of the gamma function defined in (B-12). Therefore,

$$E[R^n] = (2\sigma^2)^{n/2} \Gamma\left(1 + \frac{n}{2}\right) \quad (\text{B.36})$$

Certain properties of the gamma function are needed to simplify (B-36). An integration by parts of (B-12) indicates that  $\Gamma(1+x) = x\Gamma(x)$ . A direct integration yields  $\Gamma(1) = 1$ .

Therefore, when  $n$  is an integer,  $\Gamma(n) = (n - 1)!$ . Changing the integration variable by substituting  $y = z^2$  in (??), it is found that  $\Gamma(1/2) = \sqrt{\pi}$ .

Using these properties of the gamma function, we obtain the mean and the variance of a Rayleigh-distributed random variable:

$$E[R] = \sqrt{\frac{\pi}{2}}\sigma \quad (\text{B.37})$$

$$\sigma_R^2 = \left(2 - \frac{\pi}{2}\right)\sigma^2 \quad (\text{B.38})$$

Since  $A_1$  and  $A_2$  have zero means, the joint probability density function of the random variables  $R = \sqrt{A_1^2 + A_2^2}$  and  $\Theta = \tan^{-1}(A_2/A_1)$  is given by (B-29) with  $m = 0$ . Therefore,

$$f_{R,\Theta}(r, \theta) = \frac{r}{2\pi\sigma^2} \exp\left(-\frac{r^2}{2\sigma^2}\right), \quad r \geq 0, \quad |\theta| \leq \pi \quad (\text{B.39})$$

Integration over  $\theta$  yields (A-35), and integration over  $r$  yields the uniform probability density function:

$$f_{\Theta}(\theta) = \frac{1}{2\pi}, \quad |\theta| \leq \pi \quad (\text{B.40})$$

Since (B-39) equals the product of (B-35) and (B-40), the random variables  $R$  and  $\Theta$  are independent. In terms of these random variables,  $A_1 = R \cos \Theta$  and  $A_2 = R \sin \Theta$ . A straightforward calculation using the independence and densities of  $R$  and  $\Theta$  verifies that  $A_1$  and  $A_2$  are independent, zero-mean, Gaussian random variables with common variance  $\sigma^2$ . Since the square of a Rayleigh-distributed random variable may be expressed as  $R^2 = A_1^2 + A_2^2$ , where  $A_1$  and  $A_2$  are zero-mean independent Gaussian random variables with common variance  $\sigma^2$ ,  $R^2$  has the distribution of a central chi-square random variable with 2 degrees of freedom. Therefore, (B-18) with  $N = 2$  indicates that the square of a Rayleigh-distributed random variable has an exponential probability density function with mean  $2\sigma^2$ .

## B.5 Sum of Independent, Exponentially Distributed Random Variables

Consider the random variable

$$Z = \sum_{i=1}^N Y_i \quad (\text{B.41})$$

where the  $\{Y_i\}$  are independent, exponentially distributed random variables with unequal positive means  $\{m_i\}$ . The exponential probability density function of  $Y_i$  is

$$f_{Y_i}(x) = \frac{1}{m_i} \exp\left(-\frac{x}{m_i}\right) u(x) \quad (\text{B.42})$$

A straightforward calculation yields the characteristic function

$$C_{Y_i}(j\nu) = \frac{1}{1 - j\nu m_i} \quad (\text{B.43})$$

Since  $Z$  is the sum of independent random variables, (B-43) implies that its characteristic function is

$$C_Z(j\nu) = \prod_{i=1}^N \frac{1}{1 - j\nu m_i} \quad (\text{B.44})$$

To derive the probability density function of  $Z$ , (B-7) is applied after first expanding the right-hand side of (B-44) in a partial-fraction expansion. The result is

$$f_Z(x) = \sum_{i=1}^N \frac{B_i}{m_i} \exp\left(-\frac{x}{m_i}\right) u(x) \quad (\text{B.45})$$

where

$$B_i = \begin{cases} \prod_{\substack{k=1 \\ k \neq i}}^N \frac{m_i}{m_i - m_k} & , \quad N \geq 2 \\ 1 & , \quad N = 1 \end{cases} \quad (\text{B.46})$$

and  $m_i \neq m_k$ ,  $i \neq k$ . A direct integration and algebra yields the probability distribution function

$$F_Z(x) = 1 - \sum_{i=1}^N B_i \exp\left(-\frac{x}{m_i}\right), \quad x \geq 0 \quad (\text{B.47})$$

Equations (B-45) and (B-12) give

$$E[Z^n] = \Gamma(1 + n) \sum_{i=1}^N B_i m_i^n, \quad n \geq 0 \quad (\text{B.48})$$

When the  $\{m_i\}$  are equal so that  $m_i = m$ ,  $1 \leq i \leq N$ , then  $C_Z(j\nu) = (1 - j\nu m)^{-N}$ . Therefore, the probability density function of  $Z$  is

$$f_Z(x) = \frac{1}{(N-1)!m^N} x^{N-1} \exp\left(-\frac{x}{m}\right) u(x) \quad (\text{B.49})$$

which is a special case of the *gamma density function*. Successive integration by parts yields

$$F_Z(x) = 1 - \exp\left(-\frac{x}{m}\right) \sum_{i=0}^{N-1} \frac{1}{i!} \left(\frac{x}{m}\right)^i \quad (\text{B.50})$$

From (B-49) and (B-12), the mean and variance of  $Z$  are found to be

$$E[Z] = Nm \quad (\text{B.51})$$

$$\sigma_Z^2 = Nm^2 \quad (\text{B.52})$$

---

## C. Signal Representations

---

### C.1 Bandpass Signals

The *Hilbert transform* of a real-valued function  $g(t)$  defined on the time interval  $-\infty < t < \infty$  is

$$H[g(t)] = \hat{g}(t) = \frac{1}{\pi} \int_{-\infty}^{\infty} \frac{g(u)}{t-u} du \quad (\text{C.1})$$

Since its integrand has a singularity, the integral is defined as its Cauchy principal value:

$$\int_{-\infty}^{\infty} \frac{g(u)}{t-u} du = \lim_{\epsilon \rightarrow 0} \left[ \int_{-\infty}^{t-\epsilon} \frac{g(u)}{t-u} du + \int_{t+\epsilon}^{\infty} \frac{g(u)}{t-u} du \right] \quad (\text{C.2})$$

provided that the limit exists. Since (C-1) has the form of the convolution of  $g(t)$  with  $1/\pi t$ ,  $\hat{g}(t)$  results from passing  $g(t)$  through a linear filter with an impulse response equal to  $1/\pi t$ . The transfer function of the filter is given by the Fourier transform

$$\mathcal{F} \left\{ \frac{1}{\pi t} \right\} = \int_{-\infty}^{\infty} \frac{\exp(-j2\pi ft)}{\pi t} dt \quad (\text{C.3})$$

where  $j = \sqrt{-1}$ . This integral can be rigorously evaluated by using contour integration. Alternatively, we observe that since  $1/t$  is an odd function,

$$\begin{aligned} \mathcal{F} \left\{ \frac{1}{\pi t} \right\} &= -2j \int_0^{\infty} \frac{\sin 2\pi ft}{\pi t} dt \\ &= -j \operatorname{sgn}(f) \end{aligned} \quad (\text{C.4})$$

where  $\operatorname{sgn}(f)$  is the *signum function* defined by

$$\operatorname{sgn}(f) = \begin{cases} 1, & f > 0 \\ 0, & f = 0 \\ -1, & f < 0 \end{cases} \quad (\text{C.5})$$

Let  $G(f) = \mathcal{F}\{g(t)\}$ , and let  $\hat{G}(f) = \mathcal{F}\{\hat{g}(t)\}$ . Equations (??) and (??) and the convolution theorem imply that

$$\hat{G}(f) = -j \operatorname{sgn}(f)G(f) \quad (\text{C.6})$$

Because  $H[\hat{g}(t)]$  results from passing  $g(t)$  through two successive filters, each with transfer function  $-j \operatorname{sgn}(f)$ ,

$$H[\hat{g}(t)] = -g(t) \quad (\text{C.7})$$

provided that  $G(0) = 0$ .

Equation (C-6) indicates that taking the Hilbert transform corresponds to introducing a phase shift of  $-90$  degrees for all positive frequencies and  $+90$  degrees for all negative frequencies. Consequently,

$$H[\cos 2\pi f_0 t] = \sin 2\pi f_0 t \quad (\text{C.8})$$

$$H[\sin 2\pi f_0 t] = -\cos 2\pi f_0 t \quad (\text{C.9})$$

These relations can be formally verified by taking the Fourier transform of the left-hand side of (C-8) or (C-9), applying (C-6), and then taking the inverse Fourier transform of the result. If  $G(f) = 0$  for  $|f| > W$  and  $f_c > W$ , the same method yields

$$H[g(t) \cos 2\pi f_0 t] = g(t) \sin 2\pi f_c t \quad (\text{C.10})$$

$$H[g(t) \sin 2\pi f_0 t] = -g(t) \cos 2\pi f_c t \quad (\text{C.11})$$

A *bandpass signal* is one with a Fourier transform that is negligible except for  $f_c - W/2 \leq |f| \leq f_c + W/2$ , where  $0 \leq W < 2f_c$  and  $f_c$  is the center frequency. If  $W \ll f_c$ , the bandpass signal is often called a *narrowband signal*. A complex-valued signal with a Fourier transform that is nonzero only for  $f > 0$  is called an *analytic signal*.

Consider a bandpass signal  $g(t)$  with Fourier transform  $G(f)$ . The analytic signal  $g_a(t)$  associated with  $g(t)$  is defined to be the signal with Fourier transform

$$G_a(f) = [1 + \operatorname{sgn}(f)]G(f) \quad (\text{C.12})$$

which is zero for  $f \leq 0$  and is confined to the band  $|f - f_c| \leq W/2$  when  $f > 0$ . The inverse Fourier transform of (C-12) and (C-6) imply that

$$g_a(t) = g(t) + j\hat{g}(t) \quad (\text{C.13})$$

The *complex envelope* of  $g(t)$  is defined by

$$g_l(t) = g_a(t) \exp[-j2\pi f_c t] \quad (\text{C.14})$$

where  $f_c$  is the center frequency if  $g(t)$  is a bandpass signal. Since the Fourier transform of  $g_l(t)$  is  $G_a(f + f_c)$ , which occupies the band  $|f| \leq W/2$ , the complex envelope is a baseband

signal that may be regarded as an *equivalent lowpass representation* of  $g(t)$ . Equations (C-13) and (C-14) imply that  $g(t)$  may be expressed in terms of its complex envelope as

$$g(t) = \text{Re}[g_l(t) \exp(j2\pi f_c t)] \quad (\text{C.15})$$

The complex envelope can be decomposed as

$$g_l(t) = g_c(t) + jg_s(t) \quad (\text{C.16})$$

where  $g_c(t)$  and  $g_s(t)$  are real-valued functions. Therefore, (C-15) yields

$$g(t) = g_c(t) \cos(2\pi f_c t) - g_s(t) \sin(2\pi f_c t) \quad (\text{C.17})$$

Since the two sinusoidal carriers are in phase quadrature,  $g_c(t)$  and  $g_s(t)$  are called the *in-phase* and *quadrature* components of  $g(t)$ , respectively. These components are lowpass signals confined to  $|f| \leq W/2$ .

From Parseval's relation in Fourier analysis and (C-6), we obtain

$$\int_{-\infty}^{\infty} \hat{g}^2(t) dt = \int_{-\infty}^{\infty} |\hat{G}(f)|^2 df = \int_{-\infty}^{\infty} |G(f)|^2 df = \int_{-\infty}^{\infty} g^2(t) dt \quad (\text{C.18})$$

Therefore,

$$\begin{aligned} \int_{-\infty}^{\infty} |g_l(t)|^2 dt &= \int_{-\infty}^{\infty} |g_a(t)|^2 dt = \int_{-\infty}^{\infty} g^2(t) dt + \int_{-\infty}^{\infty} \hat{g}^2(t) dt \\ &= 2 \int_{-\infty}^{\infty} g^2(t) dt = 2\mathcal{E} \end{aligned} \quad (\text{C.19})$$

where  $\mathcal{E}$  denotes the energy of the bandpass signal  $g(t)$ .

## C.2 Stationary Stochastic Processes

Consider a stochastic process  $n(t)$  that is a zero-mean, wide-sense stationary process with autocorrelation

$$R_n(\tau) = E[n(t)n(t + \tau)] \quad (\text{C.20})$$

where  $E[x]$  denotes the expected value of  $x$ . The Hilbert transform of this process is the stochastic process defined by

$$\hat{n}(t) = \frac{1}{\pi} \int_{-\infty}^{\infty} \frac{n(u)}{t - u} du \quad (\text{C.21})$$

where it is assumed that the Cauchy principal value of the integral exists for almost every sample function of  $n(t)$ . This equation indicates that  $\hat{n}(t)$  is a zero-mean stochastic process. The zero-mean processes  $n(t)$  and  $\hat{n}(t)$  are *jointly wide-sense stationary* if their

correlation and cross-correlation functions are not functions of  $t$ . A straightforward calculation using (C-21) and (C-20) gives the cross correlation

$$R_{n\hat{n}}(\tau) = E[n(t)\hat{n}(t + \tau)] = \frac{1}{\pi} \int_{-\infty}^{\infty} \frac{R_n(u)}{\tau - u} du = \hat{R}_n(\tau) \quad (\text{C.22})$$

A similar derivation using (C-7) yields the autocorrelation

$$R_{\hat{n}}(\tau) = E[\hat{n}(t)\hat{n}(t + \tau)] = R_n(\tau) \quad (\text{C.23})$$

Equations (C-20), (C-22), and (C-23) indicate that  $n(t)$  and  $\hat{n}(t)$  are jointly wide-sense stationary.

The *analytic signal* associated with  $n(t)$  is the zero-mean process defined by

$$n_a(t) = n(t) + j\hat{n}(t) \quad (\text{C.24})$$

The autocorrelation of the analytic signal is defined as

$$R_a(\tau) = E[n_a^*(t)n_a(t + \tau)] \quad (\text{C.25})$$

where the asterisk denotes the complex conjugate. Using (C-20) and (C-22) to (C-25), we obtain

$$R_a(\tau) = 2R_n(\tau) + 2j\hat{R}_n(\tau) \quad (\text{C.26})$$

which establishes the wide-sense stationarity of the analytic signal.

Since (C-20) indicates that  $R_n(\tau)$  is an even function, (C-22) yields

$$R_{n\hat{n}}(0) = \hat{R}_n(0) = 0 \quad (\text{C.27})$$

which indicates that  $n(t)$  and  $\hat{n}(t)$  are uncorrelated. Equations (C-23), (C-26), and (C-27) yield

$$R_{\hat{n}}(0) = R_n(0) = 1/2R_a(0) \quad (\text{C.28})$$

The *complex envelope* of  $n(t)$  or the *equivalent lowpass representation* of  $n(t)$  is the zero-mean stochastic process defined by

$$n_l(t) = n_a(t) \exp(-j2\pi f_c t) \quad (\text{C.29})$$

where  $f_c$  is an arbitrary frequency usually chosen as the center or carrier frequency of  $n(t)$ . The complex envelope can be decomposed as

$$n_l(t) = n_c(t) + jn_s(t) \quad (\text{C.30})$$

where  $n_c(t)$  and  $n_s(t)$  are real-valued, zero-mean stochastic processes.

Equations (C-29) and (C-30) imply that

$$\begin{aligned} n(t) &= \operatorname{Re}[n_l(t) \exp(j2\pi f_c t)] \\ &= n_c(t) \cos(2\pi f_c t) - n_s(t) \sin(2\pi f_c t) \end{aligned} \quad (\text{C.31})$$

Substituting (C-24) and (C-30) into (C-29) we find that

$$n_c(t) = n(t) \cos(2\pi f_c t) + \hat{n}(t) \sin(2\pi f_c t) \quad (\text{C.32})$$

$$n_s(t) = \hat{n}(t) \cos(2\pi f_c t) - n(t) \sin(2\pi f_c t) \quad (\text{C.33})$$

The *autocorrelations* of  $n_c(t)$  and  $n_s(t)$  are defined by

$$R_c(\tau) = E[n_c(t)n_c(t + \tau)] \quad (\text{C.34})$$

and

$$R_s(\tau) = E[n_s(t)n_s(t + \tau)] \quad (\text{C.35})$$

Using (C-32) and (C-33) and then (C-20), (C-23), and (C-24) and trigonometric identities, we obtain

$$R_c(\tau) = R_s(\tau) = R_n(\tau) \cos(2\pi f_c \tau) + \hat{R}_n(\tau) \sin(2\pi f_c \tau) \quad (\text{C.36})$$

which shows explicitly that if  $n(t)$  is wide-sense stationary, then  $n_c(t)$  and  $n_s(t)$  are wide-sense stationary with the same autocorrelation function. The variances of  $n(t)$ ,  $n_c(t)$ , and  $n_s(t)$  are all equal because

$$R_c(0) = R_s(0) = R_n(0) \quad (\text{C.37})$$

A derivation similar to that of (C-36) gives the cross correlation

$$R_{cs}(\tau) = E[n_c(t)n_s(t + \tau)] = \hat{R}_n(\tau) \cos(2\pi f_c \tau) - R_n(\tau) \sin(2\pi f_c \tau) \quad (\text{C.38})$$

Equations (C-36) and (C-38) indicate that  $n_c(t)$  and  $n_s(t)$  are jointly wide-sense stationary. Equations (C-28) and (C-38) give

$$R_{cs}(0) = 0 \quad (\text{C.39})$$

which implies that  $n_c(t)$  and  $n_s(t)$  are uncorrelated.

Equation (C-21) indicates that  $\hat{n}(t)$  is generated by a linear operation on  $n(t)$ . Therefore, if  $n(t)$  is a zero-mean Gaussian process,  $\hat{n}(t)$  and  $n(t)$  are zero-mean jointly Gaussian processes. Equations (C-32) and (C-33) then imply that  $n_c(t)$  and  $n_s(t)$  are zero-mean jointly Gaussian processes. Since they are uncorrelated,  $n_c(t)$  and  $n_s(t)$  are statistically independent, zero-mean Gaussian processes.

The *power spectral density* of a signal is the Fourier transform of its autocorrelation. Let  $S(f)$ ,  $S_c(f)$ , and  $S_s(f)$  denote the power spectral densities of  $n(t)$ ,  $n_c(t)$ , and  $n_s(t)$ , respectively. We assume that  $S_n(f)$  occupies the band  $f_c - W/2 \leq |f| \leq f_c + W/2$  and that

$f_c > W/2 \geq 0$ . Taking the Fourier transform of (C-36), using (C-6), and simplifying, we obtain

$$S_c(f) = S_s(f) = \begin{cases} S_n(f - f_c) + S_n(f + f_c), & |f| \leq W/2 \\ 0, & |f| > W/2 \end{cases} \quad (\text{C.40})$$

Thus, if  $n(t)$  is a passband process with one-sided bandwidth  $W$ , then  $n_c(t)$  and  $n_s(t)$  are baseband processes with one-sided bandwidths  $W/2$ . This property and the statistical independence of  $n_c(t)$  and  $n_s(t)$  when  $n(t)$  is Gaussian make (C-31) a very useful representation of  $n(t)$ .

Similarly, the cross-spectral density of  $n_c(t)$  and  $n_s(t)$  can be derived by taking the Fourier transform of (C-38) and using (C-6). After simplification, the result is

$$S_{cs}(f) = \begin{cases} j[S_n(f - f_c) - S_n(f + f_c)], & |f| \leq W/2 \\ 0, & |f| > W/2 \end{cases} \quad (\text{C.41})$$

If  $S_n(f)$  is locally symmetric about  $f_c$ , then

$$S_n(f_c + f) = S_n(f_c - f), \quad |f| \leq W/2 \quad (\text{C.42})$$

Since a power spectral density is a real-valued, even function,  $S_n(f_c - f) = S_n(f - f_c)$ . Equation (C-42) then yields  $S_n(f + f_c) = S_n(f - f_c)$  for  $|f| \leq W/2$ . Therefore, (C-41) gives  $S_{cs}(f) = 0$ , which implies that

$$R_{cs}(\tau) = 0 \quad (\text{C.43})$$

for all  $\tau$ . Thus,  $n_c(t)$  and  $n_s(t + \tau)$  are uncorrelated for all  $\tau$ , and if  $n(t)$  is a zero-mean Gaussian process, then  $n_c(t)$  and  $n_s(t + \tau)$  are statistically independent for all  $\tau$ .

The autocorrelation of the complex envelope is defined by

$$R_l(\tau) = \frac{1}{2} E[n_l^*(t) n_l(t + \tau)] \quad (\text{C.44})$$

where the  $1/2$  is inserted so that

$$R_l(0) = R_n(0) \quad (\text{C.45})$$

which follows from (C-28) and (C-29). Substituting (C-30) into (C-44) and using (C-36) and (C-38), we obtain

$$R_l(\tau) = R_c(\tau) + jR_{cs}(\tau) \quad (\text{C.46})$$

The power spectral density of  $n_l(t)$ , which we denote by  $S_l(f)$ , can be derived from (C-46), (C-41), and (C-40). If  $S_n(f)$  occupies the band  $f_c - W/2 \leq |f| \leq f_c + W/2$  and  $f_c > W/2 \geq 0$ , then

$$S_l(f) = \begin{cases} 2S_n(f + f_c), & |f| \leq W/2 \\ 0, & |f| > W/2 \end{cases} \quad (\text{C.47})$$

Equations (C-36) and (C-38) yield

$$R_n(\tau) = R_c(\tau) \cos(2\pi f_c \tau) - R_{cs}(\tau) \sin(2\pi f_c \tau) \quad (\text{C.48})$$

Equations (C-48) and (C-46) imply that

$$R_n(\tau) = \text{Re} [R_l(\tau) \exp(j2\pi f_c \tau)] \quad (\text{C.49})$$

We expand the right-hand side of this equation by using the fact that  $\text{Re}[z] = (z + z^*)/2$ . Taking the Fourier transform and observing that  $S_l(f)$  is a real-valued function, we obtain

$$S_n(f) = \frac{1}{2}S_l(f - f_c) + \frac{1}{2}S_l(-f - f_c) \quad (\text{C.50})$$

If  $S_n(f)$  is locally symmetric about  $f_c$ , then (C-47) and (C-42) imply that  $S_l(-f) = S_l(f)$ , and (C-50) becomes

$$S_n(f) = \frac{1}{2}S_l(f - f_c) + \frac{1}{2}S_l(f + f_c) \quad (\text{C.51})$$

Many useful communication signals are modeled as having the form

$$s(t) = Ad_1(t) \cos(2\pi f_c t + \theta) + Ad_2(t) \sin(2\pi f_c t + \theta) \quad (\text{C.52})$$

where  $\theta$  is an independent random variable that is uniformly distributed over  $0 \leq \theta < 2\pi$ .

The modulations have the form

$$d_i(t) = \sum_{k=-\infty}^{\infty} a_{ik} \psi(t - kT - T_0 - t_i), \quad i = 1, 2 \quad (\text{C.53})$$

where  $\{a_{ik}\}$  is a sequence of independent, identically distributed random variables,  $a_{ik} = +1$  with probability 1/2 and  $a_{ik} = -1$  with probability 1/2,  $\psi(t)$  is a pulse waveform,  $T$  is the pulse duration,  $t_i$  is the relative pulse offset, and  $T_0$  is an independent random variable that is uniformly distributed over the interval  $(0, T)$  and reflects the arbitrariness of the origin of the coordinate system. Since  $a_{ik}$  is independent of  $a_{in}$  when  $n \neq k$ , it follows that  $E[a_{ik}a_{in}] = 0$ ,  $n \neq k$ . It follows that the autocorrelation of  $d_i(t)$  is

$$\begin{aligned} R_{di}(\tau) &= E[d_i(t)d_i(t + \tau)] \\ &= \sum_{k=-\infty}^{\infty} E[\psi(t - kT - T_0 - t_i)\psi(t - kT - T_0 - t_i + \tau)] \end{aligned} \quad (\text{C.54})$$

Expressing the expected value as an integral over the range of  $T_0$  and changing variables, we obtain

$$\begin{aligned} R_{di}(\tau) &= \sum_{k=-\infty}^{\infty} \frac{1}{T} \int_{t-kT-T-t_i}^{t-kT-t_i} \psi(x)\psi(x + \tau)dx \\ &= \frac{1}{T} \int_{-\infty}^{\infty} \psi(x)\psi(x + \tau)dx, \quad i = 1, 2 \end{aligned} \quad (\text{C.55})$$

This equation indicates that  $d_1(t)$  and  $d_2(t)$  are wide-sense stationary processes with the same autocorrelation.

If the sequences  $\{a_{1k}\}$  and  $\{a_{2k}\}$  are statistically independent, then the autocorrelation of  $s(t)$  is

$$R_s(\tau) = \frac{A^2}{2}R_{d1}(\tau) \cos(2\pi f_c\tau) + \frac{A^2}{2}R_{d2}(\tau) \sin(2\pi f_c\tau) \quad (\text{C.56})$$

where  $R_{d1}(\tau)$  and  $R_{d2}(\tau)$  are the autocorrelations of  $d_1(t)$  and  $d_2(t)$ , respectively. This equation indicates that  $s(t)$  is wide-sense stationary. If the sample functions of  $d_1(t)$  and  $d_2(t)$  have Fourier transforms that vanish for  $|f| \geq f_c$ , then (C-10), (C-11), (C-24), and (C-29) indicate that the complex envelope of  $s(t)$  is

$$s_l(t) = Ad_1(t) - jAd_2(t) \quad (\text{C.57})$$

Equation (C-44) and the independence of  $d_1(t)$  and  $d_2(t)$  imply that the autocorrelation of  $s_l(t)$  is

$$R_l(\tau) = \frac{A^2}{2}R_{d1}(\tau) + \frac{A^2}{2}R_{d2}(\tau) \quad (\text{C.58})$$

The power spectral density of  $s_l(t)$  is the Fourier transform of  $R_l(\tau)$ . From (C-58) and (C-55), we obtain the density

$$S_l(f) = A^2 \frac{|G(f)|^2}{T} \quad (\text{C.59})$$

where  $G(f)$  is the Fourier transform of  $\psi(t)$ .

In a quadriphase-shift-keying (QPSK) signal,  $d_1(t)$  and  $d_2(t)$  are usually modeled as independent random binary sequences with pulse duration  $T = 2T_b$ , where  $T_b$  is a bit duration. The component amplitude is  $A = \sqrt{\mathcal{E}_b/T_b}$ , where  $\mathcal{E}_b$  is the energy per bit. If  $\psi(t)$  is rectangular with unit amplitude over  $[0, 2T_b]$ , then (C-59) yields the power spectral density for QPSK:

$$S_l(f) = 2\mathcal{E}_b \text{sinc}^2 2T_b f \quad (\text{C.60})$$

which is the same as the density for PSK. For a binary minimum-shift-keying (MSK) signal with the same component amplitude,

$$\psi(t) = \sqrt{2} \sin\left(\frac{\pi t}{2T_b}\right), \quad 0 \leq t < 2T_b \quad (\text{C.61})$$

Therefore, the power spectral density for MSK is

$$S_l(f) = \frac{16\mathcal{E}_b}{\pi^2} \left[ \frac{\cos(2\pi T_b f)}{16T_b^2 f^2 - 1} \right]^2 \quad (\text{C.62})$$

### C.3 Sampling Theorems

Consider the Fourier transform  $G(f)$  of an absolutely integrable function  $g(t)$ . The periodic extension of  $G(f)$  is defined as

$$\bar{G}(f) = \sum_{i=-\infty}^{\infty} G(f + iW) \quad (\text{C.63})$$

where  $W$  is the period of  $\bar{G}(f)$  and it is assumed that the series converges uniformly. Suppose that  $\bar{G}(f)$  has a piecewise continuous derivative so that it can be represented as a uniformly convergent complex Fourier series:

$$\bar{G}(f) = \sum_{k=-\infty}^{\infty} c_k \exp\left(-j2\pi k \frac{f}{W}\right) \quad (\text{C.64})$$

where the Fourier coefficient  $c_k$  is given by

$$c_k = \frac{1}{W} \int_{-W/2}^{W/2} \bar{G}(f) \exp\left(j2\pi k \frac{f}{W}\right) df \quad (\text{C.65})$$

Substituting (C-63) into (C-65) and interchanging the order of the summation and the integration, which is justified because of the uniform convergence, we obtain

$$c_k = \frac{1}{W} \sum_{i=-\infty}^{\infty} \int_{-W/2}^{W/2} G(f + iW) \exp\left(j2\pi k \frac{f}{W}\right) df \quad (\text{C.66})$$

We change variables and observe the  $\exp(j2\pi ki) = 1$  to obtain

$$\begin{aligned} c_k &= \frac{1}{W} \sum_{i=-\infty}^{\infty} \int_{-W/2+iW}^{W/2+iW} G(f) \exp\left(j2\pi k \frac{f}{W} - j2\pi ki\right) df \\ &= \frac{1}{W} \int_{-\infty}^{\infty} G(f) \exp\left(j2\pi k \frac{f}{W}\right) df \end{aligned} \quad (\text{C.67})$$

Since  $g(t)$  is absolutely integrable, the last integral is the inverse Fourier transform of  $G(f)$  evaluated at  $t = k/W$ , and

$$c_k = \frac{1}{W} g\left(\frac{k}{W}\right) \quad (\text{C.68})$$

Substituting (C-68) into (C-64) yields the *Poisson sum formula*:

$$\bar{G}(f) = \frac{1}{W} \sum_{k=-\infty}^{\infty} g\left(\frac{k}{W}\right) \exp\left(-\frac{j2\pi kf}{W}\right) \quad (\text{C.69})$$

where the series converges uniformly.

Suppose that the Fourier transform vanishes outside a frequency band:

$$G(f) = 0, \quad |f| > W/2 \quad (\text{C.70})$$

It follows that

$$g(t) = \int_{-W/2}^{W/2} G(f) \exp(j2\pi ft) df \quad (\text{C.71})$$

Since  $G(f) = \bar{G}(f)$  for  $|f| < W/2$ , (C-71) and (C-69) and the interchange of a summation and integration yield

$$g(t) = \sum_{k=-\infty}^{\infty} g\left(\frac{k}{W}\right) \frac{1}{W} \int_{-W/2}^{W/2} \exp\left[j2\pi f\left(t - \frac{k}{W}\right)\right] df \quad (\text{C.72})$$

Evaluating this integral and defining  $\text{sinc } x = \sin(\pi x)/\pi x$ , we obtain the *sampling theorem* for deterministic signals:

$$g(t) = \sum_{k=-\infty}^{\infty} g\left(\frac{k}{W}\right) \text{sinc}(Wt - k) \quad (\text{C.73})$$

Consider a wide-sense stationary stochastic process  $n(t)$  with autocorrelation  $R_n(\tau)$  and power spectral density  $S_n(f)$ , which is the Fourier transform of  $R_n(\tau)$ . If

$$S_n(f) = 0, \quad |f| > W/2 \quad (\text{C.74})$$

then it follows from the sampling theorem that

$$R_n(\tau) = \sum_{k=-\infty}^{\infty} R_n\left(\frac{k}{W}\right) \text{sinc}(W\tau - k) \quad (\text{C.75})$$

For an arbitrary constant  $\alpha$ , the Fourier transform of  $R(\tau - \alpha)$  is  $S_n(f) \exp(-j2\pi f\alpha)$ , which is zero for  $|f| > W/2$ . Therefore, (eqC-75) can be applied to  $R'_n(\tau) = R_n(\tau - \alpha)$ , which gives

$$R_n(\tau - \alpha) = \sum_{k=-\infty}^{\infty} R_n\left(\frac{k}{W} - \alpha\right) \text{sinc}(W\tau - k) \quad (\text{C.76})$$

We define the stochastic process

$$n_\nu(t) = \sum_{k=-\nu}^{\nu} n\left(\frac{k}{W}\right) \text{sinc}(Wt - k) \quad (\text{C.77})$$

An expansion indicates that the mean square difference between  $n(t)$  and  $n_\nu(t)$  is

$$\begin{aligned} E\{[n(t) - n_\nu(t)]^2\} &= R_n(0) - 2 \sum_{k=-\nu}^{\nu} R_n\left(t - \frac{k}{W}\right) \text{sinc}(Wt - k) \\ &\quad + \sum_{i=-\nu}^{\nu} \text{sinc}(Wt - i) \sum_{k=-\nu}^{\nu} R_n\left(\frac{i - k}{W}\right) \text{sinc}(Wt - k) \quad (\text{C.78}) \end{aligned}$$

Since  $R_n(\tau) = R_n(-\tau)$ , the repeated use of (C-76) yields

$$\lim_{\nu \rightarrow \infty} E\{[n(t) - n_\nu(t)]^2\} = 0 \quad (\text{C.79})$$

which states that the mean square difference between  $n(t)$  and  $n_\nu(t)$  approaches zero.

Thus, the sampling theorem for stationary stochastic process is

$$n(t) = \sum_{k=-\infty}^{\infty} n \left( \frac{k}{W} \right) \text{sinc}(Wt - k) \quad (\text{C.80})$$

where the equality holds in the sense of (C-79).

---

## D. Adaptive Filters

---

The input and weight vectors of an adaptive filter are

$$\mathbf{x} = [x_1 \ x_2 \ \dots \ x_N]^T, \quad \mathbf{W} = [W_1 \ W_2 \ \dots \ W_N]^T \quad (\text{D.1})$$

where  $T$  denotes the transpose and the components of the vectors may be real or complex. The filter output is the scalar

$$y = \mathbf{W}^T \mathbf{x} \quad (\text{D.2})$$

The derivation of the optimal filter weights depends on the specification of a performance criterion or estimation procedure. A number of different estimators of the desired signal can be implemented by linear filters that produce (D-2). Unconstrained estimators that depend only on the second-order moments of  $\mathbf{X}$  can be derived by using performance criteria based on the mean square error or the signal-to-noise ratio of the filter output. Similar estimators result from using the maximum-*a-posteriori* or the maximum-likelihood criteria, but the standard application of these criteria entails the restrictive assumption that any interference in  $\mathbf{X}$  has a Gaussian distribution.

The difference between the desired response  $d$  and the filter output is the *error signal*:

$$\epsilon = d - \mathbf{W}^T \mathbf{x} \quad (\text{D.3})$$

The most widely used method of estimating the desired signal is based on the minimization of the expected value of the squared error magnitude, which is proportional to the mean power in the error signal. Let  $H$  denote the conjugate transpose and an asterisk denote the conjugate. We obtain

$$\begin{aligned} E[|\epsilon|^2] &= E[\epsilon^* \epsilon] = E[(d^* \mathbf{W}^H \mathbf{x}^*) (d - \mathbf{x}^T \mathbf{W})] \\ &= E[|d|^2] - \mathbf{W}^H \mathbf{R}_{xd} - \mathbf{R}_{xd}^H \mathbf{W} + \mathbf{W}^H \mathbf{R}_{xx} \mathbf{W} \end{aligned} \quad (\text{D.4})$$

where

$$\mathbf{R}_{xx} = E[\mathbf{x}^* \mathbf{x}^T] \quad (\text{D.5})$$

is the  $N \times N$  Hermitian *correlation matrix* of  $\mathbf{x}$  and

$$\mathbf{R}_{xd} = E[\mathbf{x}^* d] \quad (\text{D.6})$$

is the  $N \times 1$  *cross-correlation* vector. If we assume that  $y \neq 0$  when  $\mathbf{W} \neq \mathbf{0}$ , then  $\mathbf{R}_{xx}$  must be positive definite.

In terms of its real part  $\mathbf{W}_R$ , and its imaginary part  $\mathbf{W}_I$ , a complex weight vector is defined as

$$\mathbf{W} = \mathbf{W}_R - j\mathbf{W}_I \quad (\text{D.7})$$

The *gradient* of  $f$  with respect to the  $n$ -dimensional, real-valued vector  $\mathbf{x}$  is defined as the column vector  $\nabla_{\mathbf{x}}f$  with components  $\partial f/\partial x_i, i = 1, 2, \dots, n$ . Let  $\nabla_{wr}$  and  $\nabla_{wi}$  denote the  $N \times 1$  gradient vectors with respect to  $\mathbf{W}_R$  and  $\mathbf{W}_I$  respectively. The *complex gradient* with respect to  $\mathbf{W}$  is defined as

$$\bar{\nabla}_w = \nabla_{wr} - j\nabla_{wi} \quad (\text{D.8})$$

Let  $W_i, W_{Ri}$  and  $W_{Ii}, i = 1, 2, \dots, N$ , denote the components of  $\mathbf{W}, \mathbf{W}_R$ , and  $\mathbf{W}_I$ , respectively. Let  $g(\mathbf{W}, \mathbf{W}^*)$  denote a real-valued function of  $\mathbf{W}$  and  $\mathbf{W}^*$ . Regarding  $\mathbf{W}$  and  $\mathbf{W}^*$  as independent variables, we assume that  $g$  is an analytic function of each  $W_i$  when  $\mathbf{W}^*$  is held constant and an analytic function of each  $W_i^*$  when  $\mathbf{W}$  is held constant. We define  $\nabla_{w^*}$  as the gradient with respect to  $\mathbf{W}^*$ . Since  $W_i = W_{Ri} - jW_{Ii}$ ,

$$\frac{\partial W_i}{\partial W_{Ri}} = 1, \quad \frac{\partial W_i}{\partial W_{Ii}} = -j, \quad \frac{\partial W_i^*}{\partial W_{Ri}} = 1, \quad \frac{\partial W_i^*}{\partial W_{Ii}} = j \quad (\text{D.9})$$

The chain rule of calculus then implies that

$$\begin{aligned} \bar{\nabla}_w g(\mathbf{W}, \mathbf{W}^*) &= \nabla_{wr}g - j\nabla_{wi}g \\ &= \nabla_w g + \nabla_{w^*}g - j(-j\nabla_w g + j\nabla_{w^*}g) \end{aligned} \quad (\text{D.10})$$

Thus,

$$\bar{\nabla}_w g(\mathbf{W}, \mathbf{W}^*) = 2\nabla_{w^*}g(\mathbf{W}, \mathbf{W}^*) \quad (\text{D.11})$$

This result allows a major simplification in calculations. Since  $\nabla_{\mathbf{x}}(\mathbf{x}^T \mathbf{y}) = \nabla_{\mathbf{x}}(\mathbf{y}^T \mathbf{x}) = \mathbf{y}$ , (D-11) and (D-4) yield

$$\bar{\nabla}_w E[|\epsilon|^2] = 2\mathbf{R}_{xx}\mathbf{W} - 2\mathbf{R}_{xd} \quad (\text{D.12})$$

Since  $\nabla_{wr}g = 0$  and  $\nabla_{wi}g = 0$  imply that  $\bar{\nabla}_w g = 0$ , a necessary condition for the optimal weight is obtained from setting  $\bar{\nabla}_w E[|\epsilon|^2] = \mathbf{0}$ . Thus, if  $\mathbf{R}_{xx}$  is positive definite and hence nonsingular, the *Wiener-Hopf equation* for the optimal weight vector is

$$\mathbf{W}_0 = \mathbf{R}_{xx}^{-1}\mathbf{R}_{xd} \quad (\text{D.13})$$

Substituting  $\mathbf{W} = \mathbf{W}_0$  into (D-4), we obtain the mean square error

$$\epsilon_m^2 = E[|d|^2] - \mathbf{R}_{xd}^H \mathbf{R}_{xx}^{-1} \mathbf{R}_{xd} \quad (\text{D.14})$$

Equations (D-4), (D-13), and (D-14) imply that

$$E[|\epsilon|^2] = \epsilon_m^2 + (\mathbf{W} - \mathbf{W}_0)^H \mathbf{R}_{xx} (\mathbf{W} - \mathbf{W}_0) \quad (\text{D.15})$$

Since  $\mathbf{R}_{xx}$  is positive definite, this equation shows that the Wiener-Hopf equation provides a unique optimal weight vector and that (D-14) gives the minimum mean square error.

Since the computational difficulty of inverting the correlation matrix is considerable when the number of weights is large, and insofar as time-varying signal statistics may require

frequent computations, adaptive algorithms not entailing matrix inversion have been developed. Suppose that a performance measure,  $P(\mathbf{W})$ , is defined so that it has a minimum value when the weight vector has its optimal value. In the *method of steepest descent*, the weight vector is changed along the direction of the negative gradient of the performance measure. This direction gives the largest decrease in  $P(\mathbf{W})$ . If the signals and weights are complex, separate steepest-descent equations can be written for the real and imaginary parts of the weight vector. Combining these equations, we obtain

$$\mathbf{W}(k+1) = \mathbf{W}(k) - \mu \bar{\nabla}_w P(\mathbf{W}(k)) \quad (\text{D.16})$$

For complex signals and weights, a suitable performance measure is  $P(\mathbf{W}) = E[|\epsilon|^2]$ . Using (D-12) and (D-16), we obtain the *steepest-descent algorithm*:

$$\mathbf{W}(k+1) = \mathbf{W}(k) - 2\mu [\mathbf{R}_{xx} \mathbf{W}(k) - \mathbf{R}_{xd}] \quad (\text{D.17})$$

This ideal algorithm produces a deterministic sequence of weights and does not require a matrix inversion, but it requires the knowledge of  $\mathbf{R}_{xx}$  and  $\mathbf{R}_{xd}$ . However, the possible presence of interference means that  $\mathbf{R}_{xx}$  is unknown. In the absence of information about the direction of the desired signal,  $\mathbf{R}_{xd}$  is also unknown.

The *least-mean-square (LMS) algorithm* is obtained when  $\mathbf{R}_{xx}$  is estimated by  $\mathbf{x}^*(k)\mathbf{x}^T(k)$ ,  $\mathbf{R}_{xd}$  is estimated by  $\mathbf{x}^*(k)d(k)$ , and (D-3) is applied in (D-17). The LMS algorithm is

$$\mathbf{W}(k+1) = \mathbf{W}(k) + 2\mu\epsilon(k)\mathbf{x}^*(k) \quad (\text{D.18})$$

For a fixed value of  $\mathbf{W}(k)$ , the product  $\epsilon(k)\mathbf{x}^*(k)$  is an unbiased estimate of  $\bar{\nabla}_w E[\epsilon^2]$ . According to this algorithm, the next weight vector is obtained by adding to the present weight vector the input vector scaled by the amount of error. It can be shown [26], [1] that, for an appropriate value of  $\mu$ , the mean of the weight vector converges to the optimal value given by the Wiener-Hopf equation.

---

## References

---

- [1] D. Torrieri, *Principles of Secure Communication Systems*, 2nd ed. Boston: Artech House, 1992.
- [2] R. L. Peterson, R. E. Ziemer, and D. E. Borth, *Introduction to Spread Spectrum Communications*. Upper Saddle River, NJ: Prentice Hall, 1995.
- [3] M. K. Simon et al., *Spread-Spectrum Communications Handbook*. New York: McGraw-Hill, 1994.
- [4] S. B. Wicker, *Error Control Systems for Digital Communication and Storage*. Upper Saddle River, NJ: Prentice Hall, 1995.
- [5] G. J. Simmons, ed., *Contemporary Cryptology: The Science of Information Integrity*. New York: IEEE Press, 1992.
- [6] R. B. Ash and C. A. Doleans-Dade, *Probability and Measure Theory, 2nd ed.* San Diego: Academic Press, 2000.
- [7] D. J. Torrieri, "The Performance of Five Different Metrics Against Pulsed Jamming," *IEEE Trans. Commun.*, vol. 34, pp. 200–207, February 1986.
- [8] J.-J. Chang, D.-J. Hwang, and M.-C. Lin, "Some Extended Results on the Search for Good Convolutional Codes," *IEEE Trans. Inform. Theory*, vol. 43, pp. 1682–1697, September 1997.
- [9] C. Campbell, *Surface Acoustic Wave Devices for Mobile and Wireless Communications*. New York: Academic Press, 1998.
- [10] M. Kowatsch, "Application of Surface-Acoustic-Wave Technology to Burst-Format Spread-Spectrum Communications," *IEE Proc.*, vol. 131, pt. F, pp. 734–741, December 1984.
- [11] D. P. Morgan and J. M. Hannah, "Surface Wave Recirculation Loops for Signal Processing," *IEEE Trans. Sonics and Ultrason.*, vol. 25, pp. 30–38, January 1978.
- [12] R. B. Ward and K. P. Y. Yiu, "Acquisition of Pseudonoise Signals by Recursion-Aided Sequential Estimation," *IEEE Trans. Commun.*, vol. 25, pp. 784–794, August 1977.
- [13] H. Meyr and G. Polzer, "Performance Analysis for General PN-Spread-spectrum Acquisition Techniques," *IEEE Trans. Commun.*, vol. 31, pp. 1317–1319, December 1983.

- [14] V. M. Jovanovic, "Analysis of Strategies for Serial-Search Spread-Spectrum Code Acquisition-Direct Approach," *IEEE Trans. Commun.*, vol. 36, pp. 1208–1220, November 1988.
- [15] S.-M. Pan, D. E. Dodds, and S. Kumar, "Acquisition Time Distribution for Spread-Spectrum Receivers," *IEEE J. Select. Areas Commun.*, vol. 8, 800, June 1990.
- [16] A. Polydoros and C. L. Weber, "A Unified Approach to Serial-Search Spread Spectrum Code Acquisition," *IEEE Trans. Commun.*, vol. 32, pp. 542–560, May 1984.
- [17] V. M. Jovanovic and E. S. Sousa, "Analysis of Noncoherent Correlation in DS/BPSK Spread Spectrum Acquisition," *IEEE Trans. Commun.*, vol. 43, pp. 565–573, Feb./March/April 1995.
- [18] L.-L. Yang and L. Hanzo, "Serial Acquisition of DS-CDMA Signals in Multipath Fading Mobile Channels," *IEEE Trans. Veh. Technol.*, vol. 50, pp. 617–628, March 2001.
- [19] K. Choi, K. Cheun, and T. Jung, "Adaptive PN Code Acquisition Using Instantaneous Power-Scaled Detection Threshold under Rayleigh Fading and Pulsed Gaussian Noise Jamming," *IEEE Trans. Commun.*, pp. 1232–1235, August 2001.
- [20] S. Glisic and M. D. Katz, "Modeling of the Code Acquisition Process for Rake Receivers in CDMA Wireless Networks with Multipath and Transmitter Diversity," *IEEE J. Select. Areas Commun.*, vol. 19, pp. 21–32, January 2001.
- [21] A. Polydoros and C. L. Weber, "Analysis and Optimization of Correlative Code-Tracking Loops in Spread-Spectrum Systems," *IEEE Trans. Commun.*, vol. 33, pp. 30–43, January 1985.
- [22] W. R. Braun, "PN Acquisition and Tracking Performance in DS/CDMA Systems with Symbol-Length Spreading Sequence," *IEEE Trans. Commun.*, vol. 45, pp. 1595–1601, December 1997.
- [23] W.-H. Sheen and C.-H. Tai, "A Noncoherent Tracking Loop with Diversity and Multipath Interference Cancellation for Direct-Sequence Spread-Spectrum Systems," *IEEE Trans. Commun.*, vol. 46, pp. 1516–1524, November 1998.
- [24] L. B. Milstein, "Interference Rejection Techniques in Spread Spectrum Communications," *Proc. IEEE*, vol. 76, pp. 657–671, June 1988
- [25] H. V. Poor, "Active Interference Suppression in CDMA Overlay Systems," *IEEE J. Select. Areas Commun.*, vol. 19, 4–20, January 2001.
- [26] S. Haykin, *Adaptive Filter Theory, 4th ed.* Upper Saddle River, NJ: Prentice-Hall, 2002.

- [27] M. Medley, G. Saulnier, and P. Das, "The Application of Wavelet-Domain Adaptive Filtering to Spread-Spectrum Communications," *Proc. SPIE Wavelet Applications for Dual-Use*, vol. 2491, p. 233–247, April 1995.
- [28] C. J. Masreliez, "Approximate Non-Gaussian Filtering with Linear State and Observation Relations," *IEEE Trans. Automat. Contr.*, vol. 20, pp. 107–110, February 1975.
- [29] R. Vijayan and H. V. Poor, "Nonlinear Techniques for Interference Suppression in Spread-Spectrum Systems," *IEEE Trans. Commun.*, vol. 37, pp. 1060–1065, July 1990.
- [30] L. A. Rusch and H. V. Poor, "Narrowband Interference Suppression in CDMA Spread Spectrum Communications," *IEEE Trans. Commun.*, vol. 42, pp. 1969–1979, Feb./March/April 1994.
- [31] S. Buzzi, M. Lops, and H. V. Poor, "Code-Aided Interference Suppression for DS/CDMA Overlay Systems," *Proc. IEEE*, vol. 90, pp. 394–435, March 2002.
- [32] M. D. Srinath, P. K. Rajasekaran, and R. Viswanathan, *Introduction to Statistical Signal Processing with Applications*. Englewood Cliffs, NJ: Prentice Hall, 1996.
- [33] A. Polydoros and C. L. Weber, "Detection Performance Considerations for Direct-Sequence and Time-Hopping LPI Waveforms," *IEEE J. Select. Areas Commun.*, vol. 3, pp. 727–744, September 1985.
- [34] D. A. Hill and E. B. Felstead, "Laboratory Performance of Spread Spectrum Detectors," *Proc. IEEE Commun.*, vol. 43, pp. 243–249, August 1995.
- [35] D. V. Sarwate and M. B. Pursley, "Crosscorrelation Properties of Pseudorandom and Related Sequences," *Proc. IEEE*, vol. 68, pp. 593–619, May 1980.
- [36] M. B. Pursley, "Spread-Spectrum Multiple-Access Communications," in *Multi-User Communications Systems*, G. Longo, ed., New York: Springer-Verlag, 1981.
- [37] M. B. Pursley, D. V. Sarwate, and W. E. Stark, "Error Probability for Direct-Sequence Spread-Spectrum Multiple-Access Communications—Part 1: Upper and Lower Bounds," *IEEE Trans. Commun.*, vol. 30, pp. 975–984, May 1982.
- [38] A. R. Hammons and P. V. Kumar, "On a Recent 4-Phase Sequence Design for CDMA," *IEICE Trans. Commun.*, vol. E-76B, pp. 804–813, August 1993.
- [39] T. G. Macdonald and M. B. Pursley, "The Performance of Direct-Sequence Spread Spectrum with Complex Processing and Quaternary Data Modulation," *IEEE J. Select. Areas Commun.*, vol. 18, pp. 1408–1417, August 2000.

- [40] D. Torrieri, "Performance of Direct-Sequence Systems with Long Pseudonoise Sequences," *IEEE J. Select. Areas Commun.*, vol. 10, pp. 770–781, May 1992.
- [41] G. Zang and C. Ling, "Performance Evaluation for Band-limited DS-CDMA Systems Based on Simplified Improved Gaussian Approximation," *IEEE Trans. Commun.*, vol. 51, pp. 1204–1213, July 2003.
- [42] Y. C. Yoon, "Quadrphase DS-CDMA with Pulse Shaping and the Accuracy of the Gaussian Approximation for Matched Filter Receiver Performance Analysis," *IEEE Trans. Wireless Commun.*, vol. 1, pp 761–768, October 2002.
- [43] L. B. Milstein, "Wideband Code Division Multiple Access," *IEEE J. Select. Areas Commun.*, vol 48, pp. 1318–1327, August 2000.
- [44] J. G. Proakis, *Digital Communications*, 4th ed. New York: McGraw-Hill, 2001.
- [45] J. S. Lee and L. E. Miller, *CDMA Systems Engineering Handbook*. Boston: Artech House, 1998.
- [46] K. Higuchi et al., "Experimental Evaluation of Combined Effect of Coherent Rake Combining and SIR-Based Fast Transmit Power Control for Reverse Link of DS-CDMA Mobile Radio," *IEEE J. Select. Areas Commun.*, vol. 18, pp. 1526–1535, August 2000.
- [47] D. Torrieri, "Information-Bit, Information-Symbol, and Decoded-Symbol Error Rates for Linear Block Codes," *IEEE Trans. Commun.*, vol. 36, pp. 613–617, May 1988.
- [48] D. Torrieri, "Instantaneous and Local-Mean Power Control for Direct-Sequence CDMA Cellular Networks," *IEEE Trans. Commun.*, vol. 50, pp. 1310–1315, August 2002.
- [49] D. Torrieri, "Uplink Capacity of a CDMA Network," *IEEE Wireless Commun. and Networking Conf.*, March 2003.
- [50] S. Verdu, *Multiuser Detection*. New York: Cambridge University Press, 1998.
- [51] U. Madhow, "Blind Adaptive Interference Suppression for Direct-Sequence CDMA," *Proc. IEEE*, vol. 86, pp. 2049–2069, October 1998.
- [52] S. Buzzi and H. V. Poor, "Channel Estimation and Multiuser Detection in Long-Code DS/CDMA Systems," *IEEE J. Select. Areas Commun.*, vol. 19, pp. 1476–1487, August 2001.
- [53] M. Sawahashi et al., "Experiments on Pilot Symbol-Assisted Coherent Multistage Interference Canceller for DS-CDMA Mobile Radio," *IEEE J. Select. Areas Commun.*, vol. 20, pp. 433–449, February 2002.

## Distribution

Admnstr  
Defns Techl Info Ctr  
ATTN DTIC-OCP (Electronic Copy)  
8725 John J Kingman Rd Ste 0944  
FT Belvoir VA 22060-6218

DARPA  
ATTN S Welby  
3701 N Fairfax Dr  
Arlington VA 22203-1714

Ofc of the Secy of Defns  
ATTN ODDRE (R&AT)  
The Pentagon  
Washington DC 20301-3080

Future Centers Capabilities Development  
Directorate Science & Technology Division  
ATTN ATFEDS  
10 Whistler Lane  
FT Monroe VA 23651-5850

Dir for MANPRINT Ofc of the  
Deputy Chief of Staff for Prsnl  
ATTN J Hiller  
The Pentagon Rm 2C733  
Washington DC 20301-0300

US Military Acdmy  
Mathematical Sci Ctr of Excellence  
ATTN LTC T Rugenstein  
Thayer Hall Rm 226C  
West Point NY 10996-1786

SMC/GPA  
2435 Vela Way Ste 1613  
El Segundo CA 90245-5500

TECOM  
ATTN CSTE-DTC-CL  
Aberdeen Proving Ground MD 21005-5057

US Army ARDEC  
ATTN AMSTA-AR-TD  
Bldg 1  
Picatinny Arsenal NJ 07806-5000

US Army Avn & Mis Cmnd  
ATTN AMSMI-RD W C McCorkle  
Redstone Arsenal AL 35898-5240

US Army Info Sys Engrg Cmnd  
ATTN AMSEL-IE-TD F Jenia  
FT Huachuca AZ 85613-5300

US Army Natick RDEC  
Acting Techl Dir  
ATTN SBCN-TP P Brandler  
Kansas Street Bldg78  
Natick MA 01760-5056

US Army PEO Simulation, Training, &  
Instrmntn  
ATTN M Macedonia Chief Technology  
Officer  
12350 Research Parkway  
Orlando FL 32826-3726

US Army Tank-Automtv Cmnd RDEC  
ATTN AMSTA-TR J Chapin  
Warren MI 48397-5000

Cubic Defns Sys  
ATTN K Bakhru  
9323 Balboa Ave  
San Diego CA 92123

Hicks & Assoc Inc  
ATTN G Singley III  
1710 Goodrich Dr Ste 1300  
McLean VA 22102

Director  
US Army Rsrch Lab  
ATTN AMSRL-RO-D JCI Chang  
ATTN AMSRL-RO-EN W D Bach  
PO Box 12211  
Research Triangle Park NC 27709

US Army Rsrch Lab  
ATTN AMSRL-CI J D Gantt  
ATTN AMSRL-CI-C J Gowens

US Army Rsrch Lab (cont'd)  
ATTN AMSRL-CI-IS-R Mail & Records  
Mgmt  
ATTN AMSRL-CI-OK Techl Pub (2 copies)  
ATTN AMSRL-CI-OK-TL Techl Lib  
(2 copies)  
ATTN AMSRL-D J M Miller  
ATTN AMSRL-IS-C D Torrieri (20 copies)  
Adelphi MD 20783-1197